Wireless Powering and Communication of Implantable Medical Devices

by

Muayad Kod

Submitted in accordance with the requirements for the award of the degree of Doctor of Philosophy of the University of Liverpool

September 2016

Copyright

To my sister's soul, you are always in my mind and in my heart

To my parents, wife, lovely boys, sisters, brothers and friends: Thank you for your support.

Table of Contents

Acronyms

AC	Alternative Current
ADS	Advanced Design System
BCC	Body Centric Communication
BMI	Brain Machine Interfacing
BRs	Basic Restrictions
CC	Constant Current
CST	Computer Simulation Technology
CV	Constant Voltage
DC	Direct Current
EIRP	Effective Isotropic Radiated Power
ETSI	European Telecommunications Standards Institute
FCC	Federal Communications Commission
GPS	Global Positioning System
ICNIRP	International Commission on Non-Ionizing Radiation Protection
IEEE	Institute of Electrical and Electronics Engineers
IMD	Implantable Medical Device
ISM	Industrial Scientific & Medical
LPDA	Log Periodic Antenna

MedRadio	Medical Device Radiocommunications Service
MICS	Medical Implant Communication Service
MPEs	Maximum Permissible Exposures
MS	Modal Significance
NHS	The National Health Service
PIFA	Planar Inverted-F Antenna
RF	Radio Frequency
RMS	Root Mean Square
RX	Receiver
SAR	Specific Absorption Rate
TCM	Theory of Characteristic Mode
TX	Transmitter
UWB	Ultra-Wideband
VNA	Vector Network Analyser
WBAN	Wireless Body Area Network
WPT	Wireless Power Transfer

Acknowledgements

First of all, I thank ALLAH ALMIGHTY who has given me the power and confidence to do this work. I would like to express my deepest gratitude to my supervisor Dr Jiafeng Zhou for the continuous support of my Ph.D research, for his patience, motivation, enthusiasm, and immense knowledge. His guidance has helped me throughout the research and writing up this thesis. I would like to thank Prof. Yi Huang for his motivation and insightful comments. My sincere thanks also go to Dr. Waleed Al-Nuaamy, his advices really helped me at the beginning of the research. Thanks also go to Dr. Ali Al-Ataby for his beneficial feedback during the annual review at our department.

I should also thank my home sponsor The Higher Committee for Education Development in Iraq (HCED) for the financial fund to pursue my study. It was a great support to improve my occupation and get introduced to new cultures abroad.

Thanks must also be paid to my colleagues at the Wireless Engineering Research Group; in particular to Dr Rula Alrawashdeh, Dr Saqer Alja'afreh, Chaoyun Song, Muaad Hussein, Dr Qian Xu and Manoj Stanley for the stimulating discussions in a work related context.

I would like to thank my research lab colleagues and my friends: Dr Amir Kotb, Abed Pour Sohrab, Dr Lei Xing, Yuan Zhuang, Dr Sheng Yuan, Saidatul Izyanie, Zhouxiang Fei, Umniyyah Ulfa, Anqi Chen, Zhihao Tian, Dr Ping Cao, Dr Jingwei Zhang, Aznida Abu Bakar Sajak and Dr Neda Khiabani. I have enjoyed working with you all and I appreciate the ideas, help and good humour.

Last but not the least; I would like to offer my special thanks to my parents and family for their support, encouragement and help. I am eternally grateful for everything they have done, your prayers have been answered. I would also like to express my gratitude to my lovely wife ANSAM, your love, patient and encouragement helped me to be succeeded. My lovely boys (LAITH and AMEER), your curious and love have extremely motivated me to do the best. I would like to thank ALLAH for giving me a little angel (MAYAR).

List of Publications

[1] **Muayad Kod**, J. Zhou, Y. Huang, M. Stanley, M. Hussein, A. P. Sohrab, R. Alrawashdeh and G. Wang, " Feasibility Study of Using the Housing Cases of Implantable Devices as Antennas," *IEEE Access*, vol. 4, pp. 6939-6949, 2016.

[2] **Muayad Kod**, J. Zhou, Y. Huang, M. Hussein, A. P. Sohrab, and C. Song, " Deep Port Loop Antenna Design to Improve Wireless Power Transfer and Misalignment Tolerance into Biomedical Implants," *IEEE Transactions on Microwave Theory and Techniques*, Major revision on 15 September, 2016.

[3] **Muayad Kod**, J. Zhou, Y. Huang and M. Stanley, " Using the Housing Cases of Implantable and Wearable Devices as Antennas," *Patent*, GB Patent Application No: 1614854.6, 2016.

[4] **Muayad Kod**, J. Zhou, R. Alrawashdeh, and Y. Huang, "Wireless Charging of Implantable Battery Using Rectenna," *in Proc. in Antennas & Propagation Conference (LAPC), 2014 Loughborough*, pp. 316-317, 2014.

[5] **Muayad Kod**, J. Zhou, Y. Huang, R. Alrawashdeh, and M. Hussein, "A dual broadband butterfly loop antenna for body wearable applications," in *Antennas & Propagation Conference (LAPC), 2015 Loughborough*, pp. 1-3, 2015.

[6] **Muayad Kod**, J. Zhou, Y. Huang, and R. Alrawashdeh, "Wireless powering of implantable medical devices," in *Antennas, Wireless and Electromagnetics, IET Colloquium on*, pp. 1-18, 2015.

[7] R. S. Alrawashdeh, Y. Huang, **Muayad Kod**, and A. A. B. Sajak, "A Broadband Flexible Implantable Loop Antenna With Complementary Split Ring Resonators," *IEEE Antennas and Wireless Propagation Letters,* vol. 14, pp. 1506-1509, 2015.

[8] C. Song, Y. Huang, P. Carter, J. Zhou, S. Yuan, Q. Xu, **Muayad Kod,** *et al.*, "A Novel Six-Band Dual CP Rectenna Using Improved Impedance Matching Technique for Ambient RF Energy Harvesting," *IEEE Transactions on Antennas and Propagation,* vol. 64, pp. 3160-3171, 2016.

[9] A. P. Sohrab, Y. Huang, M. Hussein, **Muayad Kod**, and P. Carter, "A UHF RFID Tag With Improved Performance on Liquid Bottles," *IEEE Antennas and Wireless Propagation Letters,* vol. 15, pp. 1673-1676, 2016.

[10] M. Hussein, J. Zhou, Y. Huang, **Muayad Kod**, and A. Sohrab, "Dual stopband frequency selective surface by using half rings and slots," *Microwave and Optical Technology Letters,* vol. 58, pp. 1136-1139, 2016.

[11] R. Alrawashdeh, Y. Huang, A. A. B. Sajak, L. Xing, and **Muayad Kod**, "Orientation effect of flexible implantable antennas on performance," in *2014 IEEE Antennas and Propagation Society International Symposium (APSURSI)*, pp. 973-974, 2014.

[12] L. Xing, Y. Huang, S. S. Alja'afreh, Q. Xu, **Muayad Kod**, and C. Song, "Reconfigurable 3D folded monopole antenna design for DVB-H applications," in *Antennas and Propagation Conference (LAPC), 2014 Loughborough*, pp. 530-532, 2014.

[13] M. Hussein, J. Zhou, Y. Huang, **Muayad Kod**, and A. P. Sohrab, "A novel array element for wideband frequency selective surface," in *Active and Passive RF Devices Seminar*, pp. 1-3, 2016.

[14] M. Hussein, J. Zhou, Y. Huang, A. P. Sohrab, and **Muayad Kod**, "Frequency selective surface with simple configuration stepped-impedance elements," in *2016 10th European Conference on Antennas and Propagation (EuCAP)*, pp. 1-4, 2016.

Abstract

Recently, implantable medical devices become widely used because of the high quality of patient's treatment. The rapid development in technology makes the manufacturing of these devises is easy and compact. Powering is the major challenge in developing implantable medical devices. Primary battery is the mostly used power source. However, batteries limit the life and size of the implants. The promising solution to overcome this challenge is to use the wireless power transfer (WPT). Therefore, this thesis is mainly focused on developing antennas that can be used for dual purposes of WPT and communication.

One of the essential parts of WPT is the rectifier circuit. Rectifiers have been designed as follow:

- Three rectifier circuits are designed based on voltage doubler technique.
- The designed rectifiers have RF to DC conversion efficiency higher than 70%.
- The rectifier circuit has been miniaturized to dimensions of 5 x 10 mm^2 and still has more than 70% of RF to DC conversion efficiency.

Antennas are the major part of the WPT and communication system. Wearable antennas are designed for several purposes in this research as follow:

- A meandered loop wearable antenna is designed to cover the MICS band around 403 MHz and the ISM band around 433 MHz with high magnetic flux in the near field region.
- A butterfly loop antenna is designed to cover two wide bands of 0.4-1 GHz and 2-2.7 GHz. This antenna is designed to be compatible with the implantable transceiver ZL70323 by Microsemi so that MICS band is used for communication, 433 MHz for powering and 2.45 GHz for wake up signal.
- Another wearable antenna is designed based on meandering loop antenna as well. This antenna generates strong fields along two axes. The contribution of this design is to improve the magnetic field for better WPT.

Two implantable loop antennas have been designed as well to be integrated with the

rectifiers and wearable antennas to form a compact WPT system with the following characteristics:

- Both antennas cover the MICS band and the ISM band around 433 MHz.
- The antennas are flexible so that they can be used in planar and curved surfaces.

A novel implantable antenna has been designed for implantable devices that contained in a metallic case such as pacemakers. This design is based on adopting the cavity of the devices as a radiating antenna. This antenna has the following characteristics:

- The housing case itself is used as an antenna.
- It covers both the MICS band and the ISM around 433 MHz.
- It is Able to establish a communication link up to 19 m within safety limits.
- It can harvest up to 4 mW power from a transmitter 1 m away under safety limits.

Far field and near field WPT experiments have been conducted using the proposed designs as follows:

- Near Field WPT experiment in pork as body model.
- Far Field WPT experiments in pork and in a liquid body model.
- Far Field WPT experiment in pork and a rabbit using the pacemaker housing case as an antenna.

These experiments confirmed the usability of the proposed designs to provide sufficient power for many implantable medical devices.

Chapter 1

Introduction

1.1 Background

The evolution in our world is running very fast because of the rapid development of scientific research methods and tools. The base for such evolution is the human needs in different life styles including health and entertainment etc. There is no doubt in that the health has the priority over most other needs because it relates directly to human life. It attracts a lot of research funding and has a very active market. Consequently, researchers in both academic and industrial sectors are very interested in designing and developing health tools and medical devices to be more reliable, safer and more comfortable.

Some of the medical devices can be implanted inside the human body for different purposes, such as monitoring, drug delivery or specific stimulation. The first successful implanted device inside the human body was a pacemaker in 1960 [1]. This step opened a hot topic for researchers to investigate and develop many more implantable devices. Medical devices designed for implantation purposes require several considerations from different scopes such as medical, biology, electrical engineering or mechanical engineering requirements. Electrical engineering plays a significant role in developing such devices in terms of various aspects including powering and communication systems. Since these aspects are very essential for any implantable device, researchers spend great efforts to exploit the optimum solution such that the devices can work reliably and safely.

Many different implantable devices can be used for human body as shown in Fig. 1.1. Medical implants are connected with external readers through wireless communication to provide essential bio information. Such information is important for therapeutic and diagnostic purposes. Wireless communication requires efficient antennas to establish links. Many considerations should be taken into account when

the antenna is designed since it is intended to be implanted inside the human body. Some of these considerations are the size to be as small as possible, the shape to be conformal to the medical device, the radiation pattern to be suitable for the related application and more importantly the transmitted power to be within the specific absorption rate (SAR) safety limit.

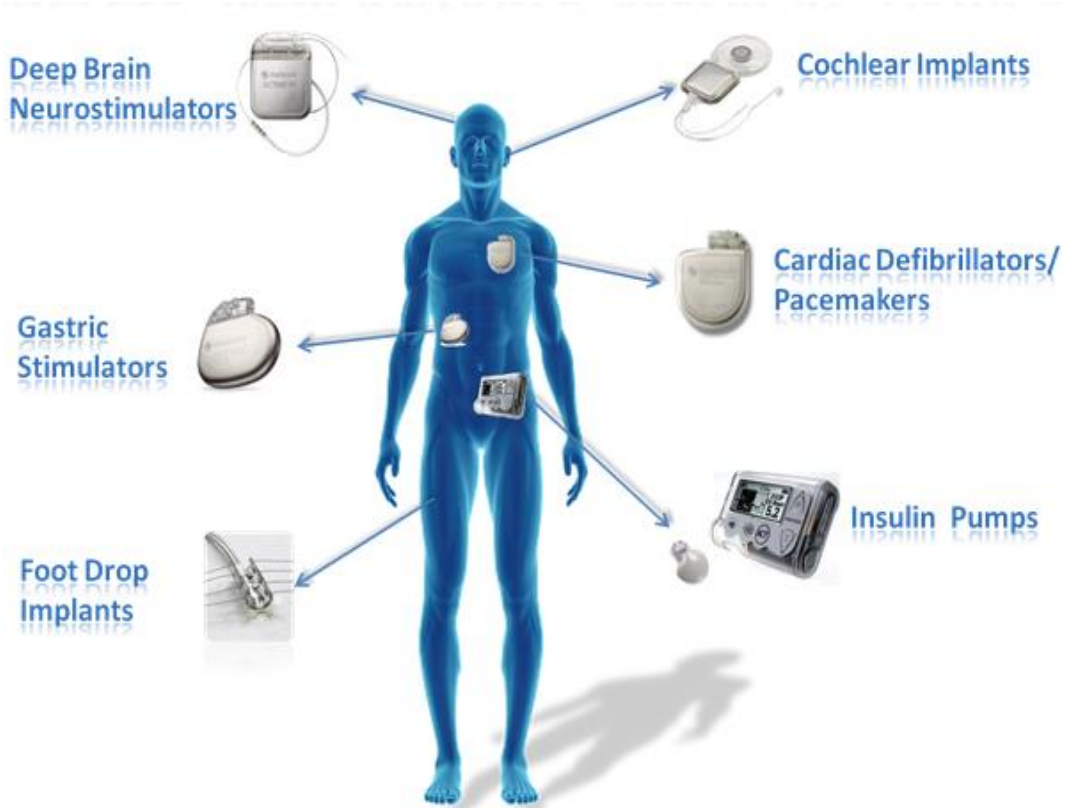

Fig. 1.1. Several wireless implantable medical devices are used in human body [2].

Mainly there are two types of methods to establish communication links for implantable device: inductive coils and Radio Frequency (RF) antennas. The working frequency bands in use are from a few kHz to several MHz through inductively coupled coils. The communication range between the inductively coupled implantable device and the programmer is limited to a few centimetres within the near field region [3, 4]. The reason for this short range is that the magnetic induction field decays rapidly with distance. In 1999, the U.S. Federal

Communications Commission (FCC) allocated the Medical Implant Communication Service (MICS) band of 402 – 405 MHz as a response to petition from Medtronic. This is to permit the use of a mobile radio device for data communication for implantable devices. The range of communication link can be extended by using the RF band, [5]. The equivalent isotropically radiated power (EIRP) of the MICS devices is limited by the regulation to -16 dBm so that the interference amongst these devices will be restrained [6]. This band is later adopted by European Telecommunications Standards Institute (ETSI) in 2002 and become the target band for implantable antenna designers [7]. The MICS band was expanded to Medical Device Radio communication (MedRadio) band (401-406 MHz) in 2009. However, the MICS band still represents the core of MedRadio band and it is reserved for implantable devices communication only with a specific channel bandwidth of 300 kHz. The expansion wings of 401-402 MHz and 405-406 MHz have channel bandwidths of 100-150 kHz and they can be used by the medical body-worn devices.

Implants are powered mostly by primary batteries. Deep brain neurostimulators and pacemakers for example are powered by non-rechargeable batteries with a predetermined lifetime. The life span of these batteries is 5 to 7 years based on the function of the device. At the end of battery life, the implantable device should be replaced surgically with a high cost and potential infection risk to the patient. The incident of infection related to such replacement of pacemakers ranges from 1%-19% [7]. Furthermore, some implantable devices that work in direct contact with blood cannot use batteries such as pH and glucose sensors due to the potential risk of poisoning in case leakage happens [8]. Batteries occupy more than 50% of some these devices volume. An alternative solution to use such batteries leads to significant reduction in the implant size. Furthermore, it leads to long term usability of the implant and is cost effective.

The information of power consumption of medical devices is very useful for the selection of proper power sources. The typical power consumption of implantable device varies from tens of μW to several mW. Examples for such power consumptions are the pacemaker which requires under normal conditions from 10 μW to 70 μW [8, 9], the nerve stimulation device requires 100 μW [10] and the glucose measurement system consumes 48 μW [11].

Power sources of implantable devices are divided into three main types. The first type is using a battery (primary or rechargeable) as the main supply. The second type is based on energy harvesting from internal resources inside the body such as piezoelectric, biology cells and thermal energy. The third type is based on Wireless Power Transfer (WPT) using dedicated external transmitters. A trade off among these power sources in terms of power density, advantage and disadvantage are summarized in Table 1.1 [12].

Table 1.1: Comparison amongst various energy sources [12].

Power source	Power density	Pros	Cons
Primary batteries	0.09 μW/mm²/year	Reliable	Limited life span
Piezoelectric	< 0.2 μW/mm²	Internal energy	Depending on moving parts
Glucose bio-fuel cell utilizing glucose from blood (5 mM)	2.8 μW/mm²	Internal energy	It's limited by the glucose enzyme density
Thermoelectric, T=5°C	0.6 μW/mm²	Internal energy	Low efficiency
Electromagnetic power transfer	10 to 1000 μW/mm²	High power density and Controllable	Limited by safety regulations

Table 1.1 shows that the most reliable source is using primary batteries (non-rechargeable). However, the batteries have a limited life span with a self-discharging which means it has to be replaced through a surgery after a certain life time. The capacity of such batteries is also limited which confines the medical devices for fewer functions in order to extend the battery life. Furthermore, it is the major contributor for the bulky volume that bothers the size and shape of the device.

On other hand, the ability of piezoelectric material such as crystalline to generate electric power based mainly on vibration or movement is a promising source. However, this limits the usage of such technique to the moving parts of the body such as heart beat or moving hands or legs which are human activity dependent otherwise there is a little generated power when the patient is idle or sleeps. Glucose bio-fuel cell is another option for power generation. It is able to transform chemical energy directly to electrical energy through electrochemical reactions [13]. However,

this technique is limited by the glucose enzyme density [14]. Another internal source for energy harvesting is the thermoelectric. This power source is limited due to the low efficiency [15]. These internal sources are advantageous for being available all the time but it is limited for several reasons such as low density, low efficiency or availability at specific parts of the body.

The electromagnetic power transfer system is the most promising solution with the highest power density compared with other possible sources as shown in Table 1.1. Although it is limited by the safety regulation for maximum permissible exposures which will be explained in the next chapter, this technique can be modified and optimized according to the application requirements. It is flexible and more controllable by the designer so that it is very attractive to be implemented.

1.2 Research Motivations and Objectives

People's life and health have the importance to motivate researchers to develop efficient and reliable solutions for medical devices. These devices play a significant role in treating or monitoring diseases or disordered organics and hence improving patients' life quality. Therefore, powering and telemetry of medical devices are of high importance to be considered as the scope of this research.

There are several considerations and requirements to design a communication and wireless powering system for medical devices including:

- Safety in terms of adverse reaction of device's material to body tissues. This can be solved by using biocompatible insulators.
- Safety in terms of low level of power to be radiated or exposed to the body. The level of transmitted power either from implantable antennas or from external antennas should be below the safety limits that issued by health authorities.
- Freedom of patient's mobility. For the cases that required long time to be processed such as charging a battery, it is important to consider the free mobility of the patient.

- Low profile and light weight antennas. Antennas are preferred to be thin so that the size of an implant is kept as small as possible.
- Sufficient power supply. The powering system should provide enough power for the implant to work properly with taking into consideration the power safety limits.
- Low interference with other applications. The frequency used and the level of the transmitted power should not affect other applications.

The inductive coils were used previously for both WPT and communication. However, the data transfer in these systems is limited and the communication range between external and internal systems is restricted for a few centimetres within the near field region [3, 4]. Since 1999 when FCC allocated MICS band, this band is become widely used in designing RF telemetry for medical devices. By adopting the home monitoring services in some medical systems, RF telemetry becomes essential service for implants. It is utilized by most Implantable Medical Device (IMD) manufactures for remote home monitoring such as Home Monitoring® system by Biotronik and CareLink® Network by Medtronic [16-18]. Although a patient can use coil to collect data and send it to the clinic by a phone or internet, some home monitoring systems are required to monitor patients even when they are sleeping [19]. This kind of wireless home monitoring requires RF antennas.

Wireless powering and telemetry of medical devices are much related topics. Both systems can be dealt simultaneously. However, many works focused on developing implantable antennas for communication regardless of what technique is adopted for powering the devices [20-28]. These designs considered mainly the communication band MICS for their antennas. On the other hand, wireless powering is considered only in [29-44]. Frequencies varied in these works. The frequency of 13.56 MHz is used at [29, 31, 40, 42], 8.1 MHz at [30], 200 MHz at [36], 10 MHz at [38], 2 MHz at [33], 94 MHz at [41] and 1.6 GHz at [44].

Both systems can be considered together to make the medical device more compact. The two techniques were integrated in one frequency by using the same coil for powering and data communications [42, 45, 46]. However, using the same frequency for both targets could cause interference or distortion to very important bio-information. Furthermore, the design in [46] used the MICS band for both targets

although it is limited to maximum EIRP of -16 dBm in order to reduce the harmful interference. Powering and communication are adopted in the same work also but with separate frequencies on one antenna [47] or using a coil and an antenna together [48, 49]. Using an antenna for communication and a coil for WPT require more space and could add more size for the implant. The most promising approach is using one implantable RF antenna to cover two bands so that one band is for RF data telemetry and the other band for WPT.

Wearable antennas have an importance for medical devices as well. These antennas are positioned on the body. It participates in establishing a communication link with the implant for in body and off body communications [50-53]. These wearable antennas were used for WPT at 300 MHz [50], for in body communication at MICS band and 430 MHz [51, 52] respectively or for off body communication as a repeater at the ISM band around 2.45 GHz [51, 53]. Wearable antennas have the potential to improve WPT by utilizing near field coupling and can extend the communication range by performing as a repeater.

From the above discussion it can be concluded that:

- Antennas are important to be considered in designing a telemetry system for medical devices because of the capability for wireless home monitoring.
- The MICS band is the main target for antenna design since it is specified for medical communications only and limited with -16 dBm of transmitting power to reduce the interference effect with other applications.
- Using one antenna to handle data communications and WPT is essential to reduce the implant size.
- The ISM band around 433 MHz is the best candidate for WPT because it is close to the MICS band so that it easy to cover both bands using one antenna.
- Wearable antennas have several advantages to be adopted in data communication in terms of extending the communication range as a repeater. It has the advantage in WPT in terms of free mobility to the patient and utilizing near field coupling in WPT.

In this research, both targets are aimed to be considered in one compact antenna design but each at a separate frequency.

- The best bands are concluded to be the MICS band for communication and ISM 433 MHz band for WPT.
- Since these two bands are close to each other, it can be easily covered by designing one antenna with sufficient bandwidth.
- Designing and developing such antennas to be integrated in powering and telemetry systems will be investigated.
- Rectifier circuits that convert the received Alternative Current (AC) signal to Direct Current (DC) power will be investigated as well. This rectifier plays essential role in converting the captured RF signal into a DC. The generated DC can be used to directly power an implant or used to recharge a battery.
- An integration to the proposed antennas and rectifiers in a compatible system will be investigated to achieve the targets so that rectifiers can be used for powering purposes, wearable and implantable antennas for transmitting and receiving RF signals.
- WPT systems will be discussed and implemented in two cases; far field WPT scenario using the proposed implantable antenna and rectifier and near field WPT using wearable and implantable antennas further to the rectifier circuit.
- Advantage and disadvantage of both near field and far field techniques will be discussed in terms of amount of the received power, safety regulations, and the comfort to the patient. Some new ideas to improve WPT and communication for medical devices will be introduced.

1.3 Organisation of the Thesis

There are seven chapters in this thesis. In Chapter 1, a brief introduction is given.

In Chapter 2, some theory and background are introduced including the safety regulation in terms of power radiation limits and exposure limits. Background of wireless power transfer and telemetry with biomedical devices will be explained. It will be supported with some related literature review.

In chapter 3, the rectifier is an important part of wireless power transfer that is designed at ISM band around 433 MHz. Battery charging experiment to one

implantable battery using one of the proposed rectifiers will be presented. Some simulation works regarding DC combining circuits will be explained as well. A summary and conclusion are given at the end of the chapter.

In chapter 4, wearable and implantable antennas designs are discussed. These antennas are used to communicate and transfer power to the implantable devices at the MICS band and the ISM 433 MHz band respectively. Two designs of implantable antennas covering these two bands will be presented. Three wearable antenna designs covering both MICS band and ISM band around 433 MHz will be demonstrated as well. A summary and conclusion are given at the end of the chapter.

In chapter 5, WPT experiments are demonstrated using the antennas and rectifiers that have been discussed in the previous chapters. Far field and near field WPT systems experiments are presented and discussed. A summary and conclusion are given at the end of the chapter.

In chapter 6, a new antenna design for IMDs is proposed. This antenna covers both MICS and ISM 433 MHz bands. This design is demonstrated for communication by experiment using a transceiver and a temperature sensor. It also demonstrated for WPT. Both experiments are carried out in Vitro using minced pork and a rabbit. A summary and conclusion are given at the end of the chapter.

In Chapter 7, the conclusions and future work are discussed.

References

[1] H. Raillard, "Development of an implantable cardiac pacemaker," *Solid-State Circuits Conference. Digest of Technical Papers, IEEE International, Philadelphia, PA, USA,* pp. 88- 89, 1962.

[2] Massachusetts Institute of Technology, "http://groups.csail.mit.edu/netmit/IMDShield/," 2011.

[3] J. A. Von Arx, W. R. Mass, S. T. Mazar, and M. D. Amundson, "Antenna for an implantable medical device," ed: US patent 7,483,752 B2, Jan. 27, 2009.

[4] S. Vajha, K. R. Maile, D. E. Larson, D. A. Chizek, and J. M. Edgell, "Folded antennas for implantable medical devices," ed: US patent 2012/0130451 A1, May 24, 2012.

[5] K. S. Nikita, *Handbook of biomedical telemetry*: John Wiley & Sons, 2014.

[6] H. S. Savci, A. Sula, Z. Wang, N. S. Dogan, and E. Arvas, "MICS transceivers: Regulatory standards and applications," *Proceedings of the IEEE SoutheastCon 2004,* pp. 179-182, 2005.

[7] E. T. S. Institute, "Ultra Low Power Active Medical Implants (ULP-AMI) and Peripherals (ULP-AMI-P) operating in the frequency range 402 MHz to 405 MHz," 2009.

[8] R. Das and H. Yoo, "Biotelemetry and Wireless Powering for Leadless Pacemaker Systems," *IEEE Microwave and Wireless Components Letters,* vol. 25, pp. 262-264, Apr 2015.

[9] J. Miller, "Wireless power for tiny medical implants," *Physics Today,* vol. 67, pp. 12-14, Aug 2014.

[10] C. S. Niu, H. W. Hao, L. M. Li, B. Z. Ma, and M. S. Wu, "The transcutaneous charger for implanted nerve stimulation device," *2006 28th Annual International Conference of the IEEE Engineering in Medicine and Biology Society, Vols 1-15,* pp. 3237-3240, 2006.

[11] K. Bazaka and M. V. Jacob, "Implantable devices: issues and challenges," *Electronics,* vol. 2, pp. 1-34, 2012.

[12] J. M. Rabaey, M. Mark, D. Chen, C. Sutardja, C. Tang, S. Gowda*, et al.*, "Powering and communicating with mm-size implants," in *2011 Design, Automation & Test in Europe*, 2011, pp. 1-6.

[13] R. A. Bullen, T. Arnot, J. Lakeman, and F. Walsh, "Biofuel cells and their development," *Biosensors and Bioelectronics,* vol. 21, pp. 2015-2045, 2006.

[14] N. Mano, "A 280 μW cm− 2 biofuel cell operating at low glucose concentration," *Chemical Communications,* pp. 2221-2223, 2008.

[15] R. Venkatasubramanian, C. Watkins, D. Stokes, J. Posthill, and C. Caylor, "Energy harvesting for electronics with thermoelectric devices using nanoscale," *2007 IEEE International Electron Devices Meeting, Vols 1 and 2,* pp. 367-370, 2007.

[16] H. Burri and D. Senouf, "Remote monitoring and follow-up of pacemakers and implantable cardioverter defibrillators," *Europace,* vol. 11, pp. 701-709, 2009.

[17] M. E. Guevara-Valdivia and P. I. Torres, *Remote monitoring of implantable pacemaker, cardioverter defibrillator, and cardiac resynchronizer*: INTECH Open Access Publisher, 2011.

[18] BostonScintefic, "https://www.bostonscientific.com/content/dam/bostonscientific/quality/education-resources/english/US_ACL_LATITUDE_Communicator_Switches_20140627.pdf," 2014.

[19] Medtronic, "http://www.medtronic.com/content/dam/medtronic-com-m/mdt/crdm/documents/uc200402712cen.pdf," 2009.

[20] R. S. Alrawashdeh, Y. Huang, M. Kod, and A. A. Sajak, "A Broadband Flexible Implantable Loop Antenna With Complementary Split Ring Resonators," *IEEE Antennas and Wireless Propagation Letters,* vol. 14, pp. 1506-1509, 2015.

[21] Z. Duan, Y. X. Guo, M. Y. Je, and D. L. Kwong, "Design and in Vitro Test of a Differentially Fed Dual-Band Implantable Antenna Operating at MICS and ISM Bands," *IEEE Transactions on Antennas and Propagation,* vol. 62, pp. 2430-2439, May 2014.

[22] S. Bakogianni and S. Koulouridis, "An Implantable Planar Dipole Antenna for Wireless MedRadio-Band Biotelemetry Devices," *IEEE Antennas and Wireless Propagation Letters,* vol. 15, pp. 234-237, 2016.

[23] A. Kiourti, K. A. Psathas, P. Lelovas, N. Kostomitsopoulos, and K. S. Nikita,

"In Vivo Tests of Implantable Antennas in Rats: Antenna Size and Intersubject Considerations," *IEEE Antennas and Wireless Propagation Letters,* vol. 12, pp. 1396-1399, 2013.

[24] A. Kiourti and K. S. Nikita, "Miniature Scalp-Implantable Antennas for Telemetry in the MICS and ISM Bands: Design, Safety Considerations and Link Budget Analysis," *IEEE Transactions on Antennas and Propagation,* vol. 60, pp. 3568-3575, Aug 2012.

[25] H. Li, Y. X. Guo, C. R. Liu, S. Q. Xiao, and L. Li, "A Miniature-Implantable Antenna for MedRadio-Band Biomedical Telemetry," *IEEE Antennas and Wireless Propagation Letters,* vol. 14, pp. 1176-1179, 2015.

[26] T. Karacolak, A. Z. Hood, and E. Topsakal, "Design of a dual-band implantable antenna and development of skin mimicking gels for continuous glucose monitoring," *IEEE Transactions on Microwave Theory and Techniques,* vol. 56, pp. 1001-1008, Apr 2008.

[27] P. Soontornpipit, C. M. Furse, and Y. C. Chung, "Design of implantable microstrip antenna for communication with medical implants," *IEEE Transactions on Microwave Theory and Techniques,* vol. 52, pp. 1944-1951, Aug 2004.

[28] W. C. Liu, S. H. Chen, and C. M. Wu, "Implantable Broadband Circular Stacked Pifa Antenna for Biotelemetry Communication," *Journal of Electromagnetic Waves and Applications,* vol. 22, pp. 1791-1800, 2008.

[29] R. F. Xue, K. W. Cheng, and M. Je, "High-Efficiency Wireless Power Transfer for Biomedical Implants by Optimal Resonant Load Transformation," *IEEE Transactions on Circuits and Systems I-Regular Papers,* vol. 60, pp. 867-874, Apr 2013.

[30] D. Ahn and S. Hong, "Wireless Power Transmission With Self-Regulated Output Voltage for Biomedical Implant," *IEEE Transactions on Industrial Electronics,* vol. 61, pp. 2225-2235, May 2014.

[31] T. Campi, S. Cruciani, F. Palandrani, V. De Santis, A. Hirata, and M. Feliziani, "Wireless Power Transfer Charging System for AIMDs and Pacemakers," *IEEE Transactions on Microwave Theory and Techniques,* vol. 64, pp. 633-642, Feb 2016.

[32] A. K. RamRakhyani and G. Lazzi, "Interference-free wireless power transfer

system for biomedical implants using multi-coil approach," *Electronics Letters,* vol. 50, pp. 853-854, Jun 5 2014.

[33] A. K. RamRakhyani and G. Lazzi, "Multicoil Telemetry System for Compensation of Coil Misalignment Effects in Implantable Systems," *IEEE Antennas and Wireless Propagation Letters,* vol. 11, pp. 1675-1678, 2012.

[34] S. Kim, J. S. Ho, and A. S. Y. Poon, "Wireless Power Transfer to Miniature Implants: Transmitter Optimization," *IEEE Transactions on Antennas and Propagation,* vol. 60, pp. 4838-4845, Oct 2012.

[35] A. S. Y. Poon, S. O'Driscoll, and T. H. Meng, "Optimal Frequency for Wireless Power Transmission Into Dispersive Tissue," *IEEE Transactions on Antennas and Propagation,* vol. 58, pp. 1739-1750, May 2010.

[36] D. Ahn and M. Ghovanloo, "Optimal Design of Wireless Power Transmission Links for Millimeter-Sized Biomedical Implants," *IEEE Transactions on Biomedical Circuits and Systems,* vol. 10, pp. 125-137, Feb 2016.

[37] S. Y. Lee, C. M. Yang, C. H. Hsieh, and J. Q. Fang, "A Wireless Front-End for Implantable Cardiac Micro-Stimulator," *Proceedings of the 2010 IEEE Asia Pacific Conference on Circuit and System (Apccas),* pp. 438-441, 2010.

[38] R. Jegadeesan, Y. X. Guo, R. F. Xue, and M. Je, "An Efficient Wireless Power Link for Neural Implant," *Proceedings of the 2012 IEEE International Symposium on Radio-Frequency Integration Technology (Rfit),* pp. 122-124, 2012.

[39] W. H. Moore, D. P. Holschneider, T. K. Givrad, and J. M. I. Maarek, "Transcutaneous RF-powered implantable minipump driven by a class-E transmitter," *IEEE Transactions on Biomedical Engineering,* vol. 53, pp. 1705-1708, Aug 2006.

[40] E. G. Kilinc, G. Conus, C. Weber, B. Kawkabani, F. Maloberti, and C. Dehollain, "A System for Wireless Power Transfer of Micro-Systems In-Vivo Implantable in Freely Moving Animals," *IEEE Sensors Journal,* vol. 14, pp. 522-531, Feb 2014.

[41] N. Xue, S. H. Cho, S. P. Chang, and J. B. Lee, "Systematic analysis and experiment of inductive coupling and induced voltage for inductively coupled wireless implantable neurostimulator application," *Journal of Micromechanics and Microengineering,* vol. 22, Jul 2012.

[42] E. G. Kilinc, M. A. Ghanad, F. Maloberti, and C. Dehollain, "A Remotely Powered Implantable Biomedical System With Location Detector," *IEEE Transactions on Biomedical Circuits and Systems,* vol. 9, pp. 113-123, Feb 2015.

[43] Q. Xu, H. Wang, Z. L. Gao, Z. H. Mao, J. P. He, and M. G. Sun, "A Novel Mat-Based System for Position-Varying Wireless Power Transfer to Biomedical Implants," *IEEE Transactions on Magnetics,* vol. 49, pp. 4774-4779, Aug 2013.

[44] A. Ma and A. S. Y. Poon, "Midfield Wireless Power Transfer for Bioelectronics," *IEEE Circuits and Systems Magazine,* vol. 15, pp. 54-60, 2015.

[45] R. Puers, R. Carta, and J. Thone, "Wireless power and data transmission strategies for next-generation capsule endoscopes," *Journal of Micromechanics and Microengineering,* vol. 21, May 2011.

[46] G. Monti, P. Arcuti, and L. Tarricone, "Resonant Inductive Link for Remote Powering of Pacemakers," *IEEE Transactions on Microwave Theory and Techniques,* vol. 63, pp. 3814-3822, Nov 2015.

[47] F. J. Huang, C. M. Lee, C. L. Chang, L. K. Chen, T. C. Yo, and C. H. Luo, "Rectenna Application of Miniaturized Implantable Antenna Design for Triple-Band Biotelemetry Communication," *IEEE Transactions on Antennas and Propagation,* vol. 59, pp. 2646-2653, Jul 2011.

[48] E. G. Kilinc, C. Baj-Rossi, S. Ghoreishizadeh, S. Riario, F. Stradolini, C. Boero*, et al.*, "A System for Wireless Power Transfer and Data Communication of Long-Term Bio-Monitoring," *IEEE Sensors Journal,* vol. 15, pp. 6559-6569, Nov 2015.

[49] J. Walk, T. Ussmueller, R. Weigel, and G. Fischer, "Improvements of Wireless Communication and Energy Harvesting Aspects for Implantable Sensor Interfaces by Using the Split Frequencies Concept," *2011 IEEE Radio and Wireless Symposium (Rws),* pp. 406-409, 2011.

[50] S. Amendola, E. Moradi, K. Koski, T. Bjorninen, L. Sydanheimo, L. Ukkonen*, et al.*, "Design and Optimization of mm-Size Implantable and Wearable On-Body Antennas for Biomedical Systems," *2014 8th European Conference on Antennas and Propagation (Eucap),* pp. 519-+, 2014.

[51] K. Kwon, J. Tak, and J. Choi, "Design of a Dual-Band Antenna for Wearable Wireless Body Area Network Repeater Systems," *2013 7th European Conference on Antennas and Propagation (Eucap),* pp. 418-421, 2013.

[52] H. Wang, Z. J. Zhang, Y. Li, and Z. H. Feng, "A Dual-Resonant Shorted Patch Antenna for Wearable Application in 430 MHz Band," *IEEE Transactions on Antennas and Propagation,* vol. 61, pp. 6195-6200, Dec 2013.

[53] S. Agneessens, P. Van Torre, E. Tanghe, G. Vermeeren, W. Joseph, and H. Rogier, "On-Body Wearable Repeater as a Data Link Relay for In-Body Wireless Implants," *IEEE Antennas and Wireless Propagation Letters,* vol. 11, pp. 1714-1717, 2012.

Chapter 2

WPT and Telemetry: Basics and Literature Review

2.1 Introduction

In this chapter, the background theory of communication and Wireless Power Transfer (WPT) with implantable medical devices is introduced. It is presented in three main sections. The first section discusses the safety regulations in terms of radiative and non-radiative fields. These regulations control the level of the radiated power by the antennas. In the second section, the antenna design for medical devices in terms of implantable and wearable antennas is given. Furthermore, frequency bands to be adopted for both communications and WPT are discussed in this section. In the third section, the WPT techniques in the near field and far field regions are given. The rectifier topologies to be utilised for WPT is presented also in this section. Examples of previous works are introduced to support the related sections. At the end of this chapter, a summary and conclusion are given.

2.2 Safety Regulation and Exposure Limits

Health committees for wireless emission and communication in several regions around the world have issued protocols to regulate the exposed power to the human body. These committees include International Commission on Non-Ionizing Radiation Protection (ICNIRP) that is presented in most European countries and many other countries [1], Federal Communications Commission (FCC) which is mainly implemented in the USA [2], Institute of Electrical and Electronics Engineers (IEEE) which is based in the USA as well [3] and SAFETY CODE 6 which is implemented in Canada [4]. Their standards control radiations that are produced

from man-made sources such as medical equipment, radio and television broadcasting, mobile phones, etc. [4]. Materials with finite conductivity including biological tissues can be heated up with RF energy absorption. So set of rules that manage emission in the frequency range from 100 kHz to 300 GHz are considered to control the adverse health effects associated with heating [3]. Limits on power levels and duty cycle factors are proposed according to studies based on preventing of heating human tissues. The upper temperature should not exceed a 1˚C rise in the tissue otherwise it could develop a potential risk to the human health [3, 4]. RF energy absorption rate depends on several parameters including body size, properties of the tissue (dielectric constant and conductivity), frequency bands and orientations of incident fields [4]. Safety regulations can be applied in two different scenarios: controlled and uncontrolled environments. The controlled environment has specific conditions to be satisfied including; RF field intensity should be adequately characterized, and the person under exposure should be conscious to the risk associated with RF energy exposure and he can mitigate their risk. Any situation does not meet these conditions will be considered as uncontrolled environment and the associated rules will be applied [2, 4]. Safety regulations can be classified into two types; the Maximum Permissible Exposures (MPEs) and the Basic Restrictions (BRs). MPEs limit the radiation from external sources with radiative fields such as far field transmitting antennas. BRs control radiations from sources inside or close to the body in terms of Specific Absorption Rate (SAR). These radiations are generated from transmitting antennas mainly in the near field region [3]. MPEs are derived from BRs but with more restrictions and greater safety factors [3].

2.2.1 Exposure Limits of the Radiative Fields

The radiative fields are mainly generated from far fields' antennas that are located far away from the body. MPEs can be classified as mentioned in the previous section into two tiers; the upper tier for controlled environments and lower tier for uncontrolled environments. The regulations for these two environments are described in Tables 2.1 and 2.2 according to the four standards [1-4]. The lower tier is more restricted and has additional safety limits because it considers the public concerns. It

is essential to work within these regulation when far field WPT in use, otherwise the patient will be in a potential risk.

It's worth mentioning that safety limits have been described in terms of 4 factors: the Root Mean Square (RMS) of electric field in (V/m), the RMS of magnetic field in (A/m), the power density in (W/m^2) and the averaging time in minutes (min). The most familiar quantity in the far field region is the power density. This factor is mostly considered for bands above 300 MHz. Since our target frequency at the band 400 MHz and above, the power density limit according to the four standards is considered as shown in Table 2.1 and Table 2.2 [1-4]. The frequency bands that have empty values in Table 2.1 and Table 2.2 are expressed in terms of electric field and magnetic field limits and it can be obtained by referring to the related references.

Table 2.1. MPEs in controlled environments at frequency bands from 0.1 to 300,000 MHz [1-4].

Exposure Limits for Controlled Environments				
Frequency (MHz)	Power Density (W/m^2), f in MHz			
	IEEE STANDARDS	ICNIRP GUIDELINES	FCC REGULATIONS	SAFETY CODE 6 REGULATIONS
0.1–1	9000	-	1000	-
1–1.34	$9000/f^2$	-	1000	-
1.34–10	$9000/f^2$	-	$9000/f^2$	-
10–30	$9,000/f^2$	10	$9000/f^2$	-
30–300	10	10	10	10
300-400	$f/30$	10	$f/30$	$f/30$
400-1,500	***f*/30**	***f*/40**	***f*/30**	***f*/30**
1,500–2,000	$f/30$	$f/40$	50	50
2,000-3,000	$f/30$	50	50	50
3,000-100,000	100	50	50	50
100,000-150,000	100	50	-	50
150,000–300,000	100	50	-	$3.33 \times 10^{-4} f$

Table 2.2. MPEs in uncontrolled environments (public) at frequency bands from 0.1 to 300,000 MHz [1-4].

Exposure Limits for Uncontrolled Environments				
Frequency (MHz)	Power Density (W/m²), f in MHz			
	IEEE STANDARDS	ICNIRP GUIDELINES	FCC REGULATIONS	SAFETY CODE 6 REGULATIONS
0.1–1.34	1000	-	1000	-
1.34–10	$1800/f^2$	-	$1800/f^2$	-
10–30	$1800/f^2$	2	$1800/f^2$	-
30–300	2	2	2	2
300-400	2	2	$f/150$	$f/150$
400-1,500	**$f/200$**	**$f/200$**	**$f/150$**	**$f/150$**
1,500–2,000	$f/200$	$f/200$	10	10
2,000-100,000	10	10	10	10
100,000-150,000	100	10	-	10
150,000–300,000	100	10	-	$6.67 \times 10^{-5} f$

Power density limits in both tables are subjected to an averaging time. The averaging time is the time period of running an experiment with the maximum power density limit before heating the tissue up to 1˚C. Our interest band in this research is 400-2500 MHz. the averaging time of IEEE standard and FCC in this band is 6 minutes and 30 minutes in the controlled and uncontrolled environments respectively. While limits of SAFETY CODE 6 and ICNIRP are averaged over 6 minutes time for both controlled and uncontrolled environments. The power density limit is higher at low frequency bands because the longer wavelength is less absorbed by body tissues. However, antennas size is related to the wavelength so that it is critical to be as small as possible inside the body.

The maximum radiation of far-field transmitting antenna can be calculated according to the power density limit by following the equation (2.1) [2].

$$S = \frac{P_T \, G_T}{4\pi R^2} \tag{2.1}$$

where S is the power density in W/m^2, P_T is the transmit power in watt that feed to the antenna, G_T is the gain of the transmitting antenna and R is the distance in meters

between the transmitting antenna and the destination where the power density is considered at.

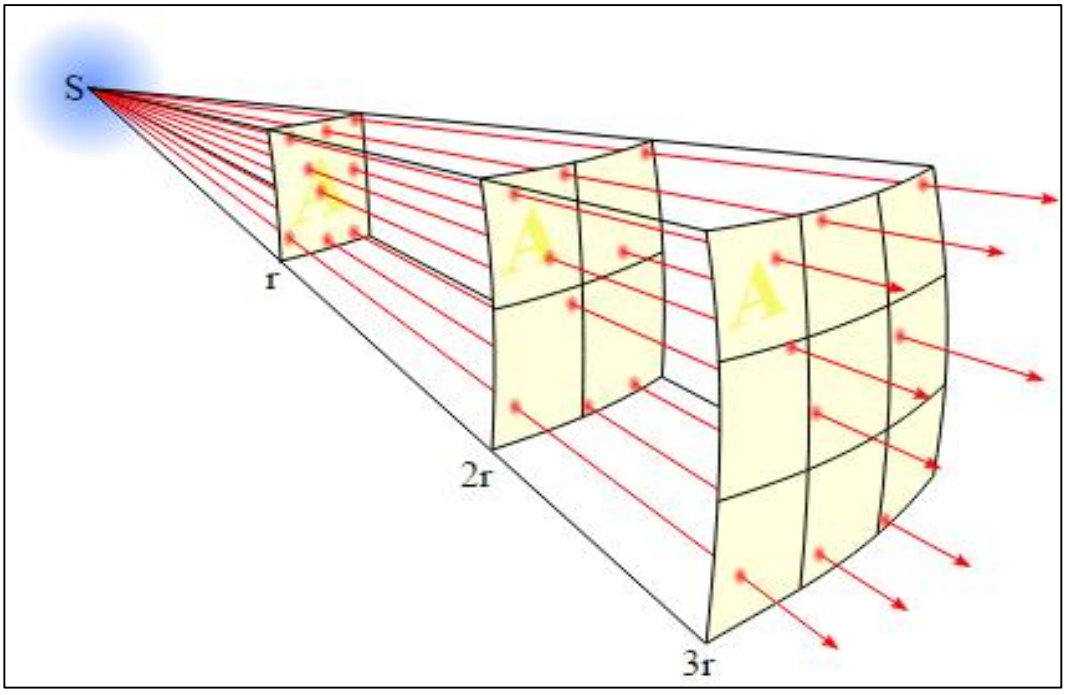

Fig. 2.1. Power density expansion over a sphere area with distance from a source [5].

The transmit power is diminished with distance from the source because it is spread over wave front of a sphere area as shown in Fig. 2.1. From equation (2.1), the level of the transmit power at any band or distance can be calculated based on MREs from Table 2.1 and Table 2.2. Furthermore, the type of the antenna in terms of radiation pattern is worth to be considered so that the reflection from ground or roof surfaces is taken into account with the omnidirectional antennas. This is excluded with directional antennas when the exposure location of interest is in the main beam [2].

2.2.2 Basic Restrictions with Fields Inside the Tissue

This kind of safety regulations restricts the generated fields from sources inside or close to the human body according to the SAR. SAR is mainly measured for the frequencies between 100 kHz and 6 GHz [4, 6]. However, IEEE reduced this upper boundary of frequency for the whole body averaging SAR from 6 GHz to 3 GHz.

Human body tissues are made mainly from cells which contain of water. This water absorbs the fields' energy and convert it into a heat. The heat could damage the cells of the tissue or the organ. SAR is primarily determined by the electric field intensity E (V/m) and the conductivity of the tissue σ (S/m) as in equation (2.2) [3, 4].

$$SAR = \frac{\sigma |E|^2}{\rho} \tag{2.2}$$

where ρ (kg/m^3) is the mass density. Electric field energy is mostly absorbed by the tissue and responsible for heating. The peak spatial average value of SAR is calculated based on the temperature rising in the tissue to be less than 1˚C. These values have been averaged on a specific volume of tissue. FCC and SAFETY CODE 6 have considered the values to be averaged over any 1gram volume of tissue in the shape of a cube [4, 6]. However, ICNIRP has considered averaging over any 10 gram of tissues. IEEE has changed the tissue averaging mass from 1 gram to 10 gram to be consistent with ICNIRP. This is because of a research done by ICNIRP showed that the RF energy is incapable of causing significant rising of local temperature in small tissue volume within the body [3]. A comparison amongst SAR limits between the four standards in controlled and uncontrolled environments is shown in Table 2.3 [1, 3, 4, 6]. From this table, the whole body averaging SAR value is the same for all of committees in both environments. While the partial body averaging SAR is varied between these standards according to the averaging of the tissue mass.

Table 2.3. SAR limits for controlled and uncontrolled environments at frequency bands from 0.1 to 6000 MHz [1, 3, 4, 6].

	Whole-Body SAR		Partial-Body SAR	
	controlled	uncontrolled	controlled	Uncontrolled
FCC	0.4	0.08	8[a]	1.6[a]
Safety Code 6	0.4	0.08	8[a]	1.6[a]
ICNIRP	0.4	0.08	10[b]	2[b]
IEEE	0.4	0.08	10[b]	2[b]
[a] : averaged over any 1 gram of tissue				
[b] : averaged over any 10 gram of tissue				

2.3 Antennas for Medical Devices

The stimulation or monitoring information of implantable medical devices is required to be communicated wirelessly with an external reader. Coils are widely used with implantable devices for such communication. However, the communication range is limited to very short range for few centimetres [7, 8]. To extend the range, Radio Frequency (RF) implantable antennas should be utilized. These antennas are embedded with the medical device. It is able to establish an RF link for implants with external far away readers. The target in this research is to find out the appropriate antennas that can be used for dual purposes: WPT and communications.

The big challenge in designing such RF antennas is the lossy and asymmetric environment of the human body. This body has multiple layers of tissues including muscle, fat, skin, veins, organs and bones. The distribution of these tissues is asymmetrical and the thickness varies at different body parts. As effect of these properties, the prediction of the antenna performance inside human body will be inaccurate so that it needs to be optimised at each position. The resonance frequency of a specific antenna will experience a shifting down with increasing of the medium's permittivity as in equation (2.3).The antenna size is scaled down accordingly.

$$f_r = \frac{f_0}{\sqrt{\varepsilon_e}} \tag{2.3}$$

where f_0 is the resonant frequency in free space (Hz). ε_e is the effective permittivity of the medium [9].

The propagated signal in lossy media including the human tissues undergoes attenuation mainly due to the following reasons:

- A large amount of the signal energy is absorbed by tissue cells. This kind of absorption is referred to as a SAR as explained in the previous section.
- The reflection from the boundary of tissues' layers. The body is constructed of several layers. Each layer has specific properties in terms of conductivity

σ (S/m), permittivity ε (F/m) and permeability μ (H/m). The permittivity ε equals to $\varepsilon_0\varepsilon_r$ where ε_r is the relative permittivity of the tissue and $\varepsilon_0 = 8.854187817 6\times10^{-12}$ F/m is the permittivity of free space. Since human body tissues are nonmagnetic, the permeability of the tissue $\mu = \mu_o = 4\pi\times10^{-7}$ H/m where μ_o is the permeability of free space [9]. These properties decide the intrinsic impedance η (Ω) of the layer at a certain frequency ω (Hz) as:

$$\eta = \sqrt{\frac{j\omega\mu}{\sigma + j\omega\varepsilon}} \tag{2.4}$$

Several layers with variable intrinsic impedances cause a reflection Γ to the propagated signal. The reflection is based on how neighbour layers impedances are mismatched and it is given by

$$\Gamma = \frac{\eta_2 - \eta_1}{\eta_2 + \eta_1} \tag{2.5}$$

the attenuation due to reflections at the tissue layers is given by L_r (dB) as

$$L_r = -20\log_{10}(\Gamma) \tag{2.6}$$

As a result, the electromagnetic signal experiences degradation in the energy that limits the range of communication.

On other hand, the propagated signal towards the implants experiences the same attenuation that causes a reduction in the efficiency of WPT. The challenge is to find a suitable antennas system that can communicate for relatively long range in far field region and it is able to deliver a sufficient amount of energy for direct powering or recharging a battery within safety limits.

2.3.1 Frequency Bands

The choice of the frequency band of operation is an important step in designing and antenna. Frequency bands are directly proportional to the attenuation of the propagated signal. The attenuation α of the signal in a lossy media is given by [10]:

$$\alpha = \omega\sqrt{\mu\varepsilon}\left[\frac{1}{2}\left(\sqrt{1+\left(\frac{\sigma}{\omega\varepsilon}\right)^2}-1\right)\right]^{1/2} \approx \sqrt{\frac{\omega\mu\sigma}{2}} \tag{2.7}$$

Each frequency can penetrate to a specific depth in a lossy media. This depth is described as skin depth δ. The skin depth δ of the propagated signal is inversely proportional to the attenuation factor α as:

$$\delta = \frac{1}{\alpha}$$

$$\delta = \sqrt{\frac{2}{\omega\mu\sigma}} \tag{2.8}$$

From equation (2.8), the skin depth is inversely proportional to the permeability and conductivity of the medium and also with the operating frequency. Since the properties of the medium cannot be changed, the only option to increase δ is to use low operating frequency bands.

Several bands have been used for communication with implantable medical devices. Some of these bands are licensed and others are free licensed. This took range from few kilohertz to few gigahertzes. Frequencies up to 100 MHz are used for near field inductive coupling using coils where antennas will be in a large scale for body usage [11]. As example for that, the Boston Scientific pacemaker which communicates at 43.4 kHz using a coil that is embedded inside the housing of the pacemaker [12]. Other low frequency bands have been used including 1 MHz [13], 8.4 MHz [14] or 13.56 MHz [15]. However, since the communication of these bands is based on the near field inductive coupling, the range will be limited to few centimetres and do not support effectively the RF telemetry of the remote home monitoring. The candidate frequency band to be used for such communication is Medical Implant

Communication Service (MICS) band. This band is relatively low frequency with accepted skin depth. It can be utilised for antenna design where the size is relatively small especially when the antenna is placed inside tissues. This band is licensed for implantable devices communication only so that it is the optimum candidate band for medical antenna design.

2.3.2 Implantable Antennas

Implantable antennas have been designed for RF telemetry at frequencies with a range of sub gigahertz and higher. These antennas are essential to establish a communication link between the implantable biosensor and far away external readers. The properties of these antennas will have direct impact on the implantable device performance. These properties are affected by body tissues. The gain of such antennas is very low with values less than 0 dB since the body loss is taken into consideration [16]. In the same time the radiation efficiency is very low due to the high absorption of the radiated signal energy by the lossy tissues. The received power at certain off body receiver can be calculated following the equation [9]:

$$P_{RX} = P_{TX} + G_{RX} + G_{TX} - L_P - e_P \tag{2.9}$$

Where P_{RX} is the received power by the off body receiver, P_{TX} is the power feed to the implantable antenna, G_{RX} and G_{TX} are the gain of receiving and transmitting antennas after taking into account the antenna impedance mismatch loss, L_P is the path loss and e_P is the polarization mismatch. Page 23 line 3

Implantable antennas have been designed at several high frequency bands such as 2.45 GHz [17-21]. The antenna in [20] was circularly polarized with foot print size of 10 × 10 × 1.27 mm^3 as shown in Fig. 2.2. However, at 2.45 GHz the interference is expected to be high since it is adopted by several applications. The power attenuation at this band is high as well so that it is not the proper choice for communications and WPT.

Another high band implantable antenna was designed around 5 GHz as shown in Fig. 2.3 [22]. This antenna was designed to work with high data rate applications. However, the size is large even with this high band and the signal energy is expected to lose large amount of energy due to the attenuation so that it is unsuitable for WPT. Wide bandwidth bands at high frequencies were also conducted. An antenna that covers the Ultra-Wideband (UWB) (3.1- 10.6 GHz) was proposed in [23] as shown in Fig. 2.4. This implantable antenna was designed for brain neural activity monitoring. Internal and external prototypes on the same design approach were presented so that the receiving (RX) antenna is located outside the head and the internal transmitter (TX1 and TX2) are located under and above skull respectively. This design can be potentially used for both WPT and communications. However, the high frequency bands experience large attenuation.

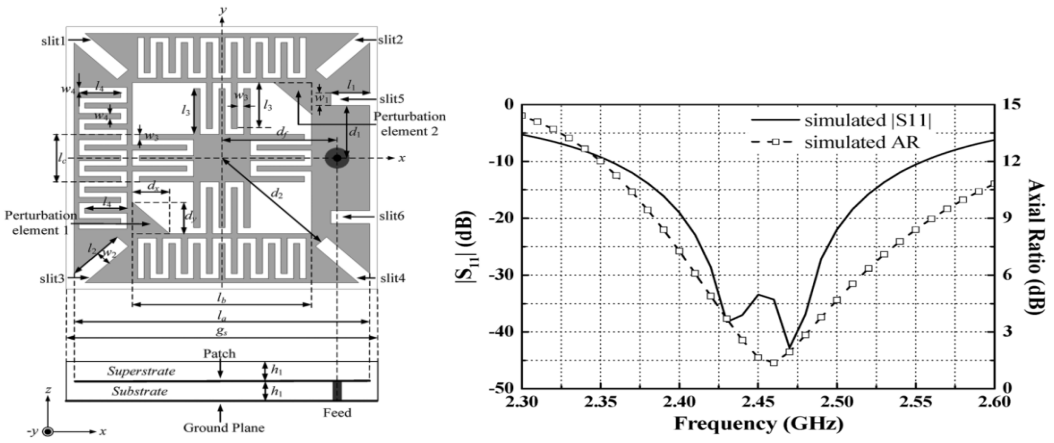

Fig. 2.2. Circularly polarized microstrip patch antenna with the reflection coefficient S_{11} [20].

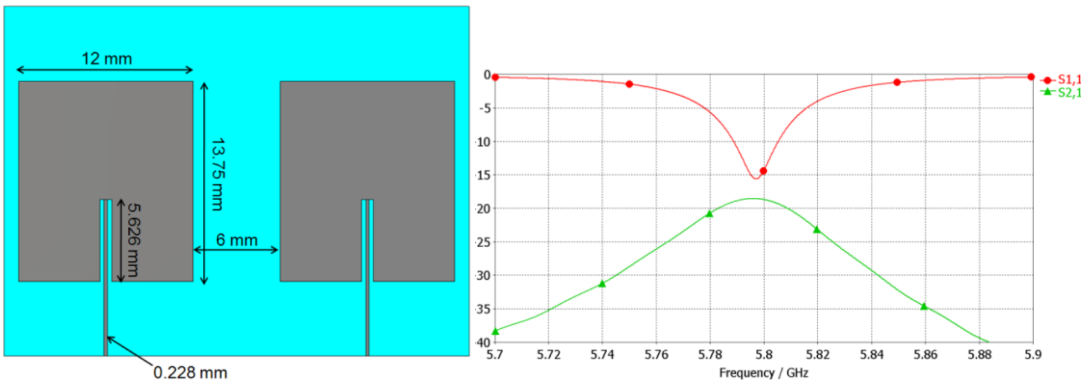

Fig. 2.3. Square Microstrip Antenna Array with S parameters [22].

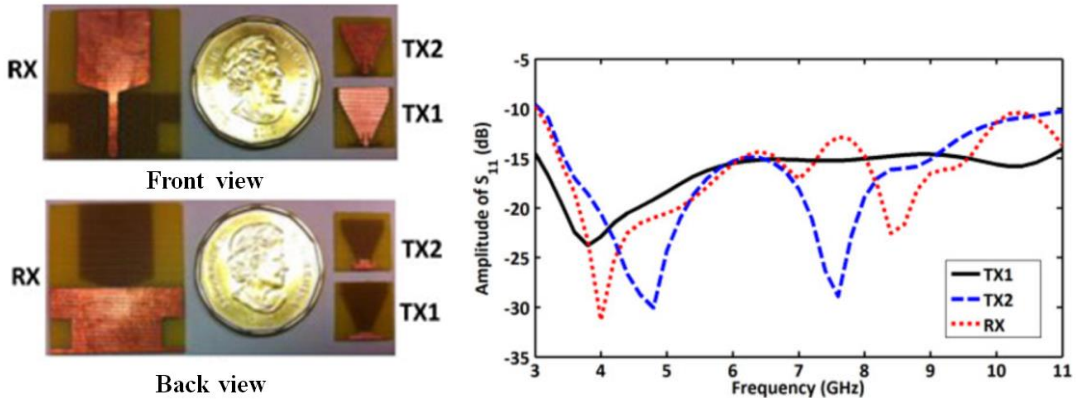

Fig. 2.4. S_{11} and prototype of a microstrip antenna combined with truncated ground plane [23].

In [24], a flexible folded slot dipole antenna was designed at ISM band around 2.45 GHz as shown in Fig. 2.5. However, this antenna has size around 25.9 × 25.9 mm^2 at 2.45 GHz, to be tuned to the MICS band a larger size is expected which is undesirable for medical applications.

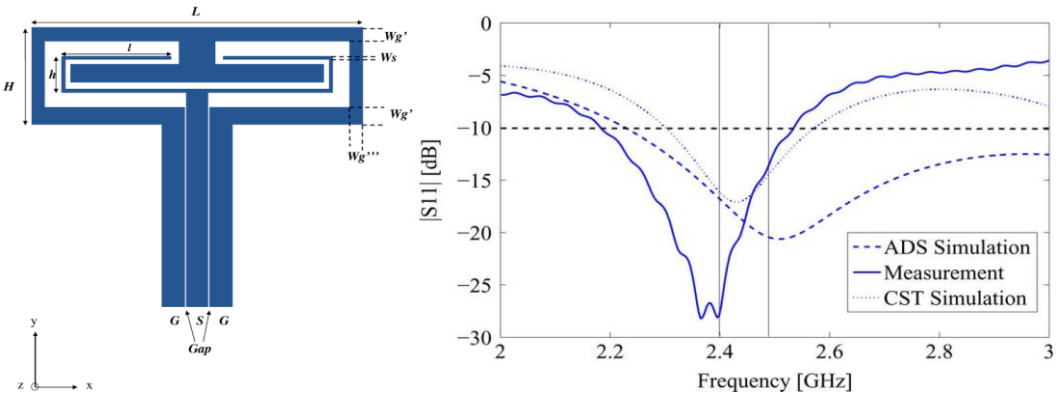

Fig. 2.5. S_{11} and structure of the coplanar waveguide-fed antenna [24]

MICS is the mostly used band for implantable antenna design [16, 24-49]. In [41], a triple band antenna was designed . It covers the MICS band for communication and the Industrial, Scientific and Medical (ISM) bands around 433 MHz and 2.45 GHz for WPT and wake up signal respectively as shown in Fig. 2.6. This antenna design is useful for implantable applications. However, the rigid structure makes it limited for specific implants.

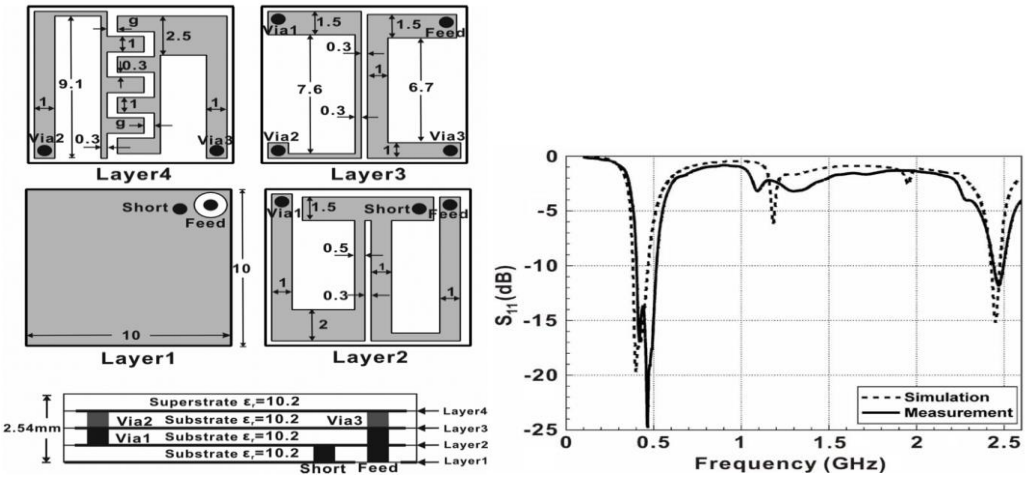

Fig. 2.6. The geometry and S_{11} of a triple-band implantable antenna [41].

In [48], an implanted spiral PIFA antenna was designed to cover MICS band. This antenna is used in a stack structure to be integrated with a rectifier circuit as rectenna for WPT as shown in Fig. 2.6. From the S11 illustration, it looks have a wide bandwidth that cover ISM band around 433 MHz, so that it can be potentially used for WPT at 433 MHz and for communication at MICS band. However, the rigid and high profile of the structure could be undesirable for some medical applications that require conformal antenna.

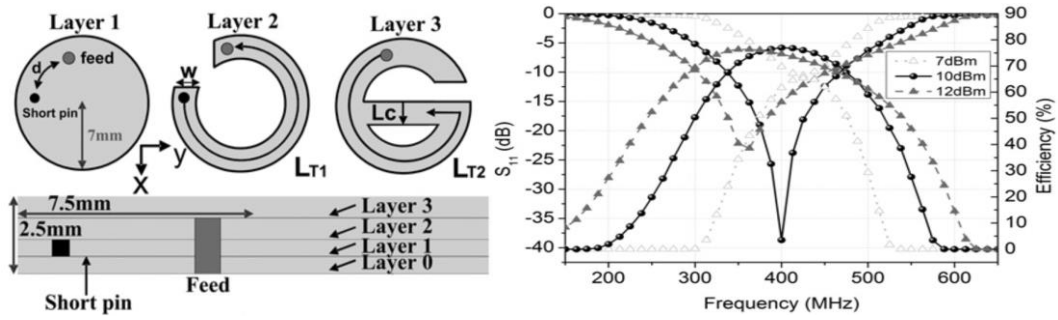

Fig. 2.7. Geometry and S_{11} of the implantable spiral PIFA antenna [49].

Flexible implantable antennas were conducted at MICS band as well. An implantable loop antenna with complementary split ring resonator was design in [30]. This antenna covers wideband range of frequencies including MICS band and ISM bands around 433 MHz and 2.45 GHz as shown in Fig. 2.8. This antenna is conformal to the implants and good candidate for dual purposes as WPT and communications.

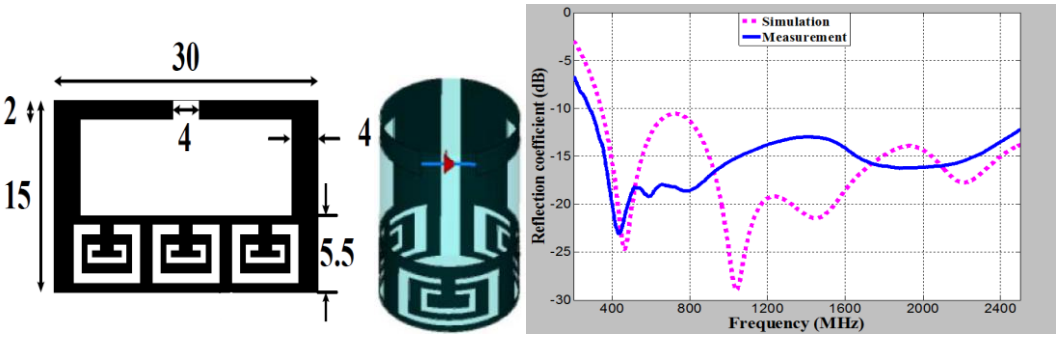

Fig. 2.8. Structure and S_{11} of implantable antenna with complementary split ring resonator [30].

Another flexible antenna was proposed at [16]. This antenna can be used in two scenarios as well; planar and flexible implantation. It covers two bands MICS band and ISM band around 2.45 GHz. It can be used potentially for dual purposes as shown in Fig. 2.9. However, WPT at 2.45 GHz experiences high attenuation as compared with 433 MHz.

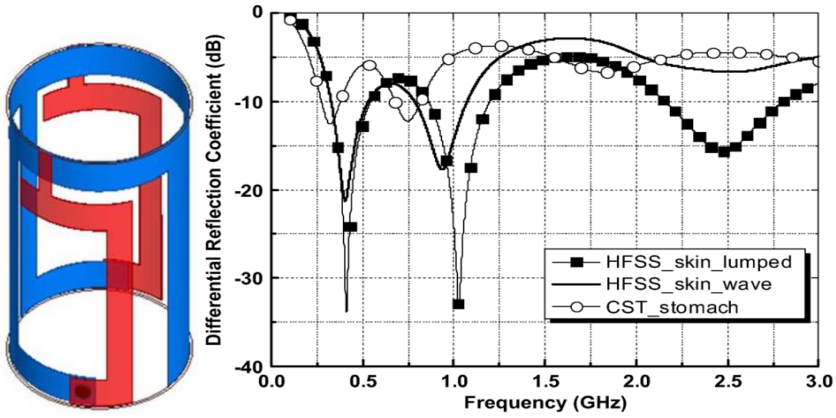

Fig. 2.9. S_{11} and the shape of an implantable flexible antenna at MICS band and 2.45 GHz [16]

Antennas to be used for WPT and for communications should have specific properties that support both targets. For far field communications, the antenna gain, radiation efficiency, bandwidth and directivity are important parameters to reflect the effectiveness of the antenna. With regard to WPT, as large of energy as possible is required to be transferred to the antenna as will be explained in the following section. The safety regulations in terms of SAR and MPEs limit the amount of the transferred

energy. Solutions that improve the antenna performance and overcome the limitation are required.

Limitations of power transfer within the lossy media as discussed before are: the high power absorption by the tissue, the reflection loss at the layer boundary and the skin depth. The reflection at the boundary of the tissue layers will not be investigated in this research. To overcome the skin depth issue, a low frequency band can be adopted. With regard to the power absorption, solutions to overcome this issue will be investigated.

According to equation (2.2), the largest energy absorbed by the tissue from a signal is that associated with the electric field. The power flow density of electromagnetic wave is defined as

$$S = E \times H \qquad (\mathrm{W/m^2}) \tag{2.10}$$

This equation is known as Poynting vector [10]. From equation (2.10), the signal is combined of electric and magnetic fields. The antenna has two main regions; near field and far field as shown in Fig. 2.10.

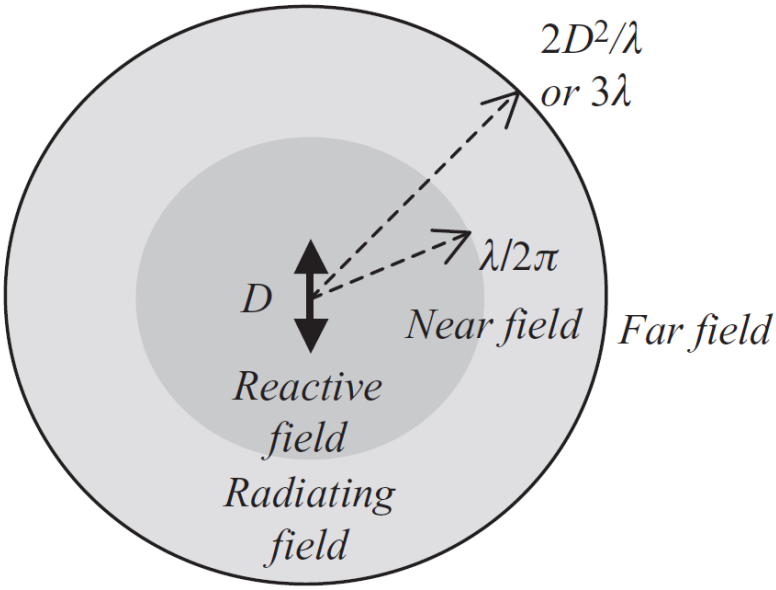

Fig. 2.10 Radiated field regions of an antenna [10].

Near field region can be divided into reactive and radiating regions. In the reactive region which is extended to $\lambda/2\pi$ from the antenna, the reactive fields are the dominant. In the radiating near field region (Fresnel region) the radiative fields are the dominant while there are some reactive fields exist. In the far field region which is started at the boundary 3λ, all fields are radiative. Within the three regions above, the magnetic and electric fields at a certain frequency are degraded with distance from the antenna as shown in Fig. 2.11.

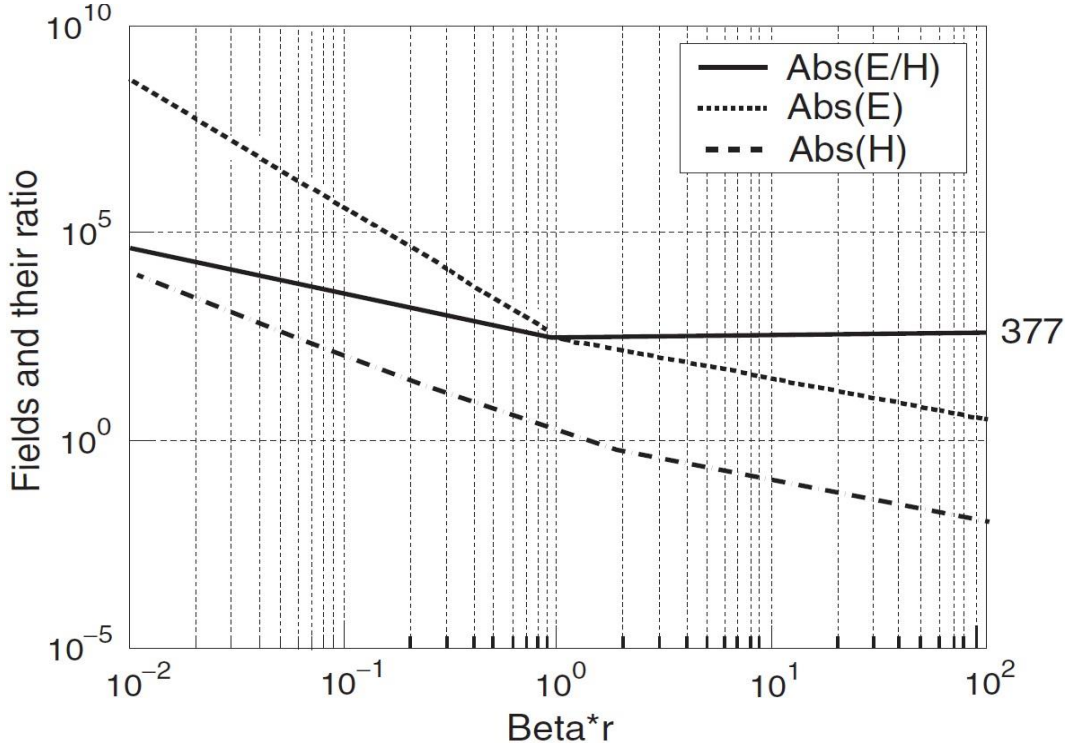

Fig. 2.11 The fields E, H and E/H as a function of β and radius (r) at a fixed frequency [10].

Beta β is known as phase constant or wave number. It is given by equation (2.11) and can be written for free loss case as in equation (2.12) [10].

$$\beta = \omega\sqrt{\mu\varepsilon}\left[\frac{1}{2}\left(\sqrt{1+\left(\frac{\sigma}{\omega\varepsilon}\right)^2}+1\right)\right]^{1/2} \tag{2.11}$$

$$\beta = \omega\sqrt{\mu\varepsilon} \tag{2.12}$$

It can be seen in the reactive near field region that the electric field is decreasing with distance from the antenna faster than the magnetic field. After the reactive region, both magnetic and electric fields are decreasing in the same rate.

Fields propagation inside body tissues have been tested using CST Microwave Studio. An implantable square loop antenna was used in the simulation inside the centre of a cubic tissue body model of dimensions of 240 × 240 × 240 mm^3. The dielectric constant of the tissue is 57.1 and the conductivity is 0.79 S/m. The antenna has dimensions of 13.8 mm × 13.8 mm × 0.04 mm with conductor width of 1.15 mm. It was found that fields are decayed with distance as well as shown in Fig. 2.12.

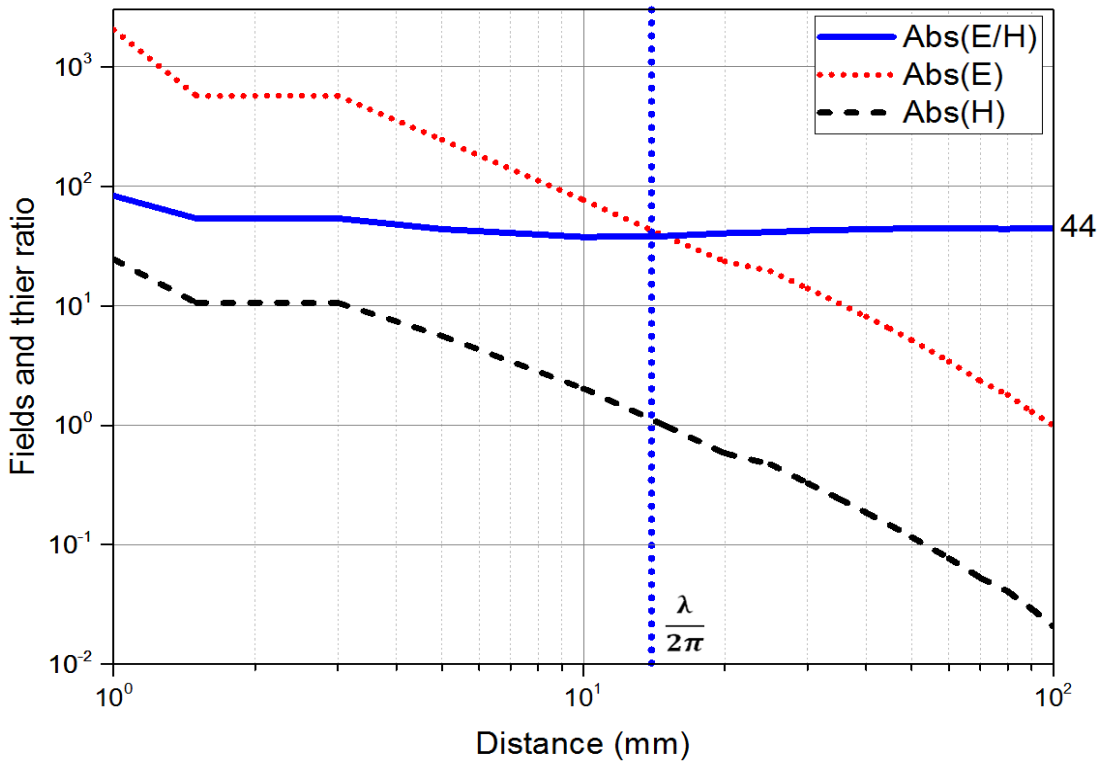

Fig. 2.12. The fields E, H and E/H as a function of distance in tissue at 433 MHz.

The wavelength of 433 MHz in this tissue has been calculated to be 0.0916 m according to the equation:

$$\lambda_r = \frac{\lambda_0}{\sqrt{\varepsilon_r}} \tag{2.13}$$

where λ_0 is the wavelength in free space. If the boundary of the reactive region in free space is applied here, then this region can be extended up to 1.45 cm in the body model. The ratio between electric and magnetic fields has dropped from 377 in free space to 44 in the tissue medium. This gives indication that the energy of the electric field is highly absorbed by the tissue.

It can be concluded from this subsection that:

- The electric field antennas such as PIFA and patch antennas have high electric field in their near field region. This electric field increases the SAR according to equation (2.2).
- Loop antennas have strong magnetic field in their near field region so that the SAR will be less [50].
- Loop antennas are flexible so that it conformal to the shape of the device and hence it can be use with planar or cylindrical implants [30]. Another advantage of using loop antenna is that the high magnetic field in the near field region can improve the WPT.
- According to the skin depth δ, the choice of low frequency bands that is suitable to the radio frequency (RF) antenna design is the optimum solution.
- MICS band is chosen as the candidate for implantable communications. In terms of WPT, the choice of the frequency band with lower signal attenuation is of a high importance. Since the target of this research is to design antennas that can be used dually for WPT and communication, then the optimum frequency choice for WPT is ISM band around 433 MHz. With ISM band around 433 MHz and MICS band, a proper loop antenna with a minimum bandwidth of 30 MHz can cover them.

2.3.3 Wearable Antennas

Antennas that lay on the body for specific application such as Global Positioning System (GPS) tracking, Body Centric Communication (BCC), Wireless Body Area Network (WBAN) and implantable communications are called wearable antennas.

The application in interest in this research is adopting wearable antennas with implantable devices. The usage of wearable antennas has several advantages:

- By using wearable antenna as external reader with implantable devices, the close range of communication will decrease the transmit power level that required to establish the link. This could help in extending the lifespan of the battery.
- The low level of transmit power by the implantable antenna will improve the safety situation by falling down further under the SAR limit.
- The wearable antenna can be potentially used as a repeater between implantable devices and a faraway programmer so that the communication range can be extended further.
- The position of wearable antenna in close proximity to the implants gives a potential advantage of using them for near field WPT.

Wearables can be available in form of rigid or flexible antennas. Several planar and rigid antennas were proposed in the literature to work as wearable antenna for medical purposes. The Vivaldi antenna was proposed in [51], this antenna is intended for in-body communication with implants. It covers Ultra-wideband (UWB) for wireless body area communication from 3 GHz to 10 GHz as shown in Fig. 2.13. The radiation pattern of this antenna is in one direction when it's employed with reflector. Although it is designed with higher frequencies of 3 GHz and above, the size of this antenna is relatively large so that it is not suitable for MICS band.

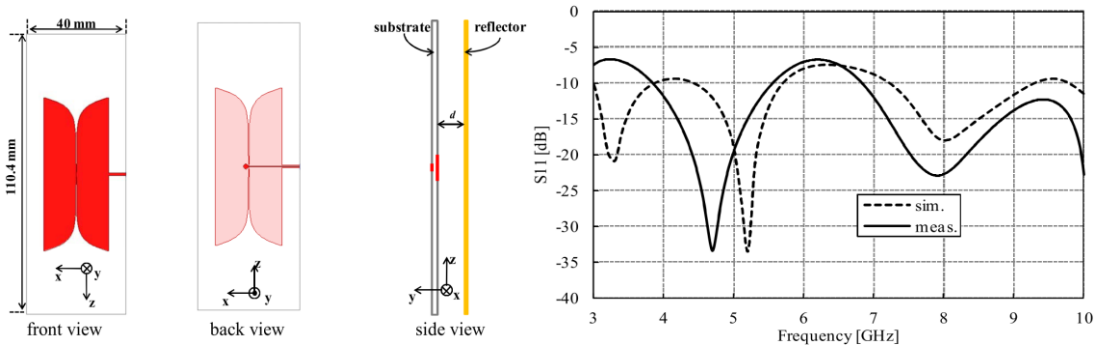

Fig. 2.13. Vivaldi antenna geometry with the measured and simulated S11 [51].

A patch antenna was designed on a textile substrate to work as a repeater with implantable devices as shown in Fig. 2.14. The function of this antenna is to communicate with implants through a patch antenna, then there is a ground plane to isolate this patch from a circuitry and an amplifier that feed a transmit antenna. The transmit antenna is used to communicate with a faraway reader. Both antennas are working at 2.45 GHz [52]. The disadvantage of this antenna is that it is adopting two antennas to function as a repeater which increase the profile significantly. Another drop back is that it is working at 2.45 GHz while most the implantable antennas are working at MICS band.

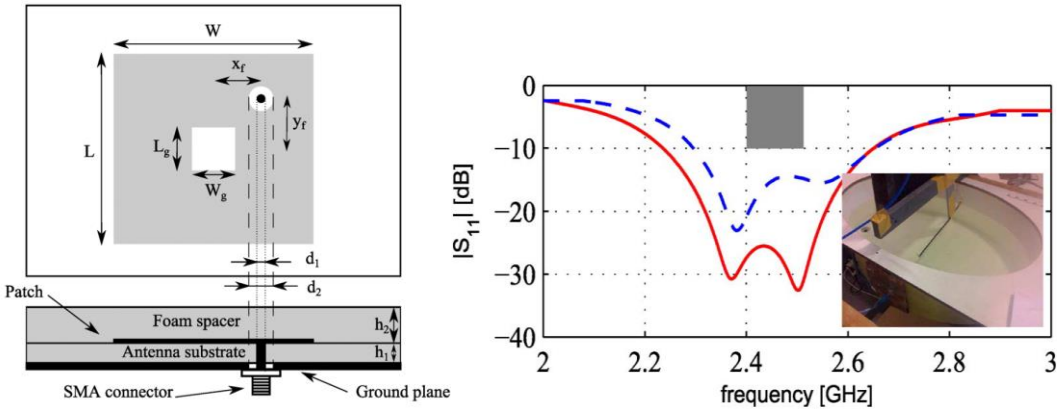

Fig. 2.14. Geometry and S_{11} of on-body wearable repeater patch antenna at 2.45 GHz [52].

Wearable antennas were mostly designed for communication purposes. The dual target of WPT and communications can be achieved by adopting wearable loop antenna. This antenna type can improve WPT due to the high magnetic field in the near field region. It can be used potentially as a repeater for in-body communication with implants and off-body communication with faraway reader. A multiple bands loop antenna can be investigated so that each band can be adopted for a specific function such as MICS band for in-body communication, 433 MHz for WPT and 2.45 GHz for off-body communication.

2.4 Wireless Power Transfer

Wireless Powering of implantable devices is a promising solution since it can avoid the frequent replacement of batteries and then improves the patient life. However, there are several challenges that should be considered carefully so that safe and comfortable solutions can be offered. WPT is classified into two techniques; the far field that based on electromagnetic radiation and near field that based on electromagnetic induction [53]. Both techniques transfer alternative waves and fields. These alternative signals require a rectifier circuit to change it into a Direct Current (DC).

Both techniques can be described in the diagram shown in Fig. 2.15. In this diagram, there are two sides; the internal side which includes the implantable antenna, rectifier circuit and a matching circuit between the antenna and the rectifier for maximum power transfer, the external side has the transmitting antenna that is connected to the reader. The external antenna can be wearable or far field antenna. The combination of the implantable antenna and rectifier including the matching circuit is called as rectenna.

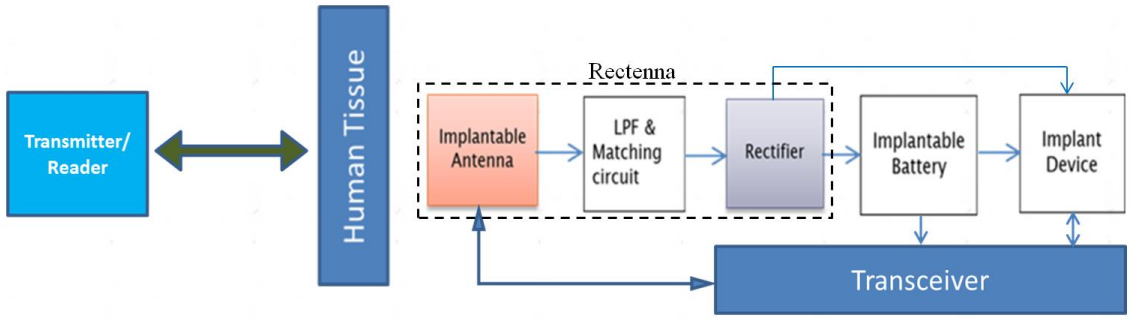

Fig. 2.15. Diagram of wireless power transfer to the human body.

2.4.1 Near Field Coupling

Inductive coupling is an efficient way for WPT. This takes place when a receiving antenna of an implant device is located within the near field region of an external antenna. This kind of coupling is mostly attributed for magnetic fields coupling [54]. However, this technique is subjected to short distance up to $\lambda/2\pi$ (reactive near field

region) from the antenna [10]. Coils have been greatly used for this application. The coil works as an inductor with current flows in the wires, a magnetic field will be generated around the current path producing closed lines of magnetic fields. The magnetic lines cut the secondary coil within the near field region to induce a voltage according to the Faraday law in equation (2.14) [55].

$$V_2 = i\omega\mu_0 \int H_1 . ds \tag{2.14}$$

where V_2 is the induced voltage at a receiver, ω is the operating frequency, H_1 is the magnetic field generated by a source with area of S.

The induced voltage level is based on the magnitude of the magnetic field. Maximum voltage can be generated when all magnetic lines link to the secondary coil. The magnetic field density is limited by exponential field decay with distance d as $1/d^6$ so that coils should be kept in close distance for strong coupling. Furthermore, the small radius of the receiving coil reduces the number of linked magnetic field lines and causes a weakness in the coupling as shown in Fig. 2.16 [54].

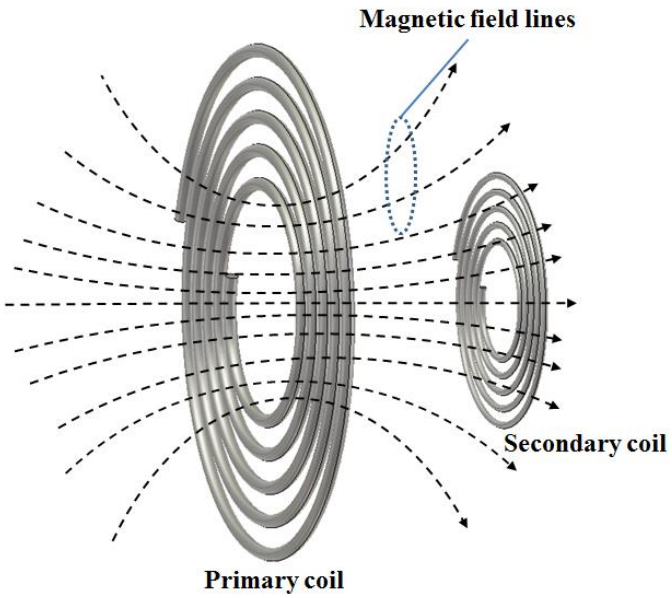

Fig. 2.16. Magnetic field induction between two coils.

From the inductive coupling theory, the coupling coefficient k between two coils is given by

$$k = \frac{M}{\sqrt{L_p L_s}} \tag{2.15}$$

where M is the mutual coupling, L_p and L_s are the self-inductance of the primary and secondary coil antennas respectively.

The magnetic flux density is directly proportional to the inductance of the antenna where the self-inductance is given by

$$L = \frac{\Phi}{I} \tag{2.16}$$

$$\Phi = BS \tag{2.17}$$

$$B = \mu H \tag{2.18}$$

where:

L: Self-inductance in Henry

Φ: Magnetic flux linkage

B: Magnetic flux density

S: area of the antenna

I: current in Ambers

So larger self-inductance results in stronger magnetic field as in equation (2.19)

$$L = \frac{\mu\, H\, S}{I} \tag{2.19}$$

For implantable applications, the transmitting and receiving coils are asymmetrical. To get better WPT, the size of both coils and the separation distance are critical parameters and should be dealt with carefully. For a separation distance of 1 cm and implantable coil with outer diameter of 1 cm, the outer diameter of the external coil should be around 4 cm as shown in Fig. 2.17 [56]. This is one of the limitations of

using coils in medical applications where there is optimum dimension for the coils radii for better WPT further to the short distance of communications.

Antennas can be used for near field coupling. Magnetic antennas such as loops are the most commonly antenna types used for WPT because of the high magnetic field in the near field region [57-64]. Magnetic field has negligible interaction with biological materials [55] and then the antenna is more robust against the detuning by the high permittivity of the body.

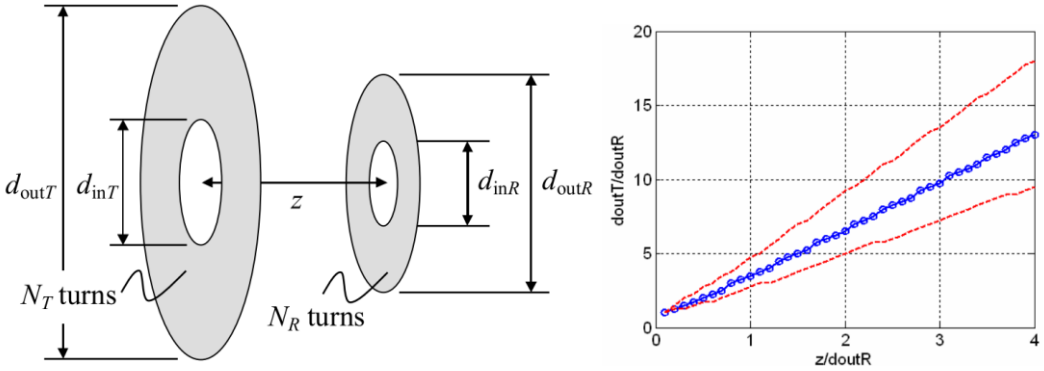

Fig. 2.17. Geometry and optimum coil size for better WPT for two circular planar coils [56]

In literature, a circular loop antenna with 30 mm radius and an implantable cubic loop antenna of 2 mm × 2 mm × 2mm were used for powering Brain Machine Interfacing (BMI) as shown in Fig. 2.18. The coupled antennas are optimized to work at 300 MHz with a separation distance of 11 mm and WPT efficiency of 0.48%. However, for implantable communication purpose, the MICS band should be the target.

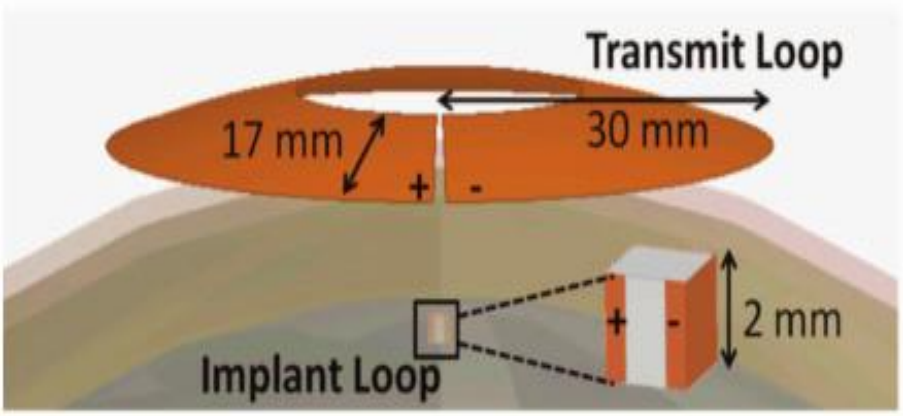

Fig. 2.18. A circular transmit loop antenna coupled to a mm-size cubic loop [64]

A pair of square loop antennas was used for WPT at 915 MHz [63]. The transmitting loop antenna has dimension of 20 mm × 20 mm and the receiving loop antenna has dimension of 2 mm × 2 mm as shown in Fig. 2.19. This pair of loops was tested in Bovine muscle phantom with a separation distance of 15 mm and WPT efficiency of 0.056%. These antennas can be optimised to work at MICS band and 433 MHz for our targets.

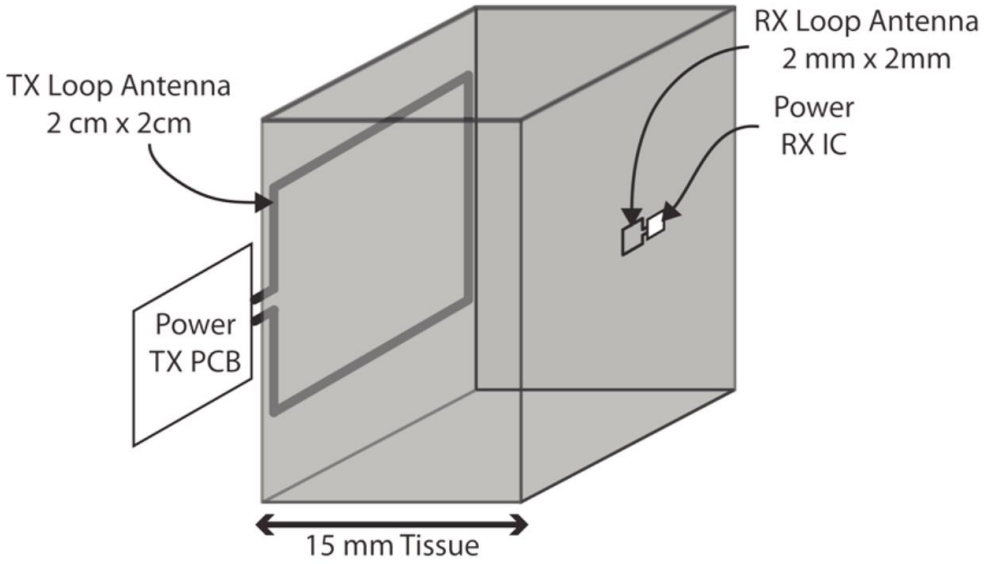

Fig. 2.19. Transmit and receive square loop antennas on a tissue phantom [63].

Implant system that powered by near field coupling requires proper alignment between the antennas as in the coils case to receive sufficient power. The big technical challenge in this application is that the sizes of the transmitting and receiving antennas are significantly different because the implantable antenna size is strictly limited. Furthermore, the patient or the doctor cannot identify the orientation or the location of the implant precisely, this elevate the challenge further. The misalignment between coupled antennas is a big issue and especially in the medical applications [65, 66]. Loop antenna can be optimized for better WPT and communication at the desire bands. It is also important to investigate ways to improve WPT and mitigate the misalignment issue using this type of antennas.

2.4.2 Far Field WPT Technique

Power and information can be transferred using far field electromagnetic radiative waves. Unlike the electromagnetic induction fields, the electromagnetic radiative fields decay with distance d as 1/d as compared with inductive fields that decay in proportional of $1/d^6$ [54]. Medical implants have been investigated with respect to far field powering and communications in [41, 49, 67-70].

This technique can be established using far field external and implantable antennas. The RF link is influenced directly by the efficiency of the antennas. Furthermore, as discussed in section 3, the electromagnetic waves with high frequencies cannot penetrate deeply through the tissue so that lower frequency bands are preferred [54].

From the literature, a triple band antenna was designed to cover the MICS band and the ISM bands around 433 MHz and 2.45 GHz as shown previously in Fig. 2.6. This antenna was connected with a dual diode rectifier type HSMS-286c to be used as a rectenna at 433 MHz for WPT. The overall rectenna dimension is 10mm × 10 mm × 2.74 mm [41]. The drawback of this design is rigid with high profile.

A wireless battery charging system was implemented at 2.4 GHz. This system consists of dual-dipole rectenna in a microstrip decoupling structure and rectifier as shown in Fig. 2.20.

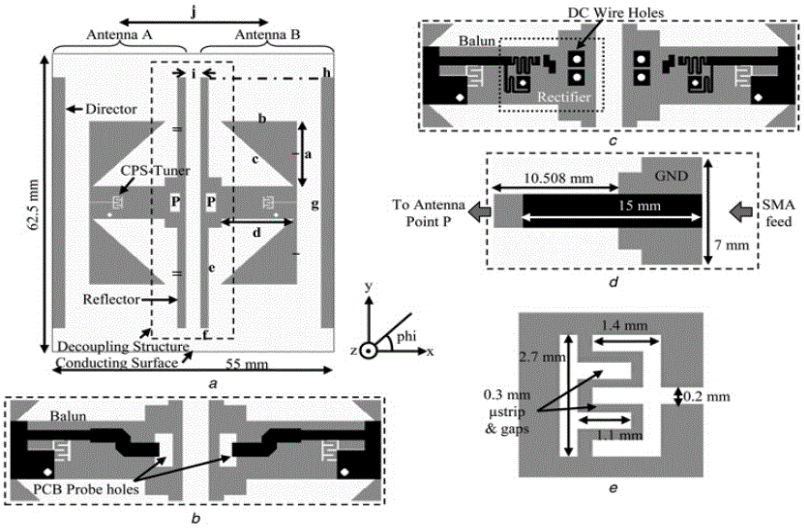

Fig. 2.20. Schematic layout of the decoupled dual dipole and decoupled dual-dipole rectenna [71].

This design was used to charge a standard NiMH battery from 4.8 V to 5.1 V fully charge in 5 hours by a transmitting power of 36 dBm from a distance of 23 centimeters [71]. This design is rigid and large.

A planar inverted-F antenna (PIFA) built on a Roger 3010 substrate was proposed at [49]. It was used with a dual rectifier circuit based on diode type HSMS-2820 as a rectenna working. This design is working at MICS band as shown previously in Fig. 2.7. This work harvested a 2 mA current when 33 dBm of power is transmitted from a distance of 50 cm. The rigid design and high profile are still undesirable for some implantable applications. The loop antenna remains the good candidate for WPT because of the low profile and flexible to be used for planar and cylindrical implants.

2.4.3 Rectifying Circuits

Rectifiers are essential part of WPT. It converts the captured AC signal into DC as shown in Fig. 2.21. The efficiency of such rectifier plays major role in deciding the overall efficiency of the WPT system. A matching impedance circuit is usually adopted between the rectifier and the antenna to provide maximum power transfer. A smoothing capacitor is also added as a shunt to the output of the rectifier in order to provide a steady DC output.

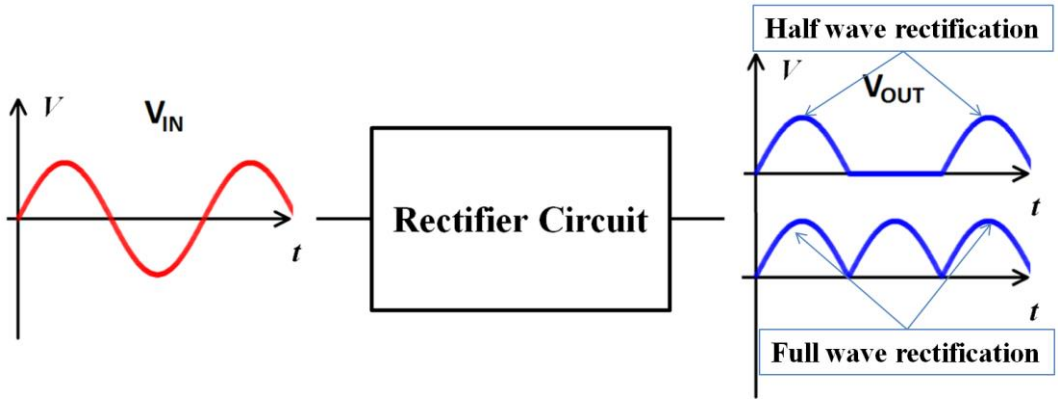

Fig. 2.21. Rectifying operation diagram in terms of half wave and full wave rectification.

Generally, there are three main topologies of rectifier circuit. The first topology is a single diode rectifier [72, 73]. This topology acts as a half wave rectifier. This rectifier has ideally a maximum conversion efficiency of 50 %. However, diodes have some forward voltage to work ON. This rectifier with a Schottky diode type HSMS-2852 has a maximum conversion efficiency of 42% since this diode still has forward threshold voltage of 0.15 V as shown in Fig. 2.22 [73].

The second type is the dual diodes rectifier. This rectifier acts usually as a voltage doubler but still as a half wave rectifier. It can perform with higher conversion efficiency than single diodes [49, 74]. It usually consists of dual diodes D1 and D2, charging capacitor C1 and smoothing capacitor C2 as shown in Fig. 2.23.

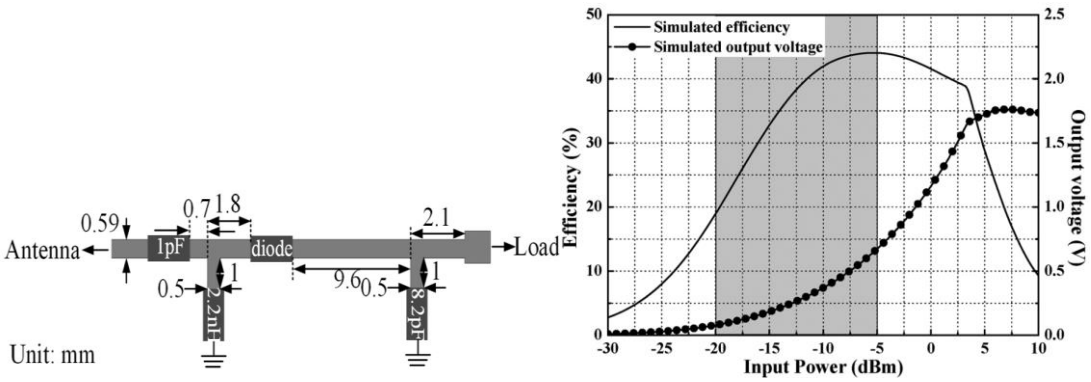

Fig. 2.22. Schematic of a single diode rectifier with the simulated results [73].

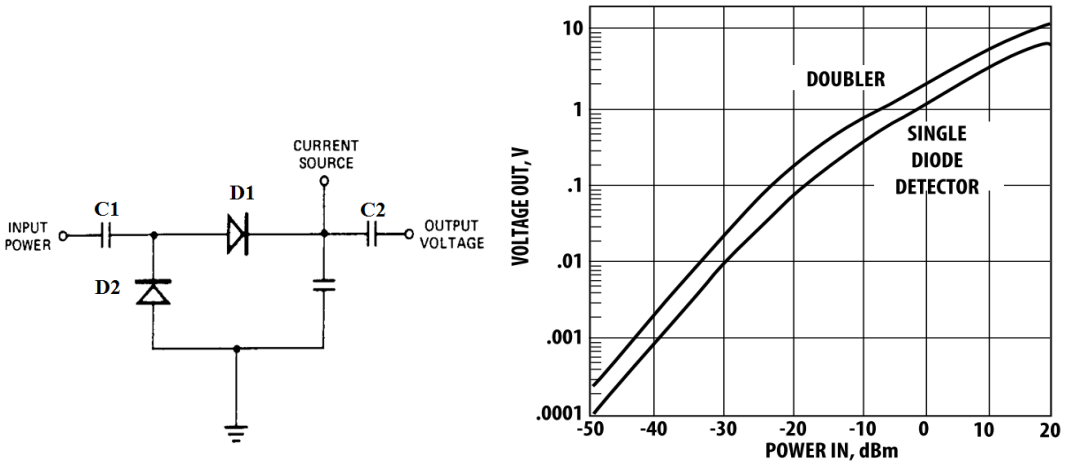

Fig. 2.23. Dual diodes voltage doubler rectifier [73].

During the negative half cycle, D1 will be OFF and D2 ON, then the capacitor C1 will be charged up to ($V_{C1} = V_{in} - V_{D2}$). At the positive cycle, D1 will be ON and D2 OFF, then the output voltage will be the sum of input voltage and the voltage of capacitor C1 excluding the forward voltage of the diodes as follows:

$$V_{C1} = V_{in} - V_{D2} \tag{2.20}$$

$$Vout = Vin + (Vin - V_{D2}) - V_{D1} \tag{2.21}$$

$$Vout = 2\,Vin - V_{D1} - V_{D2} \tag{2.22}$$

This value of $Vout$ is valid at the positive cycle of the input signal but it is zero at the negative cycle. However, by using a smoothing shunt capacitor at the output, the average of the V_{DC} will be approximated to the V_{in} max and can result in conversion efficiency up to around 80%.

The third rectifier is the full wave rectifier which consists of four diodes or two diodes rectifier [43, 75, 76] as shown in Fig. 2.24 and Fig. 2.25. In this type the positive and negative cycles of the input waveform are converted both to a DC.

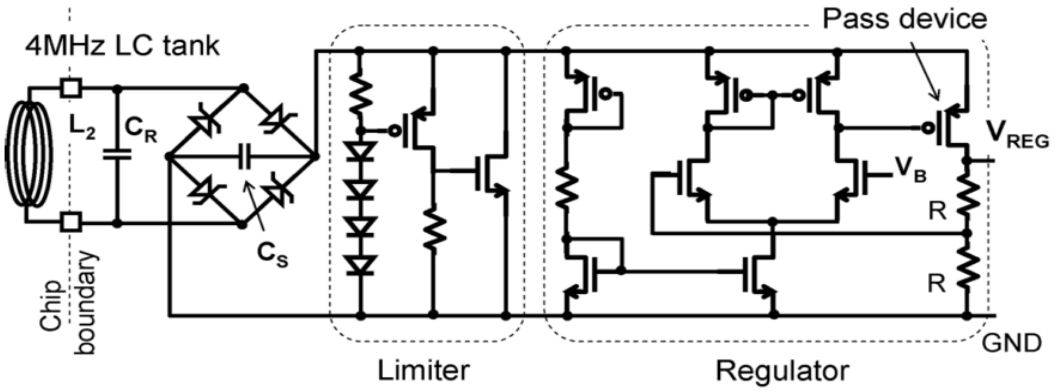

Fig. 2.24. The schematic diagram of the four diodes full wave rectifier [75]

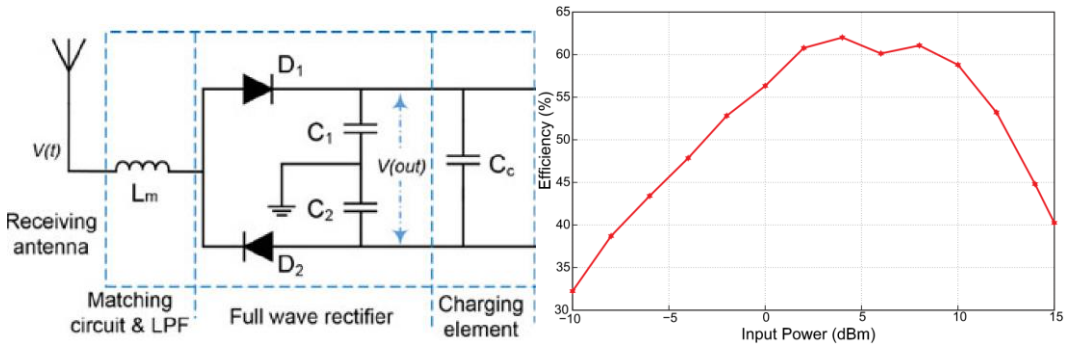

Fig. 2.25. The schematic diagram of the matching circuit and dual diodes full wave rectifier [76]

The conversion efficiency of such rectifier can reach up to 80%. However, at low input power, the output is expected to be low since the four diodes will consume forward voltage which is in total will be $4V_D$. This amount of dissipated voltage is very critical for low power application.

In low power applications including the implantable devices, the input power is expected as low as few milliwatts. With this low power inputs, the power dissipated by the circuit is become very critical. The forward voltage of the diode is one of the major parameters that reduce the output power especially with low power inputs. The choice between these topologies is decided based on the maximum efficiency can be achieved and minimum power dissipated in the circuit. The voltage doubler rectifier is the optimum choice since it requires just 2 diodes and the efficiency can be high as the full wave rectifier.

2.5 Summary and Conclusion

In this chapter, the safety standards in terms of MPEs and SAR limits have been discussed. The electromagnetic signal in terms of attenuation in lossy media and reflection at boundary of the tissue layers was discussed. The implantable and wearable antennas designs in terms of antenna type and frequency in use were introduced for communications and WPT. The WPT in terms of far field and near field were discussed further to the rectifier's designs. As a conclusion, the chapter can be summarized in the following points:

- Low frequency bands but suitable for antenna designs are preferred for lower attenuations. The MICS band is the target since it is relatively low around 400 MHz and licensed for implantable medical communications.
- ISM band around 433 MHz is the optimum band for WPT. It is close to the MICS band so that both can be covered using one antenna.
- High magnetic properties antennas are preferred for better WPT.
- Flexible antennas can be used in planar or cylindrical shapes so that it is conformal for medical devices.
- Wearable antenna is good choice with implantable devices since it is in close proximity to the implants. This has several advantages including it can be utilised in near field WPT and it can be used as a repeater so that the power required for establishing a communication link is reduced.
- Loop antenna is the best target since it is flexible and it has strong magnetic field in the near field region. It can be used with planar and cylindrical implants as implantable antenna. It can be used around all body parts as wearable antenna.
- Voltage doubler rectifier is good candidate since it adopts two diodes in the circuit only and has RF to DC conversion efficiency comparable to that of the full wave rectifier.

References

[1] ICNIRP, "Guidelines for Limiting Exposure to Time-Varying Electric, Magnetic, and Electromagnetic Fields (up to 300 GHz)," *HEALTH PHYSICS,* pp. 494-522, 1998.

[2] L. Jerry, F. Ulcek Robert, and J. Cleveland, "Evaluating Compliance with FCC Guidelines for Human Exposure to Radiofrequency Electromagnetic Fields," *Federal Communications Commission Office of Engineering & Technology,* 1997.

[3] IEEE Std C95.1™-2005, "IEEE Standard for Safety Levels with respect to Human exposure for RF electromagnetic fields 3 kHz to 300 GHz," *IEEE International Committee on Electromagnetic Safety (SCC39),* April 2006.

[4] Safety Code 6, "Limits of Human Exposure to Radiofrequency Electromagnetic Fields in The Frequency Range from 3 kHz to 300 GHz," *Environmental Health Directorate, Health Protection Branch, Health Canada, Canada,* 1999.

[5] Wikipedia, "https://en.wikipedia.org/wiki/Inverse-square law."

[6] D. L. Means and K. W. Chan, "Evaluating Compliance with FCC Guidelines for Human Exposure to Radiofrequency lectromagnetic Fields," *Federal Communications Commission Office of Engineering & Technology,* 2001.

[7] J. A. Von Arx, W. R. Mass, S. T. Mazar, and M. D. Amundson, "Antenna for an implantable medical device," US patent 7,483,752 B2, Jan. 27, 2009..

[8] S. Vajha, K. R. Maile, D. E. Larson, D. A. Chizek, and J. M. Edgell, "Folded antennas for implantable medical devices," US patent 2012/0130451 A1, May 24, 2012.

[9] R. Alrawashdeh, "Implantable antennas for biomedical applications," PhD thesis, University of Liverpool, 2015.

[10] Y. Huang and K. Boyle, *Antennas: from theory to practice*: John Wiley & Sons, 2008.

[11] A. Khaleghi and I. Balasingham, "On selecting the frequency for wireless implant communications," in *Antennas & Propagation Conference (LAPC), 2015 Loughborough*, pp. 1-4, 2015.

[12] A. J. Shah, J. D. Brunett, J. P. Thaker, M. B. Patel, V. V. Liepa, K. Jongnarangsin, *et al.*, "Characteristics of telemetry interference with pacemakers caused by digital media players," *Pacing and Clinical Electrophysiology,* vol. 33, pp. 712-720, 2010.

[13] R. Puers, R. Carta, and J. Thone, "Wireless power and data transmission strategies for next-generation capsule endoscopes," *Journal of Micromechanics and Microengineering,* vol. 21, May 2011.

[14] G. Yilmaz, O. Atasoy, and C. Dehollain, "Wireless Energy and Data Transfer for In-Vivo Epileptic Focus Localization," *IEEE Sensors Journal,* vol. 13, pp. 4172-4179, Nov 2013.

[15] A. Kiourti, "Biomedical telemetry: communication between implanted devices and the external world," *Opticon1826,* vol. 8, pp. 1-7, 2010.

[16] Z. Duan, Y. X. Guo, M. Y. Je, and D. L. Kwong, "Design and in Vitro Test of a Differentially Fed Dual-Band Implantable Antenna Operating at MICS and ISM Bands," *IEEE Transactions on Antennas and Propagation,* vol. 62, pp. 2430-2439, May 2014.

[17] S. A. Kumar and T. Shanmuganantham, "Implantable CPW-fed Z-monopole antennas at 2.45 GHz ISM band for biomedical applications," *International Journal of Microwave and Wireless Technologies,* vol. 7, pp. 529-533, Oct 2015.

[18] S. A. Kumar, J. N. Sankar, D. Dileepan, and T. Shanmuganantham, "Design and Performances of Implantable CPW Fed Apollian Shaped Antenna at 2.45 GHz ISM Band for Biomedical Applications," *Transactions on Electrical and Electronic Materials,* vol. 16, pp. 250-253, Oct 25 2015.

[19] H. Y. Lin, M. Takahashi, K. Saito, and K. Ito, "Design of Miniature Implantable Tag Antenna for Radio-Frequency Identification System at 2.45 GHz and Received Power Analysis," *IEICE Transactions on Communications,* vol. E97b, pp. 129-136, Jan 2014.

[20] C. R. Liu, Y. X. Guo, and S. Q. Xiao, "Capacitively Loaded Circularly Polarized Implantable Patch Antenna for ISM Band Biomedical Applications," *IEEE Transactions on Antennas and Propagation,* vol. 62, pp. 2407-2417, May 2014.

[21] H. Li, Y. X. Guo, and S. Q. Xiao, "Broadband circularly polarised

implantable antenna for biomedical applications," *Electronics Letters,* vol. 52, pp. 504-505, April 2016.

[22] D. G. Rucker, H. R. Khaleel, S. S. Raheem, and H. M. Al-Rizzo, "Microstrip Antenna Arrays for Implantable and Wearable Wireless Applications," *Wireless Mobile Communication and Healthcare,* vol. 55, pp. 135-143, 2011.

[23] H. Bahraini, S. A. Mirbozorgi, L. A. Rusch, and B. Gosselin, "Biological Channel Modeling and Implantable UWB Antenna Design for Neural Recording Systems," *IEEE Transactions on Biomedical Engineering,* vol. 62, pp. 88-98, Jan 2015.

[24] M. L. Scarpello, D. Kurup, H. Rogier, D. Vande Ginste, F. Axisa, J. Vanfleteren*, et al.*, "Design of an Implantable Slot Dipole Conformal Flexible Antenna for Biomedical Applications," *IEEE Transactions on Antennas and Propagation,* vol. 59, pp. 3556-3564, Oct 2011.

[25] R. Alrawashdeh, Y. Huang, and P. Cao, "Flexible meandered loop antenna for implants in MedRadio and ISM bands," *Electronics Letters,* vol. 49, pp. 1515-1516, Nov 21 2013.

[26] J. Ha, K. Kwon, and J. Choi, "Compact zeroth-order resonance antenna for implantable biomedical service applications," *Electronics Letters,* vol. 47, pp. 1267-1269, Nov 10 2011.

[27] C. M. Lee, T. C. Yo, F. J. Huang, and C. H. Luo, "Dual-resonant Pi-shape with double L-strips PIFA for implantable biotelemetry," *Electronics Letters,* vol. 44, pp. 837-U158, Jul 3 2008.

[28] C. M. Lee, T. C. Yo, C. H. Luo, C. H. Tu, and Y. Z. Juang, "Compact broadband stacked implantable antenna for biotelemetry with medical devices," *Electronics Letters,* vol. 43, pp. 660-662, Jun 7 2007.

[29] R. Q. Li and S. Q. Xiao, "Compact slotted semi-circular antenna for implantable medical devices," *Electronics Letters,* vol. 50, pp. 1675-1676, Nov 6 2014.

[30] R. S. Alrawashdeh, Y. Huang, M. Kod, and A. A. Sajak, "A Broadband Flexible Implantable Loop Antenna With Complementary Split Ring Resonators," *IEEE Antennas and Wireless Propagation Letters,* vol. 14, pp. 1506-1509, 2015.

[31] M. Asili, R. Green, S. Seran, and E. Topsakal, "A Small Implantable Antenna

for MedRadio and ISM Bands," *IEEE Antennas and Wireless Propagation Letters,* vol. 11, pp. 1683-1685, 2012.

[32] S. Bakogianni and S. Koulouridis, "An Implantable Planar Dipole Antenna for Wireless MedRadio-Band Biotelemetry Devices," *IEEE Antennas and Wireless Propagation Letters,* vol. 15, pp. 234-237, 2016.

[33] S. Chamaani and A. Akbarpour, "Miniaturized Dual-Band Omnidirectional Antenna for Body Area Network Basestations," *IEEE Antennas and Wireless Propagation Letters,* vol. 14, pp. 1722-1725, 2015.

[34] T. F. Chien, C. M. Cheng, H. C. Yang, J. W. Jiang, and C. H. Luo, "Development of Nonsuperstrate Implantable Low-Profile CPW-Fed Ceramic Antennas," *IEEE Antennas and Wireless Propagation Letters,* vol. 9, pp. 599-602, 2010.

[35] A. Khripkov, W. B. Hong, and K. Pavlov, "Integrated Resonant Structure for Simultaneous Wireless Power Transfer and Data Telemetry," *IEEE Antennas and Wireless Propagation Letters,* vol. 11, pp. 1659-1662, 2012.

[36] A. Kiourti, K. A. Psathas, P. Lelovas, N. Kostomitsopoulos, and K. S. Nikita, "In Vivo Tests of Implantable Antennas in Rats: Antenna Size and Intersubject Considerations," *IEEE Antennas and Wireless Propagation Letters,* vol. 12, pp. 1396-1399, 2013.

[37] H. Li, Y. X. Guo, C. R. Liu, S. Q. Xiao, and L. Li, "A Miniature-Implantable Antenna for MedRadio-Band Biomedical Telemetry," *IEEE Antennas and Wireless Propagation Letters,* vol. 14, pp. 1176-1179, 2015.

[38] C. R. Liu, Y. X. Guo, and S. Q. Xiao, "A Hybrid Patch/Slot Implantable Antenna for Biotelemetry Devices," *IEEE Antennas and Wireless Propagation Letters,* vol. 11, pp. 1646-1649, 2012.

[39] L. J. Xu, Y. X. Guo, and W. Wu, "Dual-Band Implantable Antenna With Open-End Slots on Ground," *IEEE Antennas and Wireless Propagation Letters,* vol. 11, pp. 1564-1567, 2012.

[40] L. J. Xu, Y. X. Guo, and W. Wu, "Miniaturized Dual-Band Antenna for Implantable Wireless Communications," *IEEE Antennas and Wireless Propagation Letters,* vol. 13, pp. 1160-1163, 2014.

[41] F. J. Huang, C. M. Lee, C. L. Chang, L. K. Chen, T. C. Yo, and C. H. Luo, "Rectenna Application of Miniaturized Implantable Antenna Design for

Triple-Band Biotelemetry Communication," *IEEE Transactions on Antennas and Propagation,* vol. 59, pp. 2646-2653, Jul 2011.

[42] A. Kiourti and K. S. Nikita, "Miniature Scalp-Implantable Antennas for Telemetry in the MICS and ISM Bands: Design, Safety Considerations and Link Budget Analysis," *IEEE Transactions on Antennas and Propagation,* vol. 60, pp. 3568-3575, Aug 2012.

[43] C. L. Yang, C. L. Tsai, and S. H. Chen, "Implantable High-Gain Dental Antennas for Minimally Invasive Biomedical Devices," *IEEE Transactions on Antennas and Propagation,* vol. 61, pp. 2380-2387, May 2013.

[44] T. Karacolak, A. Z. Hood, and E. Topsakal, "Design of a dual-band implantable antenna and development of skin mimicking gels for continuous glucose monitoring," *IEEE Transactions on Microwave Theory and Techniques,* vol. 56, pp. 1001-1008, Apr 2008.

[45] G. Monti, P. Arcuti, and L. Tarricone, "Resonant Inductive Link for Remote Powering of Pacemakers," *IEEE Transactions on Microwave Theory and Techniques,* vol. 63, pp. 3814-3822, Nov 2015.

[46] P. Soontornpipit, C. M. Furse, and Y. C. Chung, "Design of implantable microstrip antenna for communication with medical implants," *IEEE Transactions on Microwave Theory and Techniques,* vol. 52, pp. 1944-1951, Aug 2004.

[47] C. K. Wu, T. F. Chien, C. L. Yang, and C. H. Luo, "Design of Novel S-Shaped Quad-Band Antenna for MedRadio/WMTS/ISM Implantable Biotelemetry Applications," *International Journal of Antennas and Propagation,* 2012.

[48] W. C. Liu, S. H. Chen, and C. M. Wu, "Implantable Broadband Circular Stacked Pifa Antenna for Biotelemetry Communication," *Journal of Electromagnetic Waves and Applications,* vol. 22, pp. 1791-1800, 2008.

[49] H. W. Cheng, T. C. Yu, and C. H. Luo, "Direct current driving impedance matching method for rectenna using medical implant communication service band for wireless battery charging," *IET Microwaves Antennas & Propagation,* vol. 7, pp. 277-282, Mar 19 2013.

[50] A. A. Y. Ibraheem and M. Manteghi, "Performance of an implanted electrically coupled loop antenna inside human body," *Progress In*

Electromagnetics Research, vol. 145, pp. 195-202, 2014.

[51] Q. Wang, R. Hahnel, H. Zhang, and D. Plettemeier, "On-body directional antenna design for in-body UWB wireless communication," in *2012 6th European Conference on Antennas and Propagation (EUCAP)*, pp. 1011-1015, 2012.

[52] S. Agneessens, P. Van Torre, E. Tanghe, G. Vermeeren, W. Joseph, and H. Rogier, "On-Body Wearable Repeater as a Data Link Relay for In-Body Wireless Implants," *IEEE Antennas and Wireless Propagation Letters,* vol. 11, pp. 1714-1717, 2012.

[53] A. B. Islam, "Design of wireless power transfer and data telemetry system for biomedical applications," 2011.

[54] P. T. Theilmann, "Wireless power transfer for scaled electronic biomedical implants," 2012.

[55] J. S. Ho, S. Kim, and A. S. Y. Poon, "Midfield Wireless Powering for Implantable Systems," *Proceedings of the IEEE,* vol. 101, pp. 1369-1378, Jun 2013.

[56] R. R. Harrison, "Designing efficient inductive power links for implantable devices," *2007 IEEE International Symposium on Circuits and Systems, Vols 1-11,* pp. 2080-2083, 2007.

[57] D. B. Shire, S. K. Kelly, J. H. Chen, P. Doyle, M. D. Gingerich, S. F. Cogan*, et al.*, "Development and Implantation of a Minimally Invasive Wireless Subretinal Neurostimulator," *IEEE Transactions on Biomedical Engineering,* vol. 56, pp. 2502-2511, Oct 2009.

[58] F.-G. Zeng, S. Rebscher, W. Harrison, X. Sun, and H. Feng, "Cochlear implants: system design, integration, and evaluation," *IEEE reviews in biomedical engineering,* vol. 1, pp. 115-142, 2008.

[59] J. C. Schuder, J. H. Gold, and H. E. Stephenson, "An inductively coupled RF system for the transmission of 1 kW of power through the skin," *IEEE Transactions on Biomedical Engineering,* pp. 265-273, 1971.

[60] J. Schuder, H. Stephenson, and J. Townsend, "High-level electromagnetic energy transfer through a closed chest wall," *Inst. Radio Engrs. Int Conv. Record,* vol. 9, p. 119, 1961.

[61] M. R. Haider, S. K. Islam, S. Mostafa, M. Zhang, and T. Oh, "Low-Power

Low-Voltage Current Readout Circuit for Inductively Powered Implant System," *IEEE Transactions on Biomedical Circuits and Systems,* vol. 4, pp. 205-213, Aug 2010.

[62] S. Kim, R. R. Harrison, and F. Solzbacher, "Influence of System Integration and Packaging on Its Inductive Power Link for an Integrated Wireless Neural Interface," *IEEE Transactions on Biomedical Engineering,* vol. 56, pp. 2927-2936, Dec 2009.

[63] S. O'Driscoll, A. Poon, and T. H. Meng, "A mm-sized implantable power receiver with adaptive link compensation," in *2009 IEEE International Solid-State Circuits Conference-Digest of Technical Papers*, 2009.

[64] S. Amendola, E. Moradi, K. Koski, T. Bjorninen, L. Sydanheimo, L. Ukkonen*, et al.*, "Design and Optimization of mm-Size Implantable and Wearable On-Body Antennas for Biomedical Systems," *2014 8th European Conference on Antennas and Propagation (Eucap),* pp. 519-522, 2014.

[65] M. Q. Nguyen, Z. Hughes, P. Woods, Y. S. Seo, S. Rao, and J. C. Chiao, "Field Distribution Models of Spiral Coil for Misalignment Analysis in Wireless Power Transfer Systems," *IEEE Transactions on Microwave Theory and Techniques,* vol. 62, pp. 920-930, Apr 2014.

[66] Y. H. Liao and X. Q. Yuan, "Compensation topology for flat spiral coil inductive power transfer systems," *IET Power Electronics,* vol. 8, pp. 1893-1901, Oct 2015.

[67] P. D. Bradley, "An ultra low power, high performance medical implant communication system (MICS) transceiver for implantable devices," in *2006 IEEE Biomedical Circuits and Systems Conference*, pp. 158-161, 2006.

[68] Z. N. Chen, G. C. Liu, and T. S. P. See, "Transmission of RF Signals Between MICS Loop Antennas in Free Space and Implanted in the Human Head," *IEEE Transactions on Antennas and Propagation,* vol. 57, pp. 1850-1854, Jun 2009.

[69] A. J. Johansson, "Performance of a radio link between a base station and a medical implant utilising the MICS standard," *Proceedings of the 26th Annual International Conference of the IEEE Engineering in Medicine and Biology Society, Vols 1-7,* vol. 26, pp. 2113-2116, 2004.

[70] A. J. Johansson, "Performance measures of implant antennas," in *2006 First*

European Conference on Antennas and Propagation, pp. 1-4, 2006.

[71] W. S. Yeoh, W. S. T. Rowe, and K. L. Wong, "Decoupled dual-dipole rectennas on a conducting surface at 2.4 GHz for wireless battery charging," *IET Microwaves Antennas & Propagation,* vol. 6, pp. 238-244, Jan 31 2012.

[72] P. Lipinski, "On charging the battery of an Implantable device," *Modern Problems of Radio Engineering, Telecommunications and Computer Science, Proceedings,* pp. 365-366, 2002.

[73] C. R. Liu, Y. X. Guo, H. C. Sun, and S. Q. Xiao, "Design and Safety Considerations of an Implantable Rectenna for Far-Field Wireless Power Transfer," *IEEE Transactions on Antennas and Propagation,* vol. 62, pp. 5798-5806, Nov 2014.

[74] Avago Technologies, "Schottky Diode Voltage Doubler," *Application Note 956-4,* 2010.

[75] P. F. Li and R. Bashirullah, "A wireless power interface for rechargeable battery operated medical implants," *IEEE Transactions on Circuits and Systems Ii-Express Briefs,* vol. 54, pp. 912-916, Oct 2007.

[76] S. M. Asif, J. Hansen, M. S. Khan, S. D. Walden, M. O. Jensen, B. D. Braaten*, et al.*, "Design and In Vivo Test of a Batteryless and Fully Wireless Implantable Asynchronous Pacing System," *IEEE Transactions on Biomedical Engineering,* vol. 63, pp. 1070-1081, May 2016.

Chapter 3

Rectifier Circuits at 433 MHz

3.1 Introduction

In this chapter, rectifiers work at 433 MHz band are designed. The characteristics of the rectifier and the appropriate rectifying diodes within the target band will be investigated. Then battery charging characteristics will be introduced. Three voltage doubler rectifiers are discussed in this chapter. The first rectifier is designed on an FR4 substrate. It is intended to be used in charging experiment of a 50 mA•h implantable battery. The second rectifier is designed on a Roger substrate. It will be used later with one of the designed implantable antenna in far field Wireless Power Transfer (WPT) experiment. The third rectifier is designed on a Roger substrate as well. It is miniaturized to a small size to be used later with one of the implantable antennas in near field WPT experiment. DC combination techniques to increase the output voltages and currents are investigated in this chapter. Conclusions and summary are given at the end of this chapter.

3.1.1 Rectifier Characteristics

The main function of a rectifier is to convert AC to DC. The output DC is used for direct powering of a specific device or for charging a battery. The voltage doubler rectifier was chosen and discussed in Chapter 2. This circuit consists of dual diodes, charging capacitor and DC pass and smoothing capacitor as shown in Fig. 3.1 [1, 2]. It is able to double the input voltage as compared with a single diode rectifier as shown in Fig. 3.2.

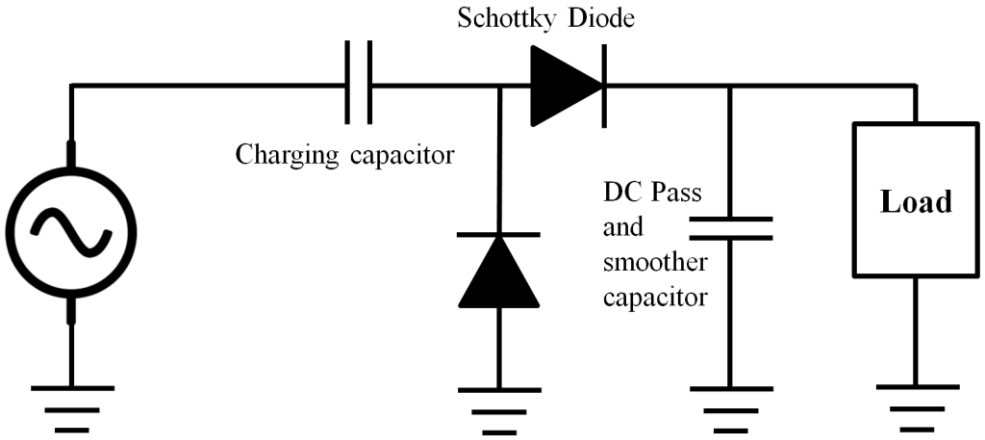

Fig. 3.1. Voltage doubler rectifier circuit diagram.

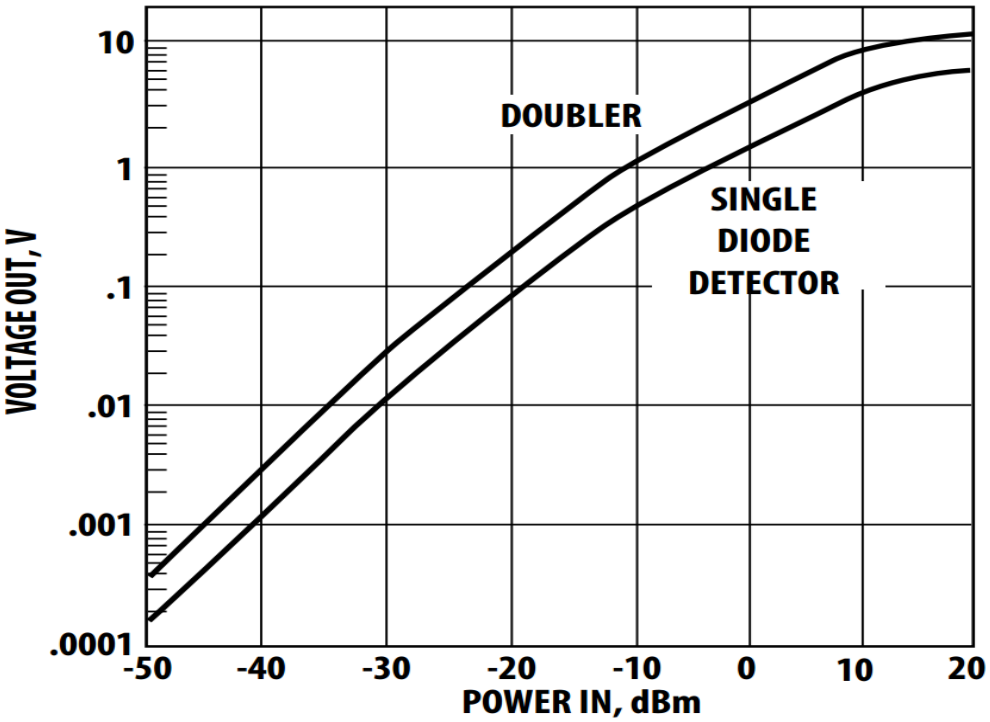

Fig. 3.2. Voltage doubler output at sweep of inputs power as compared with single diode rectifier [2]

A diode is an essential component that has significant impact on the rectifier performance. It cuts the AC in a certain polarity and let it go in another according to the diode direction. Diodes are chosen to a certain application according to several characteristic properties [3]. For RF applications that deal with low power inputs, Schottky diodes are usually used since it has a low forward voltage. However, these

diodes are nonlinear. The resistance junction R_j is variable as shown in Fig. 3.3. where R_S is the series resistance and C_j is the junction capacitance. R_j is given by

$$R_j = \frac{8.33 \times 10^{-5} nT}{I_b + I_s} \tag{3.1}$$

where

I_b = External bias current applied in amperes

I_s = Saturation current (from SPICE parameters)

T = Temperature in K

n = Ideality factor (from SPICE parameters)

I_b is usually zero since Schottky diodes are almost zero biased. The input impedance of these diodes is changing with the input power level and with the frequency. The matching impedance design for wide range of frequencies or variable power levels is challenging.

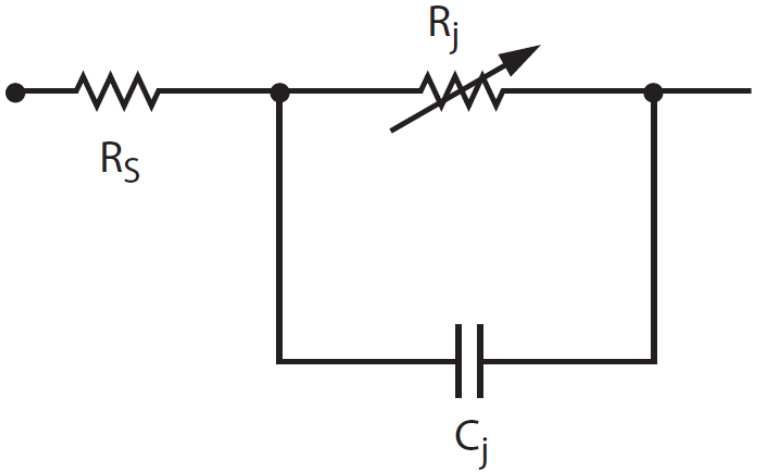

Fig. 3.3. Linear Equivalent Circuit Model of a Diode Chip [3].

The selection of the Schottky diode type is important. Each type is designed to be optimal for specific power levels and frequency bands. The series HSMS-282x from Avago Technologies can be used for power levels greater than -20 dBm with frequency bands below 4 GHz, while HSMS-286x series is applicable for the same power levels but with frequency bands above 4 GHz. Another series HSMS-285x is applicable for frequency bands below 1.5 GHz with power levels less than -20 dBm [4]. Since our application bands is around 400 MHz and the power input levels is

expected to be greater than -20 dBm, the series HSMS 282x is the candidate diode. A comparison amongst the three series in terms of spice parameters is shown in Table 3.1.

Table 3.1. Spice parameters of series HSMS-282x, 286x and 285x [3-5].

Parameter	Units	HSMS-282x	HSMS-286x	HSMS-285x
Maximum Forward Voltage ($\mathbf{V_F}$)	mV	340	350	250
Reverse breakdown voltage ($\mathbf{B_V}$)	V	15	7	3.8
Zero-bias junction capacitance ($\mathbf{C_{J0}}$)	pF	0.7	0.18	0.18
Activation energy ($\mathbf{E_G}$)	eV	0.69	0.69	0.69
Reverse breakdown current ($\mathbf{I_{BV}}$)	A	10^{-4}	10^{-5}	3×10^{-4}
Saturation current ($\mathbf{I_S}$)	A	2.2×10^{-8}	5×10^{-8}	3×10^{-6}
Emission coefficient (**N**)		1.08	1.08	1.06
Series resistance ($\mathbf{R_S}$)	Ω	6	6	25

3.1.2 Battery Charging Characteristics

The rectifier to be developed will be used to charge batteries. Lithium-ion (Li-ion) rechargeable batteries are the best candidate for medical applications. It has no memory effect and a very slow loss of charge when not in use. It can provide large energy density and can be used as a lightweight power source for portable devices [1, 6]. This makes them very attractive for implantable applications. The characteristics of Li-ion batteries can be summarized as follow:

1. Rechargeable, small size, high energy density, low self-discharging rate and long lifespan.

2. The battery charge rate is typically defined as a ratio of C-rate. C is the battery nominal capacity expressed in terms of milliamp hours (mA•h).

3. 1C-rate is defined as the constant charging current that will fully charge a battery in one hour. The recommended current charging rate is 0.5 C.

4. Nominal voltages are 3.6 to 3.7 volts. The maximum charging voltage is 4.2 volts.

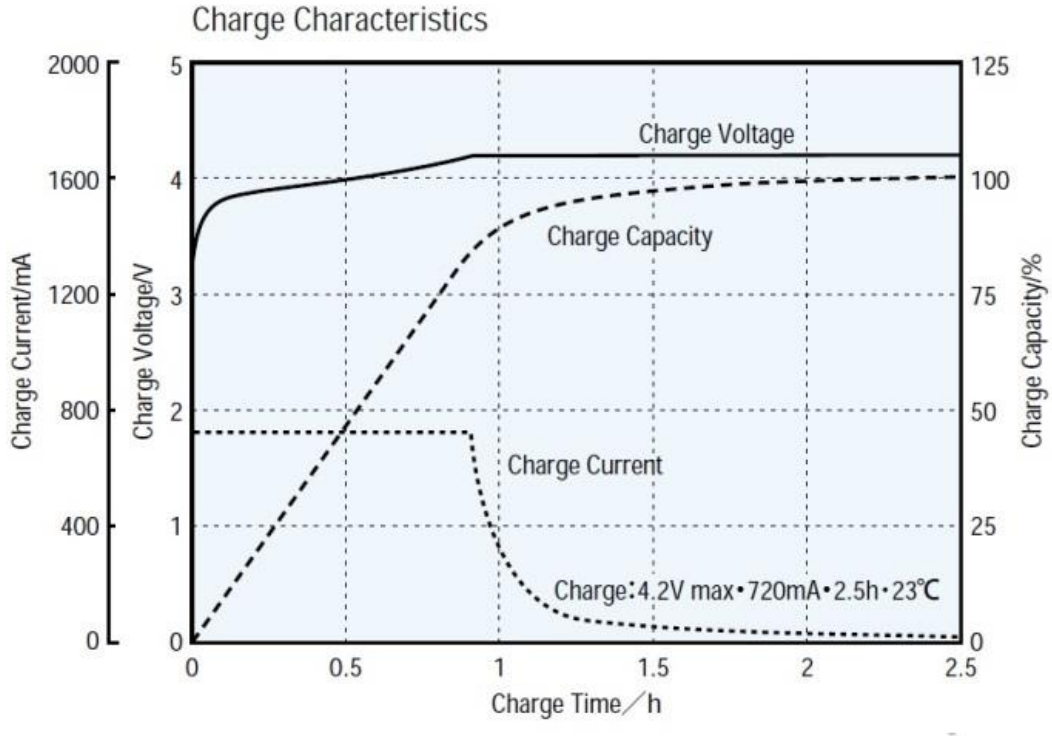

Fig. 3.4. Battery charging process [7].

Charging can be done using two main techniques. The first technique is to charge the battery using a Constant Current (CC) followed by a Constant Voltage (CV) as shown in Fig. 3.4 [1, 8]. This technique is usually used when the rated current is 0.18C or above [9]. The constant current is applied to the battery until the voltage reaches to 4.1 V then the charging voltage is fixed until the charging current reduces to 10% of the initial value as shown in Fig. 3.4. At this level the battery has been charged to the full capacity. The second technique is to charge the battery with a lower rated constant current. With this technique a fixed current is applied to the rechargeable battery until the voltage reaches to 4.1 or 4.2 V. At this stage the battery has reached the full capacity.

3.2 Rectifier Circuit Design on an FR4 Substrate

In this section, the rectifier design on an FR4 substrate will be presented. Then an experiment of charging a realistic implantable battery using this rectifier will be demonstrated.

3.2.1 Rectifier Design

A voltage doubler rectifier circuit based on the Schottky diode type HSMS-2822 was designed. This diode type is a part of the HSMS-282x series with a dual Schottky diodes compact in one chip. This circuit includes two capacitors further to the diodes chip. The first capacitor is located at the input of the rectifier as denoted by C240 in the schematic diagram shown in Fig. 3.5. This capacitor is charged by the input voltage during the negative cycle when the diode D62 is ON and the diode D61 is OFF. Then it discharges during the positive cycle and acts as a bias voltage to the input so that the output will equal to the input voltage added to the voltage of the capacitor. The second capacitor is located at the output of the rectifier and is denoted by C239 in the schematic diagram. This capacitor is used to smooth the output DC. Since almost devices are optimized to 50 Ω impedance, the input impedance of the rectifier circuit accordingly should be optimized to 50 Ω. The diode is nonlinear device; the input impedance of the diode is changing with variable input power, so that a broadband matching with variable inputs is challenge. Since this rectifier is intended for charging an implantable battery, an input power of 10 mW was used during the rectifier circuit design. Microstrip transmission lines have been added to the circuit to join circuit elements to each other.

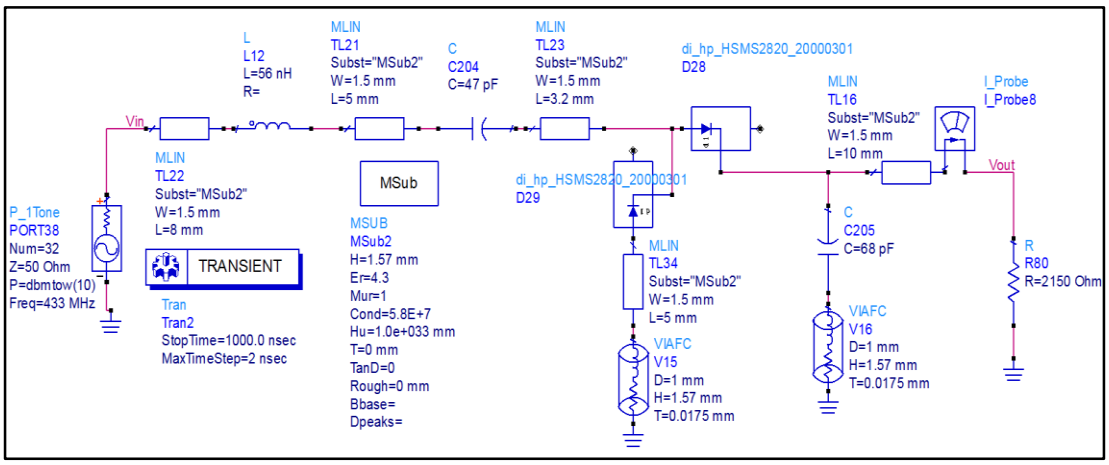

Fig. 3.5. The schematic diagram of rectifier circuit on an FR4 substrate.

It is important to consider the layout of the circuit which includes the substrate type, the size of transmission lines and the size and number of vias to be drilled to the ground plane. Initial values to the capacitors are used. Then the input impedance of

the rectifier circuit is calculated using The Advanced Design System (ADS) software. This step is very important in order to design a matching circuit between the rectifier and the source. Since this circuit showed impedance of capacitive reactance and resistance near to 50 Ω, an inductor was used at the input of the rectifier to tune the reactance components. The overall components have been tuned until getting maximum output voltage on the load. With the power input of 10 mW, the output voltage and current on a load value of 2.15 kΩ were around 4.1 V and 1.9 mA respectively as shown in Fig. 3.6. This output is equivalent to 79% AC to DC conversion efficiency. This circuit was fabricated then on an FR4 substrate with a relative dielectric constant of 4.3 and a thickness of 1.57 mm as shown in Fig. 3.7.

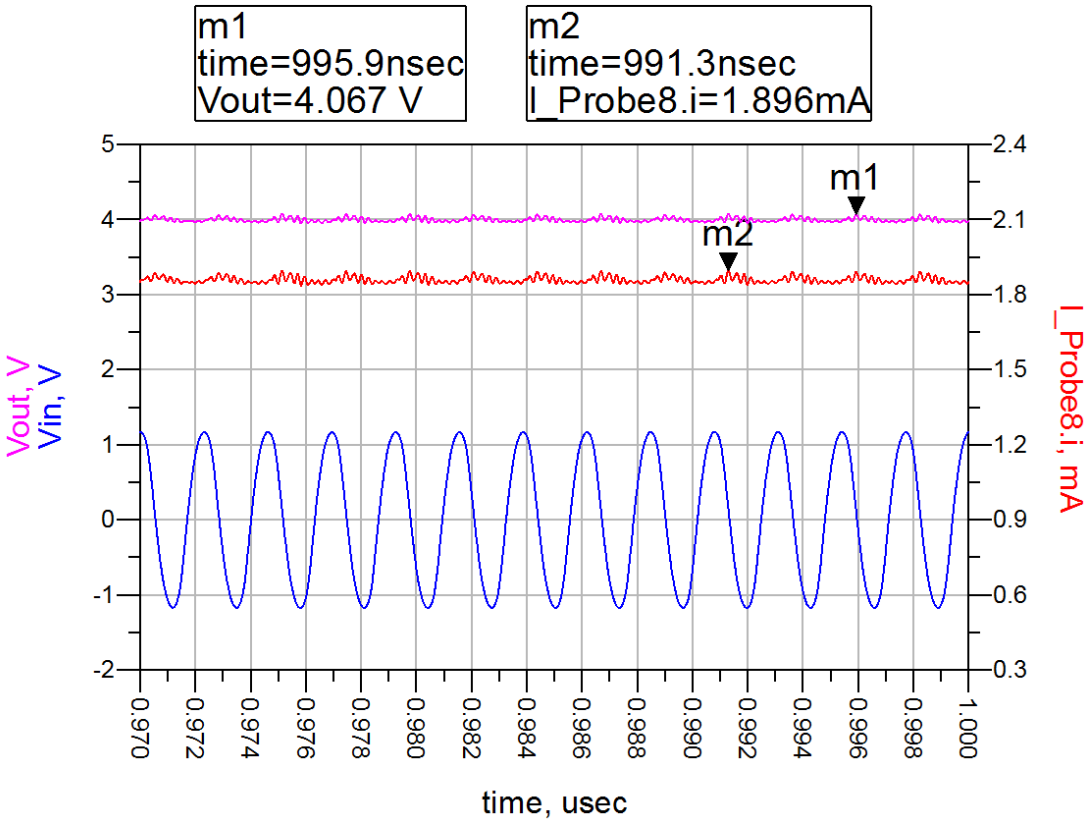

Fig. 3.6. The simulation results of the voltage doubler rectifier on an FR4 substrate.

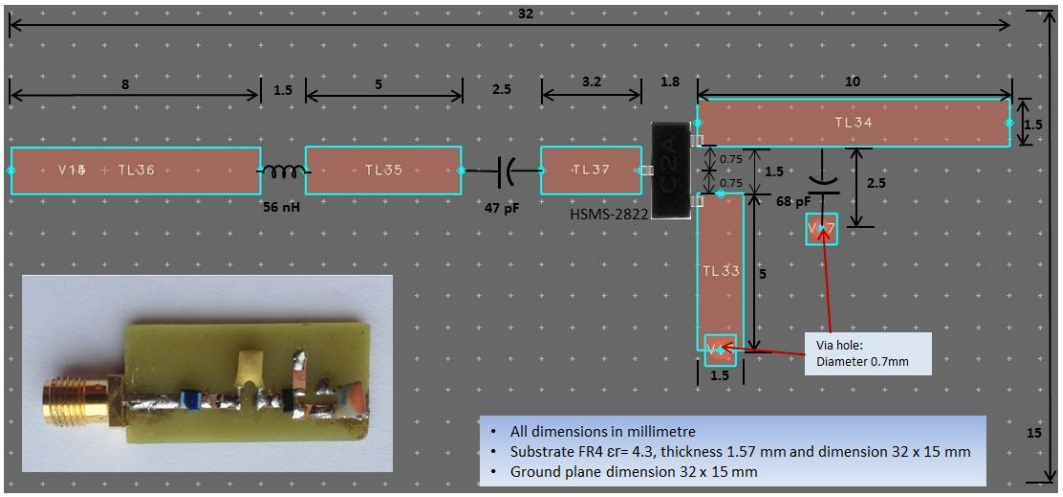

Fig. 3.7. The layout and fabrication of the rectifier circuit on an FR4 substrate.

The measurement setup of the fabricated circuit is shown at Fig. 3.8. This setup includes a signal generator to feed the rectifier with RF signal at 433 MHz and a voltmeter to measure the output voltage on the load.

Fig. 3.8. The measurement setup of the rectifier circuit test experiment with a sweep of power input at 433 MHz.

The measured voltage on the load was 3.7 V and 4.11 V at an input power of 10 dBm and 11 dBm respectively. This is equivalent to an RF to DC conversion efficiency of 62.5%. This efficiency is low as compared with the simulated one. The reason is due to use approximated values to the components and the fabrication precision. It was found by tuning the input frequency during the experiment that the circuit can produce more than 70% conversion efficiency at 405 MHz. this means that the circuit was not matched perfectly to the source at 433 MHz.

3.2.2 Battery Charging Experiment

To demonstrate the validity of the designed rectifier circuit for recharging batteries, an implantable battery was sampled from Eaglepicher Company. The capacity of this battery is 50 mA•h and it has size as shown in Fig. 3.9.

A charging current of 2 mA is generated using the proposed rectifier to charge the 50 mA•h battery. This represents 4% of the capacity. This level of current doesn't follow the charging diagram in Fig. 3.4. The rectifier can charge the battery with relatively constant current of 2 mA. When the voltage of the battery reaches 4.1 V, it means the battery is fully charged.

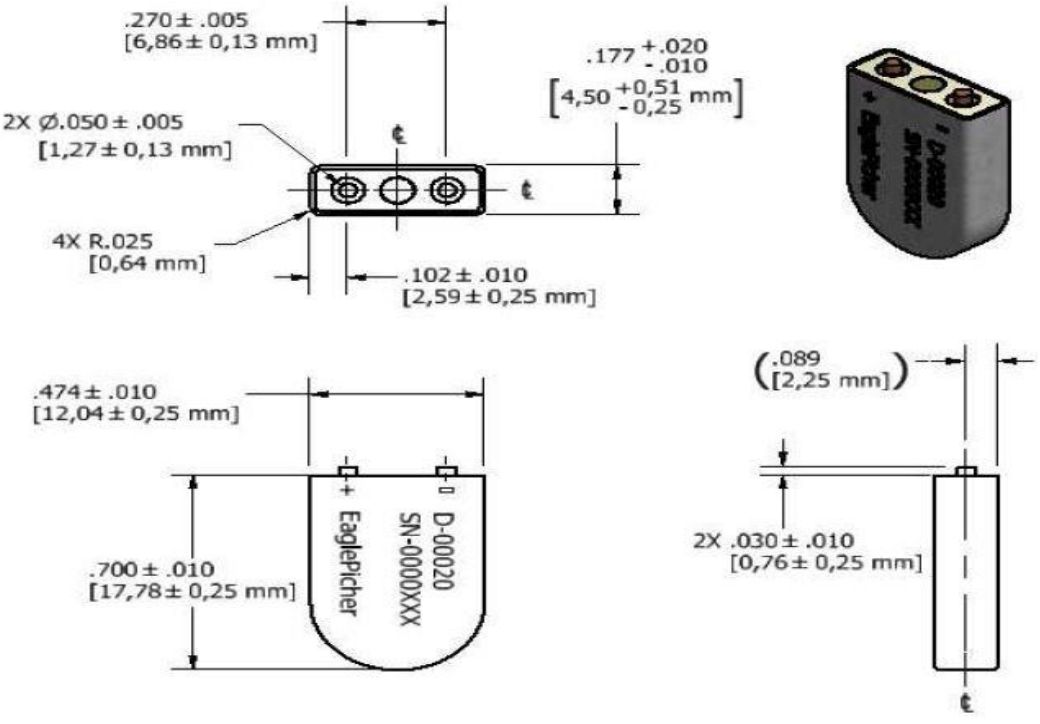

Fig. 3.9. Dimensions of the contego 50 mA•h implantable battery.

The soldering of the battery electrodes was a bit challenging. The posts of the battery are made of Molybdenum material which does not accept direct soldering. The problem was solved by using laser welding of Nickel or stainless steel wire or ribbon to be joined to the battery posts. The laser welding was done in a jewelry shop in Liverpool.

The Nickel wire was failed to be firmly joined to the battery using laser welding. The second option was to use a steel wire. However, the steel wire doesn't accept direct soldering. Some techniques to make a steel wire accepting solder can be utilized such as scratch the wire by a blade (It is not effective), use special solder has some flux inside such as multicore ARAX 96s (its expensive), and the third solution is to use phosphoric acid flux with solder. Phosphoric Acid Flux shown in Fig. 3.10 can help in preparing surfaces for soldering.

The steel wire should be pre-tinned to a solder from one side while the other side should be connected to the battery through laser welding. The electrode posts of the battery are finally attached to the steel wire and the charging experiment was done. The experiment setup includes a signal generator to supply 10 mW power at 433 MHz, multimeters to monitor the charging voltage and current simultaneously, and the battery and rectifier under test as shown in Fig. 3.11.

Fig. 3.10. Phosphoric Acid Flux that used to prepare the surface of the steel wire for soldering.

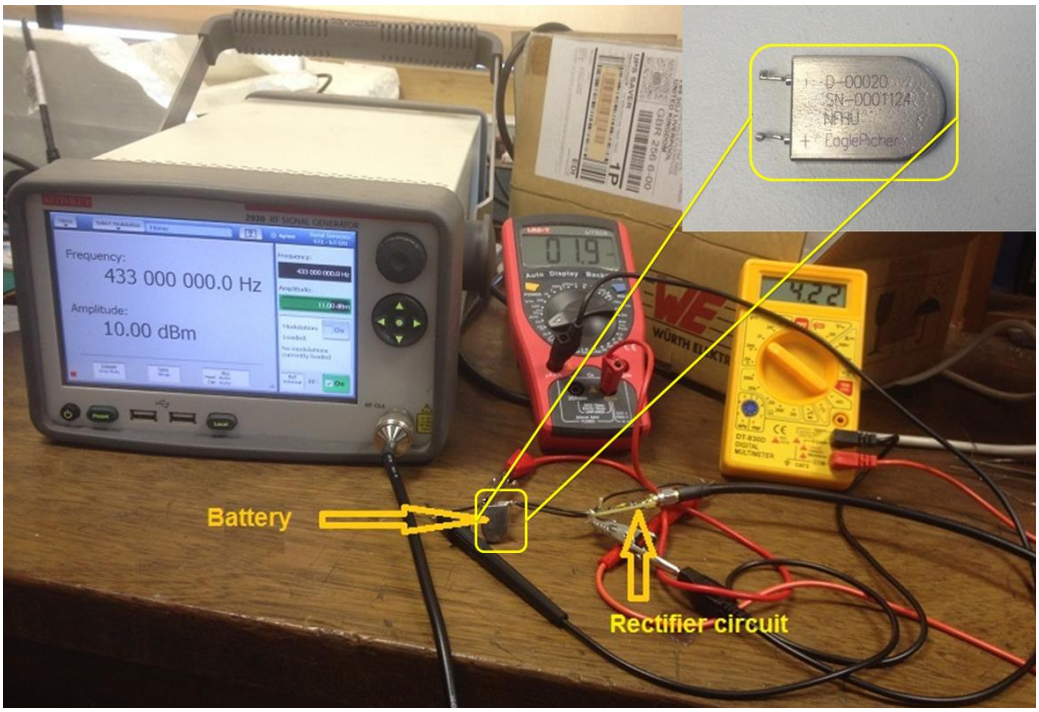

Fig. 3.11. Charging experiment setup of 50 mA•h implantable battery using the fabricated rectifier on an FR4 substrate.

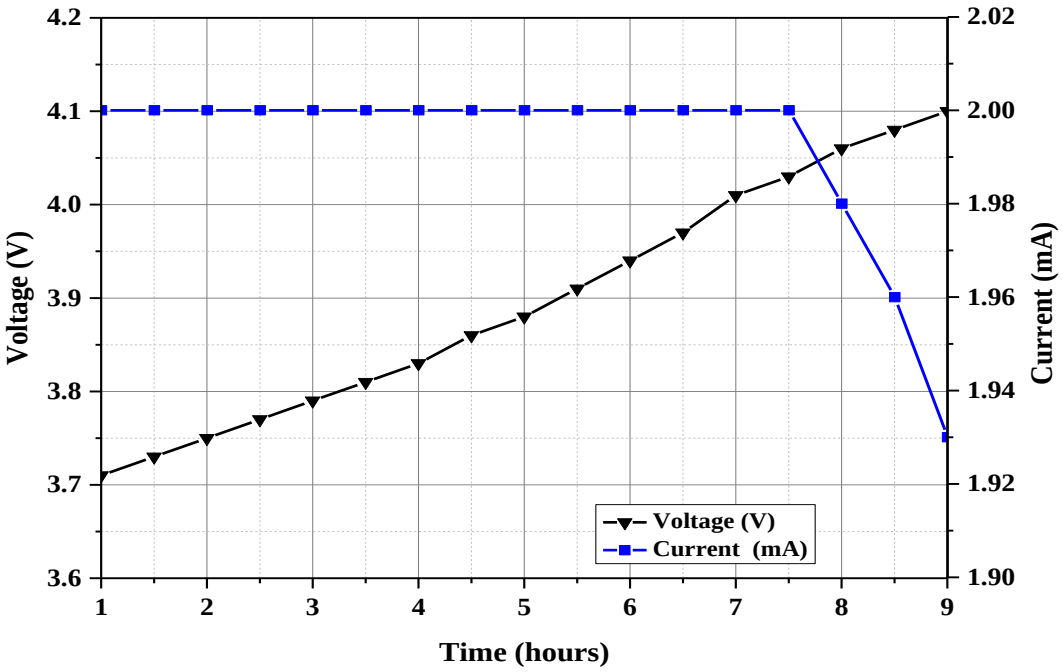

Fig. 3.12. Charging experiment process of the 50 mA•h implantable battery using the fabricated rectifier on an FR4 substrate.

The battery was successfully charged using our system from 50% state of charge to 100% of the capacity within 9 hours as shown in Fig. 3.12. as a conclusions of this experiment:

- The charging process of Lithium ion batteries is nonlinear because it is based on chemical reactions.
- The capacity in terms of energy is the current capacity times the nominal voltage. The energy capacity of the battery in this experiment can be calculated as 50 mA•h × 3.6 V = 180 mW•h.
- With charging power of 10 mW for 9 hours, a 90 mW•h of energy has been applied which is equivalent to 50% of the battery capacity.
- Batteries with smaller capacities can be recharged quicker with charging power of 10 mW or current of 2 mA.

3.3 Rectifier Circuit Design on a Roger Substrate

The FR4 substrate is widely used but it has a higher dissipation factor with higher frequency bands [10]. A new voltage doubler rectifier was designed on a Roger 5880 substrate with a relative dielectric constant of 2.2 and thickness of 1.57 mm. The dual Schottky diodes type HSMS-2822 by Avago technologies was utilized in designing the circuit. The rectifier circuit was optimized with realistic components that can be available on the shelf. The overall schematic diagram of the rectifier circuit is shown in Fig. 3.13. Since the transmission lines contribute with some impedance, the overall components including the charging capacitor C288 and smoothing capacitor C287 were optimized with the size of the transmission lines. As in the previous rectifier, other circuit parts like vias are considered before turning to the circuit. This rectifier was especially designed to be matched with an implantable antenna that will be discussed in the following chapter.

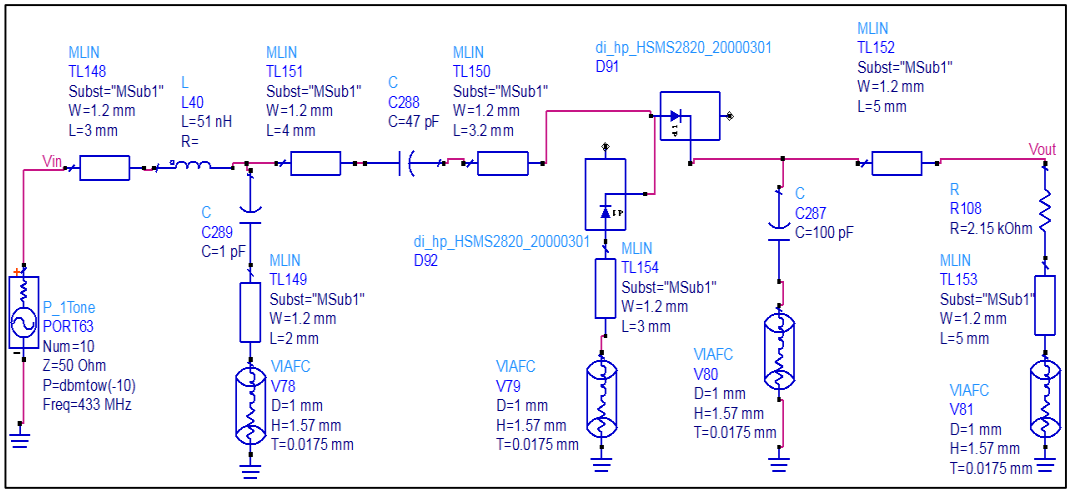

Fig. 3.13. Schematic diagram of the rectifier on a Roger substrate.

The input impedance of the rectifier is calculated by using Large Signal S Parameters (LSSP) simulation as shown in Fig. 3.14. The input impedance of the rectifier was found to be (145.7 − j215.8Ω). It is required to connect this rectifier to the candidate implantable antenna. The input impedance of the antenna is (56.2 + j10.17Ω). A matching network between the antenna and the rectifier is required. An LC matching circuit (L= 51nH and C= 1pF) was used to match the rectifier to the antenna as shown in Fig. 3.13. The overall rectifier size was optimized to be 11 mm × 21 mm. As a result, the new circuit achieved a size reduction by around 50%.

By adopting the optimization technique that includes the size of the microstrip transmission lines, smaller size with high RF to DC conversion efficiency can be obtained. The Roger substrate has contributed with some improvement since it has dissipated power factor less than that for an FR4 substrate. This new rectifier design offered better efficiency and around 50% reduction in size as shown in Fig. 3.16. The simulated and measured efficiencies versus the power fed to the rectifier are shown in Fig. 3.17.

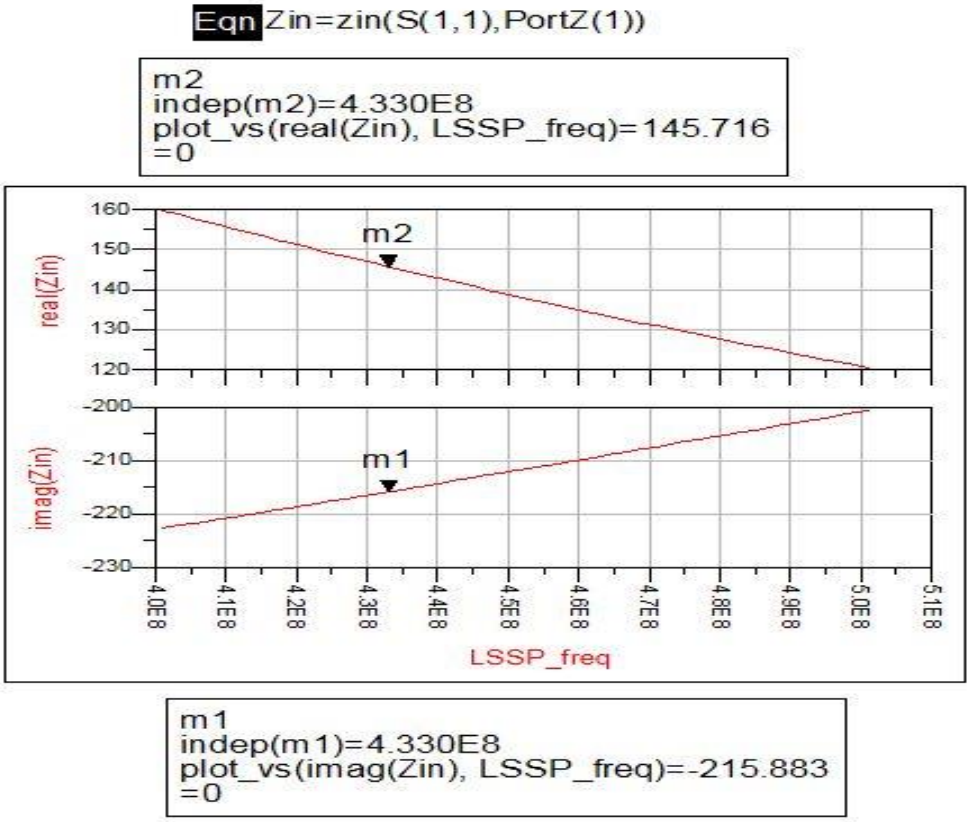

Fig. 3.14. input impedance of the rectifier circuit using LSSP simulation.

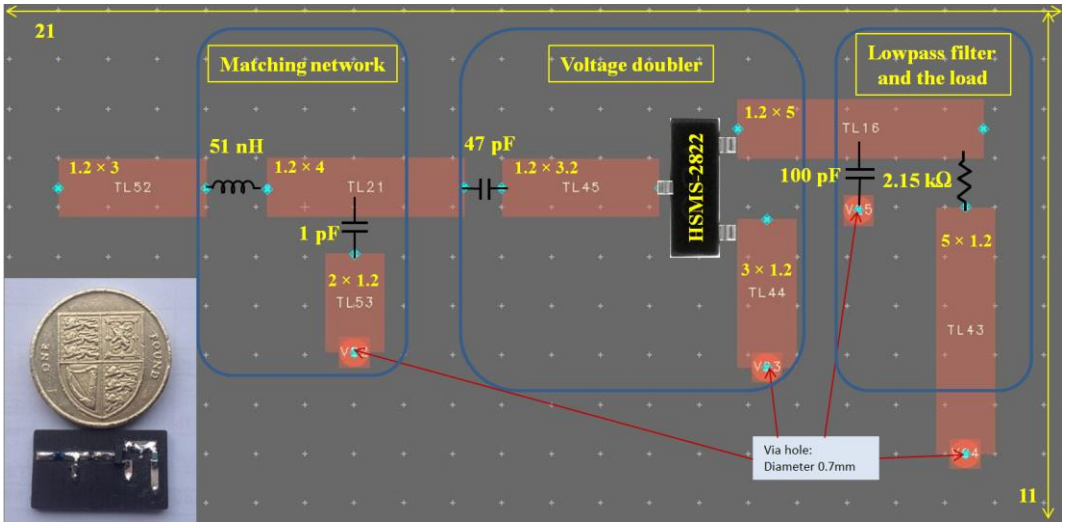

Fig. 3.15. The layout of the new rectifier on a Roger substrate, all dimensions in (mm).

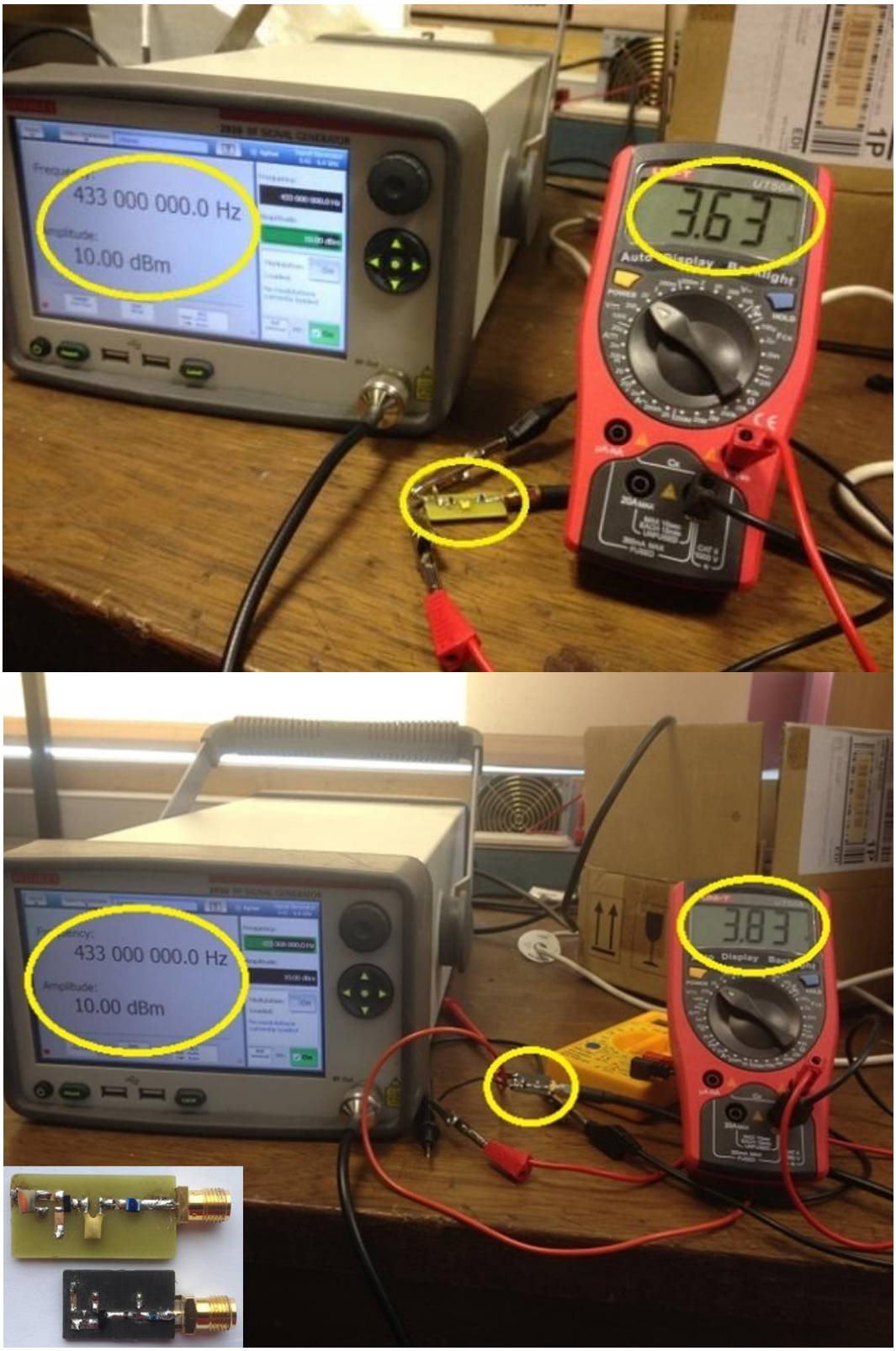

Fig. 3.16. Practical comparison between the rectifier circuits on an FR4 and a Roger substrates.

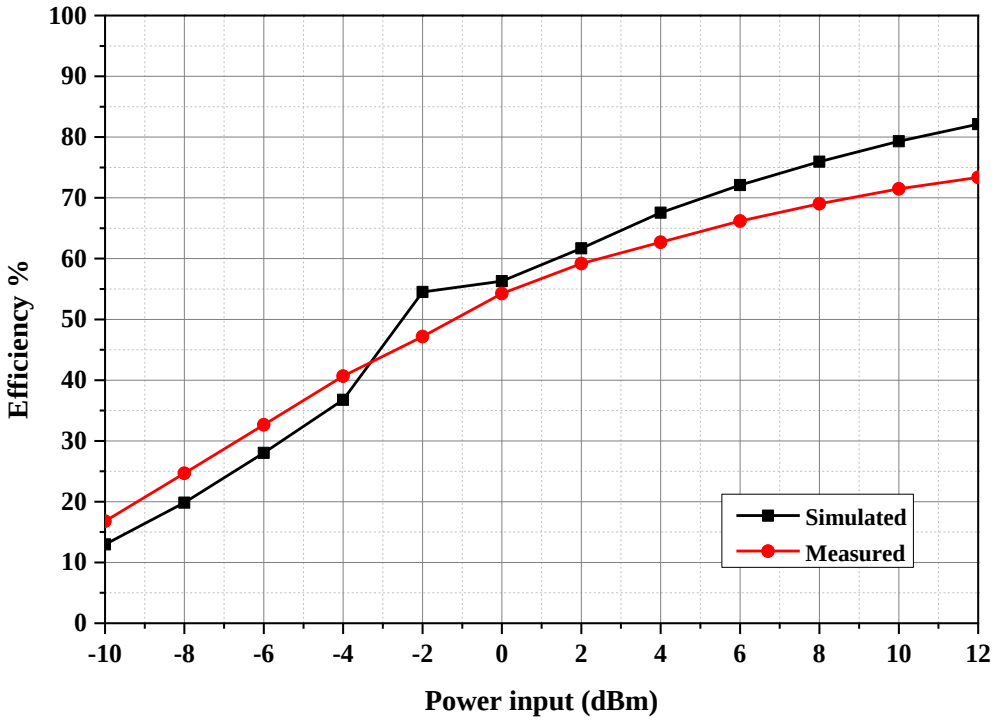

Fig. 3.17. The simulated and measured efficiency versus power input.

3.4 Miniaturized Rectifier on a Roger Substrate

A new rectifier circuit with a size of 10 mm × 5 mm was proposed to be integrated with an implantable antenna to form a rectenna. This design is also based on the principle of a voltage doubler circuit using dual Schottky diodes HSMS-2822 from AVAGO technologies [3]. The schematic diagram and layout details of the rectifier are shown in Fig. 3.198 and Fig. 3.189 respectively. The optimization process to miniaturize this rectifier is similar to the second design. However, it was found that by reducing the size of transmission lines the overall performance of the rectifier can be compensated by tuning the lumped element further. Furthermore, the lumped components of the rectifier can be approximated to realistic values, and then the size of the transmission lines is tuned to retrieve the optimum performance of the rectifier. This process is repeated many times to get smaller rectifier until reach the maximum miniaturization. The overall circuit tuning includes even components of the matching network.

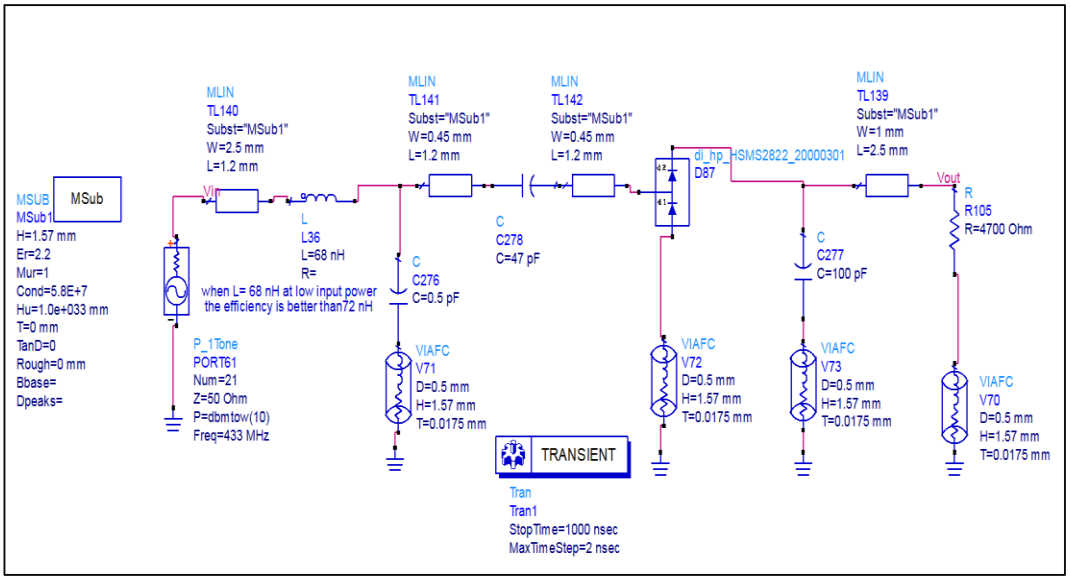

Fig. 3.18. Schematic diagram of the miniaturized rectifier on a Roger substrate.

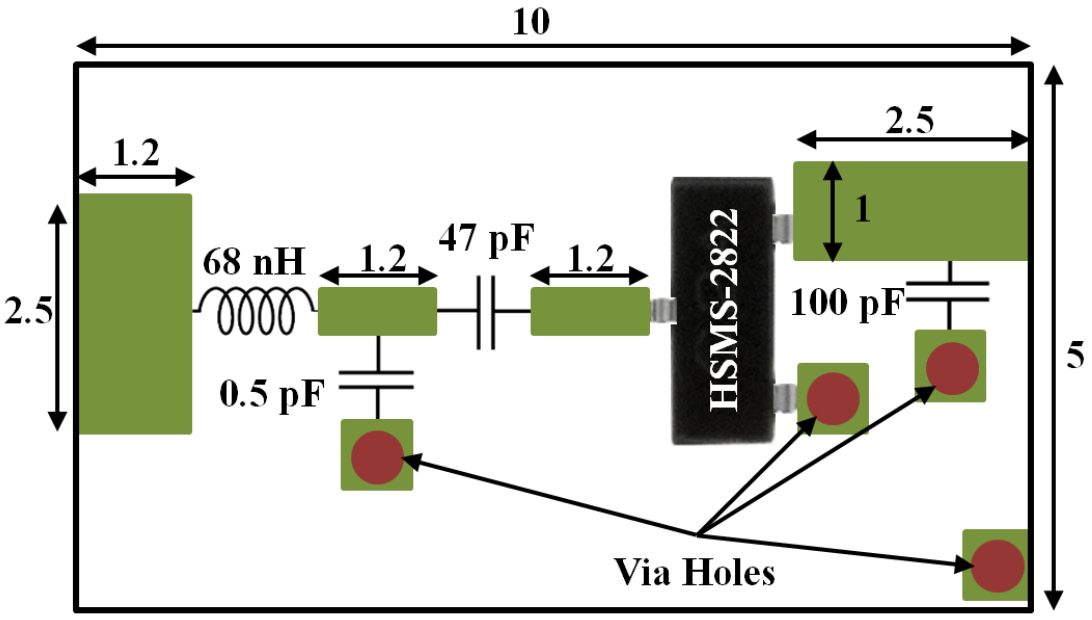

Fig. 3.19. Layout of the miniature rectifier, all dimensions in mm.

The ADS was used to develop the circuit. The rectifier has an AC to DC conversion efficiencies of 28% at -10 dBm input power up to more than 70% at 10 dBm. The reason for this difference in efficiencies is that the diode is nonlinear device where the input impedance of the diode is changed with the input power level and hence a certain mismatch occurs at a certain input power. The circuit was fabricated on a Roger 5880 substrate with a relative dielectric constant of 2.2 and thickness 1.57

mm. The measurement setup of this rectifier is shown in Fig. 3.20. This rectifier can offer around 60% efficiency at 0 dBm input power. The simulated and measured efficiencies on a load of 4.7 kΩ are in very good agreement as depicted in Fig. 3.21.

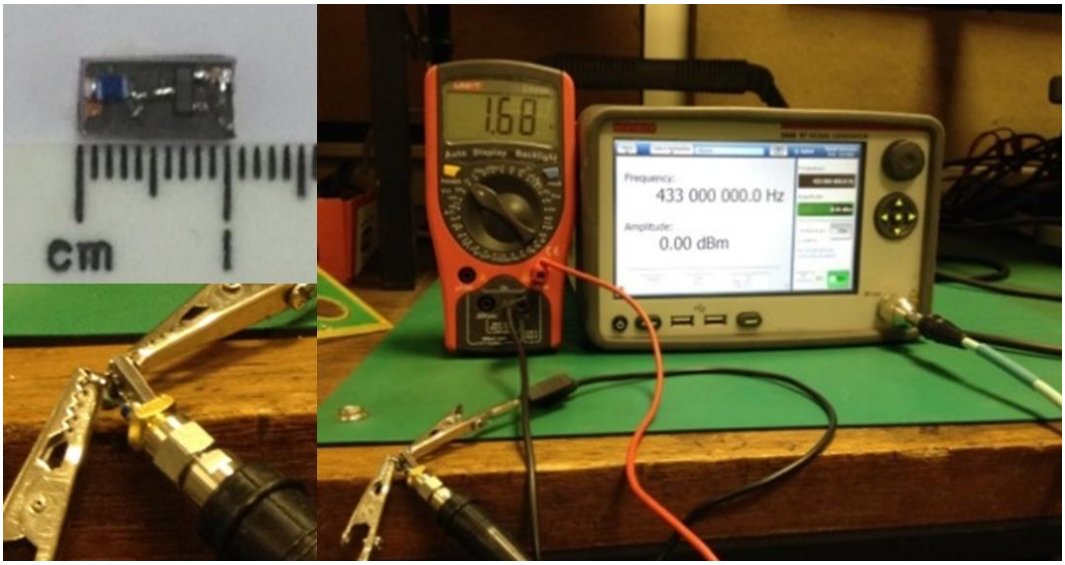

Fig. 3.20. The measurement setup of the miniaturized rectifier.

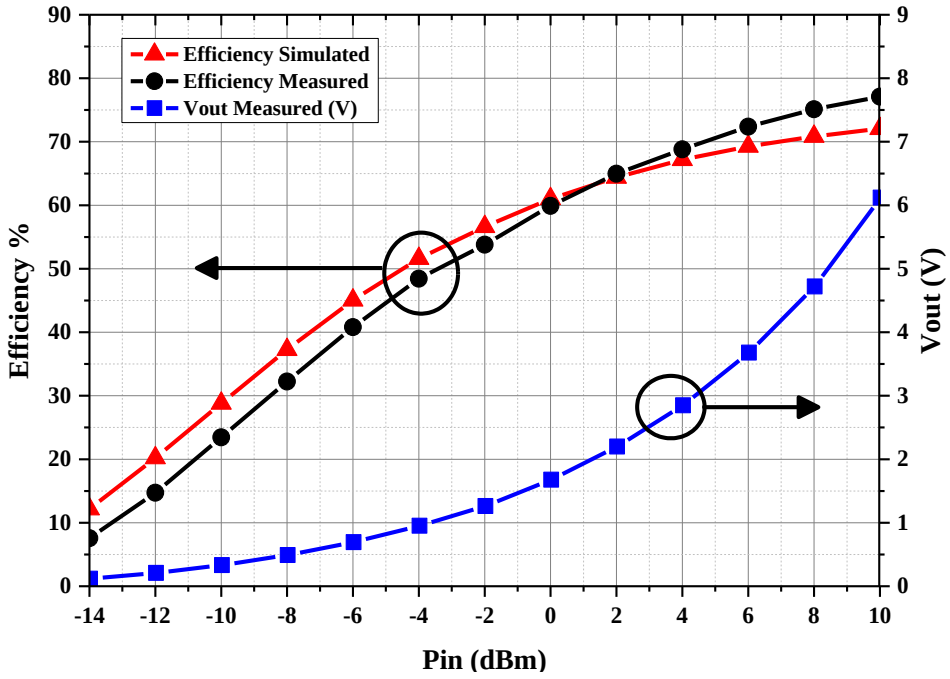

Fig. 3.21. The comparison of the simulated and measured efficiencies of the rectifier, and measured DC output voltages.

3.5 DC Combining Investigation

In this section the aim is to investigate the possibility of combining the DC output of two or more voltage doubler rectifiers. This can help to increase the harvested power in two cases; if there is one antenna receiving multiple bands or multiple antennas regardless if they work over the same or different bands.

The one stage doubler rectifier is shown in Fig. 3.22. This rectifier is matched to 50 Ω source. The output current and voltage are recorded as in Fig. 3.23.

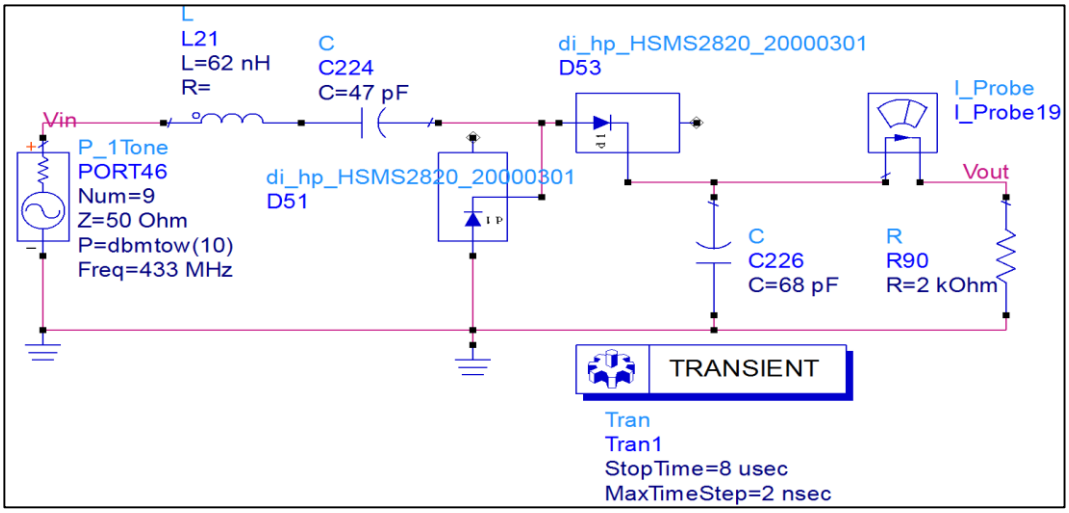

Fig. 3.22. One stage doubler rectifier.

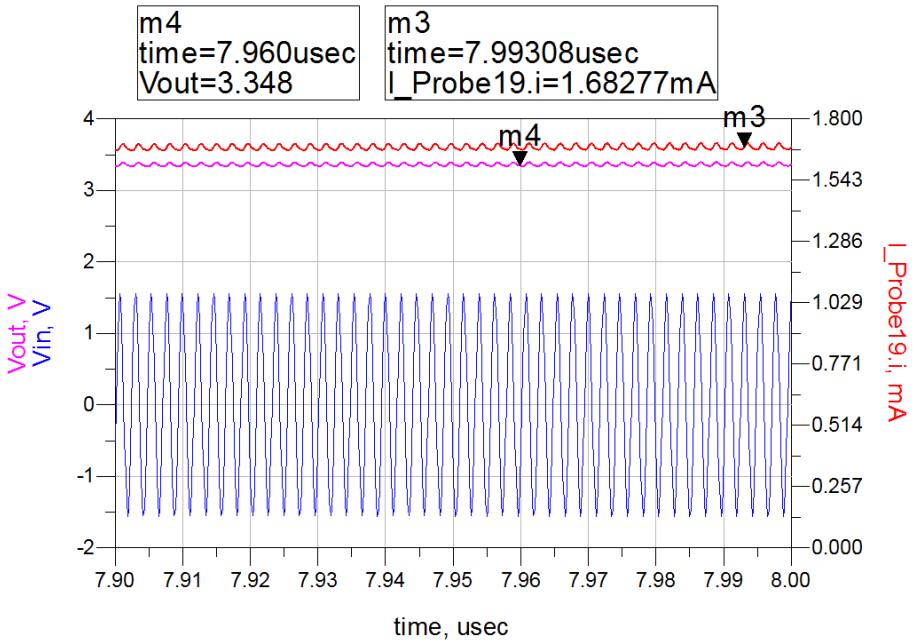

Fig. 3.23. Output records of one stage rectifier.

Then two identical rectifiers but reversed in diode direction are combined to one source and load as shown in Fig. 3.24. The direction of diode is reversed to enable the combined circuit to convert both the positive and negative cycles of the input into DC. However, the output of this case is same as the one stage rectifier regardless of use two sources or one source as shown in Fig. 3.25. The reason is that the output should be taken from Vout+ to Vout− and not from Vout+ to the ground.

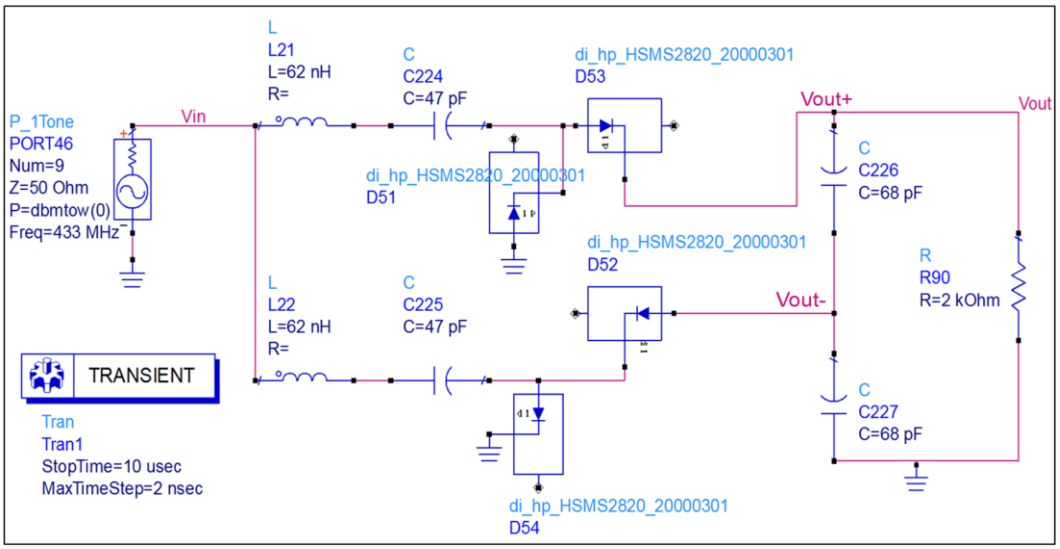

Fig. 3.24. Two stages with reversed dual diodes.

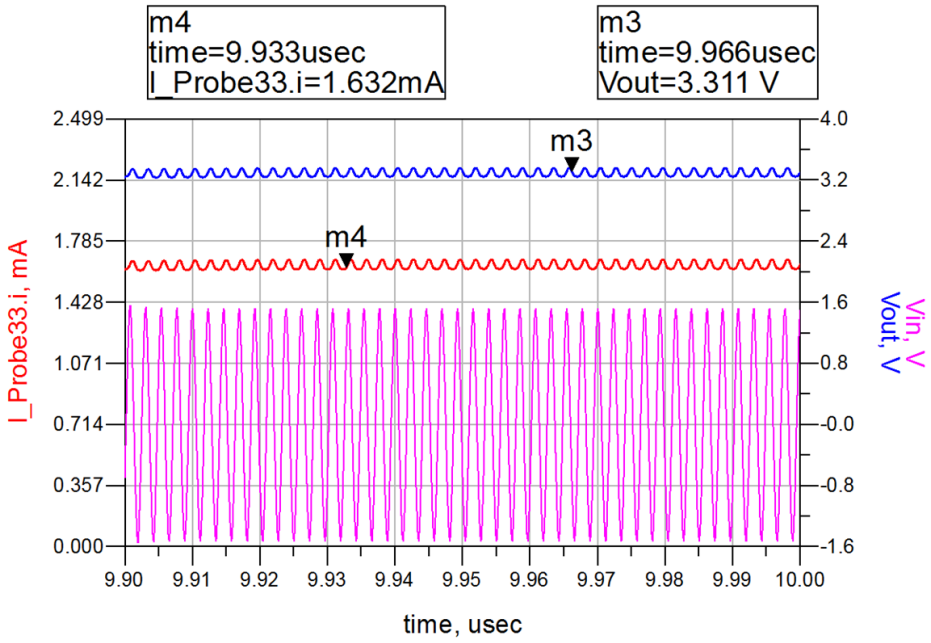

Fig. 3.25. Results of two stages reversed doubler diodes.

This kind of connection is shown in Fig. 3.26 which improves the output voltage. However, the current is decreased to a low value. The voltages may be added together but the currents were added destructively as shown in Fig. 3.27.

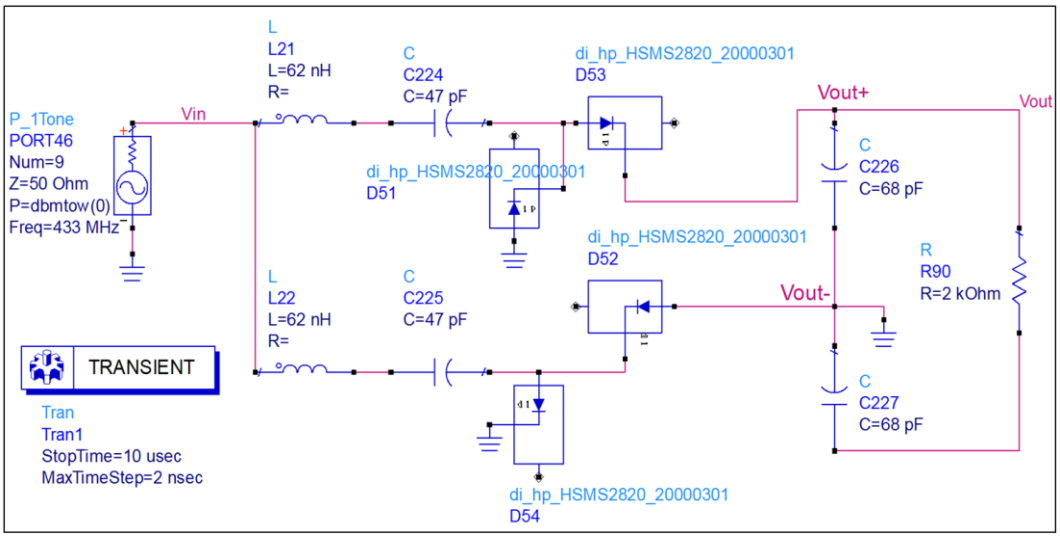

Fig. 3.26. Two stages circuit with the correct output connection.

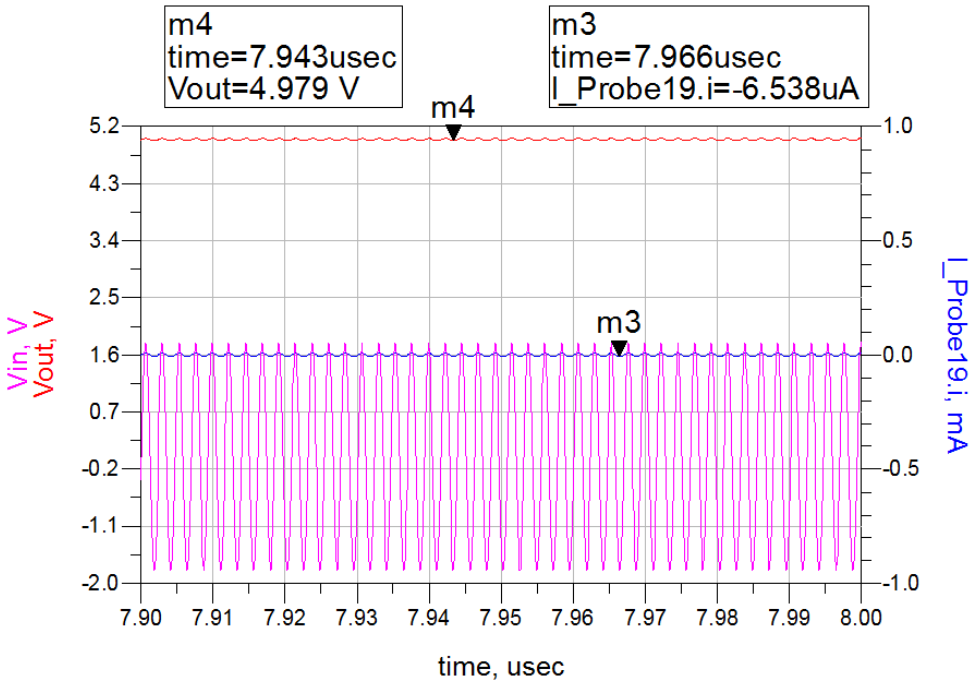

Fig. 3.27. The output record of the two stages.

The output connection was changed to the diagram shown in Fig. 3.28. This connection is called push pull. The outputs Vout+ and Vout− are 2.35 V and -2.35 V each and the current that flows in the resistor is 2.3 mA as shown in Fig. 3.29. If

multiply the current times the resistor then the real voltage across the resistor can be known as “0.0023 × 2150 = 4.9 V”. when Vout+ and Vout− are added together, the results is around 4.7 V which approximate to the value gotten from multiplying the current by the resistor load. This connection produced higher voltage and current.

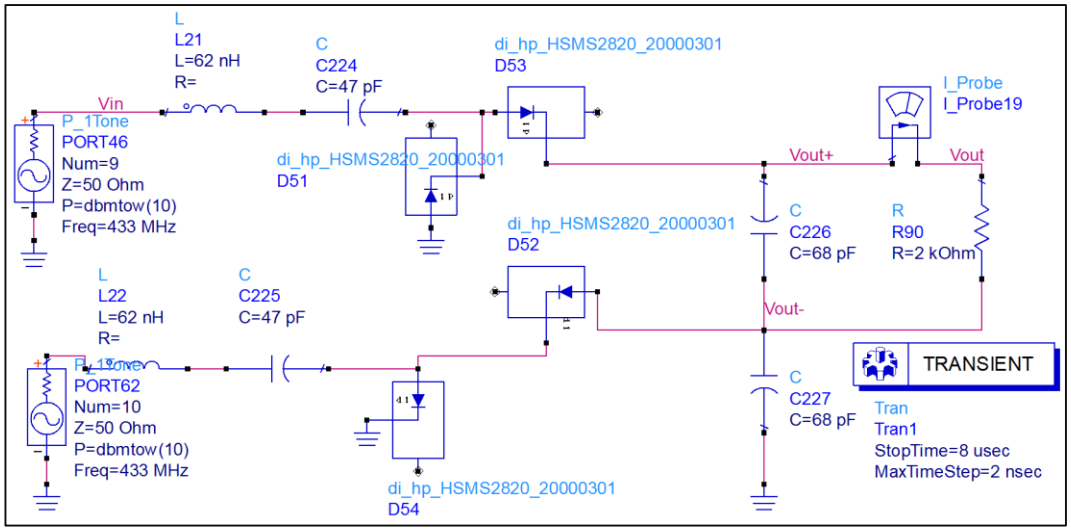

Fig. 3.28. Push pull circuit diagram.

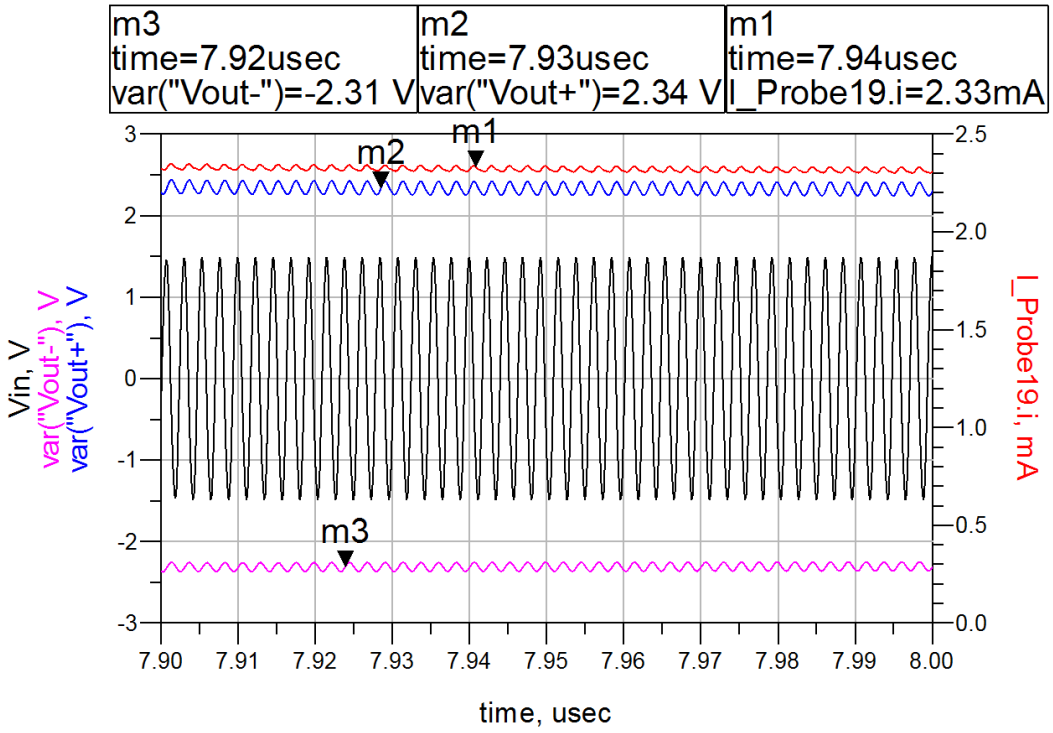

Fig. 3.29. The output of the push pull circuit.

The drawback of this combination is that up to 2 circuits can be only combined. If more stages are needed, then pairs of circuits can be cascaded.

Now the same connection is tested with one source as shown in Fig. 3.30. The output current and voltage will be reduced as shown in Fig. 3.31. The output current of this combined circuit as compared to the single stage current shows an improvement of about 7%. This is low improvement as compared with the complexity that has been added to the circuit.

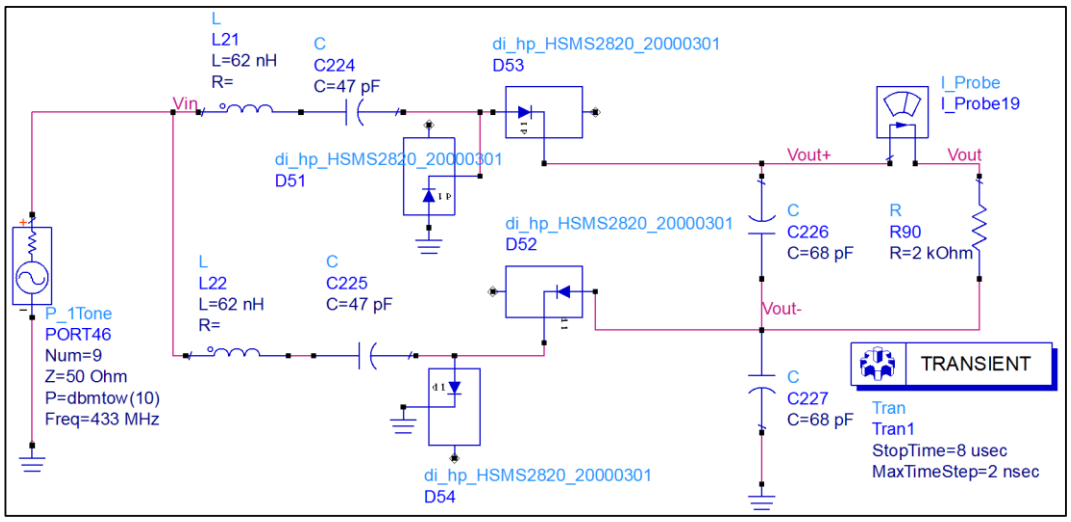

Fig. 3.30. Push Pull circuit with single source.

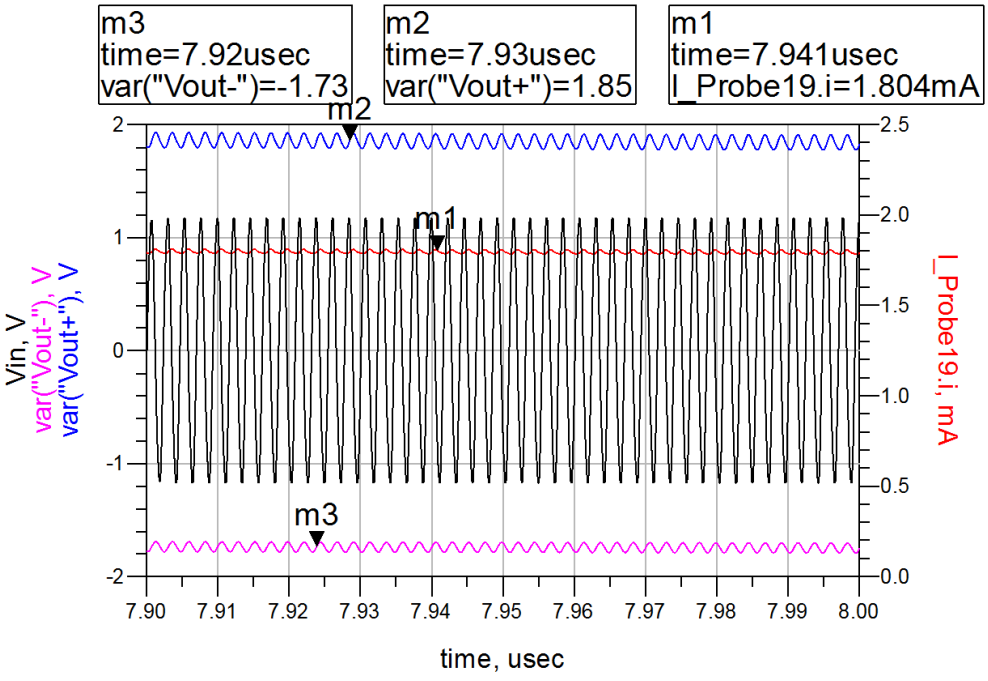

Fig. 3.31. The output of push pull circuit with one source.

On other hand, the series connection method is investigated as well. It gives constructive combining for the current and the voltage as shown in Fig. 3.32. The advantage of this combination is that multiple circuits can be cascaded to get higher output power at the load.

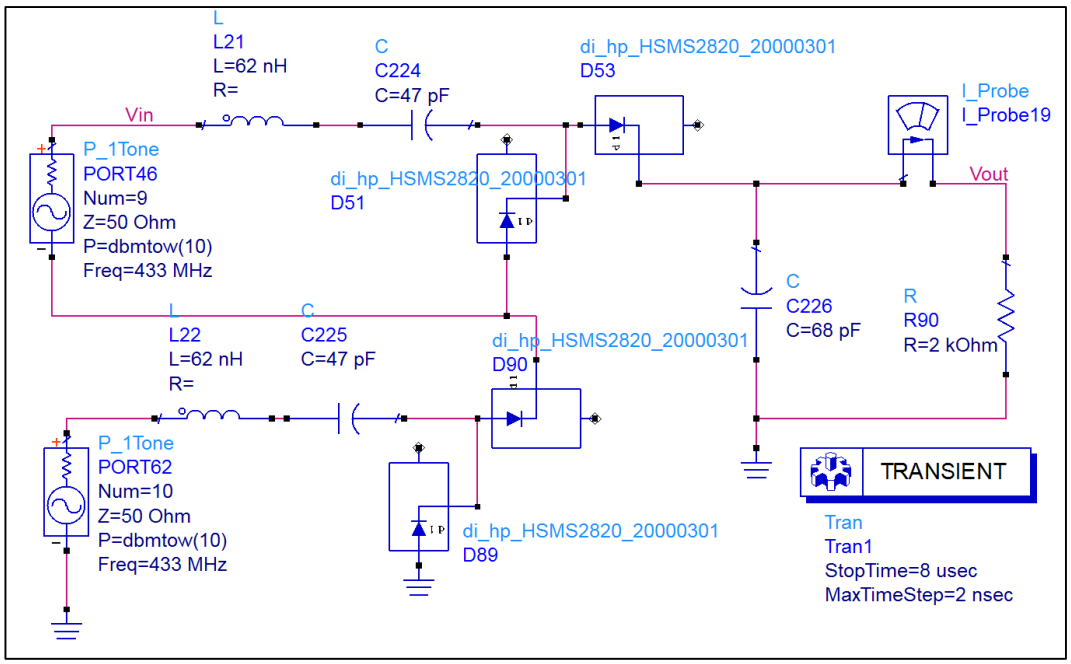

Fig. 3.32. Series connection of two stages rectifiers.

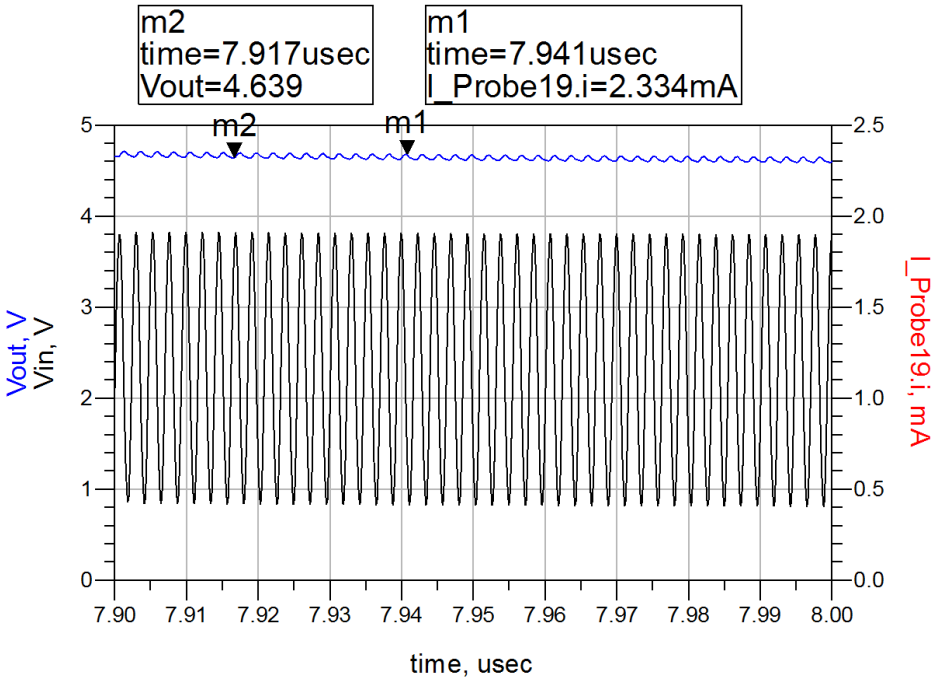

Fig. 3.33. Results of series connection

When more stages are cascaded in series as shown in Fig. 3.34, a higher voltage and current are gained at the load as shown in Fig. 3.35.

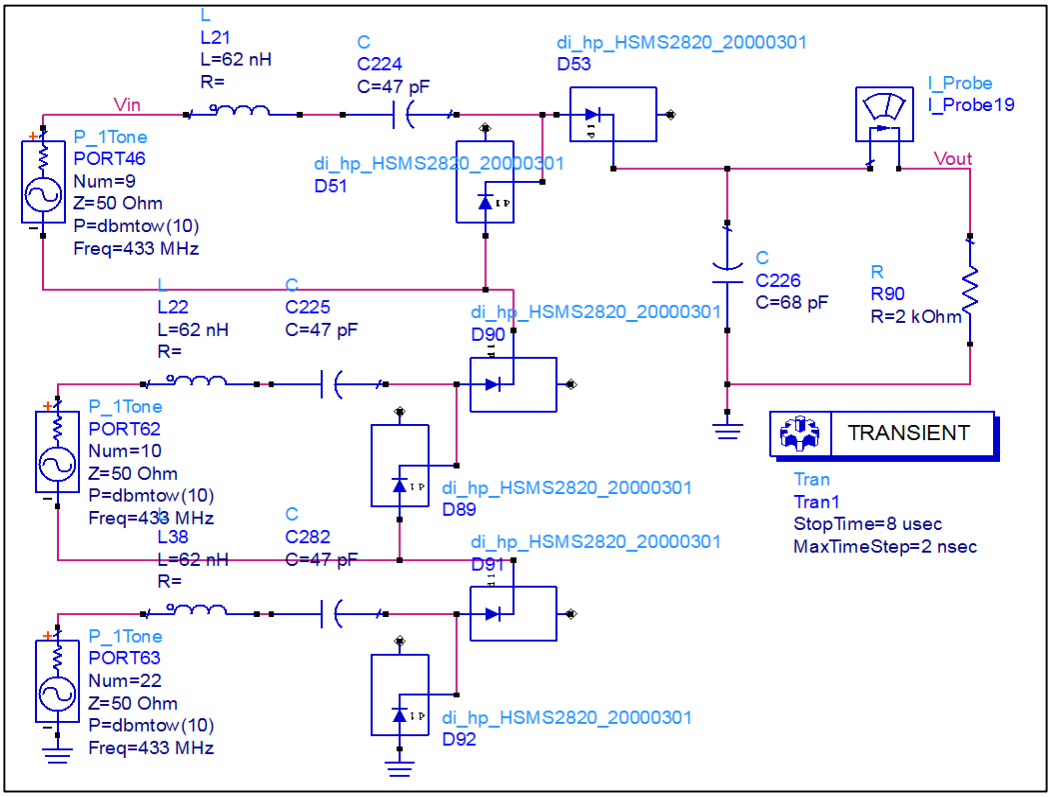

Fig. 3.34. more than two stages in series.

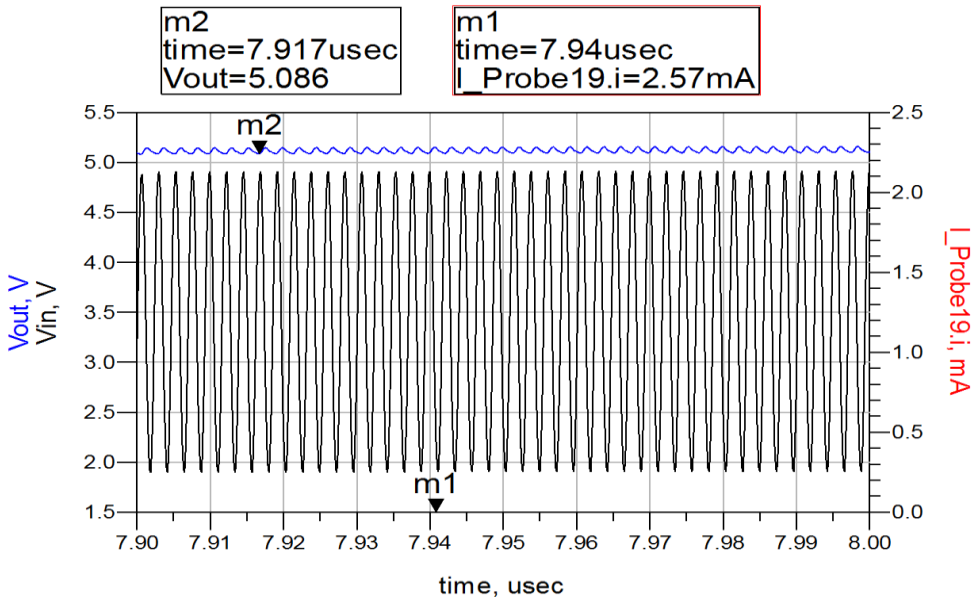

Fig. 3.35. Results of three stages.

This kind of connection is very useful for multiple sources. However, the series connection is difficult to be used with one antenna since each stage requires an individual feed. The idea of connection multiple stages here is that each stage will act as a DC bias to the next one and then the accumulation of multiple stages will result in a higher voltage and current.

This section can be concluded as:

- Two or more stages can be cascaded together to get combined DC power at the load.
- Parallel cascading approach can be done with two circuits. The two circuits can be fed using one source or two sources. For more stages, pairs of circuits can be cascaded together.
- Series cascading approach is effective way to get combined DC power at the load. Several circuits can be cascaded together. However, an individual source is required for each stage.

3.6 Summary and Conclusions

In this chapter, the design of voltage doubler rectifier circuits at the 433 MHz band was investigated. Three rectifiers have been proposed for several purposes. The first rectifier was design on an FR4 substrate and used to charge a realistic implantable battery. The second rectifier was designed on a Roger substrate for a specific implantable antenna to be used for far field WPT experiment that will be presented in the following chapters. The third rectifier was miniaturized on a Roger substrate and optimized for working with 50 Ω antennas to work as implantable rectenna. The DC combination techniques of multiple rectifiers were investigated next. It is concluded that:

- Voltage doubler rectifiers are useful to get high AC to DC conversion efficiency.
- Rectifier circuits can be miniaturized to very small size by optimizing the components together including the transmission lines.

- The designed rectifier circuits can be used effectively to charge batteries with capacity less than 10 mA•h. these batteries are useful for low power medical applications such as drug delivery.

References

[1] H. W. Cheng, T. C. Yu, and C. H. Luo, "Direct current driving impedance matching method for rectenna using medical implant communication service band for wireless battery charging," *IET Microwaves Antennas & Propagation,* vol. 7, pp. 277-282, Mar 19 2013.

[2] Avago Technologies, "Schottky Diode Voltage Doubler," *Application Note 956-4,* 2010.

[3] Avago Technologies, "HSMS-282x Surface Mount RF Schottky Barrier Diodes," *Data Sheet,* 2014.

[4] Avago Technologies, "HSMS-285x Series Surface Mount Zero Bias Schottky Detector Diodes," *Data Sheet,* 2009.

[5] Avago Technologies, "HSMS-286x Series Surface Mount Microwave Schottky Detector Diodes," *Data Sheet,* 2009.

[6] H. Chi-Chun, Y. Shou-Fu, and W. Chua-Chin, "A Li-ion battery charging design for biomedical implants," in *Circuits and Systems, 2008. APCCAS 2008. IEEE Asia Pacific Conference on*, pp. 400-403, 2008.

[7] L. I. R. Batteries, "Technical handbook," *Disponible: http:/cardi. igeofcu. unam. mx/techdocs/PowerSonic_batteries. pdf,* vol. 25, pp. 27-29, 2013.

[8] B. D. Valle, C. T. Wentz, and R. Sarpeshkar, "An Area and Power-Efficient Analog Li-Ion Battery Charger Circuit," *IEEE Transactions on Biomedical Circuits and Systems,* vol. 5, pp. 131-137, 2011.

[9] S. Keeping, "A Designer's Guide to Lithium Battery Charging," *Digikey corporation, Hearst Electronic Products,* 2012.

[10] J. Coonrod, "Understanding When to Use FR4 or High Frequency Laminates," *Rogers Corporation, Advanced Circuit Materials Division,* 2011.

Chapter 4

Wearable and Implantable Antennas

4.1 Introduction

In this chapter, flexible loop antennas are designed for the purpose of powering implantable medical devices and for communication. These antennas include wearables and implantable. Three wearable antenna designs are introduced. The first design is proposed to cover multiple bands with wide bandwidths. The second design is proposed to improve the magnetic field in the near field region of the antenna for better Wireless Power Transfer (WPT). The third design is proposed to improve WPT and coupling with offset in some directions. Implantable loop antennas are presented as well. These antennas are simple and proposed to be a part of system for WPT and communication. A summary and conclusion will be given at the end of this chapter.

4.2 Wearable Antenna Design

Wearable antennas are usually designed for the purpose of communication. It is used on the human body for off-body, on-body or in-body communications [1-3]. It can be used also for WPT [4]. Several wearable antennas have been proposed to cover a single band [5] or multiple bands such as the Fractal Koch antenna at 0.915, 2.45 and 5.8 GHz [6], a planar inverted antenna at 1.9 and 2.45 GHz [7], a meandered dipole antenna at 0.915, 1.575 and 2.4 GHz [8] and a bow-tie antenna to cover 0.45, 0.8 and 1.4 GHz [9].

The aim of this research is to design a wearable antenna for both purposes: WPT and communication with implants. The main bands to be covered are Medical Implant Communication Service (MICS) band and the Industrial, Scientific and Medical (ISM) band around 433 MHz. A loop antenna was already chosen as a candidate because of the flexibility to be conformal to the body parts and the high magnetic field in the near field region. In this section, three designs are introduced. The first

design can cover multiple bands with wide bandwidths. The second design investigates the possibility of improving the magnetic field in the near field region of the antenna. The third design is to investigate a solution to improve WPT.

4.2.1 Dual Broadband Butterfly Loop Antenna

The target of the first design is to cover multiple wide bands that support a wide range of medical applications. The advantage of having a wide band is to be robust against the detuning by human tissues. The antenna size can be reduced and multiple bands can be covered by using two approaches. The first approach is to use Hilbert curves where multiple line segments are used to construct a close loop antenna as shown in Fig. 4.1 [10]. However, the generated bands are usually with narrow bandwidths. The second approach is based on multiple straight meandered strips [11, 12].

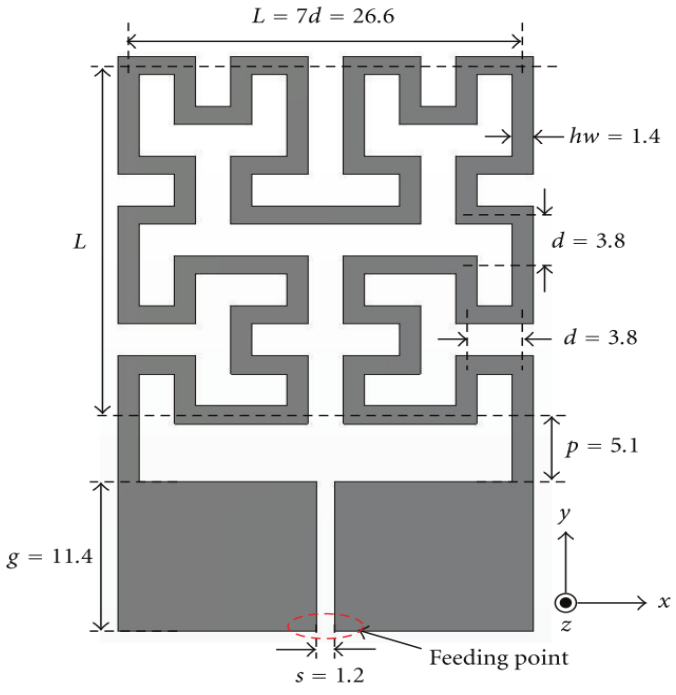

Fig. 4.1. Geometry and dimensions of Hilbert-curve loop antenna [10].

In this work a novel antenna is designed by using curved meandered lines rather than straight lines. This approach can cover multiple bands and produce wide bandwidth.

This feature is much desired for in-body wearable application to resist the detuning effects by tissues. The process of optimising the antenna shape and performance is shown in Fig. 4.2.

Fig. 4.2. The process of optimising the dual wideband butterfly antenna.

The feeding point's size are adjusted to provide a suitable matching to the antenna. The antenna shape was drawn based on overlapping multiple ovals. This shape is

symmetrical around y-axis. The size of the antenna and the fabricated prototype are shown in Fig. 4.3. The ovals' size details are given in Table 4.1.

This antenna has two wide bandwidths of 600 MHz from 400 to 1000 MHz and 700 MHz from 2 to2.7 GHz. These bandwidths cover multiple medical bands including the MICS band and the ISM bands around 433 MHz, 868 MHz, 915 MHz and 2.45 GHz. The simulated and measured reflection coefficients of the proposed antenna are shown in Fig. 4.4.

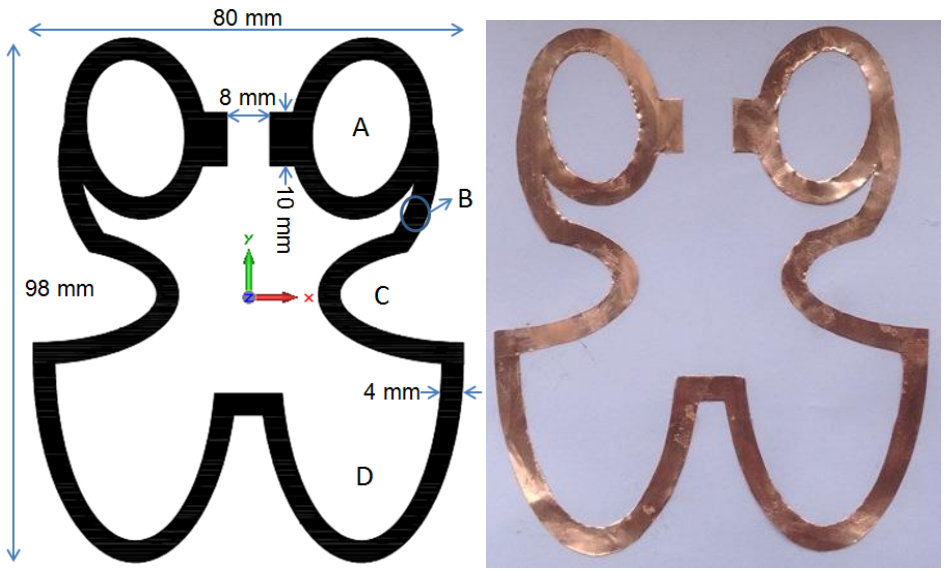

(a) **(b)**

Fig. 4.3. The proposed butterfly loop antenna: (a) dimension details and (b) the fabricated prototype antenna.

Table 4.1. The dimension details of ovals that construct the butterfly antenna

Oval label	(x, y, z) centre coordinate	Radius in x-direction	Radius in y-direction	longer diameter's angle with respect to y-axis
A	(20, 30, 0)	11	15	10˚
B	(12, 20, 0)	18	23	35˚
C	(40, 0, 0)	25	11	90˚
D	(21, -12, 0)	17	36	0˚

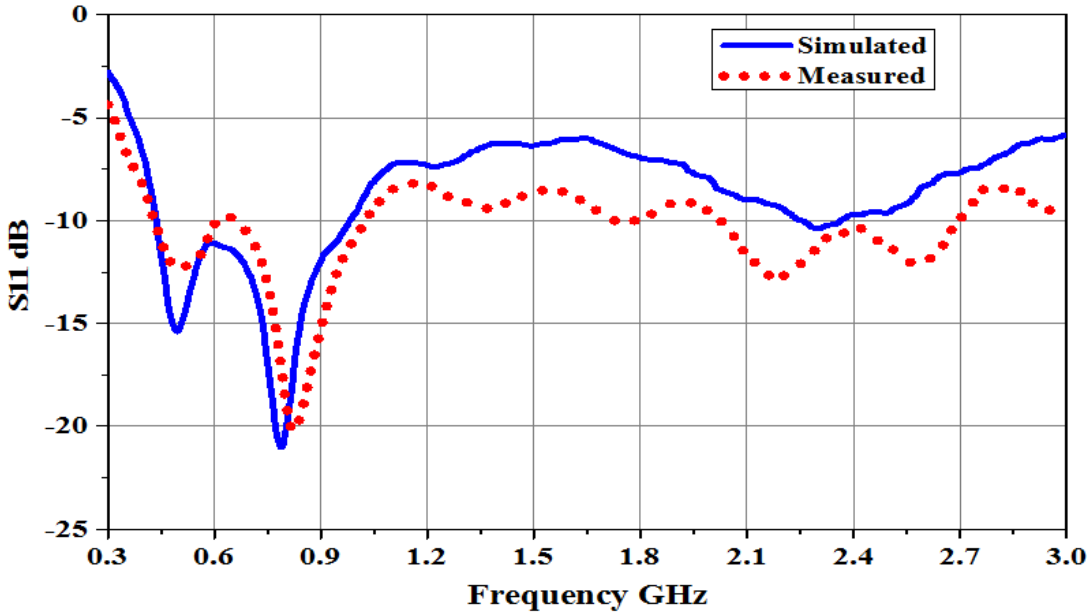

Fig. 4.4. The measured and simulated refection coefficient S_{11} of the butterfly loop antenna.

This antenna can achieve a wide bandwidth where the two small loops are responsible for the high frequency band while the whole circumference including the small loops is responsible for the low frequency band response as indicated in Fig. 4.5.

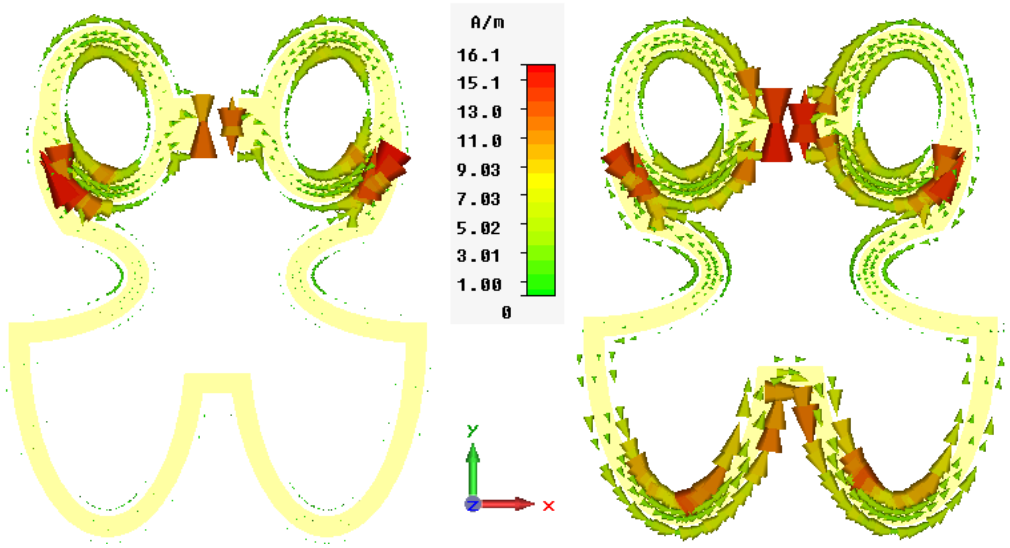

(a) **(b)**

Fig. 4.5. Surface current distribution at: (a) 2.4GHz and (b) 0.43 GHz.

The antenna was tested on two body phantoms, one to mimic flat surfaces and the other for curved surfaces with a radius of 73 mm for a typical human arm as shown in Fig. 4.6. Each phantom consists of four layers of muscle, fat, skin and clothes. The muscle has a radius of 67 mm for cylindrical phantom and a thickness of 67 mm for the flat phantom. The thickness of the fat, skin and clothes are 3mm, 1 mm and 2 mm respectively for both shapes. The properties of these layers are shown in Table 4.2. The reflection coefficients S_{11} of the proposed antenna on flat and bending body surfaces are in very good agreement as shown in Fig. 4.7. The antenna showed a robust in performance to the different surface curvatures. It is worth mentioning that the fabricated antenna was tested in flat case on pork that mimics human body properties.

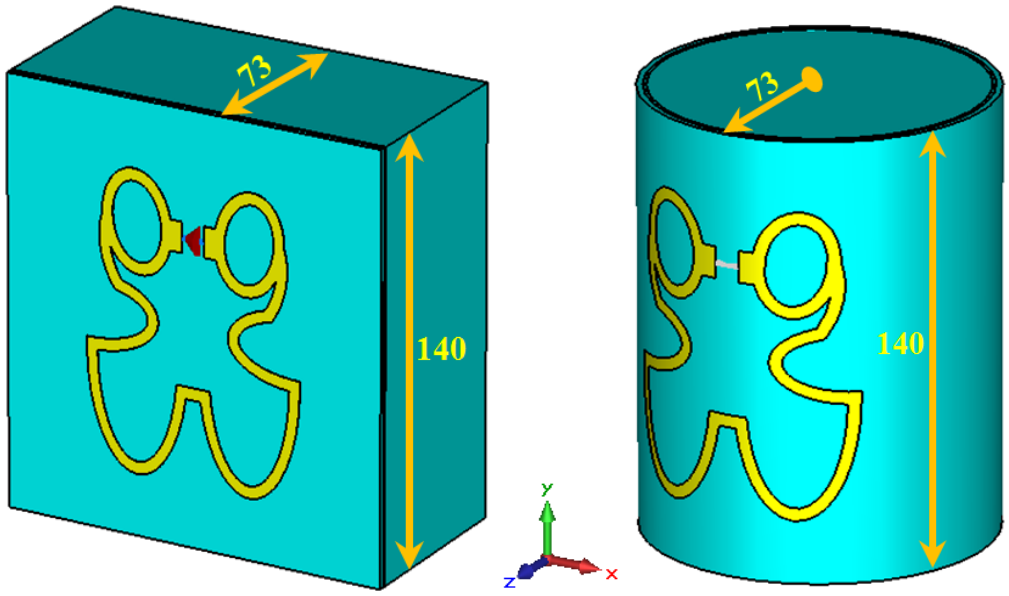

Fig. 4.6. Testing the proposed antenna on the flat and bending surfaces, all dimensions in mm.

Table 4.2. Bio Tissue Broadband Properties from 0.1 – 3 Ghz from CST Voxel Family.

Prosperities🡻\Tissue type 🡺	Muscle	Fat	Skin
Mue	1	1	1
Rho ρ (kg/m^3)	1041	910	1100
Dielectric constant ε_r	57.1	5.6	46.7
Conductivity σ (S/m)	0.79	0.04	0.69
Thermal cond. (W/K/m)	0.53	0.201	0.293
Heat capacity (kJ/K/kg)	3.546	2.5	3.5
Thermal Diffusivity (m^2/s)	1.436×10^{-7}	8.8352×10^{-8}	7.611×10^{-8}
Blood flow (w/k/m^3)	2700	1700	9100
Metabolic rate (w/m^3)	480	300	1620

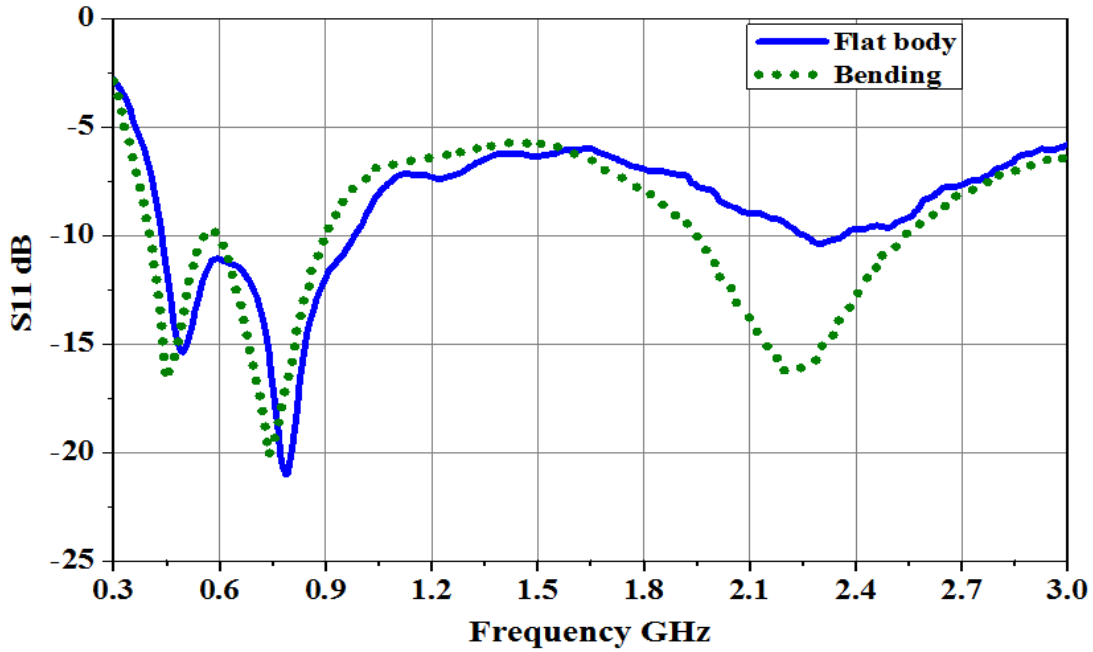

Fig. 4.7. The simulated S_{11} of the butterfly loop antenna in flat and bending surfaces.

In the bending case, the antenna showed better matching at high frequencies while kept approximately the same response at low frequencies. This is because the size of the feeding port has effect on tuning the antenna impedance especially at higher frequencies. The little bending of feeding will detune the input impedance of the antenna for better matching at this band.

The radiation pattern of the butterfly at multiple frequencies is shown in Fig. 4.8. In these figures, the z-direction represents the off-body direction. This antenna has the

main magnitude in direction towards the body at the bands 405 and 433 MHz which is required for the communication and transferring power into the implants respectively. The patterns at 0.915 and 2.45 GHz are mainly off-body. This feature gives the antenna the advantage to be used potentially as a repeater between the implants and a faraway external reader. As a repeater, the proposed antenna can adopt MICS band for in-body communication with the implant and the ISM around 2.45 GHz for off-body communication with a faraway reader.

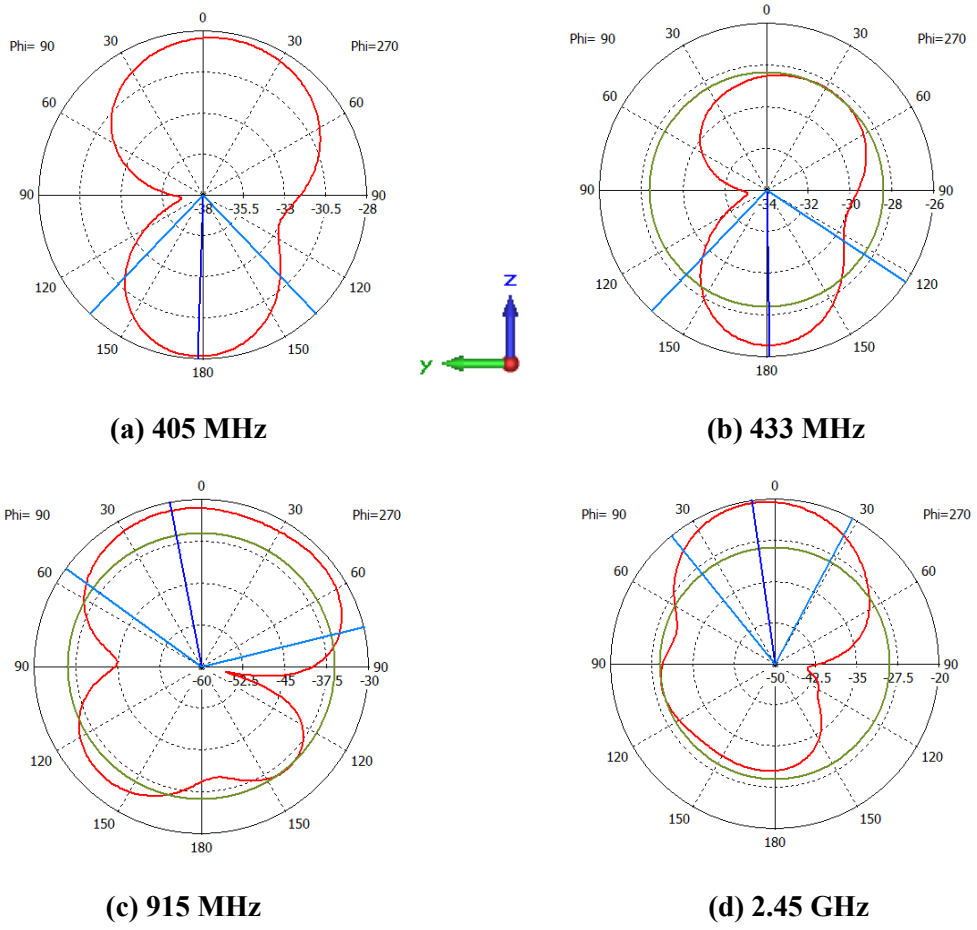

(a) 405 MHz **(b) 433 MHz**

(c) 915 MHz **(d) 2.45 GHz**

Fig. 4.8. The polar power pattern of the proposed antenna at: (a) 405 MHz, (b) 433 MHz, (c) 915 MHz and (d) 2.45 GHz.

4.2.2 Meandered Square Loop Antenna

In this design, an approach to improve the magnetic field in the near field region of the antenna for WPT is proposed. In near field region, the inductive coupling is the

main technique for WPT. The inductive coupling follows equation (2.13) mentioned in Chapter 2. According to equation (2.13), the induced voltage is directly proportional to the magnetic field, so that improving the magnetic field of the wearable antenna yields to better power reception at the receiver.

According to Faraday's law, when a current flows in a conductor, a magnetic field will be generated around the conductor and the direction of this field follows the right hand rule as shown in Fig. 4.9

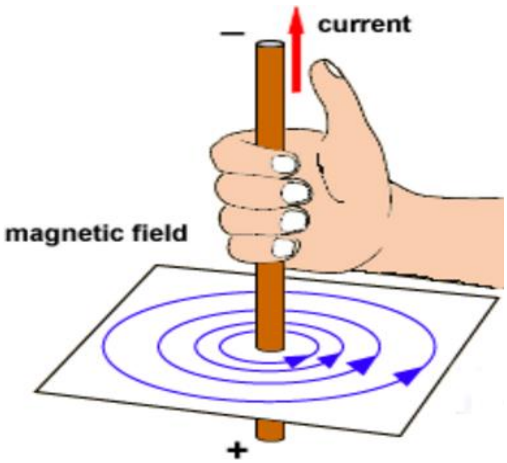

Fig. 4.9. Right hand rule for magnetic field direction according to Faraday's law [13].

Since loops are wire antennas, the current in the wire generates a magnetic field around the wire according to Fig. 4.9.

Loop antennas can be electrically small or large according to the antenna size as compared with the wavelength at the operating frequency. Surface current is uniform with electrically small antennas while it is no-uniform with electrically large antennas. Wearable antennas have relatively large dimension comparable to the wavelength. A conventional wearable square loop with size of 9 cm × 9 cm works around 400 MHz on the body tissue. With same size it resonates at around 1 GHz in free space as shown in Fig. 4.10.

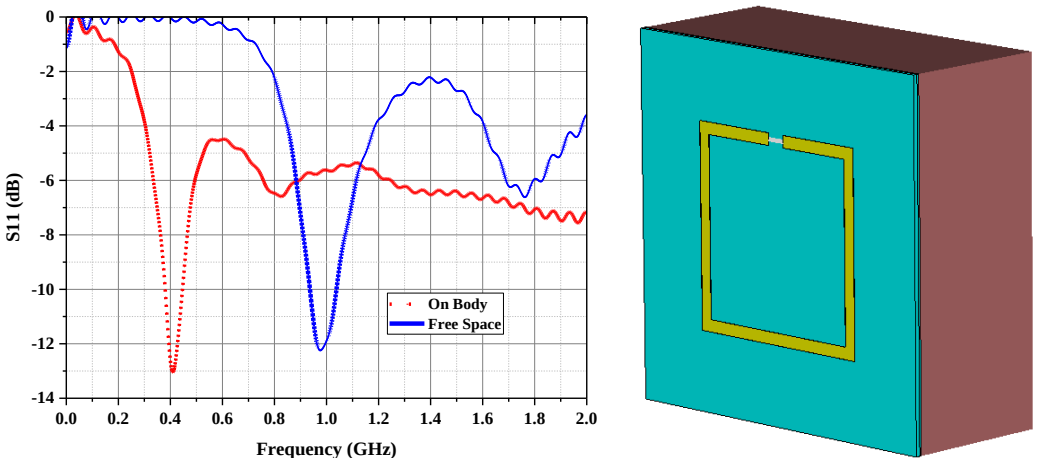

Fig. 4.10. S_{11} of the conventional square loop antenna on body and in free space.

The generated magnetic fields are combined destructively or constructively according to the field's directions. Square loop antenna with a perimeter of about one λ (wavelength) long behaves as a folded dipole antenna with two λ/2 dipoles. The directions of the currents along the two halves are the same as shown in Fig. 4.11(a). The surface current along each halve will be maximal at the center and be minimal at the ends. The generated fields from the two conductors are in opposite directions in the center area of the conventional loop antenna and will cancel out each other. This leads to weak magnetic field at the middle area and stronger at the edges.

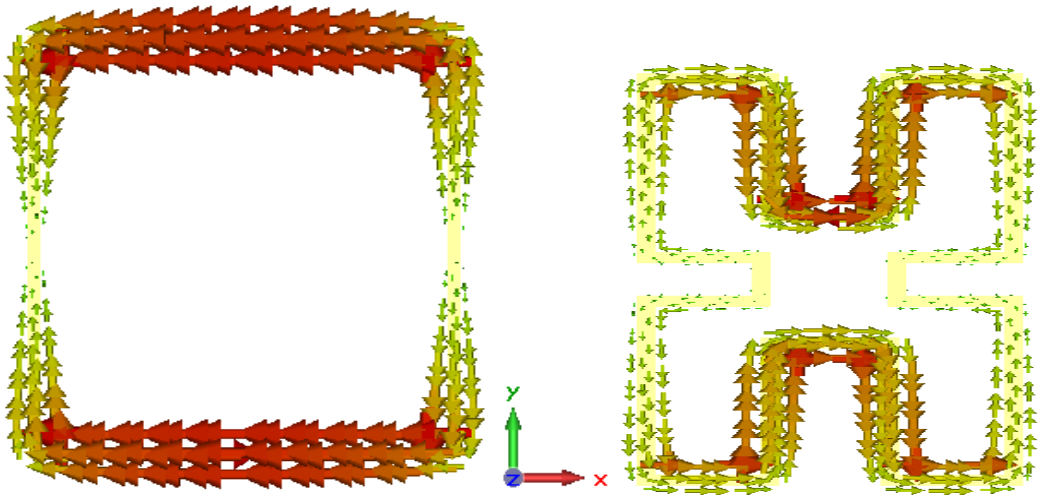

(a) **(b)**

Fig. 4.11. Current distribution of: (a) the square loop and (b) the meander loops.

A meander loop design could contribute with a stronger field in the near field region. To design a meandered square loop antenna, the meandered lines and the excitation port location can be chosen in such way that more combined fields can be generated as shown in Fig. 4.11(b). The constructive magnetic fields offer high magnetic field density into the human tissues and as a result the WPT to the implantable system can be improved.

The generated magnetic fields from both square and meandered square loops have been compared along x-axis and y-axis. Along x-axis, surface currents of the square loop are strong and in the same direction but the associated magnetic fields will be opposite to each other. As a result the generated magnetic field will be weak due to the destructive combination. In the case of meandered square loop, the antenna segments along x-axis have surface currents with opposite directions. The associated magnetic field will be in the same direction. This yields to constructive combined fields as shown in Fig. 4.12.

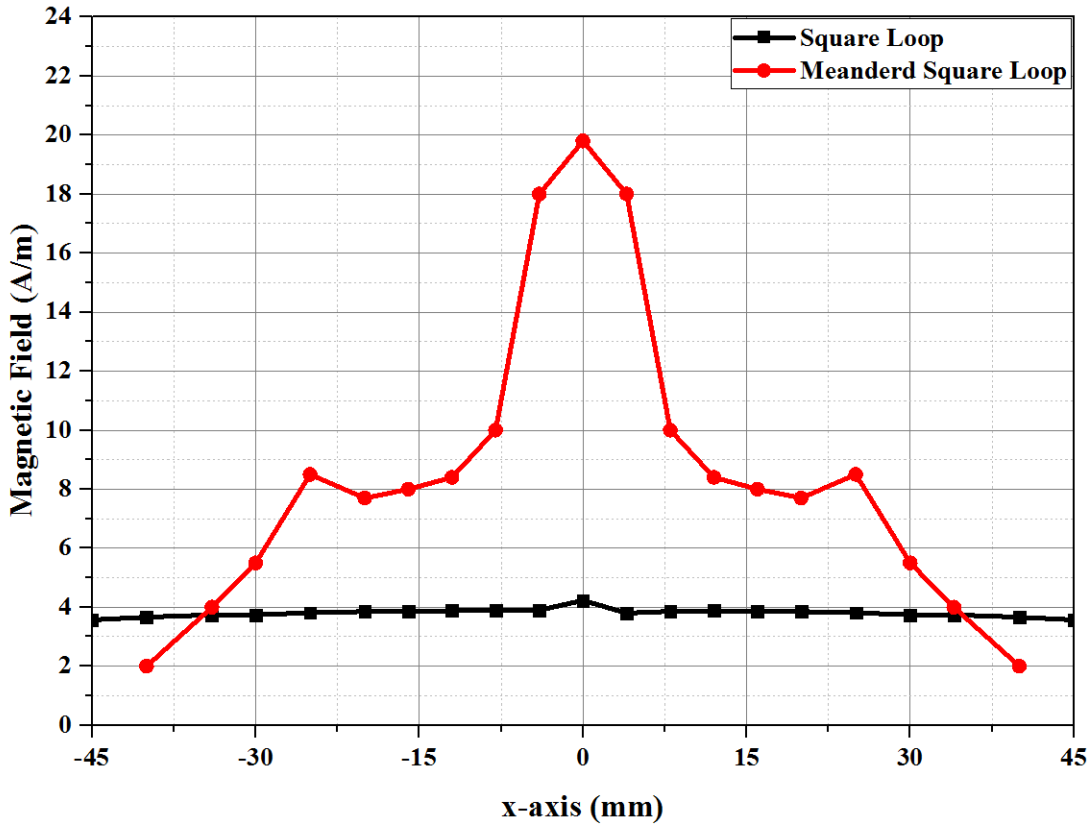

Fig. 4.12. Comparison of the generated magnetic field from meandered square loop and the conventional square loop antennas along x-axis.

Along y-axis, the segments of square loop carry very weak surface currents at the middle and become stronger at the edges. The resultant magnetic field will be stronger at the edges as well. On other hand, the segments of the meander square loop carry strong surface currents in opposite directions along almost the segments except the middle distance. The generated magnetic fields will be then combined constructively. This results in strong magnetic field as compared with the conventional square loop as shown in Fig. 4.13.

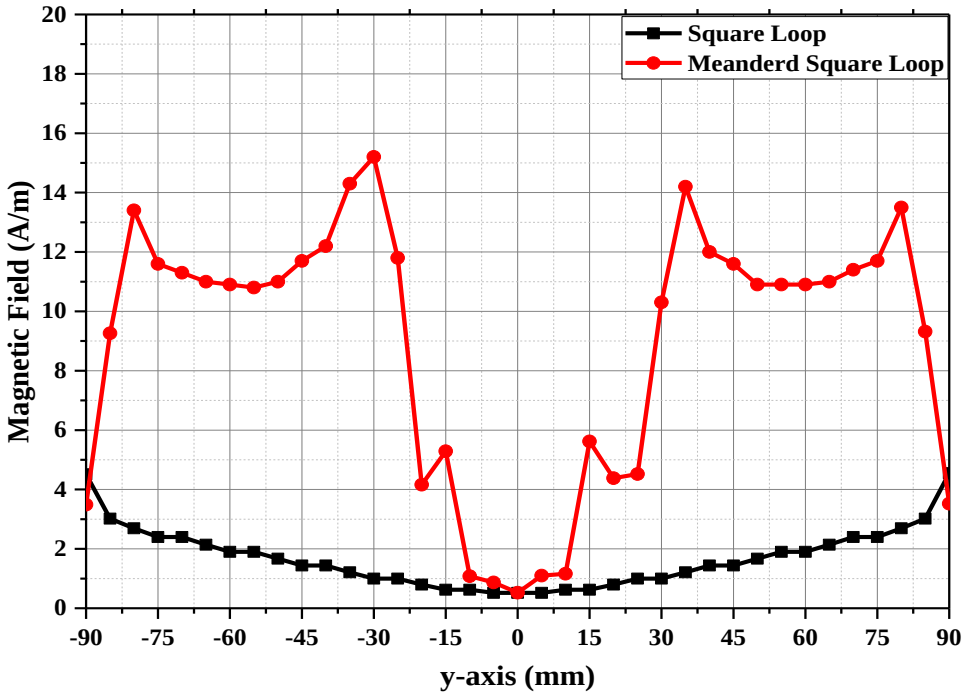

Fig. 4.13. Comparison of the generated magnetic field from meandered square loop and the conventional square loop antennas along y-axis.

The proposed antenna was fabricated by cutting 0.1mm copper sheet into shape. The fabricated prototype and the dimension details of the proposed antenna are depicted in Fig. 4.14. The measured reflection coefficient S_{11} is in very good agreement with the simulation as shown in Fig. 4.15. This antenna covers both the MICS band and ISM band around 433 MHz.

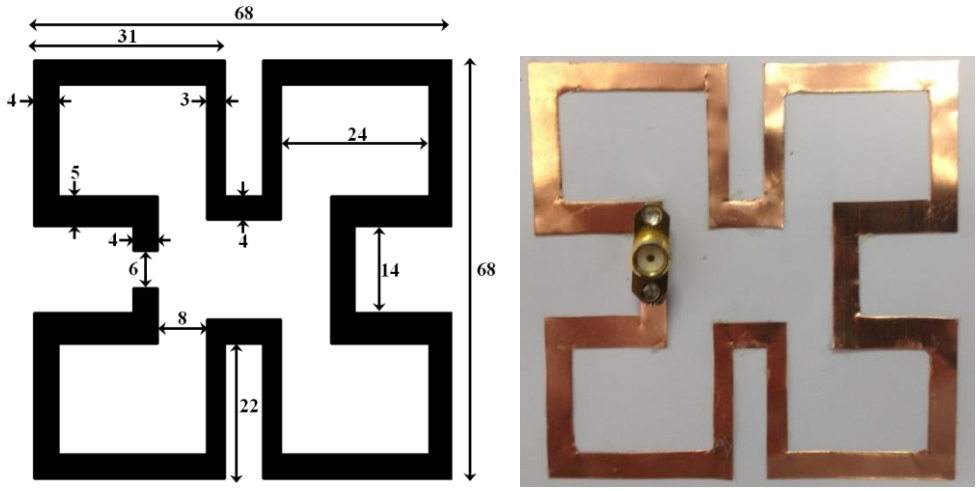

(a) **(b)**

Fig. 4.14. The meander square loop: (a) dimension details (all in mm) and (b) the fabricated prototype.

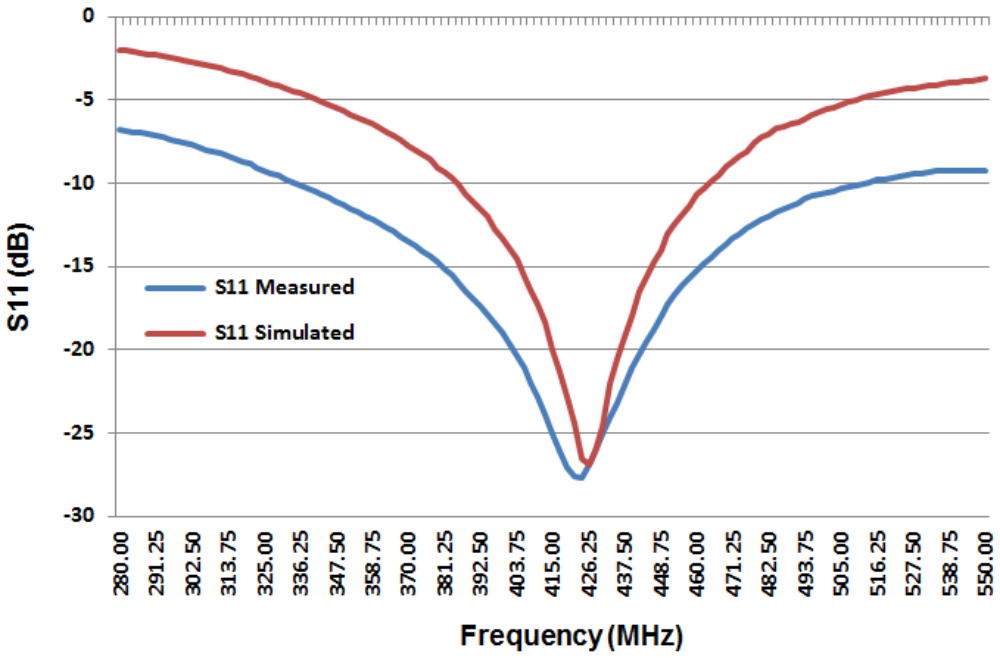

Fig. 4.15. The simulated and measured reflection coefficients of the meandered square loop antenna.

The magnetic field of both the conventional square loop and meander square loop antennas is measured by using an H-field probe as shown in Fig. 4.16. The measurement setup includes a signal generator to feed the antenna under test, an H-field probe to capture the generated field and a spectrum analyzer to read the power strength of the captured field.

The received power is measured at several distances from the antennas. Then the power is converted into equivalent flux density by using flux density calculators in spread sheet provided by the manufacturer of the probes.

A comparison between the flux density of the square and meandered square loops is depicted in Fig. 4.17. This figure shows that the meandered square loop antenna has stronger magnetic field in the near field region.

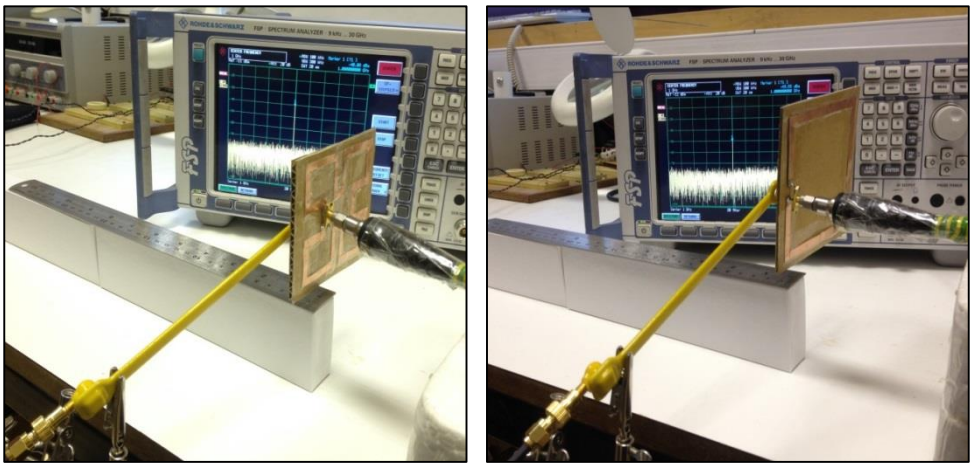

Fig. 4.16. The experiment setup of measuring the magnetic field of the meandered and conventional square loop antennas using H-field probe.

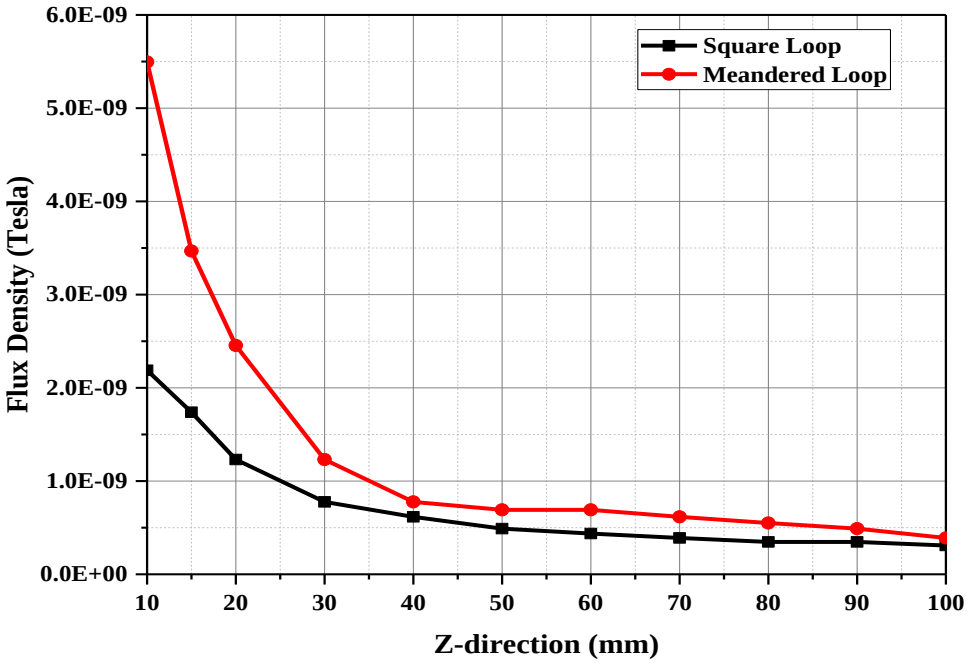

Fig. 4.17. The measured magnetic field for both square and meandered square loops using H-field probe.

4.2.3 High Magnetic Loop Wearable Antenna

This design is proposed to improve the magnetic field in near field WPT. The magnetic field in the internal area of the loop can be consolidated through creating fields that can be combined constructively as discussed in subsection (4.2.2). A redirection of the surface current is proposed in this work. A strong magnetic field and redistribution to the magnetic flux can be achieved by dragging the exciting port into the internal area deeply to form a High Magnetic loop antenna as shown in Fig. 4.18(a). The antenna has been meandered more at the sides to get a smaller antenna size at the same operating frequency. The proposed antenna covers both the MICS band and the ISM band around 433 MHz. A photograph of the fabricated prototype of the proposed antenna is shown in Fig. 4.18(b). This antenna was fabricated by cutting a copper sheet into shape. The thickness of the copper sheet is 0.1 mm.

The new design offers strong surface currents along two different axes x and y as shown in Fig. 4.19. With this design two advantages have been achieved: the first one is to generate combined magnetic fields constructively in the antenna area. The second one is that the generated magnetic field is strong along two different axes in

the xy-plane of the antenna. Currents along two axes generate magnetic lines vertically and horizontally in closed lines as shown in Fig. 4.20. The dense orthogonal lines provide better coupling with the receiver at different locations and then improve WPT.

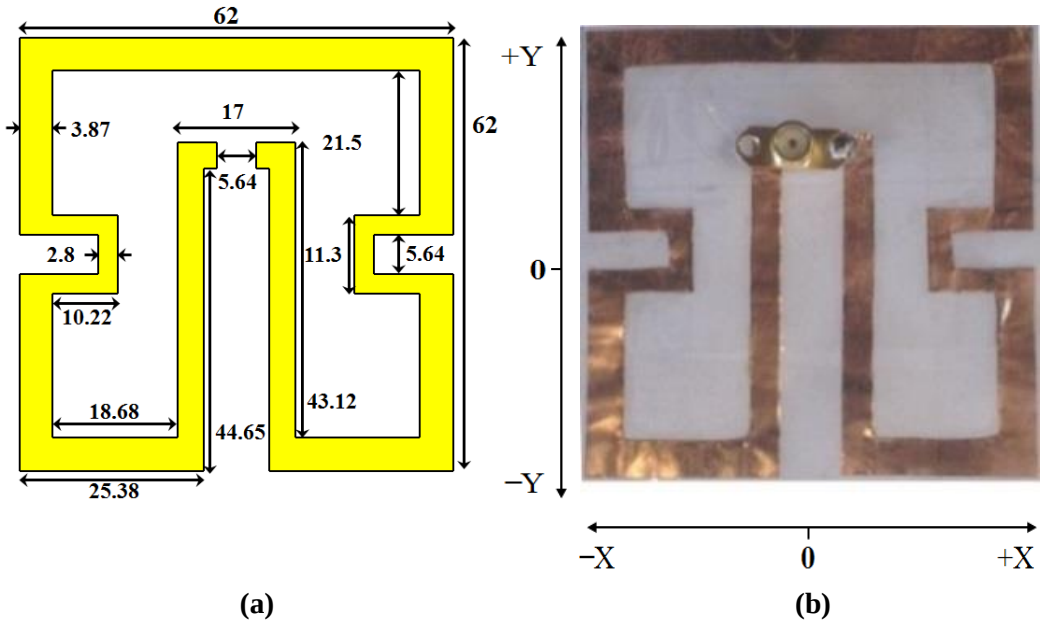

Fig. 4.18. The proposed antenna: (a) detailed dimensions in mm and (b) the fabricated prototype.

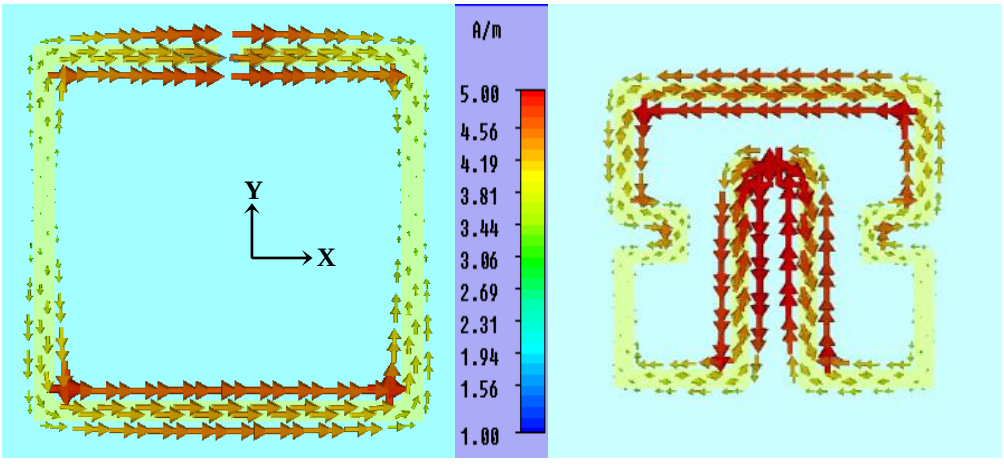

Fig. 4.19. Surface current distribution of (a) the square loop antenna and (b) the High Magnetic loop antenna.

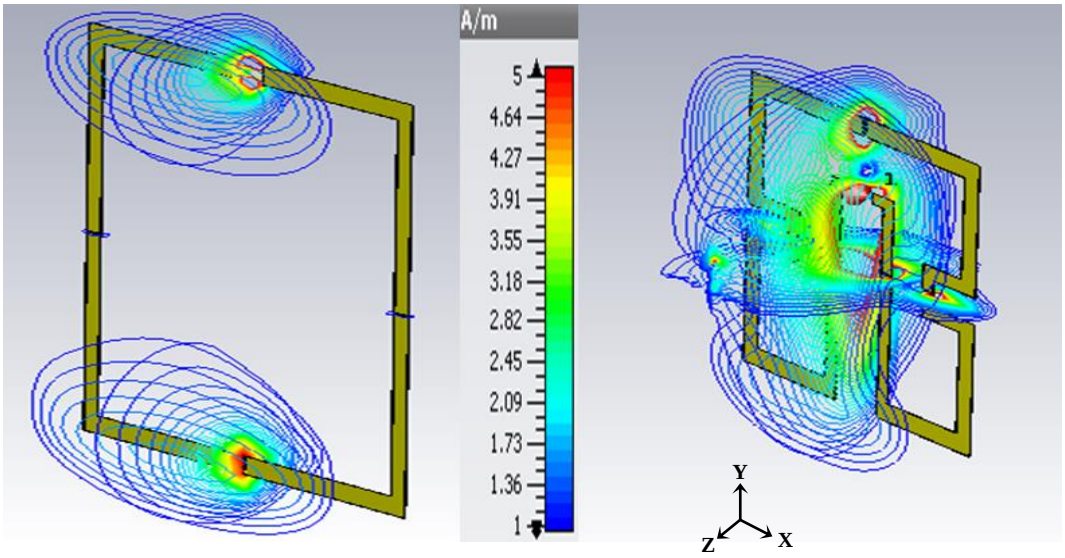

Fig. 4.20. Comparison between the square and the proposed antennas in term of magnetic field distribution.

The simulated total radiation efficiency and gain of this antenna are 1.13% and -16.5 dB respectively. These values are expected to be low due to the high power absorption by the tissue. The antenna is suitable for in-body communication at the MICS band with an implantable antenna and for off-body communication as a repeater between the implantable antenna and an external far away reader based on the link budget [14].

To validate the advantages of the High Magnetic loop antenna, a square loop is optimized to cover the desired bands using CST software. It has size of 90 mm × 90 mm with a 5.4 mm strip width and a 8.6 mm feeding gap. The reflection coefficients S_{11} of the standard square loop and the proposed High Magnetic loop antennas are shown in Fig. 4.21. The proposed loop has a narrower bandwidth due to the meandering structure but still has sufficient bandwidth of 65 MHz to cover the desired bands. The proposed loop antenna was evaluated using CST Microwave Studio on a Gustav voxel body model and a simplified body model as shown in Fig. 4.22.

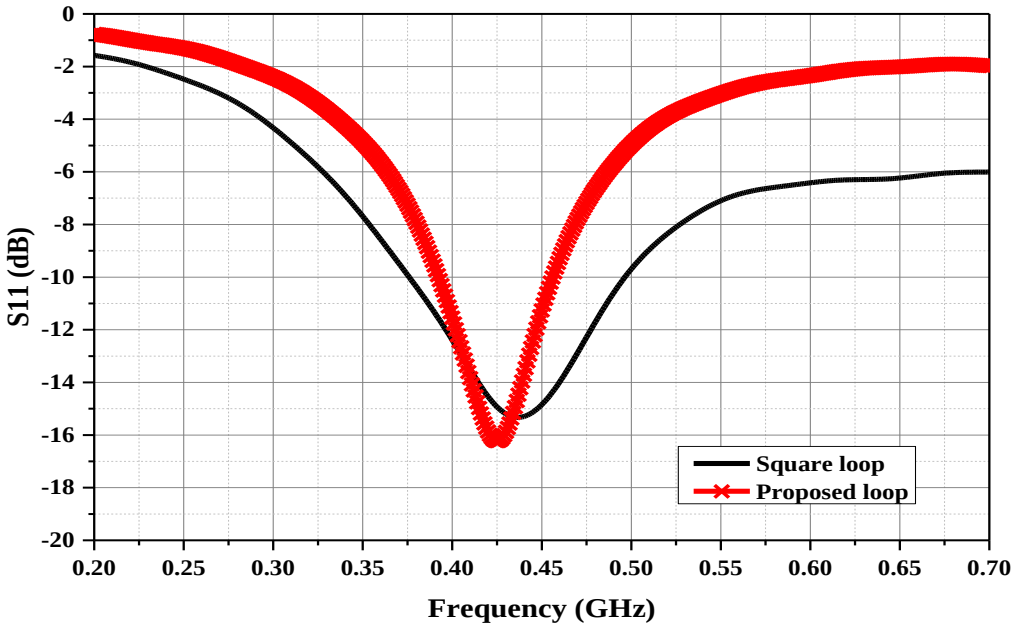

Fig. 4.21. The S_{11} of the proposed High Magnetic loop and the traditional square loop antennas.

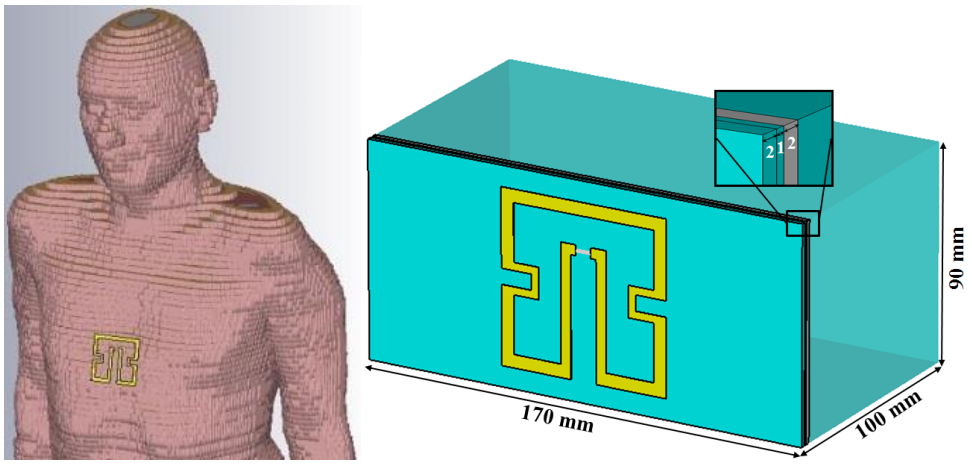

Fig. 4.22. Gustav voxel body model and a simplified body model that used for the simulation.

The simplified body model consists of 4 layers with properties defined as a bio tissue from the CST Voxel family. These properties are broadband from 0.1 – 3 GHz as previously shown in Table 4.2. The thicknesses of these layers are 2 mm, 1 mm, 2 mm and 95 mm for clothes, skin, fat and muscle, respectively. The results on both body models are found in good agreement so the simplified body model was used in

most simulations. The size of the simplified body model is chosen to be consistent with a container that will be used for WPT measurements as will be shown in the following chapter.

The generated magnetic field strength for the proposed antenna in z-direction was examined along two major axes of the xy-plane and compared with the conventional square loop antenna as shown in Fig. 4.23. In this figure, the field of the traditional square loop is shown in grid which is dominant mostly along x-axis. The internal area has weak field because the field lines are combined destructively as mentioned before. However, the field still exists although weak because the conductor that contains the feeding port has the highest surface current and will contribute with stronger field. The effect of this weakness on the coupling will be very obvious when the receiver is moved along y-axis. In the case of the High Magnetic loop antenna, the combined magnetic fields exist along both x and y axes and stronger than the conventional case as indicated by horizontal bars shown in Fig. 4.23.

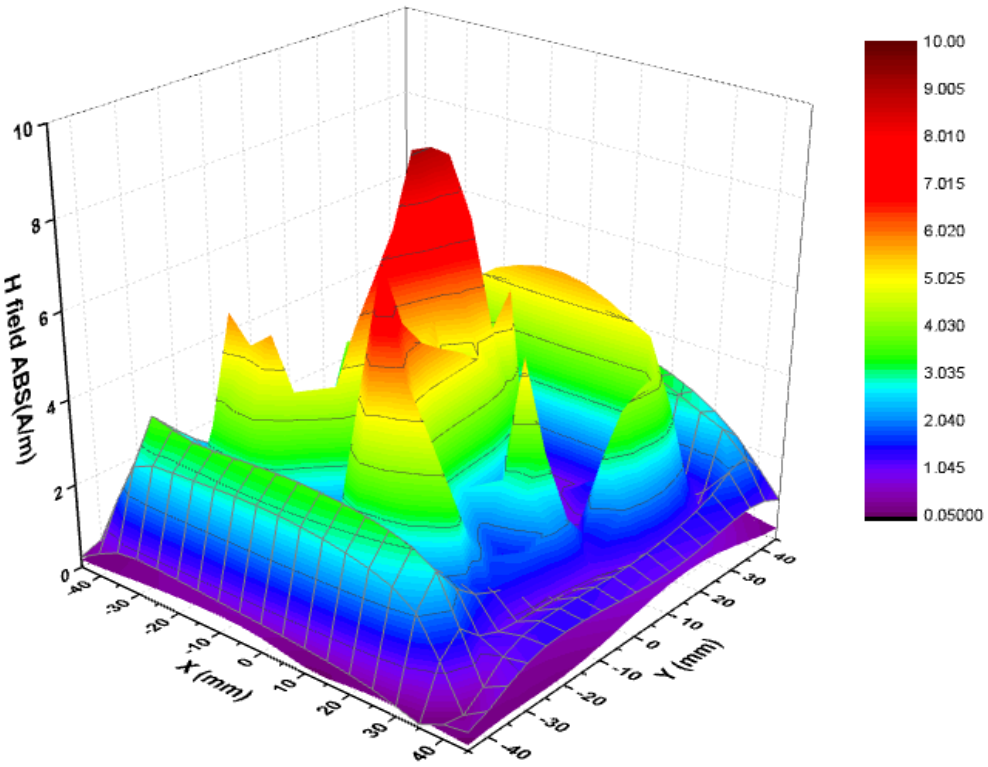

Fig. 4.23. The magnetic field strength along x and y offsets for the proposed and the square loop antennas. The square loop antenna results are indicated by grids. The results for the proposed deep-port antenna are indicated by horizontal bars.

It is noticed also that the middle area has the strongest field because it contains the excitation port. These fields come from the entire area of the antenna as compared with the traditional one which generates field mostly along the sides. This gives more flexibility and better coupling to the receiver in terms of offset in some directions as will be seen in the following chapter.

The maximum transmit power to be used within the safety regulations can be computed according to SAR limits as explained in chapter 2. The FCC SAR regulation of 1.6 W/kg per 1-g averaging was considered to determine the usability of the proposed wearable antenna limits. It was found by calculating the SAR using CST Microwave Studio that the proposed design can be used with a transmit power of up to 274 mW.

4.3 Implantable Antenna Design

Design of implantable antenna is a big challenge since it is aimed to operate inside a human body. The body is an asymmetrical and inhomogeneous medium. The performance of the antenna will vary based on the following:

- The part of the body that the antenna is implanted into.
- The depth of the antenna inside the body.
- The thickness variation of the tissue layers around the antenna.

Since our target in this research is to investigate the possibility of using antennas for WPT and communications in one compact antenna, simple implantable antennas will be used in this research.

As discussed in chapter 2, the target bands for this research are the MICS band for communications and the ISM band around 433 MHz for WPT. The implantable antenna to be used in this investigation should cover both bands. A loop antenna was already chosen as the candidate. In this section, two implantable loop antennas will be discussed. The first one is a simple loop that was used with one of the designed rectifiers for the far-field WPT experiment as will be discussed in the following chapter. The second antenna is an optimized one based on the High Magnetic loop wearable antenna. This antenna was used in the following chapter with the wearable antenna for near-field WPT experiment.

4.3.1 Flexible Loop Implantable Antenna

The proposed antenna is a flexible loop antenna. It was designed for implantable applications and fabricated by using a very thin layer of a copper sheet with a thickness of 0.04 mm. The loop structure antenna can be bent around implants. It provides good matching at the MICS band and the ISM band around 433 MHz. The antenna diagram and dimension details are shown in Fig. 4.24.

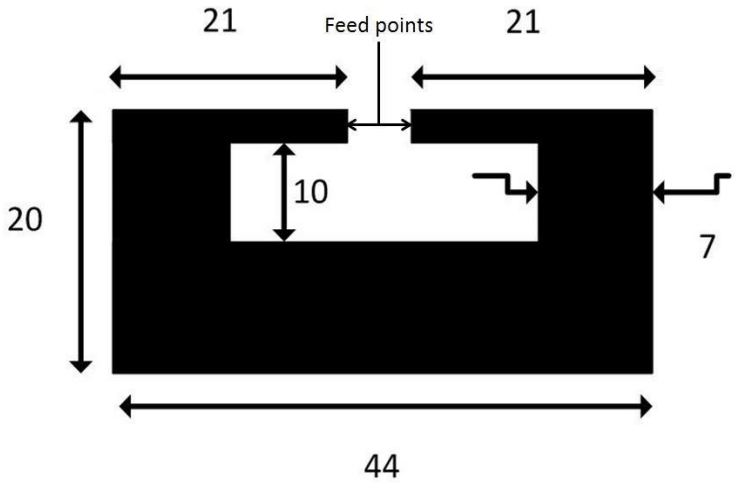

Fig. 4.24. Dimension details of the implantable loop antenna (all units in mm).

This antenna can be used for implants of a radius 7.5 mm and a length of 20 mm. The antenna is simulated and measured in cylindrical shape body model with dimensions as shown in Fig. 4.25. The tissue properties of dielectric constant and conductivity are 57.1 and of 0.79 S/m respectively. It has a realized gain of -20.1 dB including the body loss. The total radiation efficiency of the antenna is 0.387 %. These parameters are relatively large as compared with other implantable antennas because the size of the antenna is relatively larger [15, 16]. The three-dimensional radiation pattern of the proposed antenna is shown in Fig. 4.26.

Safety limits according to SAR are calculated for this antenna. The FCC SAR of 1.6 W/kg averaged on 1-g of tissue is considered. This antenna can be used with up to 13 mW of transmitted power. This antenna can be used with up to 65 mW of transmitting power according to ICNIRP regulation.

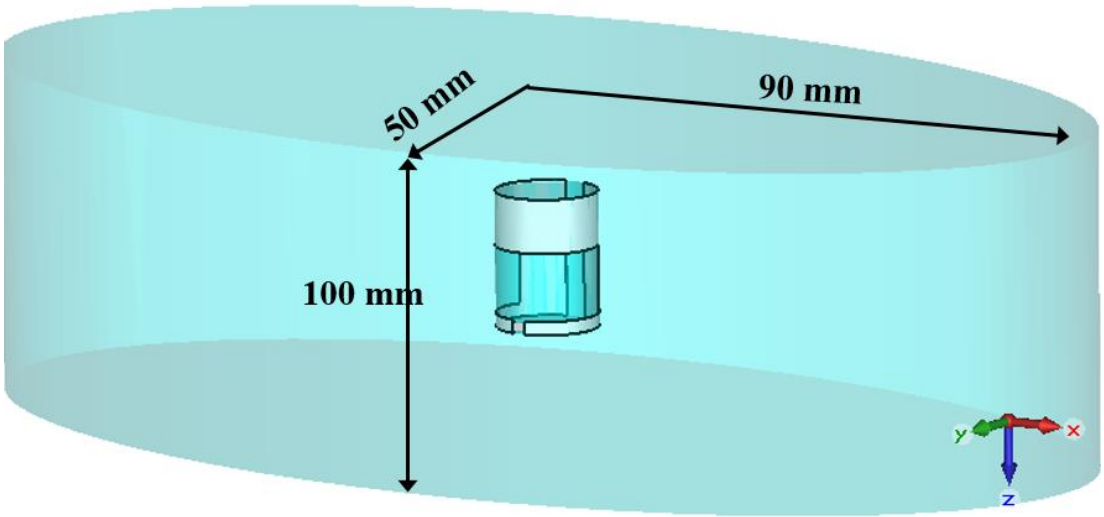

Fig. 4.25. Body model to test the implantable loop antenna (all units in mm).

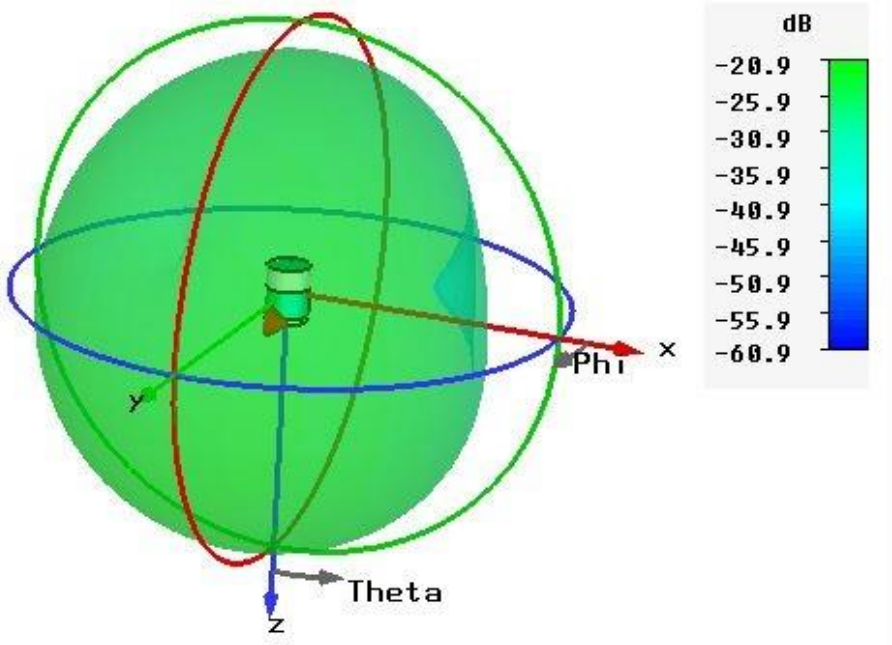

Fig. 4.26. The simulated three-dimensional radiation pattern of the proposed antenna.

The reflection coefficient of the antenna was measured. It is in good agreement with the simulated one as shown in Fig. 4.27.

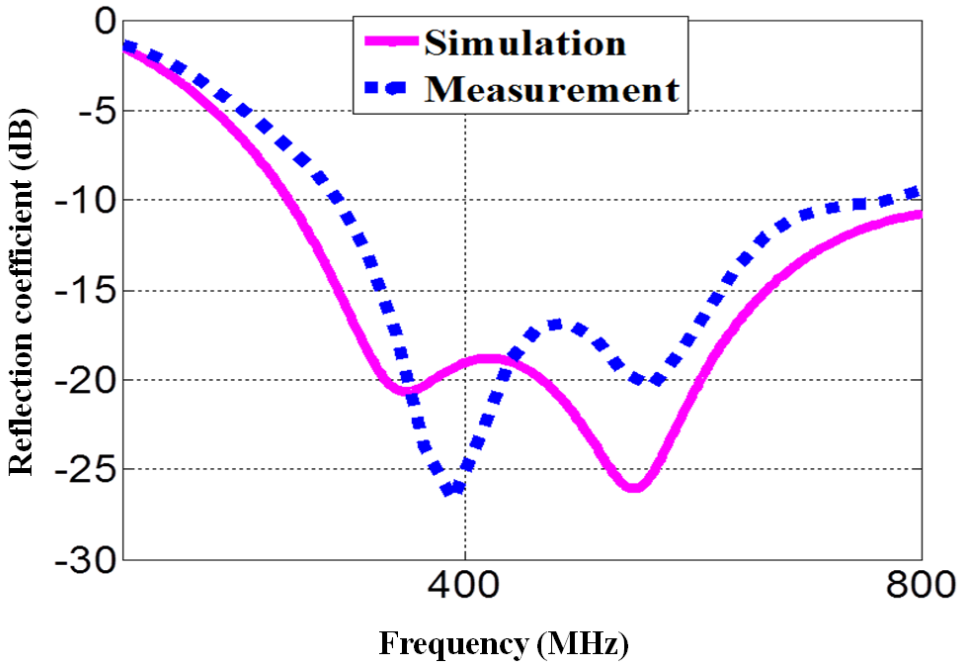

Fig. 4.27. The simulated and measured S_{11} of the implantable loop antenna.

4.3.2 Meandered Flexible Loop Implantable Antenna

An implantable loop antenna was designed to have a structure similar to the proposed High Magnetic loop wearable antenna as shown in Fig. 4.28. This structure can be bent around cylindrical implants with a minimum size of 11 mm in length and 3.5 mm in radius so that very little space will be occupied by the antenna. This implantable antenna shows broadband response in both cases, flat and bent, as shown in Fig. 4.29.

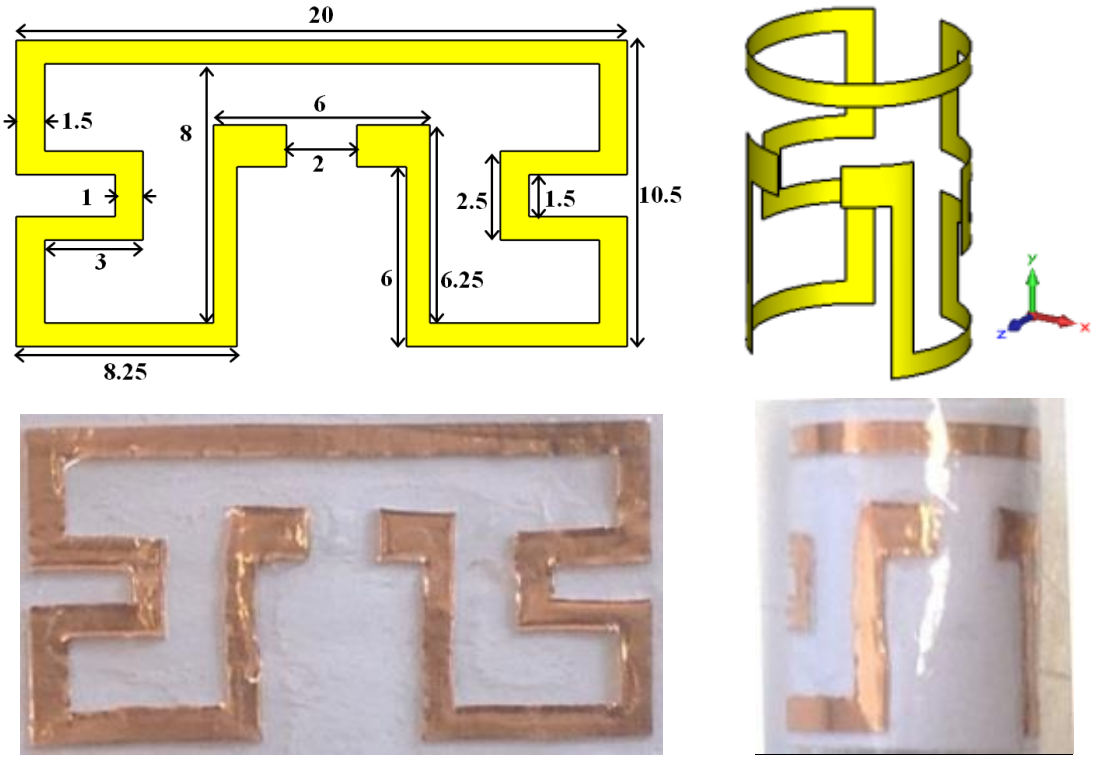

Fig. 4.28. Size and photographs of the fabricated implantable antenna, all dimensions in mm.

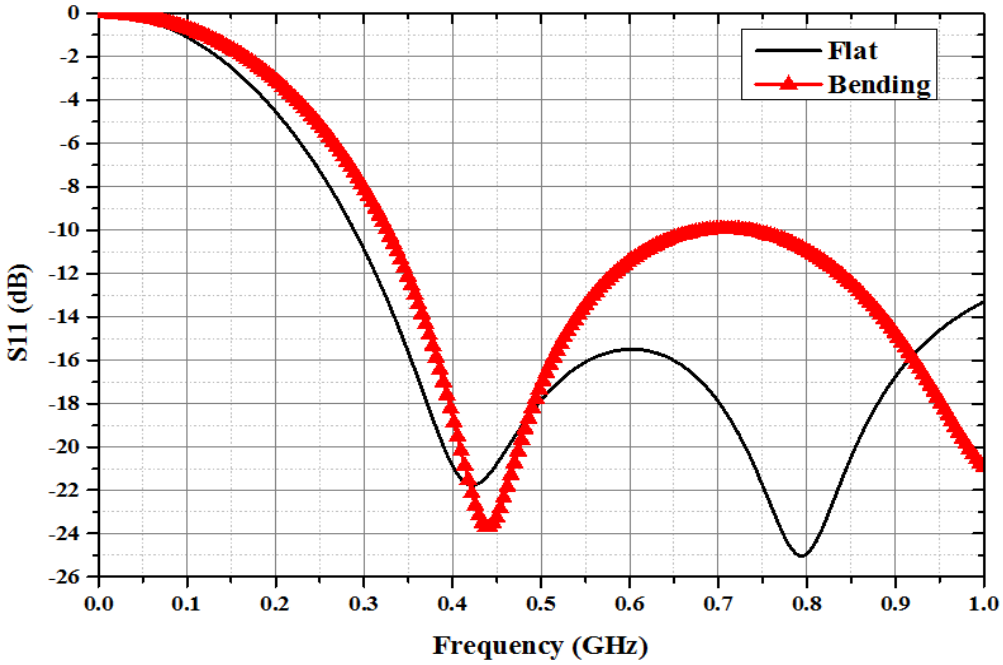

Fig. 4.29. The reflection coefficient S_{11} of the proposed implantable antenna in two cases: flat and bending.

The discrepancy in the response shape might be from the bending surfaces. These surfaces could generate parasitic capacitance which causes a bit mismatching at certain frequencies. However, both structures cover well the desired bands of 402-405 MHz and 433 MHz. The radiation efficiency and gain of the implantable antenna are 0.056% and -28.5 dB respectively. These values are expected due to the high loss of body tissues and the small size of the antenna.

The implantable antenna was fabricated by cutting a thin copper sheet with a thickness of 0.04 mm into shape. To prevent direct contact of the antenna material with the tissue, the implantable antenna was surrounded by a thin Polypropylene adhesive tape of 0.04 mm. This thin layer has negligible effect on the antenna performance.

4.4 Summary and Conclusion

In this chapter, wearable and implantable antenna designs have been introduced. The wearable antenna can be used on body for in body communications and for WPT. It can be used potentially as a repeater between the implantable antenna and a faraway external reader. In this chapter, three wearable antenna designs were proposed:

- A novel butterfly wearable loop antenna was designed to cover several medical bands with two wideband of 600 MHz from 400 to1000 MHz and 700 MHz from 2 to 2.7 GHz.
- A meandered square loop wearable antenna was designed to improve the magnetic field in the near field region of the antenna for better WPT.
- A novel approach to improve the efficiency of WPT is proposed. This was done by introducing the High Magnetic loop wearable antenna. This antenna is able to generate two orthogonal strong magnetic fields.

Implantable loop antennas are introduced as well. These antennas are intended to be integrated with rectifier circuits to form rectennas. The overall rectenna and wearable antennas or far field transmitting antennas can form a compact system for WPT and communication.

References

[1] H. Wang, Z. J. Zhang, Y. Li, and Z. H. Feng, "A Dual-Resonant Shorted Patch Antenna for Wearable Application in 430 MHz Band," *IEEE Transactions on Antennas and Propagation,* vol. 61, pp. 6195-6200, Dec 2013.

[2] Q. Wang, R. Hahnel, H. Zhang, and D. Plettemeier, "On-body directional antenna design for in-body UWB wireless communication," in *2012 6th European Conference on Antennas and Propagation (EUCAP)*, pp. 1011-1015, 2012.

[3] E. Moradi, K. Koski, T. Bjorninen, L. Sydanheimo, J. M. Rabaey, J. M. Carmena*, et al.*, "Miniature Implantable and Wearable On-Body Antennas: Towards the New Era of Wireless Body-Centric Systems," *IEEE Antennas and Propagation Magazine,* vol. 56, pp. 271-291, Feb 2014.

[4] J. S. Ho, A. J. Yeh, E. Neofytou, S. Kim, Y. Tanabe, B. Patlolla*, et al.*, "Wireless power transfer to deep-tissue microimplants," *Proceedings of the National Academy of Sciences,* vol. 111, pp. 7974-7979, 2014.

[5] Z. H. Jiang, D. E. Brocker, P. E. Sieber, and D. H. Werner, "A Compact, Low-Profile Metasurface-Enabled Antenna for Wearable Medical Body-Area Network Devices," *IEEE Transactions on Antennas and Propagation,* vol. 62, pp. 4021-4030, Aug 2014.

[6] M. E. Jalil, M. K. A. Rahim, N. A. Samsuri, O. Ayop, M. A. Abdullah, and M. F. Ismail, "Investigation the performance of Koch fractal multiband textile antenna for on-body measurement," in *2012 Asia Pacific Microwave Conference Proceedings*, pp. 1373-1375, 2012.

[7] M. M. Khan, M. Magani, A. Rahman, and C. Parini, "A dual band planar inverted F antenna for body-centric wireless communications," in *Passive RF and Microwave Components, 3rd Annual Seminar on*, pp. 57-64, 2012.

[8] T. Thalmann, Z. Popovic, B. M. Notaros, and J. R. Mosig, "Investigation and Design of a Multi-band Wearable Antenna," *2009 3rd European Conference on Antennas and Propagation, Vols 1-6,* pp. 425-428, 2009.

[9] R. Nagarjun, G. George, D. Thiripurasundari, R. Poonkuzhali, and Z. C. Alex, "Design of a Triple Band Planar Bow-Tie Antenna for Wearable Applications," *2013 IEEE Conference on Information and Communication*

Technologies (Ict 2013), pp. 1185-1189, 2013.

[10] D.-O. Kim, C.-Y. Kim, and D.-G. Yang, "Flexible Hilbert-curve loop antenna having a triple-band and omnidirectional pattern for WLAN/WiMAX applications," *International Journal of Antennas and Propagation,* vol. 2012, 2012.

[11] K. L. Wong, W. Y. Chen, and T. W. Kang, "On-Board Printed Coupled-Fed Loop Antenna in Close Proximity to the Surrounding Ground Plane for Penta-Band WWAN Mobile Phone," *IEEE Transactions on Antennas and Propagation,* vol. 59, pp. 751-757, Mar 2011.

[12] Y. W. Chi and K. L. Wong, "Internal compact dual-band printed loop antenna for mobile phone application," *IEEE Transactions on Antennas and Propagation,* vol. 55, pp. 1457-1462, May 2007.

[13] herbzinser, "http://region2.herbzinser03.com/blogenginenet/herb09/image.axd?picture=%2F2015%2F06%2Fcurrent-causing-magnetic-field-right-hand-rule-2.png."

[14] S. Agneessens, P. Van Torre, E. Tanghe, G. Vermeeren, W. Joseph, and H. Rogier, "On-Body Wearable Repeater as a Data Link Relay for In-Body Wireless Implants," *IEEE Antennas and Wireless Propagation Letters,* vol. 11, pp. 1714-1717, 2012.

[15] R. S. Alrawashdeh, Y. Huang, M. Kod, and A. A. Sajak, "A Broadband Flexible Implantable Loop Antenna With Complementary Split Ring Resonators," *IEEE Antennas and Wireless Propagation Letters,* vol. 14, pp. 1506-1509, 2015.

[16] A. Kiourti and K. S. Nikita, "Miniature Scalp-Implantable Antennas for Telemetry in the MICS and ISM Bands: Design, Safety Considerations and Link Budget Analysis," *IEEE Transactions on Antennas and Propagation,* vol. 60, pp. 3568-3575, Aug 2012.

Chapter 5

Experimental of Far Field and Near Field WPT

5.1 Introduction

This chapter focuses mainly on experiments for Wireless Power Transfer (WPT). These experiments are done in two techniques: far-field and near-field. For far field experiment, the implantable system mainly consists of our designs including the rectifier and the implantable antenna while the external transmitter can be represented by any traditional far field antenna. This experiment is to confirm the usability of flexible antennas in this technique and how efficient can be achieved within safety limits. Near field WPT is mostly done using a system of our designs including the transmitting wearable antenna, the implantable antenna and the rectifier. This system is proposed to improve WPT.

5.2 Far Field WPT

Far field WPT is a promising solution to transfer power to the implantable medical devices. The setup usually consists of an external transmitter, implantable antenna and implantable rectifier to convert RF signal to DC. The efficiency of this technique depends mainly on the performance of the implantable system since the transmit power by the external antenna is restricted to a certain level by safety regulations. This performance is associated with the conversion efficiency of the rectifier and the gain, the total radiation efficiency and the radiations pattern of the implantable antenna. In this section, experiments to study the far field technique are proposed. The proposed implantable loop antenna and rectifier shown in Fig. 5.1 are used in these experiments.

The rectifier and antenna are integrated with a cylindrical tube of biocompatible Propylene material as an implant as shown in Fig. 5.2. The dielectric properties of this implant has negligible effect on the performance of the antenna [1].

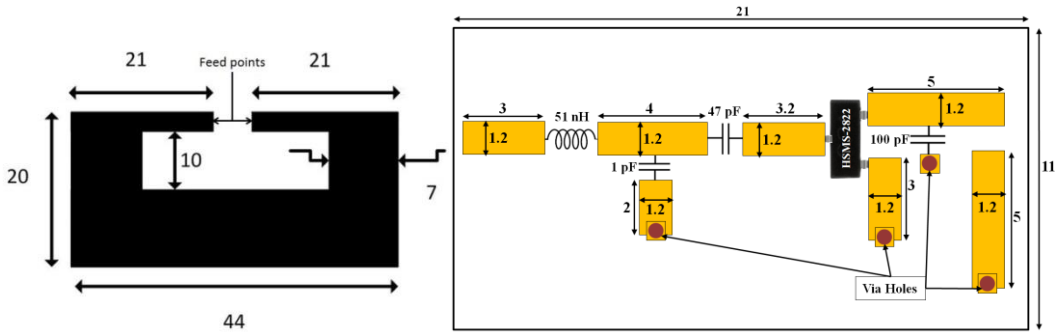

Fig. 5.1. Implantable antenna and rectifier circuit that used in the far field WPT experiments.

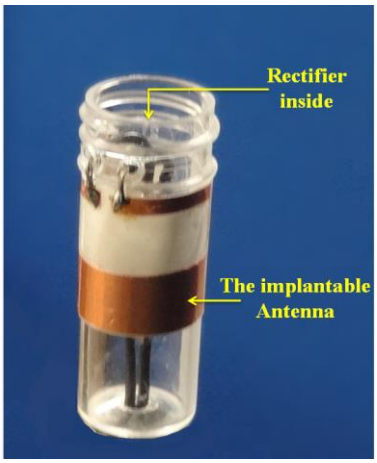

Fig. 5.2. The implantable antenna and rectifier are integrated on a tube of Propylene.

The far field WPT experiments are done using a Log Periodic Antenna (LPDA) with a gain of around 6 dBi. The body model phantoms that used in the experiments to mimic human tissues are pork and liquid body models. The liquid body model is prepared by adding mixture of salt and sugar to the water while heating the water up until getting dielectric constant of 57.1 and conductivity of 0.79 S/m. The properties of this liquid is measured using an Agilent 87050E dielectric probe [1].

5.2.1 Voltage Measurement on a Load

In this experiment, the received voltage on a load of 4.7 kΩ was measured first when the implantable rectenna is placed in pork. The experiment setup includes the transmitting LPDA antenna, a voltmeter to measure the voltage on the load, and pork

as a body phantom as shown in Fig. 5.3. A signal generator is used to feed the transmit antenna with a 433 MHz signal and an amplifier to boost the transmit power. The rectenna was placed inside pork with a depth of 3 cm and the experiment was done in an anechoic chamber. The voltage was measured at different separations (from 10 cm to 100 cm) between the transmitting and receiving antennas. At each separation distance, the voltage was recorded versus a sweep of the transmit power (EIRP) from 27 dBm to 46 dBm as shown in Table. 5.1. The received voltage was increasing with decreasing the separation distance and with increasing the transmit power. This response is expected due to the attenuation in the free space and in pork.

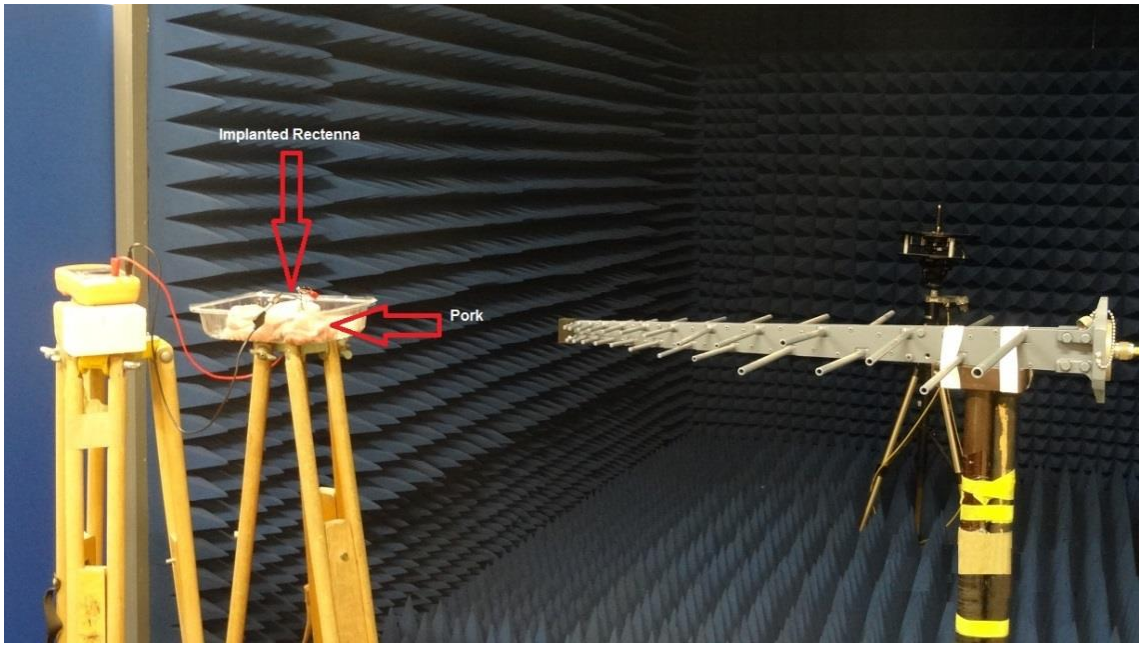

Fig. 5.3. Far field WPT experiment of the rectenna that placed in pork.

The experiment was carried out again but this time in a liquid body model as shown in
Fig. 5.4. In this experiment, the antenna is placed inside the liquid after insulation by a thin Polypropylene adhesive tape of 0.04 mm. the rectifier is connected to the implantable antenna through a coaxial cable. The received voltage was measured versus separation distances (from 10 cm to 50 cm). At each distance, the voltage was measured against sweep of transmit power (from 27 dBm to 46 dBm) as shown in Table. 5.2.

Table. 5.1. Received voltage on a load versus distance and sweep of transmit power.

Pork	Log periodic transmitting Antenna and 4.7 KΩ Load								
EIRP dBm ➔	27	31	35	40	41	42	43	44	46
Distance (cm) ↓	V_{OUT} (V) ↓								
100	0.17	0.42	0.84	1.56	1.72	2.12	2.28	2.5	3.2
75	0.28	0.61	1.18	2.12	2.37	2.89	3.17	3.47	4.3
50	0.36	0.75	1.42	2.61	2.9	3.55	3.87	4.3	5.66
40	0.5	0.96	1.75	3.2	3.53	4.28	4.76	5.25	7
30	0.51	1.01	1.89	3.35	3.78	4.66	5.13	5.5	7.3
25	0.6	1.13	2.05	3.67	4.1	5.05	5.5	5.92	7.77
20	0.62	1.2	2.15	3.81	4.24	5.2	5.7	6.2	7.95
15	0.66	1.22	2.25	3.95	4.4	5.36	5.86	6.35	8
10	0.68	1.3	2.35	4.1	4.53	5.54	6.03	6.49	8.2

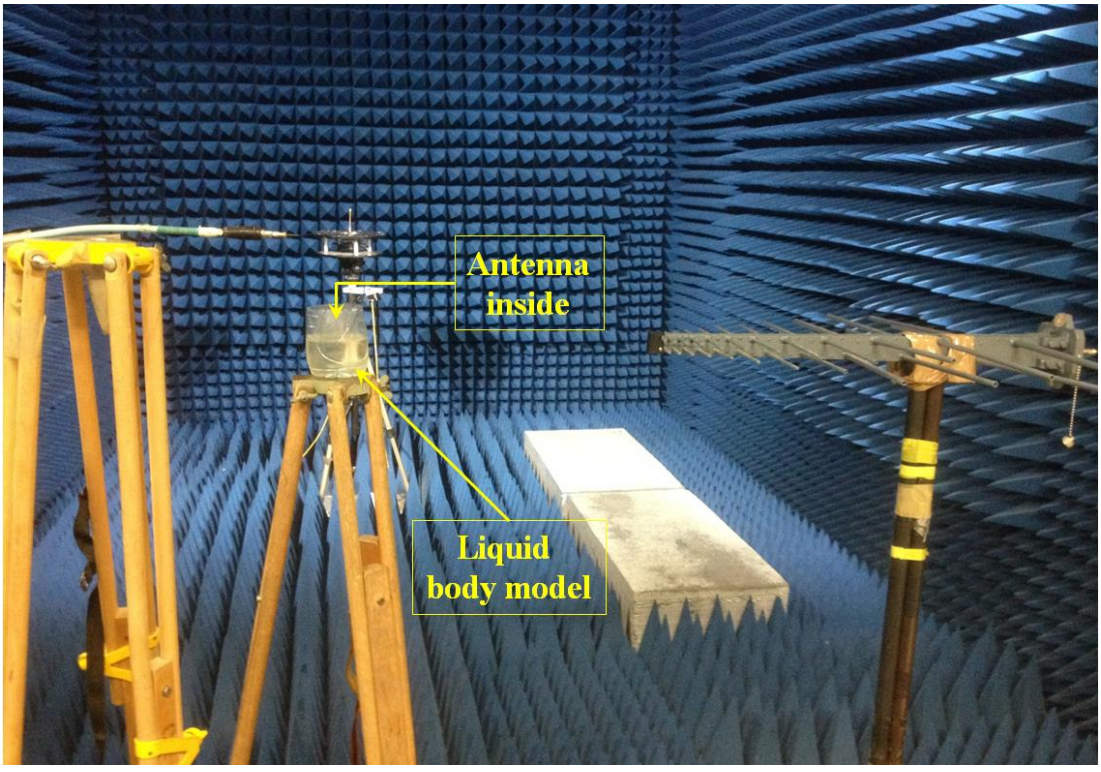

Fig. 5.4. Far field WPT experiment inside anechoic chamber in Liquid body model.

The received power in the liquid body model is less than that in pork. The reason for this is that the liquid absorbs more power than pork. As discussed in Chapter 2, the

major parameter for absorbing power is the water in cells of the tissue. Since the human body consists of tissues that contains water, then the experiment results with pork tissue is more accurate than results with liquid. A comparison between the received power in pork and liquid body models is depicted in Fig. 5.5.

Table. 5.2. Received voltages in liquid body model.

Liquid	Log periodic transmitting Antenna and 4.7 KΩ Load					
EIRP dBm ➔	27	31	35	40	44	46
Distance (cm) ↓	V_{OUT} (V) ↓					
50	0.14	0.4	0.87	1.66	2.72	3.58
40	0.18	0.47	1	1.86	3.05	3.9
30	0.2	0.51	1.05	1.96	3.13	4.15
25	0.22	0.55	1.12	2.06	3.35	4.33
20	0.25	0.58	1.18	2.18	3.58	4.47
15	0.28	0.65	1.28	2.32	3.74	4.75
10	0.33	0.74	1.45	2.62	4.16	5.25

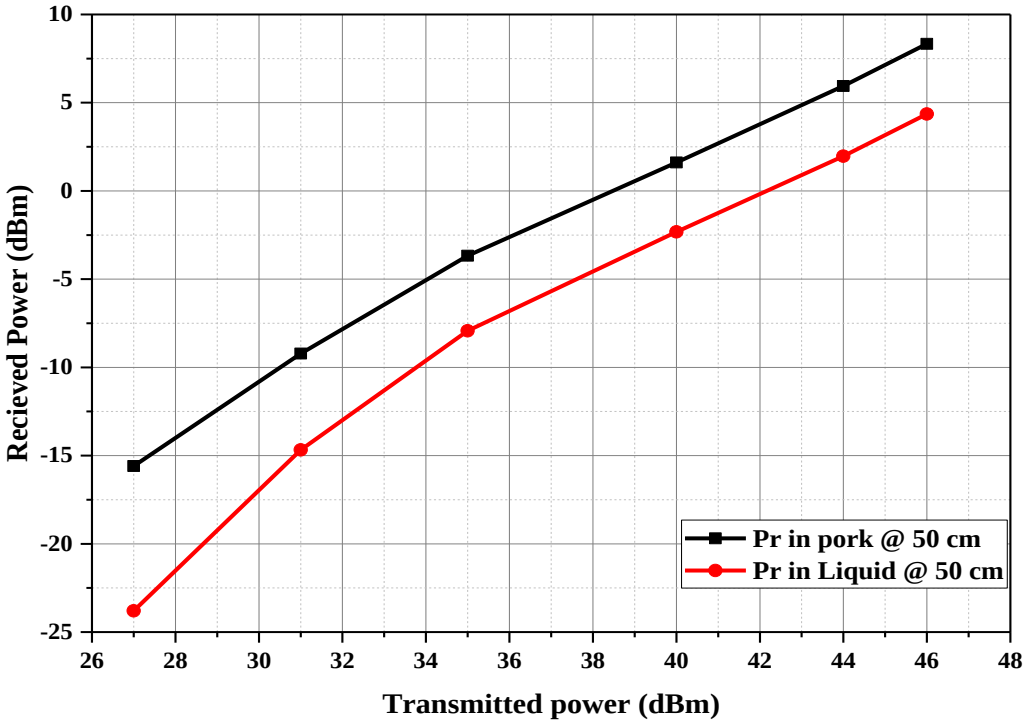

Fig. 5.5. A comparison between the received power in pork and liquid body models at 50 cm separation.

5.2.2 Charging Current Delivered to the Battery

The charging current was measured on a realistic implantable battery of 50 mA•h that reported in Chapter 3. The measurement was done at different separations (from 10 cm to 50 cm) between the transmitting and receiving antennas with a sweep of the transmitted power (from 27 dBm to 46 dBm). Charging currents of about 1 mA and 3 mA were confirmed at a separation of 50 cm when the transmit power is within the public and controlled safety limits respectively. Larger harvested currents were obtained at closer distances because of the path loss. A comparison between the received currents at 25 cm and 50 cm separation distances is shown in Fig. 5.6. Charging currents measurement versus distance is shown in Table. 5.3.

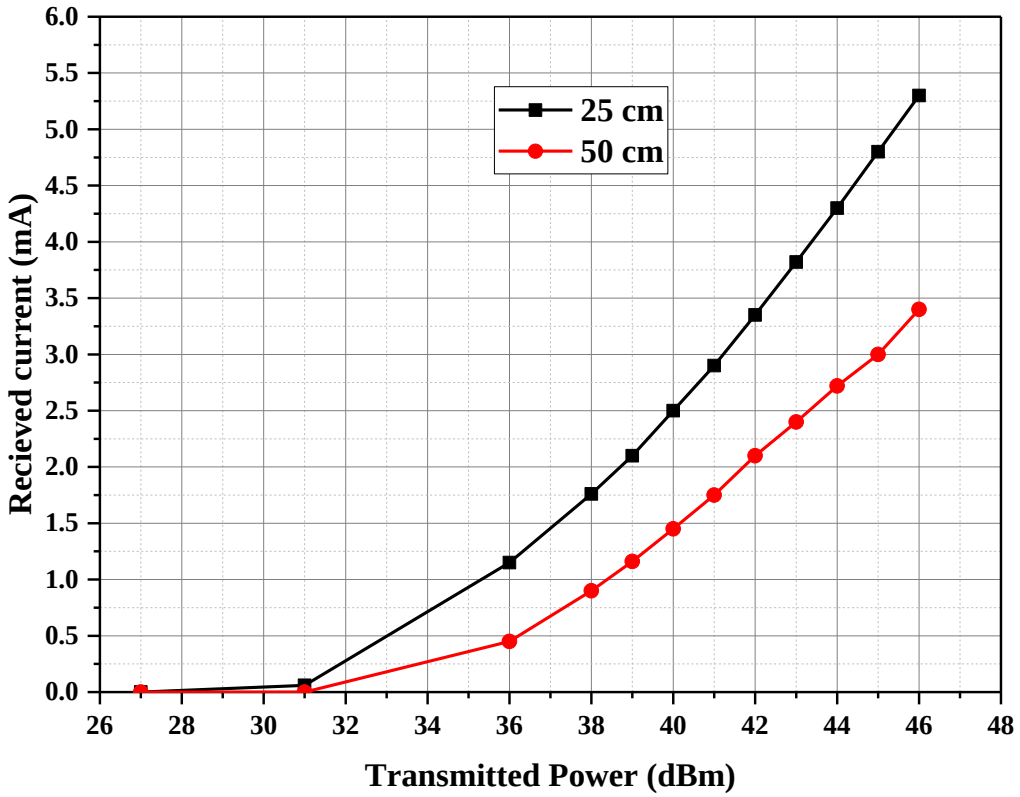

Fig. 5.6. The measured charging current of the candidate battery at 25 cm and 50 cm separation distances.

Table. 5.3. Charging current experiment of the battery in pork.

Pork	The charging current for the implantable Lithium battery load of 50 mA•h											
EIRP dBm ➔	27	31	36	38	39	40	41	42	43	44	45	46
Distance (cm) ➔	Received current (mA) ➔											
50	0	0	0.45	0.9	1.16	1.45	1.75	2.1	2.4	2.72	3	3.4
40	0	0	0.71	1.24	1.53	1.86	2.2	2.6	2.95	3.33	3.7	4
30	0	0	0.93	1.5	1.84	2.2	2.6	3.06	3.5	4	4.45	4.9
25	0	0.06	1.15	1.76	2.1	2.5	2.9	3.35	3.82	4.3	4.8	5.3
20	0	0.15	1.3	1.95	2.34	2.75	3.18	3.67	4.17	4.69	5.2	5.7
10	0	0.26	1.53	2.23	2.63	3	3.53	4	4.55	5.1	5.66	6.15

5.2.3 Discussion of Safety Limits

Far field WPT is controlled by Maximum Permissible Exposures (MPEs) that was explained in Chapter 2. This means that the level of the transmit power by far field external antenna to the body at any distance should fall within the safety limits. For WPT at 433 MHz, the power density allowed to be exposed to the human body in the public environment is (2.165 – 2.88) W/m^2. In the controlled environment the safety power density limit is higher up to (10.825 - 14.4) W/m^2 [2-5]. The maximum transmit power versus distance at 433MHz can be calculated according to the power density equation (2.1) that was described in Chapter 2 as

$$S = \frac{P_T\, G_T}{4\pi R^2}$$

Where $P_T G_T$ represents Effective Isotropic Radiated Power (EIRP). This EIRP will be considered for the maximum transmitted power from the transmitting antenna. The lowest power density limits of 2.165 W/m^2 for public and 10.825 W/m^2 for controlled environment are considered in calculations. The EIRP versus distance is depicted in Fig. 5.7.

The proposed design of implantable antenna and rectifier was able to deliver certain levels of voltage and current to the load. The voltage level versus distance that can be delivered to the load using the proposed design within safety limits is shown in Fig. 5.8. These voltages on the load of 4.7 kΩ represent a receiving power of (2.24 mW to 0.32 mW) in public environment and (9 mW to 1.33 mW) in controlled environment for separation distances from 10 cm to 100 cm. The charging current versus distance that can be supplied within the safety limits to the custom battery using the proposed design is shown in Fig. 5.9. The generated currents are able to charge efficiently small batteries with capacity of equal or less than 10 mA•h.

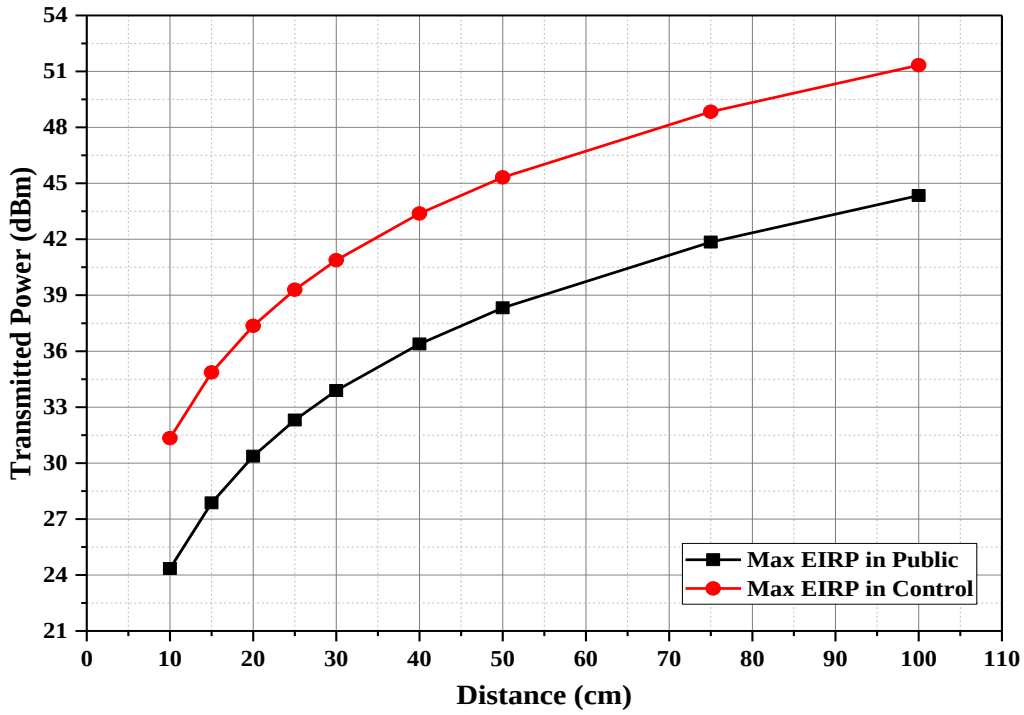

Fig. 5.7. Maximum transmitted power versus distance according to the maximum exposure limit at 433 MHz for both the public and controlled environments.

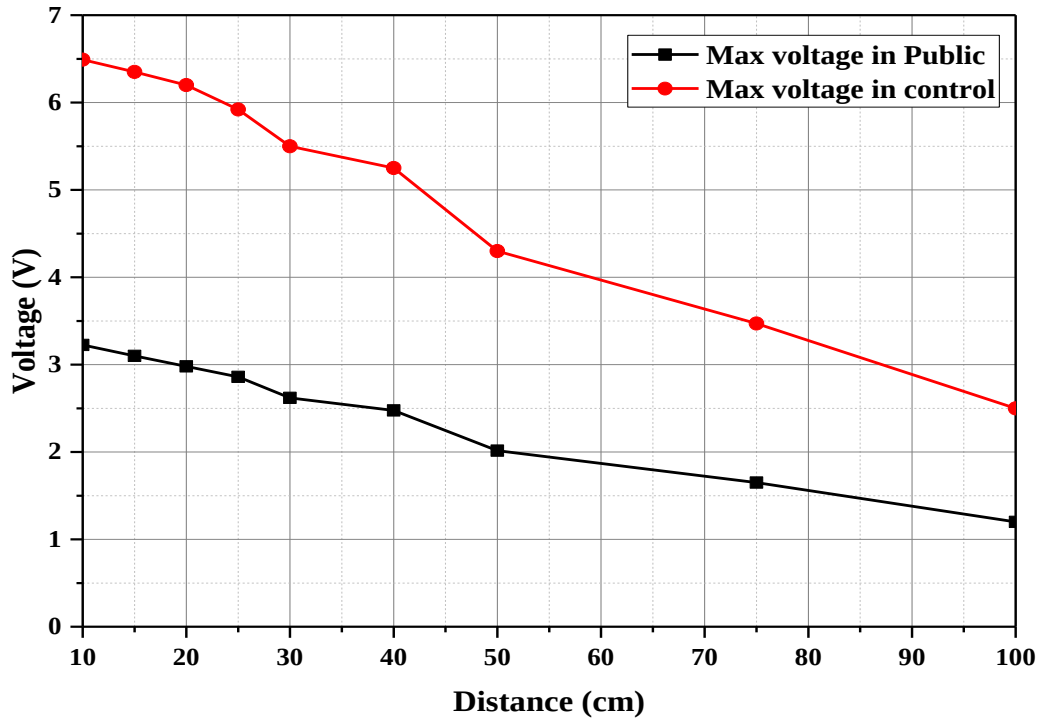

Fig. 5.8. Maximum delivered voltage to the load versus distance that the proposed design can provide within the safety limits.

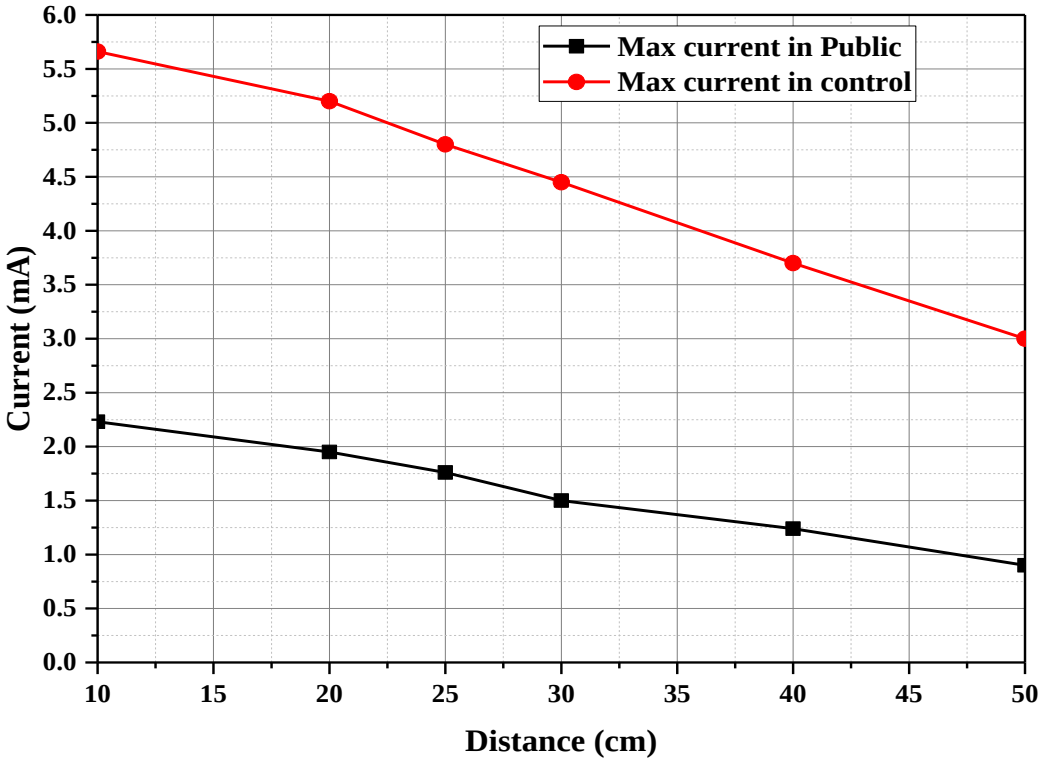

Fig. 5.9. Maximum charging currents within the safety limits that the proposed design can provide.

5.3 Near Field WPT

Near field inductive coupling between transmitters and receivers is an efficient way for WPT when they are in very close distance. For medical applications, wearable antennas are a promising candidate for inductive coupling to replace traditional coils. This is because that antennas can be useful for both far field and near field techniques. Loop antennas are the most commonly used antenna types on the body because of the high magnetic field in the near field region. Magnetic field has negligible interaction with biological materials [6] and then this antenna type is more robust against the detuning by the high permittivity of the body.

A loop antenna can be considered as a coil with one turn. The inductive coupling between two loops can be presented in the simplified circuit model as shown in Fig. 5.10. L, R and C are the self-inductance, resistance and capacitance of an antenna respectively. The mutual coupling between two loops is denoted by M. The subscripts p and s refer to the primary and the secondary loops respectively.

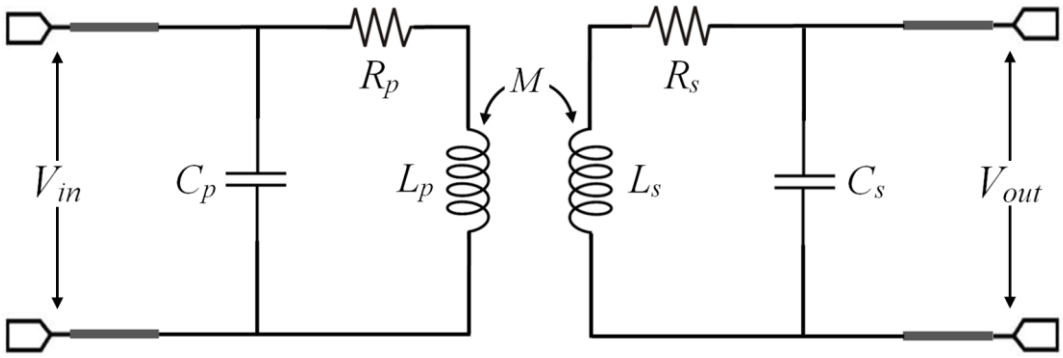

Fig. 5.10. Equivalent circuit of two coupled loops.

The improvement of WPT comes from better coupling coefficient k due to higher M according to the equation (2.15) from Chapter 2:

$$k = \frac{M}{\sqrt{L_p L_s}}$$

The traditional approach to improve WPT is to increase the magnetic field by increasing the self-inductance through adding more turns to the coil. This leads to

higher induced voltage at the receiver according to Faraday law in equation (2.14) from Chapter 2:

$$V_2 = i\omega\mu_0 \int H_1 . ds$$

However, any misalignment between coils can cause loss of the flux linkage and then reduction in WPT. WPT for implants is established between asymmetrical antennas where the implantable antenna is much smaller than the primary wearable transmitter. This is due to the effect of the high permittivity of body tissues. An accurate position for the implantable antenna with respect to the wearable is unguaranteed during implantation and hence the misalignment and then a reduction in WPT efficiency can occur.

It is important to find a proper design that can provide larger coupling when the receiver encounters a misaligned position. An understanding of the flux lines distribution can help in modifying this distribution to get better flux linkage with the receiver.

The magnetic field is distributed in closed lines around the source conductor. Larger induced voltage can be generated at the receiver when these lines cut the effective parts of the receiver antenna in an appropriate direction. This means that the z components of magnetic lines from horizontal conductor along x-axis by referring to Fig. 4.20 are distributed in vertical closed lines. It can induce voltage at the horizontal conductor of the receiver while it is less effective at the vertical conductors. The same scenario is true for the horizontal closed lines fields from vertical conductor.

As explained in Chapter 4, surface currents along antenna conductors generate a magnetic field around these conductors in a direction following the right hand rule. As a result, the generated fields can be in the same or opposite directions. In the case of the conventional loop antenna, the generated fields are in opposite direction in the centre area of the antenna and will cancel out each other. This leads to a weak magnetic field at the middle area and stronger at edges. A reshape for the generated magnetic field distribution was proposed in Chapter 4 by designing the High Magnetic loop antenna. This antenna can generate two orthogonal magnetic fields at the target receiver. These fields offer better coupling and an improvement in WPT.

5.3.1 Analysis of Coupling with Misalignment

The misalignment issue breaks the optimum operating condition of the WPT system and consequently the WPT efficiency can be significantly reduced. Previous works have been conducted to investigate and resolve this issue. Multiple circular coils were used as a solution for retinal implant system to improve WPT and reduce the misalignment effect in [7]. The typical receiver orientation and position for better WPT based on the magnetic field distribution were studied using spiral coils to tolerate the misalignment in [8]. In [9], a repeater coil between multiple transmitting and receiving coils was used. This repeater was proposed to reduce the misalignment effect and improve WPT by altering the orientation of the repeater. In [10], an adaptive impedance matching at the transmission side was used to improve axial misalignment. Other researchers suggested a solution to solve the misalignment by using parallel and orthogonal winding at the secondary coil in [11, 12]. In [13] a mix of circular spiral and helical coils in bowl shape have been used to compensate the misalignment issue. Another solution using square loop antennas was introduced in [14] by using distributed array of transmitting loops to improve lateral misalignment of WPT. Most of the suggested solutions are complicated and bulky especially for biomedical applications.

The proposed design of High Magnetic wearable and implantable loop antennas suggests a planar compact solution. No matching solutions or extra array elements are required to improve WPT. Furthermore, this design as antenna covers two bands Medical Implant Communication Service (MICS) and The Industrial, Scientific and Medical (ISM) around 433 MHz. These features make the proposed design very suitable for biomedical applications in terms of communication at MICS band and WPT at ISM around 433 MHz.

To demonstrate the feasibility of the design, the implantable antenna that presented in subsection (4.3.2) will be used as a receiver to work with the High Magnetic loop wearable antenna. To examine the WPT coupling improvement, the transmission coefficient S_{21} along different offset scenarios is simulated first using CST Microwave Studio. The implantable antenna was inserted 30 mm in depth in a body model. The body model consists of tissue, fat, skin and cloth layers as described in Chapter 4. The antenna then was shifted along x, y and (x, y) offsets and rotated

around the azimuth angle θ as indicated in Fig. 5.12. The simulated S_{21} is compared with S_{21} results from a standard square loop pair tested in the same scenario.

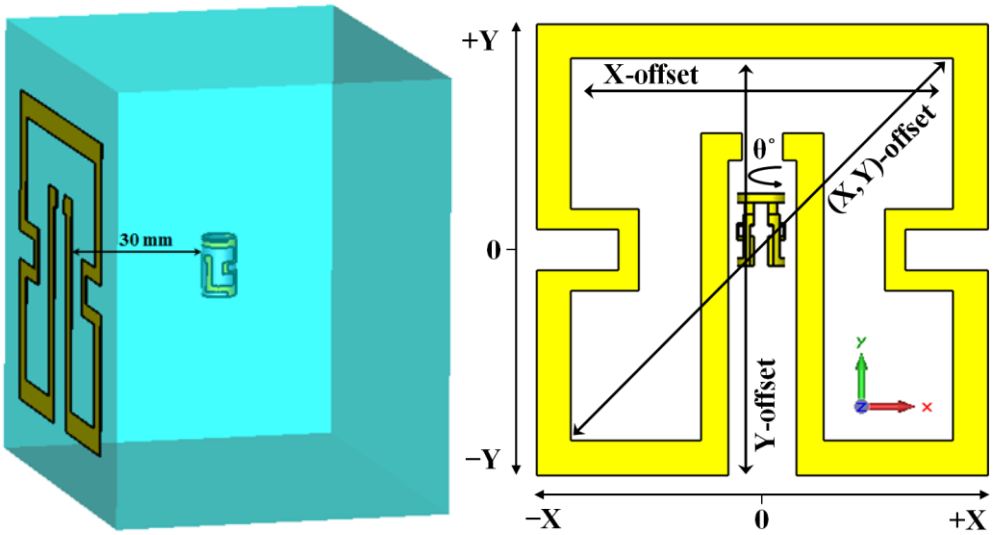

Fig. 5.11. The setup of testing S_{21} between the proposed pair of antennas.

The investigation was run first along x-axis as shown in Fig. 5.13. It is shown that when the implantable antenna has an offset along the x-axis, the proposed design has a similar response to the square loop. This is because that both pairs have relatively strong magnetic fields along the x-axis. However, the proposed pair offers improved efficiency with a magnitude of S_{21} is about 4 dB better as a result of the stronger magnetic field.

When the implantable antenna has an offset along y-axis, the effect of the orthogonal magnetic axes is very obvious. The proposed pair has approximately stable response against the offset with a better coupling in terms of S_{21}. The improved coupling is around 5 dB on average as compared with the square loop as shown in Fig. 5.14.

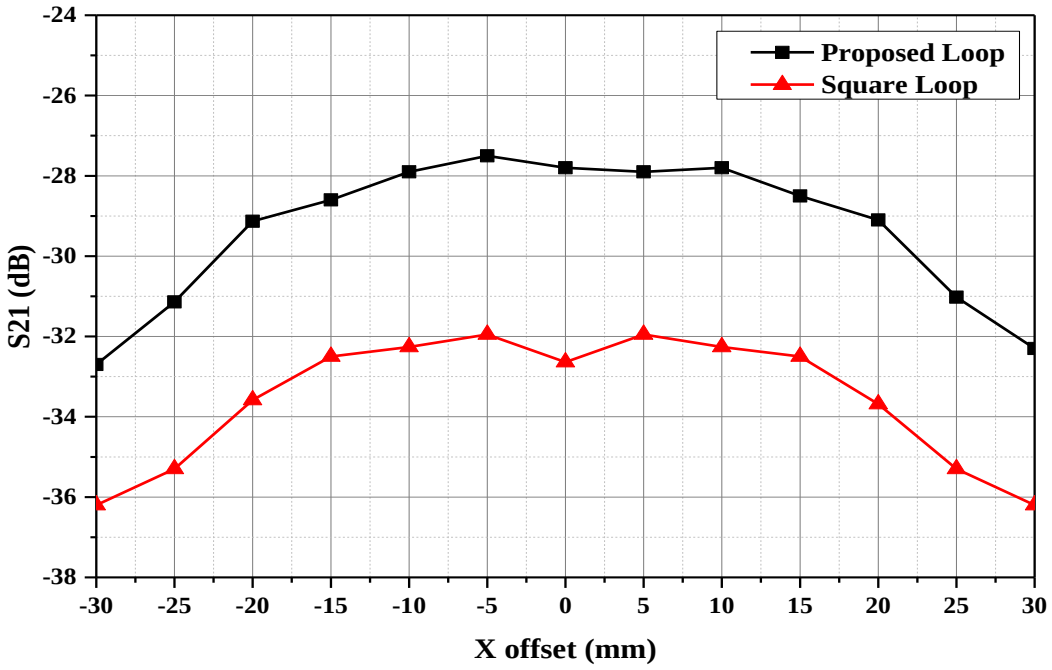

Fig. 5.12. The S_{21} comparison between the proposed and the square loop antennas along x-axis.

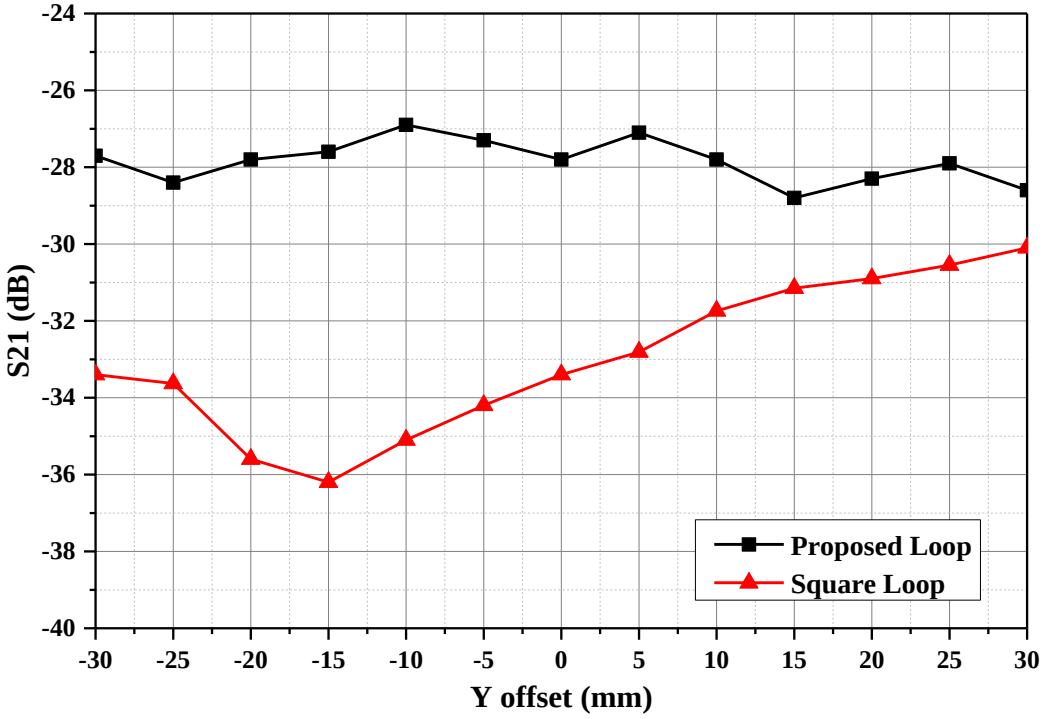

Fig. 5.13. The S_{21} comparison between the proposed and square loop antennas along y-axis.

The diagonal offset is shown in Fig. 5.15. The proposed pair has a more stable response compared with the square loop. In the case of the proposed pair, the difference between the highest and lowest coupling in terms of offset is around 5 dB while it is more than 7 dB in the case of square loop pair. The coupling is improved as well with an advantage of 2 dB up to 7 dB. This advantage comes from the strength of magnetic field along both x and y axes so that the weak coupling from one polarisation can be compensated by the other. The location of the exciting port in the internal area adds more advantages to the proposed design. The response is smoother and relatively symmetrical while the response of the square loop case is more biased toward the side where the exciting port is located.

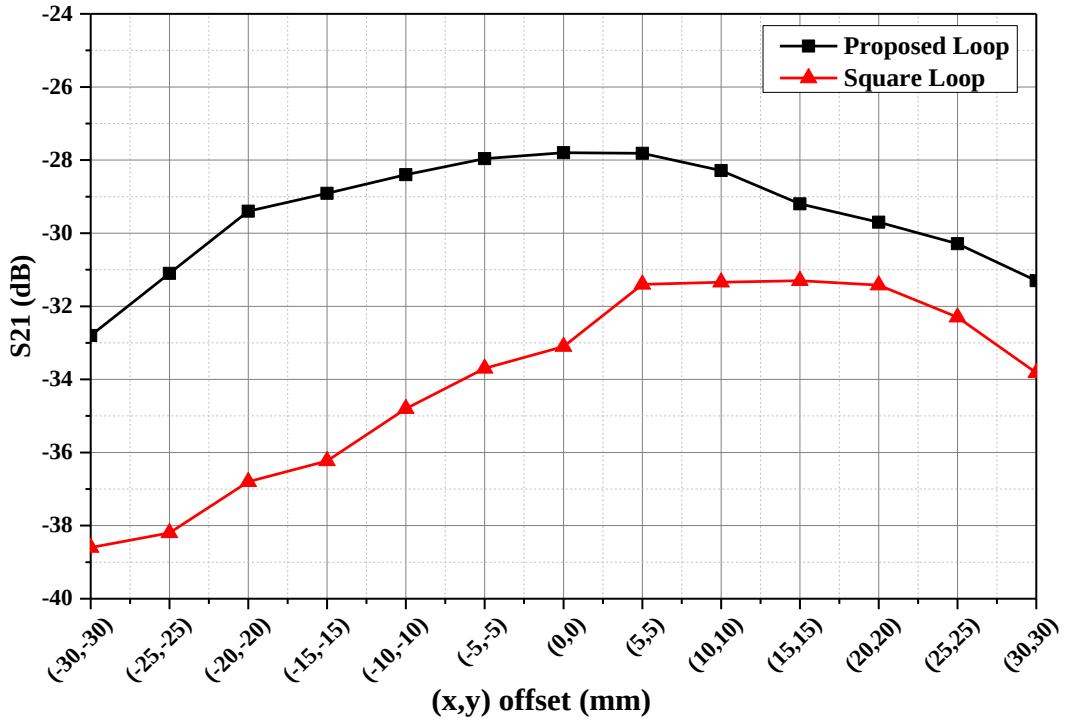

Fig. 5.14. The S_{21} comparison between the proposed and the square loop antennas along diagonal (x,y) offset.

The two pairs have been examined and compared with an angle offset. This offset was done by rotating the implantable antenna around the azimuth. The implantable antenna is rotated at the same position of 3 cm depth in the tissue. Wearable antennas were kept in the same position and orientation through the experiment. Responses of both pairs were similar so that the highest coupling occurs when the alignment angle

is 0˚ or 180˚ and the worst coupling when the transmitting and receiving antennas are misaligned by 90˚ angle. However, the proposed design still has higher coupling with S_{21} of up to 4 dB better as shown in Fig. 5.16.

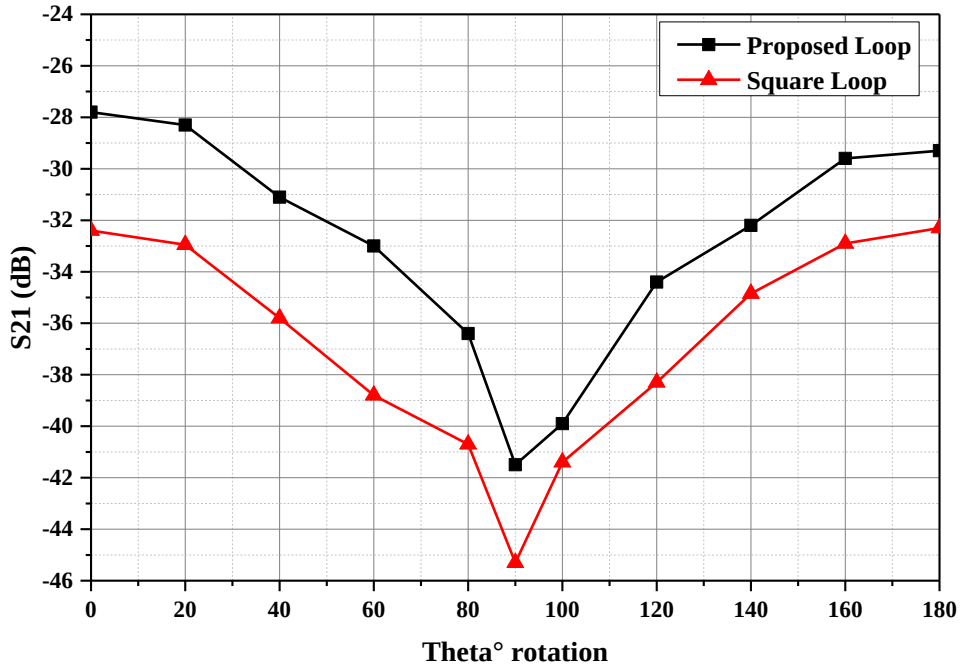

Fig. 5.15. The S_{21} comparison between the proposed and the square loop antennas along azimuth angle θ.

5.3.2 S_{21} Measurement for the Proposed System

The proposed design of the wearable and implantable antennas was fabricated and tested in minced pork. The transmission coefficient S_{21} was measured to validate the simulation.

The same procedure of examining S_{21} mentioned in section (5.3.1) was carried out. The offsets along x-axis, y-axis, diagonally with (x, y), and rotation around the azimuth angle θ were examined. The experiment setup includes a Vector Network Analyser (VNA) to measure S_{21} and a cubic container with size 9 cm × 10 cm × 17 cm filled with minced pork to mimic body tissues as shown in Fig. 5.17.

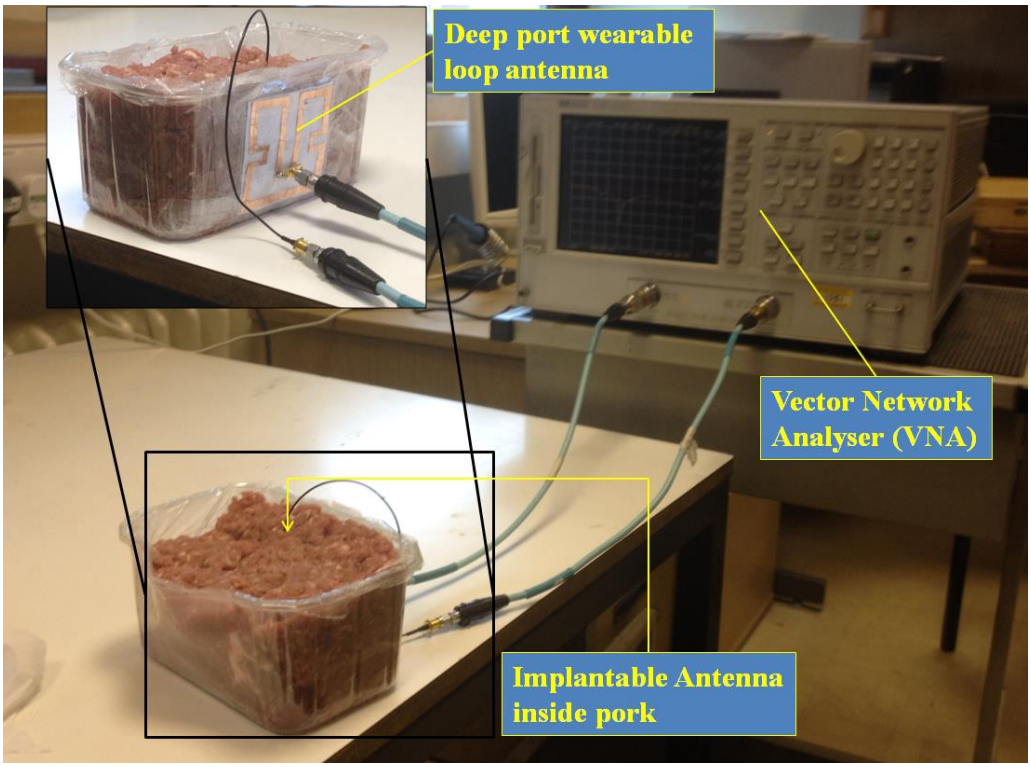

Fig. 5.16. The experiment setup of measuring S_{21} versus offsets of the proposed pair.

The measured result along x-axis showed similar response to the simulated one as shown in Fig. 5.18. A difference in magnitude of 1 dB on average is noticed. This might be due to the inhomogeneous of minced pork around the implantable antenna during the experiment. The S_{21} along y-axis offset was measured as well as shown in Fig. 5.19. The result showed very good agreement with the simulated results with around 1 dB difference in magnitude.

Along diagonal offset of (x,y), the measured results of S_{21} agreed with the simulation. However, measured results showed a little bit higher magnitudes towards the negative part of x and y axes shown in Fig. 5.20. This is logical if it is referred to Fig. 4.21 in Chapter 4. In that figure the magnitude of the magnetic field in the negative part of the antenna is higher than the positive part. This is because of the location of the exciting port near the middle and the surface current on the internal conductor along y-axis is stronger towards the negative part.

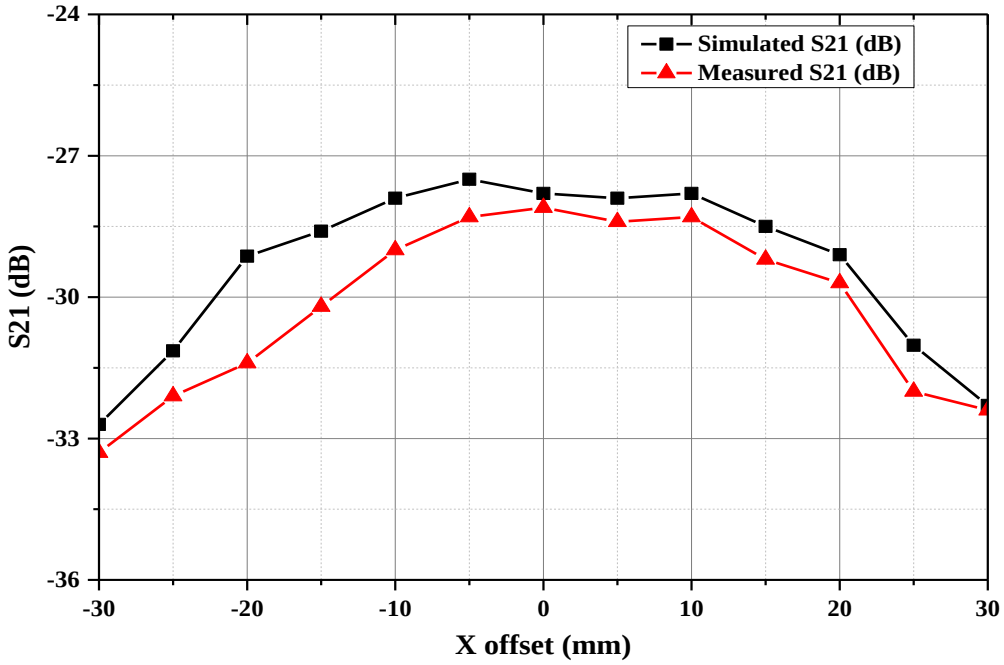

Fig. 5.17. The simulated and measured S_{21} of the proposed pair antennas with x-axis offset.

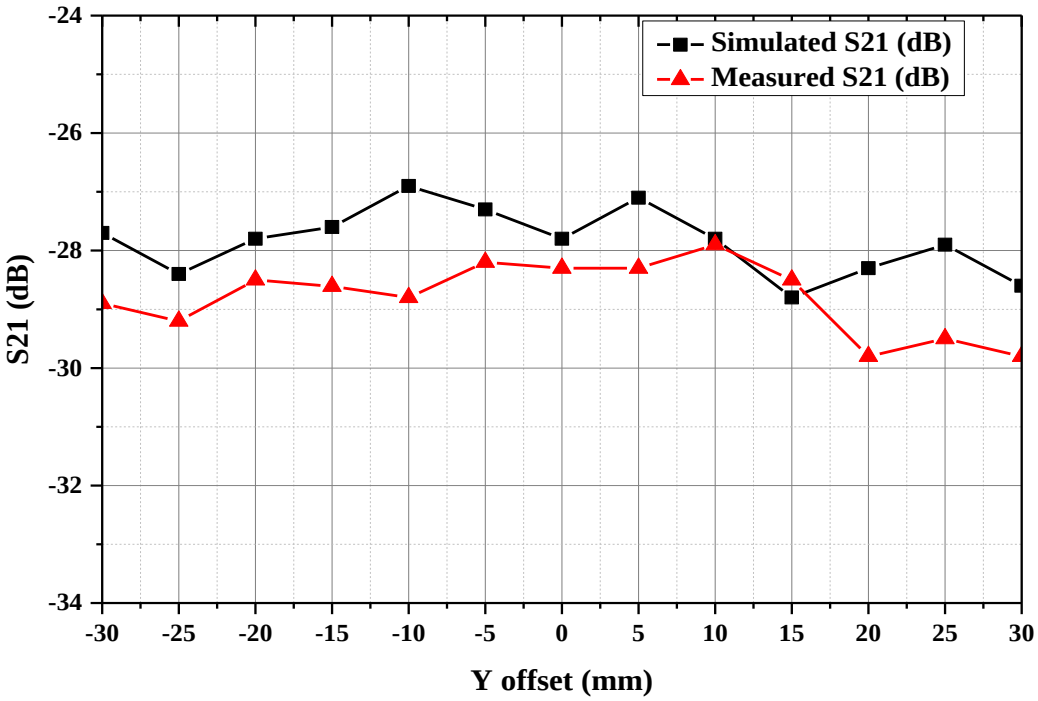

Fig. 5.18. The simulated and measured S_{21} of the proposed pair antennas with y-axis offset.

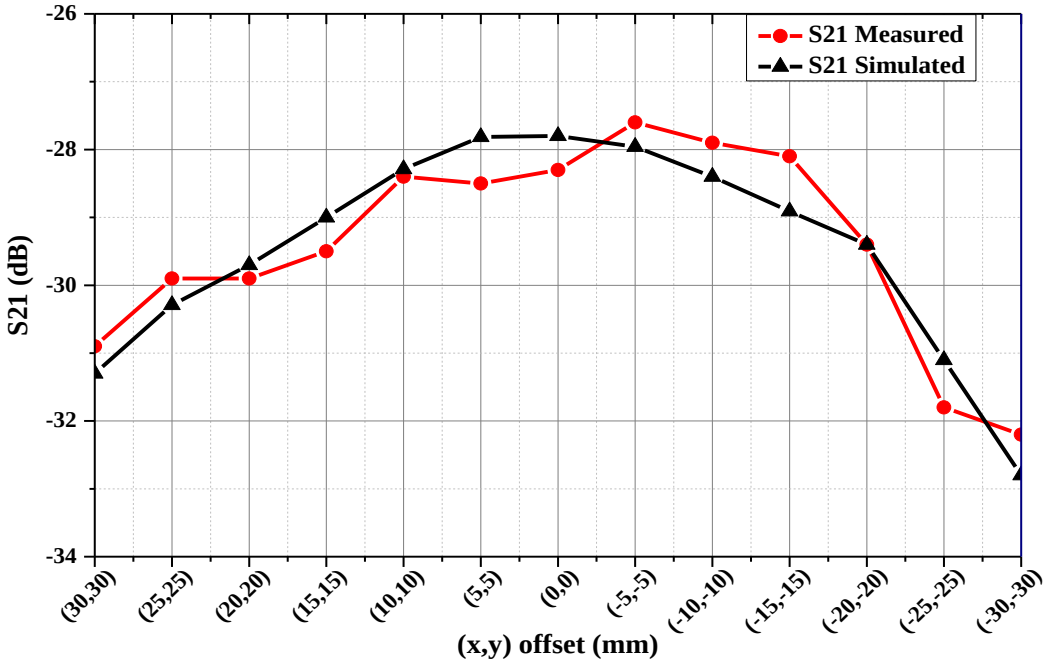

Fig. 5.19. The simulated and measured S_{21} of the proposed pair antennas with diagonal (x,y) offset.

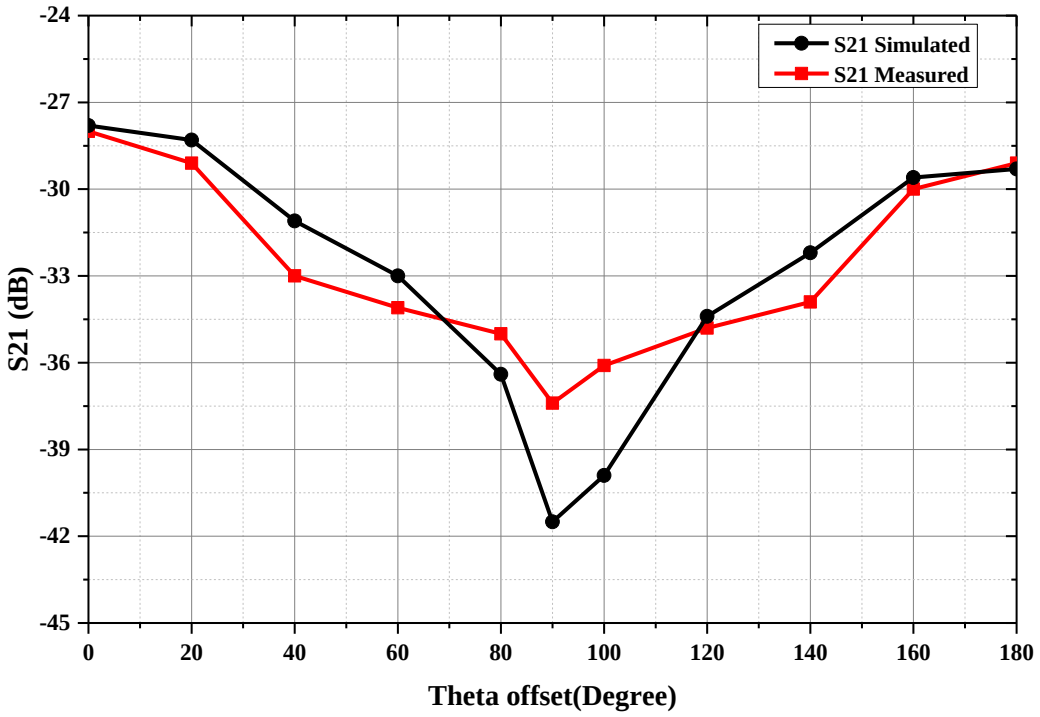

Fig. 5.20. The simulated and measured S_{21} of the proposed pair antennas with Theta offset.

The measurement of S_{21} with angle offset around the azimuth θ˚ showed good agreement with the simulation. However, at the misaligned angle 90˚ the measured result recorded higher magnitude as compared with the simulation. The coupling around the angle 90˚ is very sensitive even in simulation; where S_{21} at misaligned angle of 90˚ is lower that at 80˚ by more than 4 dB, so that a precise angle during measurement of S_{21} is unguaranteed. In general, measured results of S_{21} are in good agreement with the simulated ones. These results validate the advantage of the proposed design.

5.3.3 DC Power Received on a Load

WPT was investigated in terms of the real power that can be delivered to the target device using the proposed antennas. The miniaturized rectifier circuit that was developed in Chapter 3 section (3.4) was integrated with the implantable antenna to form a rectenna. The role of the rectenna is to capture the RF signal from the transmitter and convert it into DC. This DC can be used for powering implantable devices directly or recharging a battery.

The maximum achievable output power within the safety limit was tested using the wearable antenna and implantable rectenna. The experiment setup contains a signal generator, the cubic container filled with minced pork and a voltmeter to measure the voltage as shown in Fig. 5.22. It is worth mentioning that the rectifier was placed outside the minced pork and connected to the antenna by a 50 Ω mini coaxial cable. The reason for that is to make it easy measuring the voltage on the load using the voltmeter.

The safety regulation that restricts the transmit power in near field WPT is SAR limits. A power amplifier was used to boost the level of the transmit power up to 274 mW which is the SAR limit of the proposed wearable antenna. Both the output DC voltage and the power were measured against a sweep of input power not exceeding the safety limit as shown in Fig. 5.23.

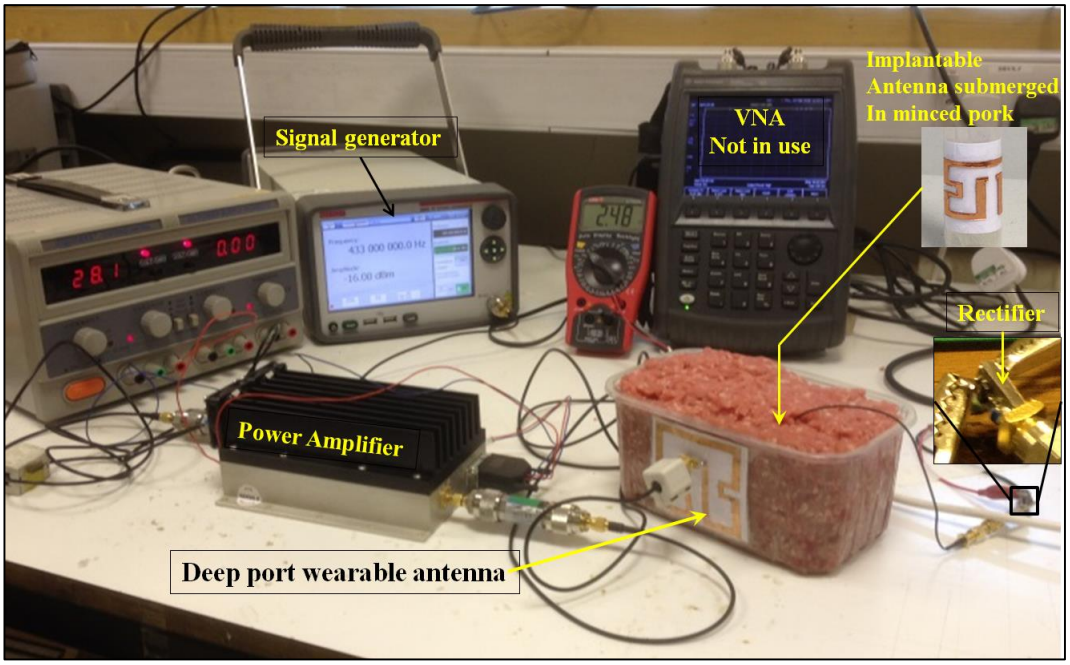

Fig. 5.21. The experiment setup of measuring the output power versus different input power.

In terms of WPT efficiency, the total power transfer efficiency is defined by

$$\eta = \frac{P_{dc}}{P_{in}} \times 100 \tag{5.1}$$

where η is the total wireless power transfer efficiency including RF to RF and RF to DC conversion efficiencies. P_{dc} and P_{in} are the power delivered to the load and the power available to the transmitting wearable antenna respectively. The measured received power at the load indicated a total power transfer efficiency of 0.1 % when the power available to the wearable antenna was 10 mW.

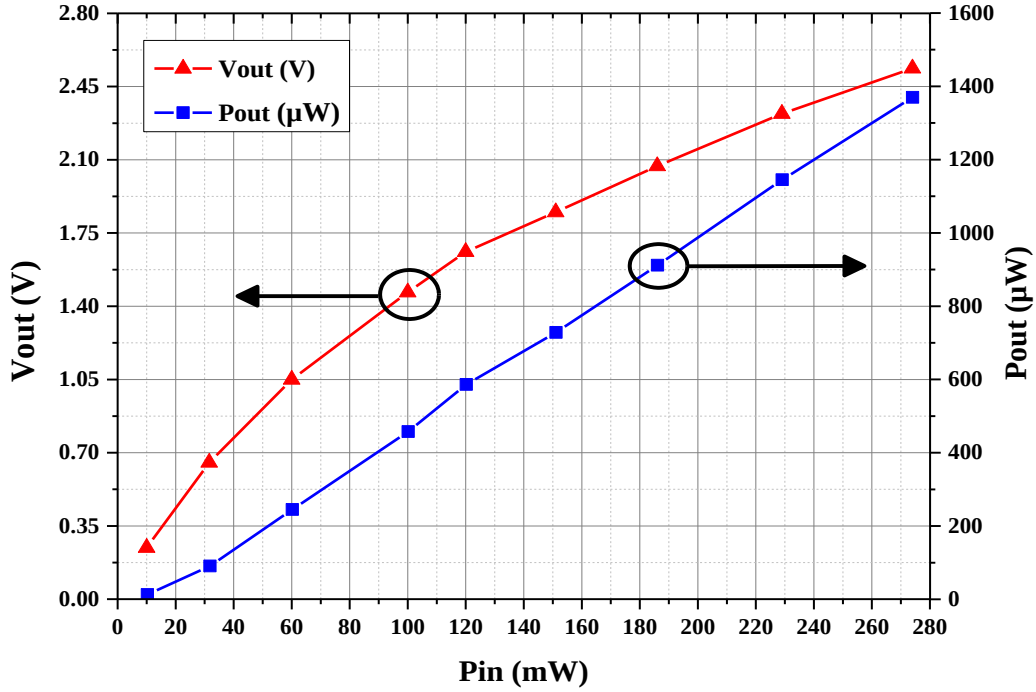

Fig. 5.22. The measured output power and voltage as a function of the input power.

The efficiency is relatively low mainly because of the low RF to RF transfer efficiency due to the high tissue loss and low RF to DC conversion by the rectifier at low power inputs. The efficiency can be increased up to 0.5 % when the available power exceeded 50 mW. This efficiency leads other works who adopted antennas in their designs as shown in Table. 5.4.

From Table. 5.4, a high frequency around 1.5 GHz was used in transferring power to a deep coil at 5.5 cm and 5 cm in Porcine with transfer efficiencies of 0.059% and 0.039% respectively [15, 16]. This technique is based on focusing the fields using a patterned metal plate antenna in close proximity to the skin. However, focusing fields requires well known to the location of the implantable antenna which is difficult to be achieved inside human body. Our proposed system although was tested at depth of 3 cm with transfer efficiency of 0.5%, it is expected to do better at depth 5 cm as compared with these works.

On the other hand, the proposed work at [17] used square loops for near field WPT at 915 MHz. Their system was tested in Bovine muscle at depth of 15 mm with WPT efficiency of 0.056%. Another work was published at [18], this work proposed circular loops for near field WPT. Their system was tested in liquid body model at

300 MHz and depth of 11 mm with WPT efficiency of 0.48%. Our proposed system still more efficient than these works even with implanted antenna inserted deeper than what they have proposed.

Table. 5.4. Comparison amongst approaches for WPT to biomedical implants using antennas

Ref.	Frequency	Antennas type	Transmitted Power	Implant depth	Received Power	Body Model	Power transfer efficiency %	Year
[15]	1.5 GHz	Antenna - coil	500 mW	55 mm	0.29 mW	Porcine heart	0.059	2015
[16]	1.6 GHz	Antenna - coil	500 mW	50 mm	0.195 mW	Porcine tissue	0.039	2014
[17]	915 MHz	Square loop	250 mW	15 mm	0.14 mW	Bovine muscle	0.056	2009
[18]	300 MHz	Circular loop	86 mW	11 mm	0.415 mW	Liquid body model	0.48	2014
This work	433 MHz	High Magnetic loop	230 mW	30 mm	1.15 mW	Minced pork	0.5	2016

A DC power of more than 1000 μW can be harvested with an input power under safety limits. This received power is enough to power many common implantable medical devices such as a pacemaker, a nerve stimulation device and a glucose measurement system that require 70 μW [15], 100 μW [19] and 48 μW [20] power, respectively.

5.4 Summary and Conclusion

This chapter presented experiments for both far field and near field WPT. In the far field experiment, our designs of implantable loop antenna and doubler rectifier circuit were used. The results and key contributions with far field WPT can be summarized as:

- The maximum transmitted EIRPs within the safety regulation at 433 MHz were calculated and depicted in Fig. 5.7. Safety regulations of both public and controlled environments were considered.

- The maximum voltage and currents that can be provided within safety limits using the proposed design were shown in Fig. 5.8 and Fig. 5.9 respectively. These values are sufficient for powering directly some implantable applications or recharging small batteries.
- Flexible loop antennas are feasible for far field WPT as demonstrated in experiments and applicable for communications based on the antenna far field parameters.
- Far field WPT has some drawback including the restricted movement for the patient and exposing all the body for radiation in order to power a specific spot.

In near field WPT, a novel approach to design loop antennas that generates strong magnetic fields along two orthogonal axes was proposed. The new design showed advantage in terms of improving WPT as compared with traditional square loop antennas. It can be summarized as

- Two deep-port loop antennas were designed to form a pair of compatible wearable and implantable antennas.
- The proposed pair was compared with a pair of conventional square loop antennas. It showed good coupling with offset in some directions and better in power transmission.
- A miniature rectifier circuit was used with the implantable antenna to form a rectenna. The rectenna and the wearable antenna perform as a WPT system.
- The overall results demonstrated significant advantages of the proposed design. The received power on the load within the safety limits was measured. A DC power of more than 1000 μW can be harvested under the condition that the transmitted power by the wearable antenna is under safety limits. This amount of power is sufficient to directly power many common implantable medical devices including a pacemaker, a nerve stimulation device or a glucose measurement system.
- By adopting the near field WPT with wearable antenna, a free mobility for the patient is offered and the transmitting power is for the intended spot only.

Both experiments in terms of far field and near field demonstrated the possibility of WPT using antennas. These techniques can be summarized in general as:

- Both techniques can provide sufficient power for direct powering of some implantable applications or charging batteries with relatively small capacities around 10 mA•h.
- Antennas can be used for RF communications based on antenna far field parameters in terms of gain, total antenna radiation efficiency and directivity. The antenna was demonstrated for WPT usage. The antenna with multiple bands can be used for both purposes.
- Loop antennas with wide bandwidth at 400 MHz can be used for communications at MICS band and for WPT at 433 MHz.

References

[1] R. Alrawashdeh, "Implantable antennas for biomedical applications," PhD thesis, University of Liverpool, 2015.

[2] IEEE Std C95.1™-2005, "IEEE Standard for Safety Levels with respect to Human exposure for RF electromagnetic fields 3 kHz to 300 GHz," *IEEE International Committee on Electromagnetic Safety (SCC39),* April 2006.

[3] L. Jerry, F. Ulcek Robert, and J. Cleveland, "Evaluating Compliance with FCC Guidelines for Human Exposure to Radiofrequency Electromagnetic Fields," *Federal Communications Commission Office of Engineering & Technology,* 1997.

[4] ICNIRP, "Guidelines for Limiting Exposure to Time-Varying Electric, Magnetic, and Electromagnetic Fields (up to 300 GHz),", 1998.

[5] Safety Code 6, "Limits of Human Exposure to Radiofrequency Electromagnetic Fields in The Frequency Range from 3 kHz to 300 GHz," *Environmental Health Directorate, Health Protection Branch, Health Canada, Canada,* 1999.

[6] J. S. Ho, S. Kim, and A. S. Y. Poon, "Midfield Wireless Powering for

Implantable Systems," *Proceedings of the IEEE,* vol. 101, pp. 1369-1378, Jun 2013.

[7] A. K. RamRakhyani and G. Lazzi, "Multicoil Telemetry System for Compensation of Coil Misalignment Effects in Implantable Systems," *IEEE Antennas and Wireless Propagation Letters,* vol. 11, pp. 1675-1678, 2012.

[8] M. Q. Nguyen, Z. Hughes, P. Woods, Y. S. Seo, S. Rao, and J. C. Chiao, "Field Distribution Models of Spiral Coil for Misalignment Analysis in Wireless Power Transfer Systems," *IEEE Transactions on Microwave Theory and Techniques,* vol. 62, pp. 920-930, Apr 2014.

[9] M. Q. Nguyen, Y. Chou, D. Plesa, S. Rao, and J. C. Chiao, "Multiple-Inputs and Multiple-Outputs Wireless Power Combining and Delivering Systems," *IEEE Transactions on Power Electronics,* vol. 30, pp. 6254-6263, Nov 2015.

[10] S. G. Lee, H. Hoang, Y. H. Choi, and F. Bien, "Efficiency improvement for magnetic resonance based wireless power transfer with axial-misalignment," *Electronics Letters,* vol. 48, pp. 339-U120, Mar 15 2012.

[11] Z. Zhang and K. T. Chau, "Homogeneous Wireless Power Transfer for Move-and-Charge," *IEEE Transactions on Power Electronics,* vol. 30, pp. 6213-6220, Nov 2015.

[12] J. P. W. Chow, N. Chen, H. S. H. Chung, and L. L. H. Chan, "An Investigation Into the Use of Orthogonal Winding in Loosely Coupled Link for Improving Power Transfer Efficiency Under Coil Misalignment," *IEEE Transactions on Power Electronics,* vol. 30, pp. 5632-5649, Oct 2015.

[13] J. Kim, D. H. Kim, J. Choi, K. H. Kim, and Y. J. Park, "Free-Positioning Wireless Charging System for Small Electronic Devices Using a Bowl-Shaped Transmitting Coil," *IEEE Transactions on Microwave Theory and Techniques,* vol. 63, pp. 791-800, Mar 2015.

[14] W. S. Lee, S. Park, and J. Lee, "A Loosely Coupled Distributed Antenna Array for Lateral Misalignment-Improved near-Field Wireless Power Transfer System," *Microwave and Optical Technology Letters,* vol. 57, pp. 2829-2833, Dec 2015.

[15] R. Das and H. Yoo, "Biotelemetry and Wireless Powering for Leadless Pacemaker Systems," *IEEE Microwave and Wireless Components Letters,* vol. 25, pp. 262-264, Apr 2015.

[16] J. S. Ho, A. J. Yeh, E. Neofytou, S. Kim, Y. Tanabe, B. Patlolla*, et al.*, "Wireless power transfer to deep-tissue microimplants," *Proceedings of the National Academy of Sciences,* vol. 111, pp. 7974-7979, 2014.

[17] S. O'Driscoll, A. Poon, and T. H. Meng, "A mm-sized implantable power receiver with adaptive link compensation," in *2009 IEEE International Solid-State Circuits Conference-Digest of Technical Papers*, 2009.

[18] S. Amendola, E. Moradi, K. Koski, T. Bjorninen, L. Sydanheimo, L. Ukkonen*, et al.*, "Design and Optimization of mm-Size Implantable and Wearable On-Body Antennas for Biomedical Systems," *2014 8th European Conference on Antennas and Propagation (Eucap),* pp. 519-522, 2014.

[19] C. S. Niu, H. W. Hao, L. M. Li, B. Z. Ma, and M. S. Wu, "The transcutaneous charger for implanted nerve stimulation device," *2006 28th Annual International Conference of the IEEE Engineering in Medicine and Biology Society, Vols 1-15,* pp. 3237-3240, 2006.

[20] K. Bazaka and M. V. Jacob, "Implantable devices: issues and challenges," *Electronics,* vol. 2, pp. 1-34, 2012.

Chapter 6

Design and In-*Vitro* Measurement of a Novel Pacemaker Antenna

6.1 Introduction

This chapter introduces novel antenna design for medical devices that are enclosed in a housing case such as pacemakers. In specific, the definition of pacemakers in terms of the function and challenges will be described first. A literature review from previous art in terms of RF pacemaker antenna will be reviewed. Then, the proposed antenna design will be explained. The safety limits with regards to use this antenna will be given as well. After that, the Wireless Power Transfer (WPT) in vitro experiments for the proposed antenna will be presented. The communication experiment using a transceiver and a base station with the proposed antenna will be introduced later. A conclusion and discussion will be finally given at the end of this chapter.

6.1.1 Pacemaker

A pacemaker is an important implantable device that is used to monitor and regulate heartbeats. It is implanted in the chest area under skin and enclosed normally inside a metal case as shown Fig. 6.1. The case is usually made of biocompatible conducting material such as Titanium. This device contains a pulse generator that produces electrical impulses through wires called pace leads. These leads are going to the heart through veins as shown in Fig. 6.1 and Fig. 6.2 [1].

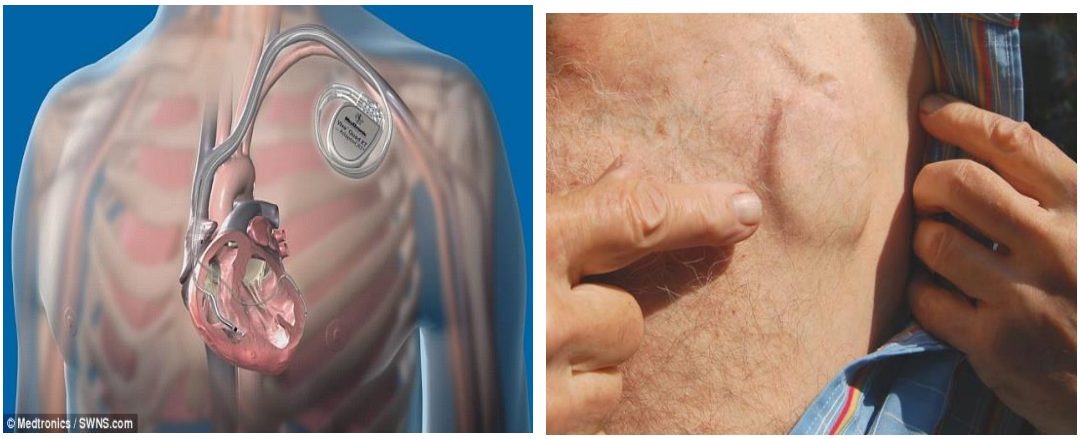

Fig. 6.1. A pacemaker implanted in the chest area under skin [2, 3].

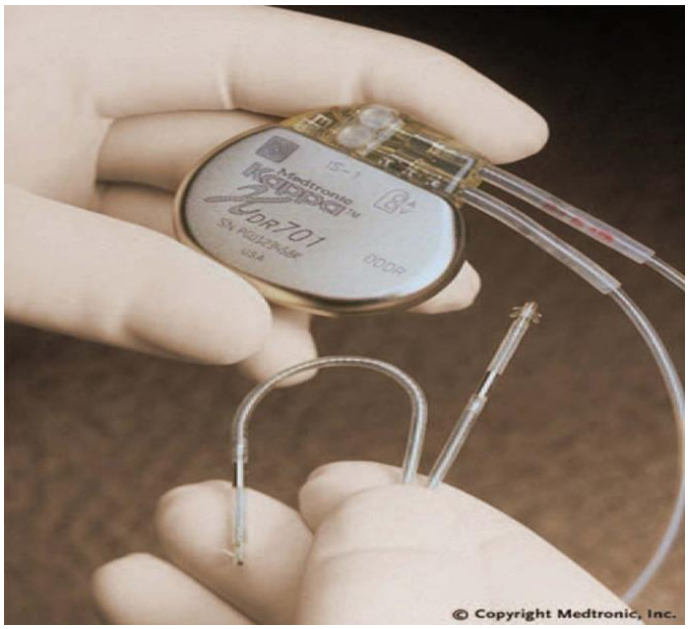

Fig. 6.2. A pacemaker with leads [2].

The National Health Service (NHS) has reported that in 2013 more than 75,500 people have fitted with pacemakers and 10,000 people with defibrillators [1]. Traditionally, the device communicates with an external programmer through near field magnetic coupling by using coil antenna as shown in Fig. 6.3. This is mainly done by using coils at low frequencies at several kHz as shown in Fig. 6.4 [4, 5].

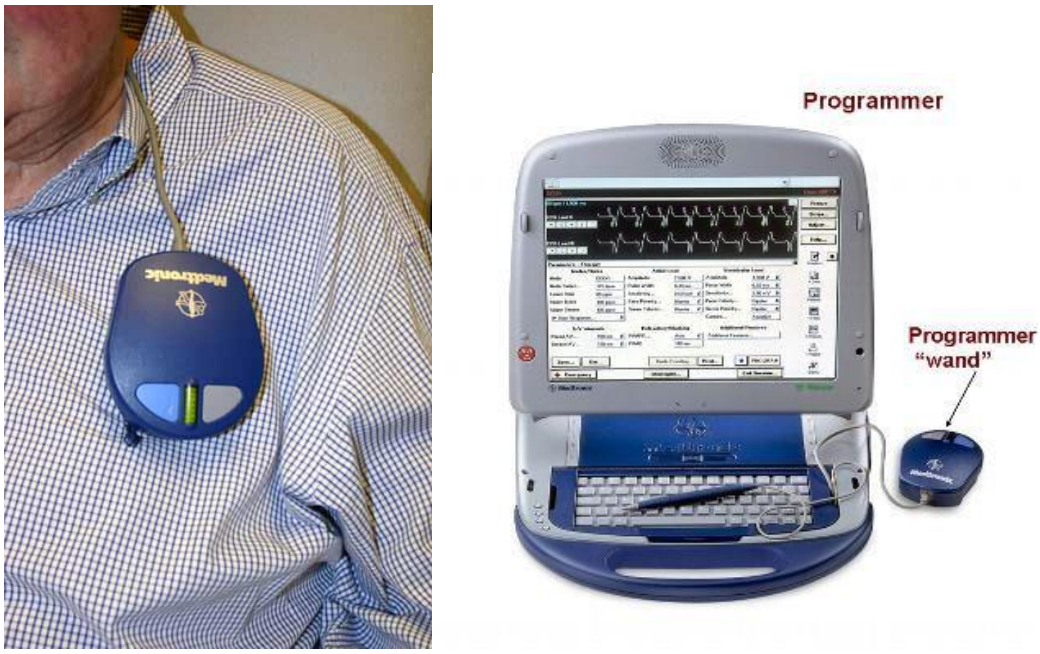

Fig. 6.3. A base station reader from Medtronic to read pacemaker and defibrillator information [6, 7].

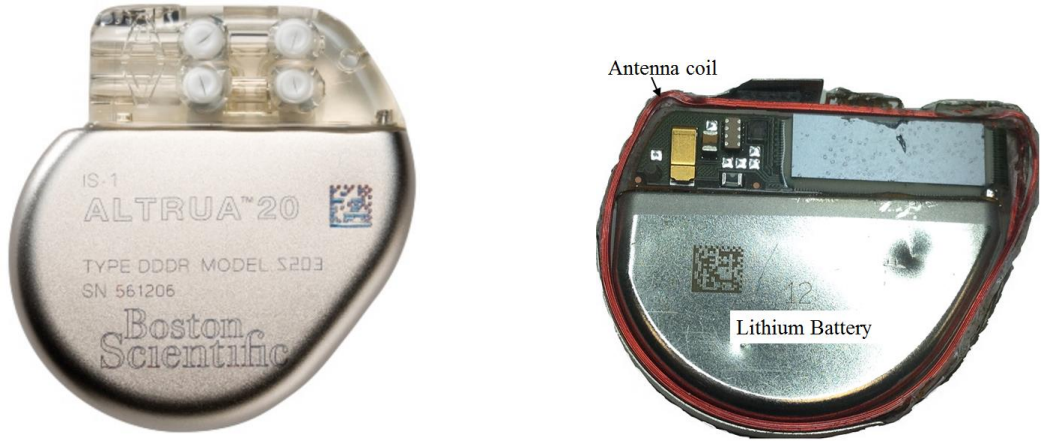

(a) **(b)**

Fig. 6.4. A pacemaker from Boston Scientific: (a) Pacemaker with the housing case and header, (b) Internal components of an ALTRUA~20 Pacemaker.

6.1.2 MICS Band and Literature Review

In 1999, FCC allocated MICS band to permit the use of a mobile radio device for data communication for implantable devices [8]. Using an RF band can extend the communication range significantly [9]. Devices with MICS bands are limited to EIRP of -16 dBm to restrain the interference to other medical devices [10]. This band is later adopted by ETSI in 2002 and become the popular band for implantable antenna design [11].

The conducting material of the case of an implantable device, such as a pacemaker, can attenuate electromagnetic RF signals significantly so that implantable RF antennas could not be totally placed inside the case. A significant amount of work has been done to design RF antennas for implantable devices. A loop antenna was proposed to work at MICS band and embedded inside the header of the pacemaker [12]. A microstrip antenna was proposed to be attached to the pacemaker case but this adds extra thickness to the pacemaker profile [13]. A PIFA antenna working at the MICS band was placed at the surface side of the pacemaker by considering the housing case as ground plane. The same group designed another PIFA but this time it was placed at the top side of the pacemaker [14, 15]. In both cases, the implant size was increased. In another study, an inverted-E antenna was proposed to be embedded to the pacemaker header [16].

A monopole antenna has been investigated for the pacemaker RF telemetry. The monopole was proposed with a folded shape to get the required length for resonance at the desired band. It was embedded to the pacemaker header in [17]. A helical monopole antenna was proposed to be embedded in the pacemaker header as well. With the increase of the helix turns, a desired length of quarter wavelength can be obtained [18]. A circumference monopole antenna was proposed in [19]. This monopole was rotated around the pacemaker case. An optional telemetry antenna was proposed in [20]. This antenna looked like a monopole and had a connection end with the electrode lead of the pacemaker. It can be utilized as an antenna by itself as the authors suggested or in collaboration with another existing telemetry antenna. These previous designs added extra elements to the implant that would increase the size and complexity of implantable devices.

A slot antenna was investigated as well for the pacemaker. A slot was made at one

side of the case in [21]. The length of the slot can be increased to adapt the desired band. However, the physical length of the slot mainly determines the resonant frequency of the antenna and most power is radiated in the slot region.

In this chapter, an approach to design an antenna using the housing case of implantable devices is presented for the first time. This design exploits the radiating characteristic current modes of the case to create a radiating antenna from the housing case itself at the frequency bands of interest. It is worth mentioning that a copper metal is used in this design, this metal prevents any field to be propagated either from inside the pacemaker to outside or vice versa. A comparison amongst the proposed antenna and previous works is shown in Table 6.1. The radiating current modes of the case are excited using a capacitive coupling element aided by a matching circuit. The proposed antenna has a radiation pattern that is outgoing from the housing case in normal direction to the pacemaker surface, which is very suitable for implantable devices as will be explained in the following sections.

Table 6.1. Comparison amongst antennas that are proposed for pacemakers.

Ref.	Antenna type	Location	Frequency	Year
[19]	Monopole Antenna	Circumference of the case	N/A	2004
[14]	PIFA Antenna	Surface side of the case	MICS	2007
[21]	Slot Antenna	Surface side of the case	MICS	2008
[18]	Helical Antenna	Pacemaker Header	N/A	2009
[12]	Loop Antenna	Pacemaker Header	MICS	2011
[13]	Microstrip Antenna	Surface side of the case	MICS	2011
[17]	Monopole Antenna	Pacemaker Header	MICS	2011
[15]	PIFA Antenna	Top side of the case	MICS	2011
[16]	Inverted E-antenna	Pacemaker Header	MICS	2015
This work	Housing antenna	The case itself	MICS	2016

6.2 Pacemaker Antenna Design

From the original shape of the pacemaker, a cavity with a small slot on the top side can be recognized as shown in Fig. 6.5(a). This small slot is reserved for lead electrodes to pass through into the pacemaker circuitry. The slot can be potentially

used as an antenna. The characteristics of the slot antenna depend on the size of the slot. Typically, the length of the slot is about half wavelength for resonance. The average length of the top side of a typical pacemaker is about 30 mm. The slot within this side could be widened up to 26 mm so that a margin metal of width 2 mm can be kept for header contact and insulation as shown in Fig. 6.5(b). A rectangular box is considered in this study to approximate a commercial pacemaker and also for easy fabrication as shown in Fig. 6.5(c). The same design method could also be applied to other implantable devices with different cavity shapes.

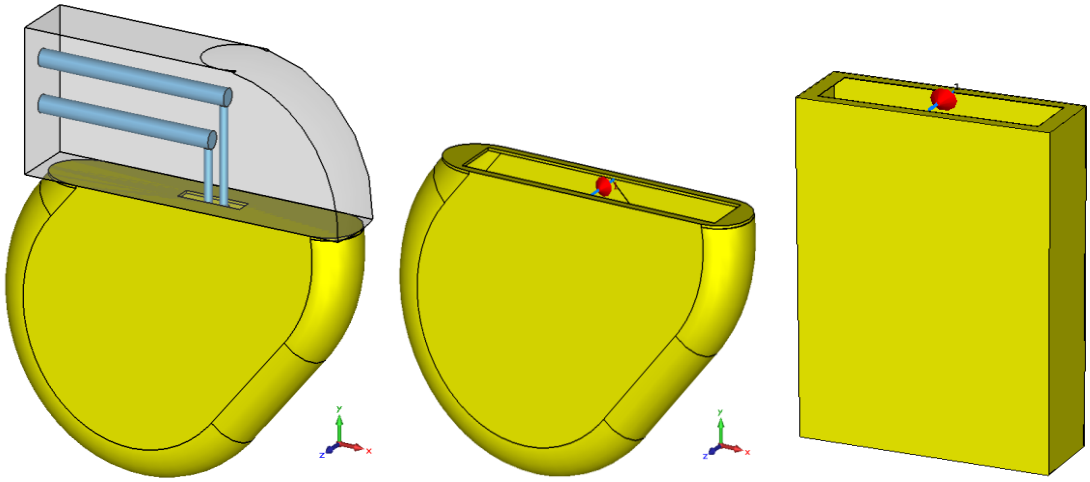

(a) **(b)** **(c)**

Fig. 6.5. The pacemaker housing antenna (a) The structure of a pacemaker (b) Creating a slot from the pacemaker's housing case and (c) A rectangular box shape slot antenna to validate the approach for easy fabrication.

The reflection coefficient S_{11} of both structures in the original shape and the rectangular shape is simulated using CST microwave studio. It shows that the two structures are resonating at 5.6 GHz which is equivalent to the slot size of 26 mm at a half wavelength as shown in Fig. 6.6.

The simulation confirmed the relationship between the resonance and the slot length. Since the target frequency of implantable devices is in the MICS band, the radiating frequency of the slot antenna is too high with this dimension. More importantly, for a slot antenna, most power is radiated in the slot region, which is unfavorable for

pacemaker applications since most power will be radiated to the body rather than off body as illustrated by the radiation pattern shown in Fig. 6.7.

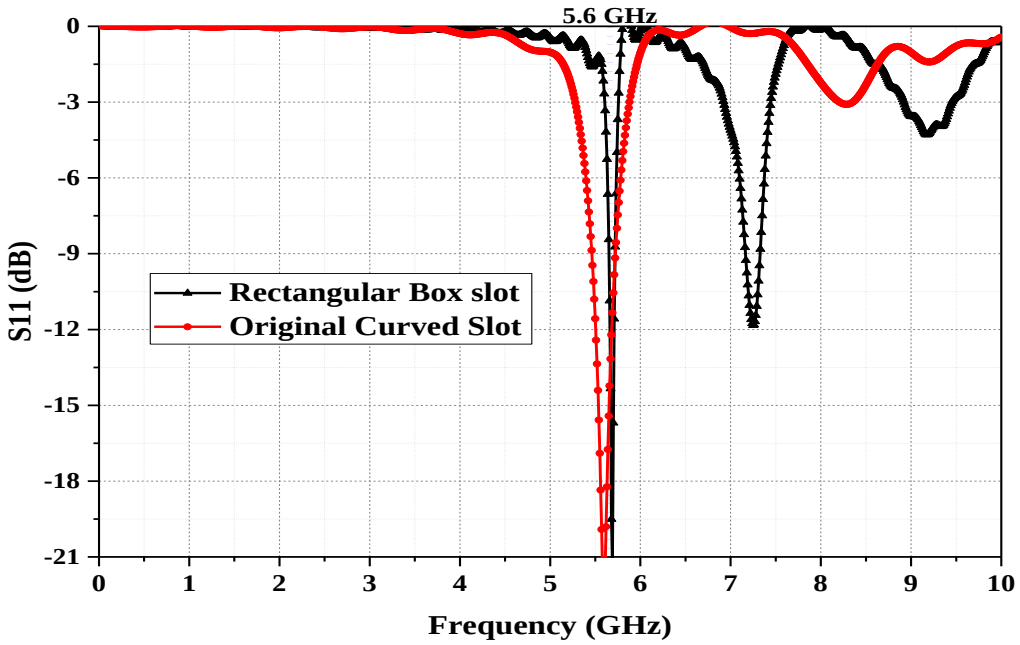

Fig. 6.6. The reflection coefficient S_{11} of the slot antenna in two cases: the original pacemaker curved shape and the rectangular box shape.

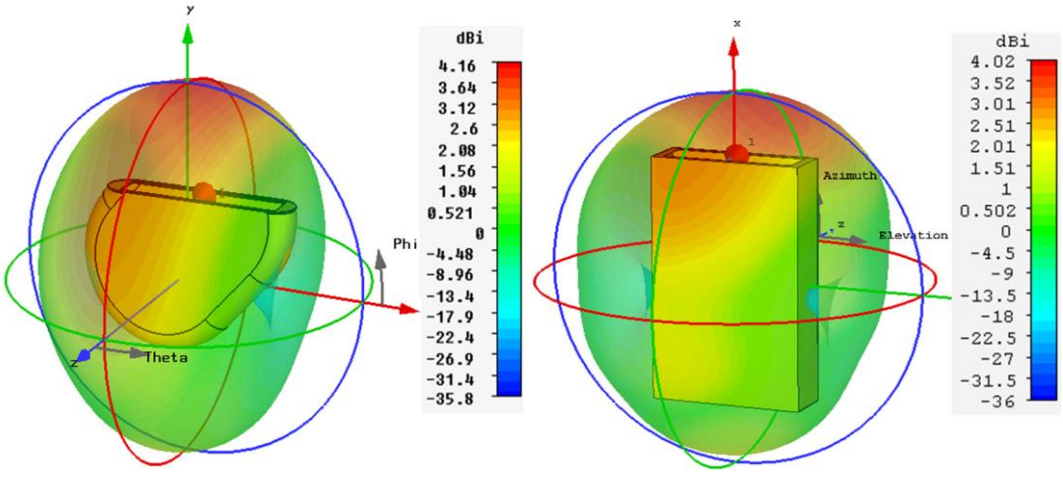

Fig. 6.7. The radiation pattern of the slot antenna at 5.6 GHz in the two cases: the original pacemaker shape and the rectangular box shape.

One of the techniques that have been adopted to the design of RF antennas recently is

to create an antenna by utilizing a large ground plane or chassis by exploiting the characteristic current modes. The surface current distribution of conducting planes or chassis is constructed from infinite orthogonal characteristics current modes [22]. The radiation current modes of the chassis can be explored using the Theory of Characteristic Mode (TCM) analysis. The principle of TCM is explained well in [22, 23]. This approach of antenna design is mainly investigated for mobile terminals [23-25].

For a specific conducting surface, the current density J is given by

$$J = \sum_n \alpha_n J_n \tag{6.1}$$

where J_n represents the characteristic current modes, these characteristic mode currents are able to radiate power independently [23]. α_n is the associated weighing coefficient of the current mode and it is related to the excitation modal and eigenvalues as:

$$\alpha_n \propto \frac{V_n}{1 + j\lambda_n} \tag{6.2}$$

where V_n is the excitation coefficient which denotes the applied excitation coupling to the current mode, the phase and magnitude of V_n affect the contribution of the current mode on the whole current distribution [22]. λ_n is the eigenvalue related to the current mode. The current density can be then given by

$$J = \sum_n \frac{V_n}{1 + j\lambda_n} J_n \tag{6.3}$$

From equation (6.3) it can be seen that the current density is related to the eigenvalues and the excitation state of V_n in terms of phase and magnitude. The radiation characteristics of any specific current mode can be estimated by the associated eigenvalue λ_n. Whenever this value is close to zero, the current mode

radiates. The magnitude of the term $\left|\frac{1}{1+j\lambda_n}\right|$ can be used to analyze the current mode rather than the individual eigenvalues. This term represent the normalized value of the current mode and is called Modal Significance (MS) [23]. The MS does not depend on the excitation and but is determined by the shape and size of the conducting surface [23].

Previous studies utilized ground planes to be effective radiative antennas for mobile terminals using simple and non-resonance coupling elements with the help of an external matching circuit [24, 26]. In this study, the housing of a pacemaker is considered as a kind of chassis with a cavity structure. The radiation characteristics from the housing itself will be investigated using this approach. The housing case is analyzed by TCM analysis in free space using FEKO software. The ISM band around 2.45 GHz is investigated since the dimension of cavity is comparable with the wavelengths at this band. The modal significance (MS) method is used to exploit the radiative current modes. This MS, the magnitude of $\left|\frac{1}{1+j\lambda_n}\right|$ as given in (6.3), has a maximum value of 1. Whenever its value is close to one then the current mode can effectively contribute to the radiation [23].

The result of the TCM analysis for the proposed antenna is shown in Fig. 6.8. It can be seen from this figure, the first two modes have the highest MS at 2.45 GHz and in particular the first mode has an MS very close to 1. Mode 4 is dominant at the bands above 2.5 GHz.

The surface currents associated with the first two modes are shown in Fig. 6.9. The current distribution of the first mode is longitudinal with the cavity surface and has high current density at the top side slot. The second mode is latitudinal on the surface including the area of the slot. The best excitation places for the current modes are at the maxima of the current distribution [22].

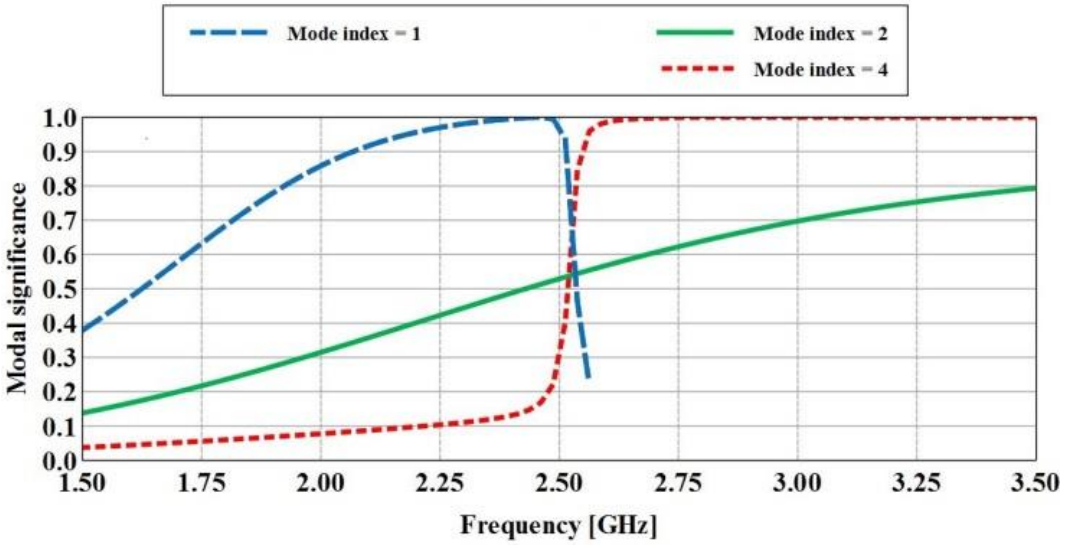

Fig. 6.8. Characteristic mode analysis of the proposed antenna in the rectangular box shape.

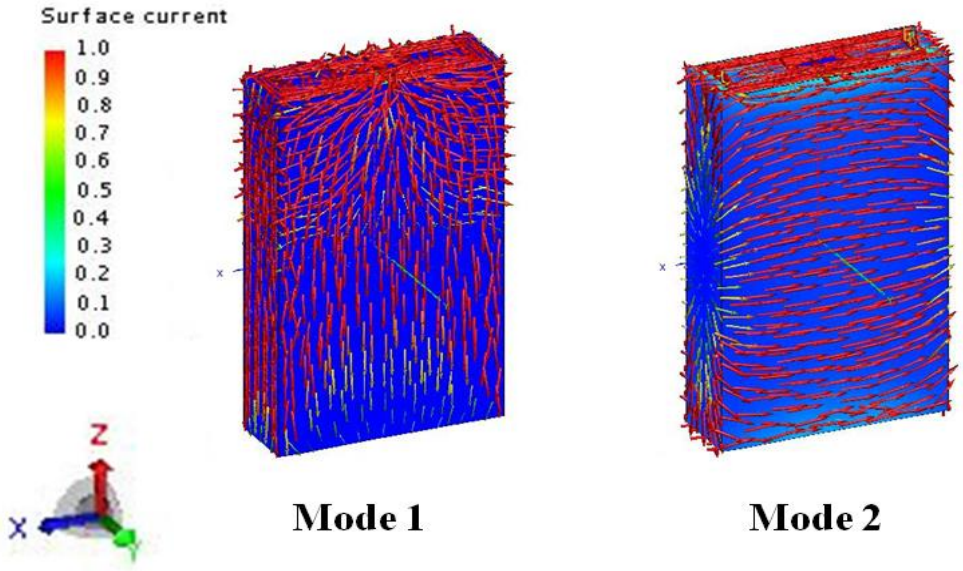

Fig. 6.9. The current distribution of the first three mode of the proposed housing antenna.

Since the dominant modes at this band have dense currents at the top slot side, the excitation would be useful at this position. The current modes have symmetric distribution around the cavity surface so that the excitation at the middle position of the slot will provide balanced excitation to the current modes. To excite the current modes of the housing at 2.45 GHz, a coupling element is used with the cavity. To

avoid adding extra element to the pacemaker and keep the shape of the opening of the case as original, an element part is cut from the top side of the housing cavity as shown in Fig. 6.10. The housing cavity and the coupling element are made of copper. A tiny slot with the size of 2 mm × 8 mm is left at the center of the coupling element for the original usage of pacemaker to lead electrode to pass-through to the internal circuit as shown in Fig. 6.10(b). This slot has negligible effect on the antenna performance.

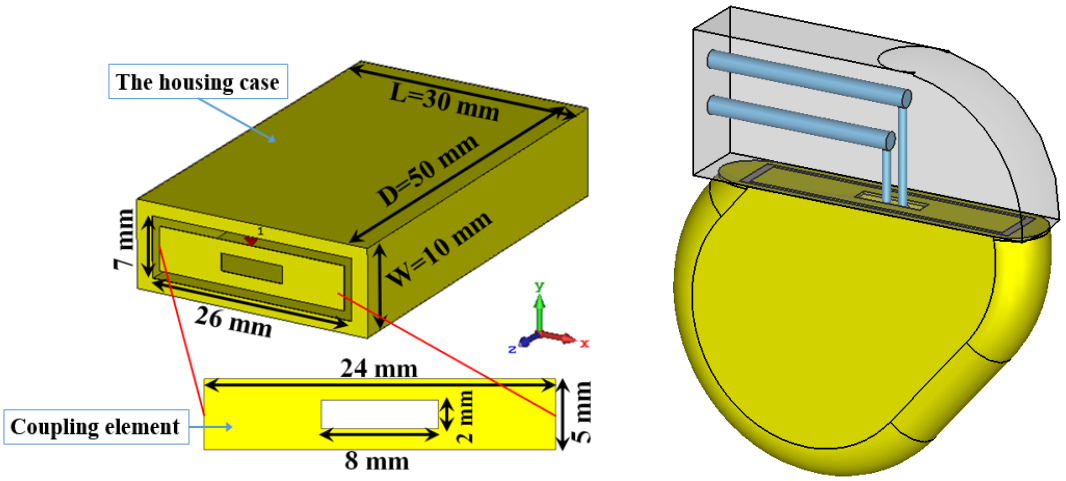

(a) **(b)**

Fig. 6.10. The proposed antenna (a) Dimension details of the proposed rectangular box antenna (b) the proposed antenna in the original pacemaker shape.

The proposed antenna has the same shape and dimension as the slot antenna except the added coupling element. The performance of both antennas are simulated and compared. It is worth mentioning that the size of this box have been chosen so that it is close to the dimension of the original pacemaker and also to fit a transceiver circuit that will be used in the following sections to test the communication ability of the proposed antenna. The proposed housing antenna with the coupling element is simulated and compared with the slot antenna. The housing antenna has a resonance similar to the slot antenna but the resonance is shifted to a slightly lower frequency as shown in Fig. 6.11. The performance of the antenna around the resonant frequency of 5.6 GHz has been slightly changed mainly due to the capacitive effect of the coupling element. This can be explained as the gap space between the slot sides is reduced by placing the coupling element between them. As a result the capacitance

in the input port between the coupling element and the slot side is increased and hence the resonance frequency is shifted down accordingly.

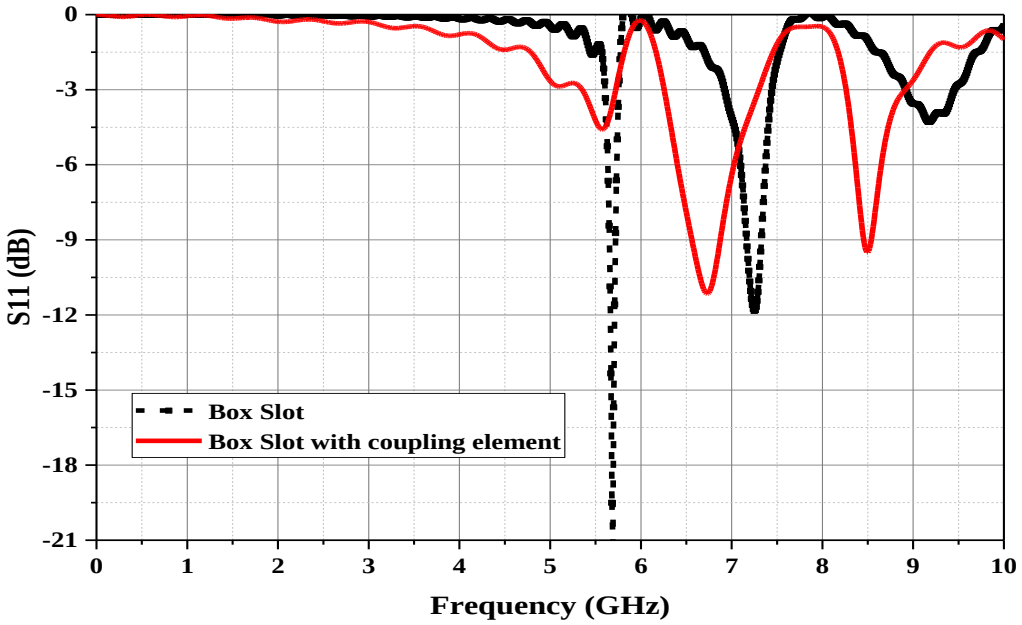

Fig. 6.11. Comparison of the reflection coefficient S_{11} of the rectangular box in the proposed housing antenna design and the slot antenna design.

Then an external matching circuit is added to the coupling element to excite the modes at 2.45 GHz in free space. This is to validate the approach of exciting surface current modes for radiation. The matching circuit can be designed automatically using CST with connection to specialist software in designing matching circuit such as Optenni lab. This software has libraries of real commercial components. The matching circuit is designed using this software based on the imported file from CST with flexibility to choose the order and topology of the circuit. The designed circuit is imported back to the CST to be attached to the antenna port. The reflection coefficient of the antenna after adding L-matching circuit is shown in Fig. 6.12. It has 28 MHz bandwidth at -10 dB return loss. The gain of the proposed antenna at this band is 2.59 dB and the total radiation efficiency is 75%. The total antenna efficiency is slightly low due to the use of the matching circuit.

A matching circuit at 2.45 GHz is applied to the slot antenna to find out the difference in performance as compared with the proposed one.

The matching circuits and surface current distributions of the housing antenna with

the coupling element and the slot antenna are shown in Fig. 6.13. The radiative current modes at 2.45 GHz have been excited using the coupling element as shown in Fig. 6.13(a). As a result, the surface current along the sides of the case is activated which is associated with the first current mode. While the surface current in the middle of the front face is mostly related to the second mode. These surface currents will participate in forming the radiation pattern. On the other hand, the surface current of the slot antenna is mostly distributed along the slot aperture. As a result, the radiation will be generated mainly from the slot aperture itself as shown in Fig. 6.13(b).

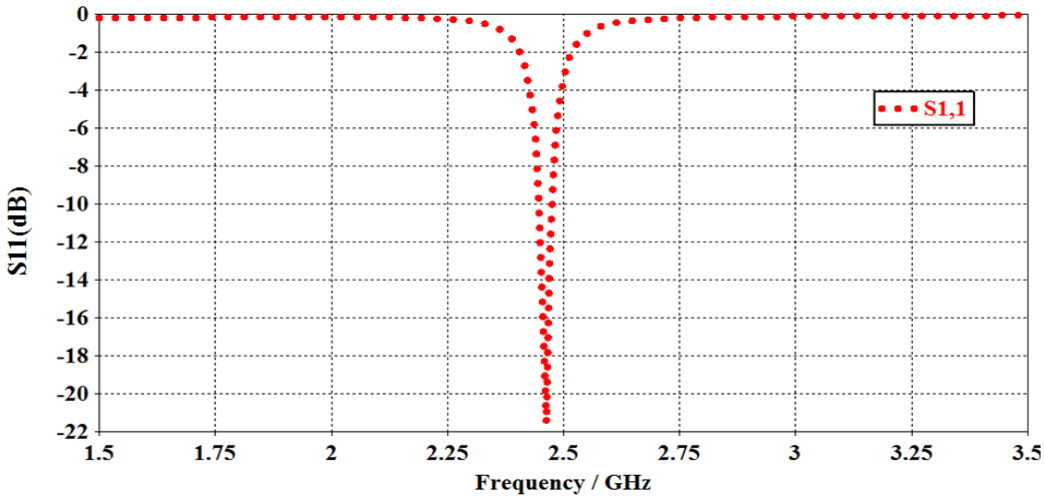

Fig. 6.12. The reflection coefficient S_{11} of the housing antenna at 2.45 GHz after adding the matching circuit to the coupling element.

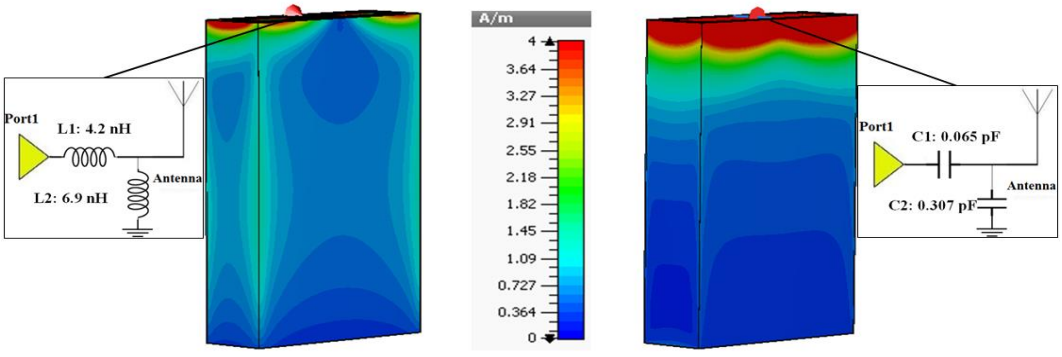

(a) **(b)**

Fig. 6.13. Matching circuit and surface current at 2.45 GHz of (a) the proposed housing antenna (b) the slot antenna.

The excitation of the proposed antenna results in radiation from the housing case itself with a radiation pattern normal to the housing surface as shown in Fig. 6.14(a) and (b). The reason for radiation mainly in one direction is the unbalanced excitation to the cavity surface where the feeding is applied between one side of the cavity and the coupling element. On contrast, the radiation of the slot antenna is still mainly from the slot aperture as shown in Fig. 6.14(c) and (d).

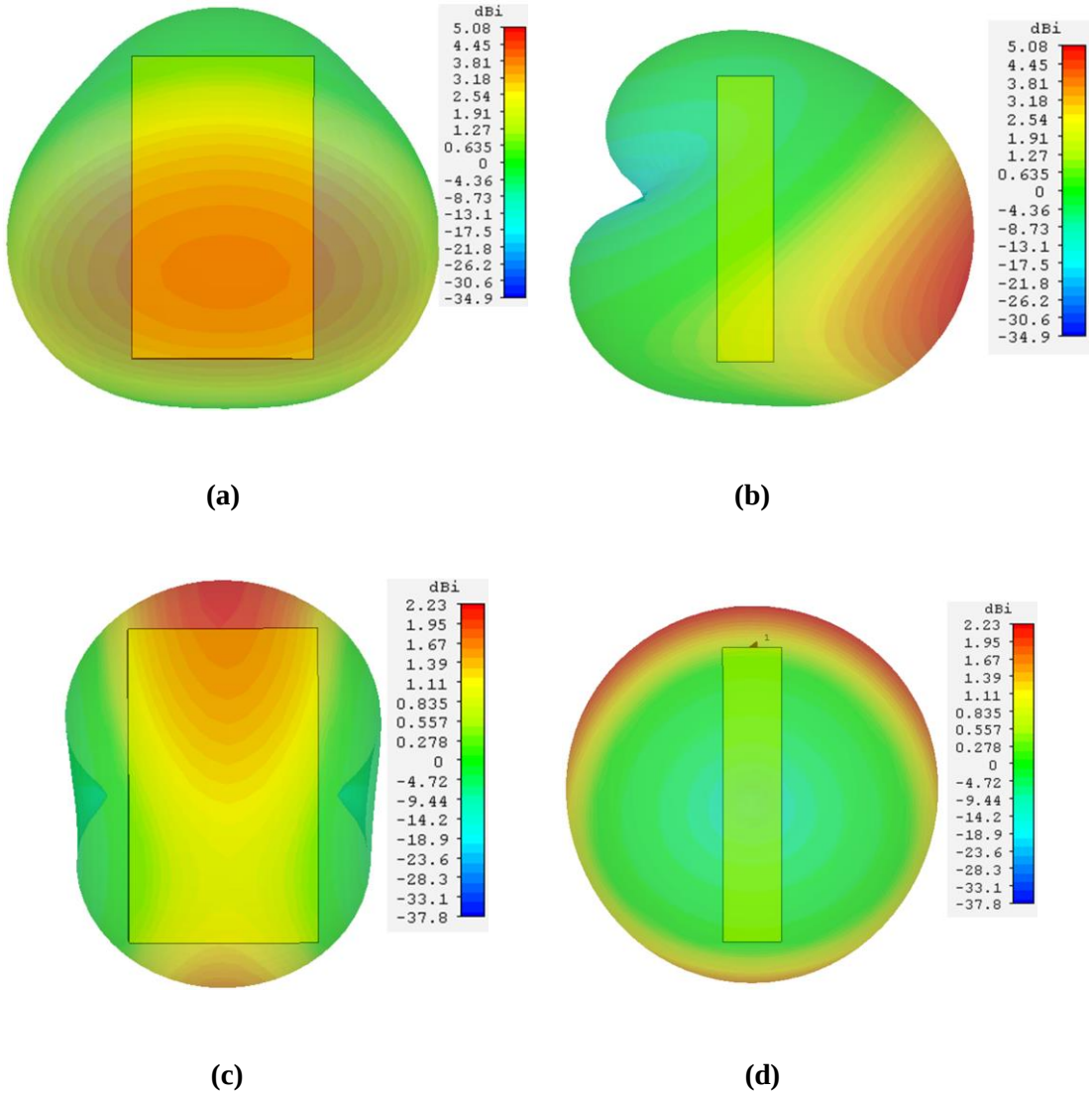

Fig. 6.14. Radiation pattern at 2.45 GHz with a matching circuit. (a) Front view of the proposed antenna (b) Side view of the proposed antenna (c) Front view of the slot antenna (b) Side view of the slot antenna.

The proposed design has a significant advantage over the performance of the equivalent slot antenna in terms of radiation from the housing itself with radiation pattern going away from the pacemaker off the body. This design represents an advantage for the pacemaker application due to the flexibility to choose the desired band and to generate the desired radiation pattern.

Since the pacemaker is used inside a human body, the properties of the housing antenna are investigated with the presence of body tissues. The high dielectric properties of the body tissues change the antenna performance. The resonance frequency of the antenna inside the body is related to the free space resonant frequency according to the properties of the tissue and is given by

$$f_r = \frac{f_0}{\sqrt{\varepsilon_e}} \tag{4}$$

where f_0 is the resonant frequency in free space, f_r is the resonant frequency in the body medium and ε_e is the equivalent effective relative permittivity of that medium. The resonant frequency of the antenna will move to a lower value due to the effect of body tissues. The body tissue properties in terms of dielectric constant at 403 MHz are 57.1, 11.6 and 46.7 for muscle, fat and skin, respectively.

The same procedure that was done in free space is then carried out to the housing antenna with the coupling element in the body model. The coupling element with the matching circuit is used to excite the current modes of the antenna at the MICS band. The simulation results confirm that the principle of performance is similar to that in free space. The surface current is activated on the case antenna surface with most power radiated in the direction perpendicular to the front surface of the antenna as shown in Fig. 6.15.

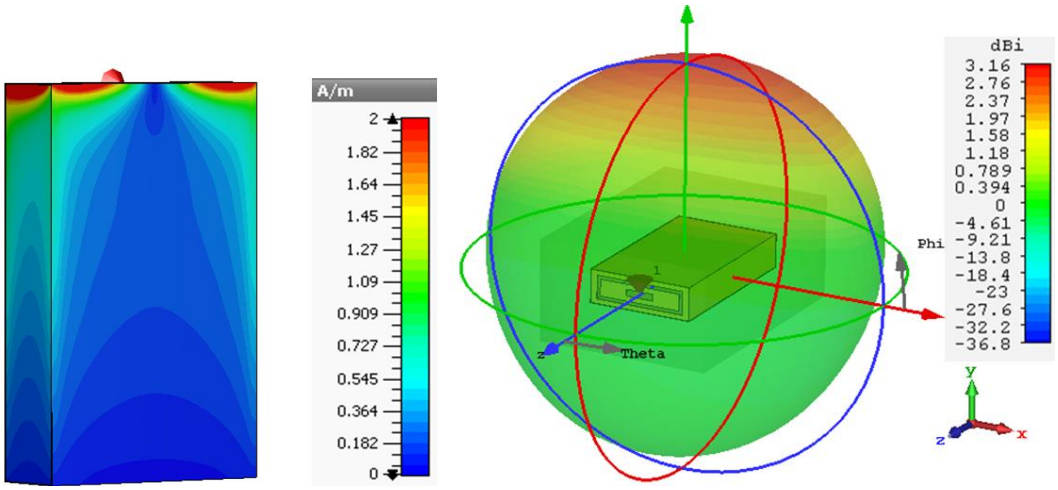

Fig. 6.15. Simulated surface current and radiation pattern of the proposed antenna at 403 MHz.

6.2.1 S_{11} Measurement

To validate this design, the housing case is fabricated by cutting 0.1 mm copper sheet into shape. The coupling element is fabricated on a 0.57 mm thick FR4 substrate. Then a T-matching network circuit is constructed on the coupling element as shown in Fig. 6.16. Minced pork is used as a mimic to human tissues to test the proposed antenna. The reflection coefficient S_{11} of the prototype antenna is measured using a portable VNA as shown in Fig. 6.17.

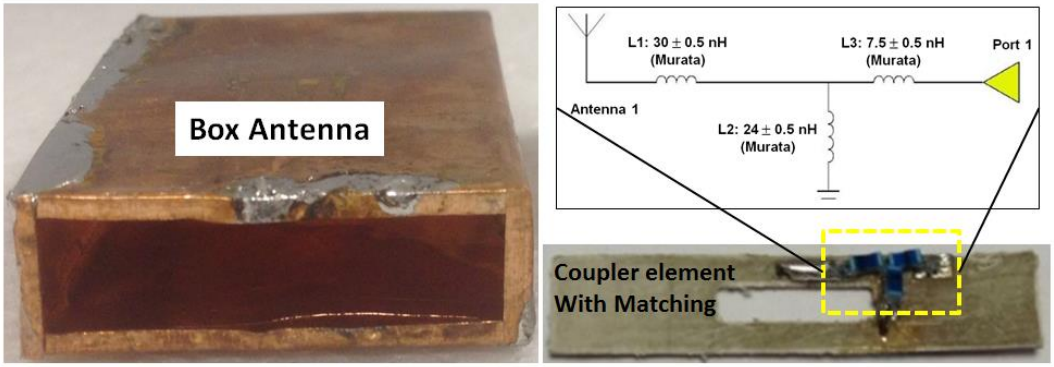

Fig. 6.16. The fabricated prototype of the proposed antenna and the matching circuit.

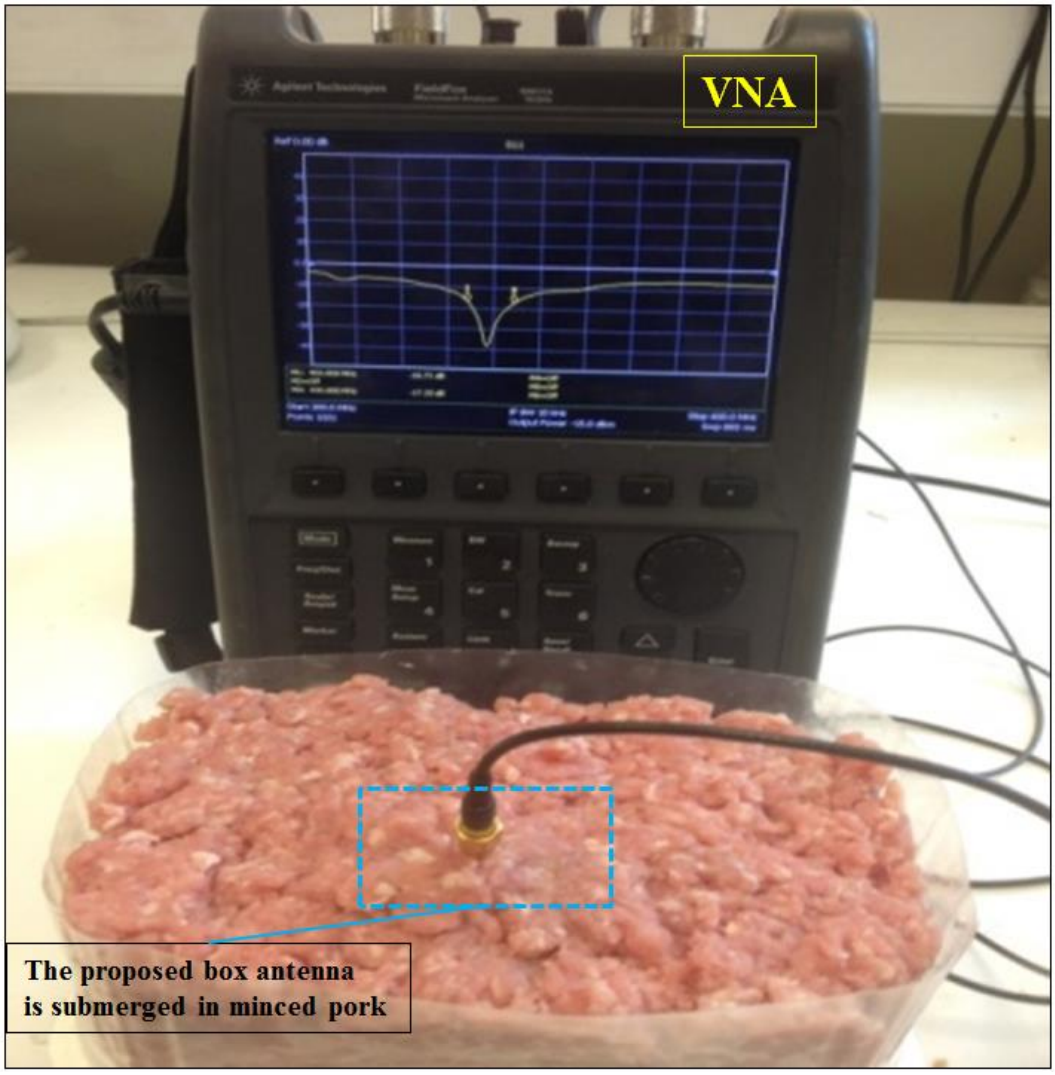

Fig. 6.17. The S_{11} measurement setup of the proposed housing antenna inside minced pork.

The antenna response has a good agreement with the simulated results as shown in Fig. 6.18. From the figure, it can be shown that a very small frequency shift is encountered due to fabrication precision. However, it still covers the desired bands of the MICS band and the ISM band at 433 MHz. The proposed antenna is investigated in terms of the effect of pacemaker parts including the battery and the PCB board. It is found that the resonance is slightly shifted up by 14 MHz but the desired bands are still covered. Furthermore, this slightly shift can be compensated by tuning the matching circuit if necessary.

The simulation results of the proposed antenna also show that the realized gain and radiation efficiency are -30 dB, 0.038% and -30.1 dB, 0.04% at 433 MHz and 403

MHz, respectively. These values are relatively small as expected due to the large loss of human body tissues [27]. Nonetheless, these values are enough to build up a communication link over 1 m when the power fed by the transceiver to the antenna is 25 µW. A longer range of up to 19 m can also be established with a larger transmit power within the safety limits as will be shown in the following sections.

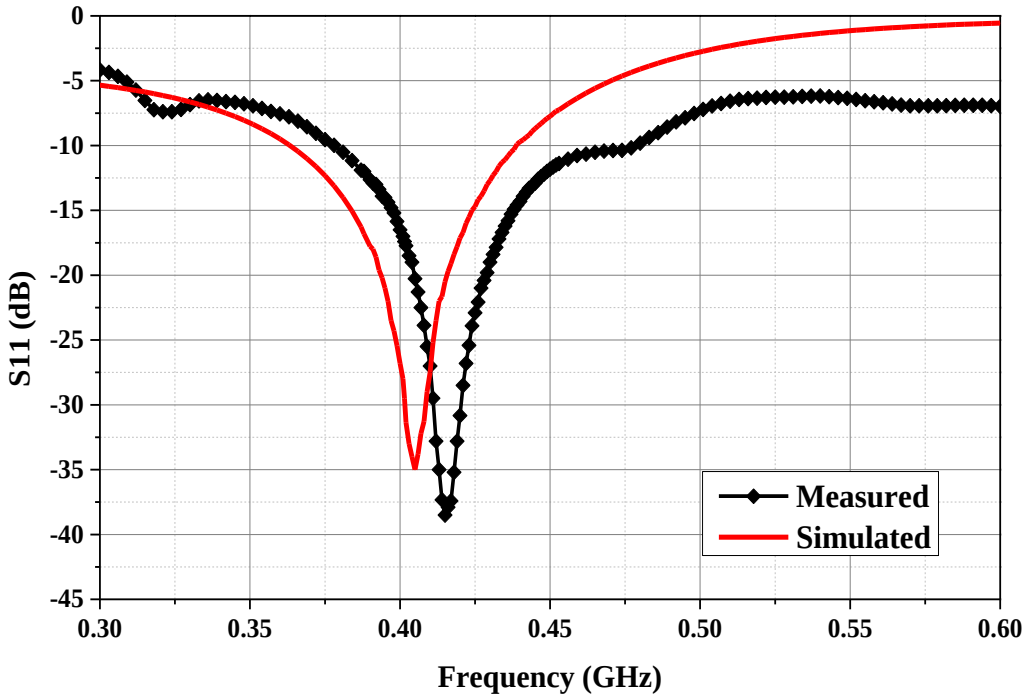

Fig. 6.18. The simulated and measured S_{11} of the proposed rectangular box antenna.

6.3 Energy Harvesting Experiments

The proposed housing case antenna is tested for WPT. The experiment of far field WPT is done inside an anechoic chamber as shown in Fig. 6.19. The experiment setup includes a signal generator, a power amplifier to boost the transmit power with a gain of 53 dB, a transmitting antenna, a wideband power sensor and a laptop to read the received power. The proposed antenna is tested inside two different body phantoms: minced pork and a rabbit. The transmitting antenna is a meandered loop resonating at 433 MHz in free space with a gain of 2.3 dB and a radiation efficiency of 96%. It is worth mentioning that there is a measurement error of 1 dB in all measurement results. This experiment is carried out in two scenarios.

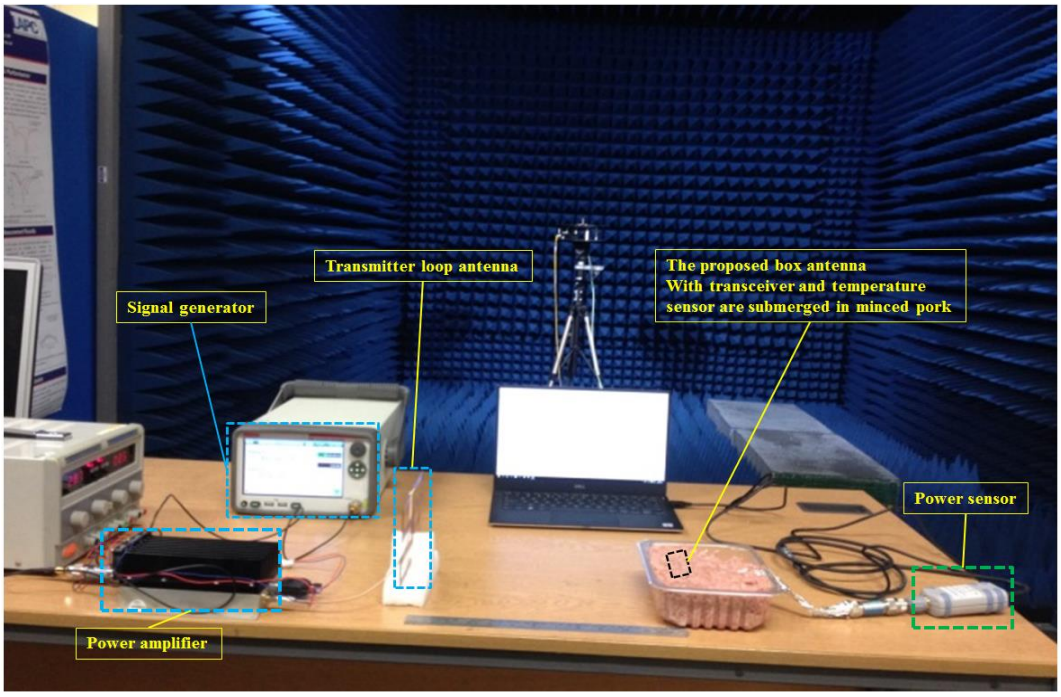

Fig. 6.19. The experiment setup of the WPT using the proposed antenna in minced pork inside an anechoic chamber.

6.3.1 Experiment in Minced Pork

Minced pork that mimics human tissues is used to test the proposed antenna for WPT. In the receiving side, the antenna is buried in the pork. The thickness of the pork between the case and the pork container is 2 cm. The received power by the antenna is fed to a power sensor that is connected to a laptop to read the power level. The transmitting side includes the signal generator that feeds a power amplifier. The output of the amplifier feeds the transmitting loop antenna. An EIRP of 140 mW was transmitted during the experiment. The received power by the antenna is measured with several distances as shown in Fig. 6.20. In the near field region of the antenna, smaller steps of measurement are used for higher accuracy. At the distance of 1 m, the received power was 6.2 μW when the transmit power is 140 mW.

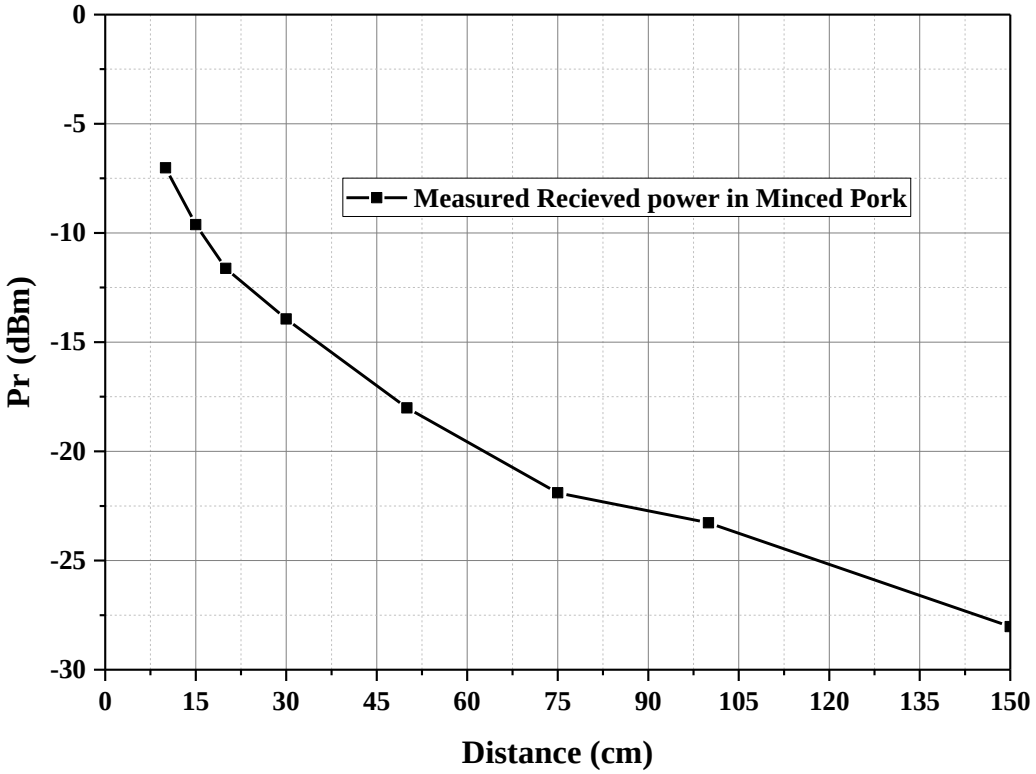

Fig. 6.20. The measured received power in minced pork with respect to distance. The EIRP transmit power is 140 mW.

To measure the received power at several misalignment angles, the proposed antenna and the transmitting antenna are kept apart for 1 m. Then the transmitting antenna is rotated around the azimuth in several angles of 15˚ then 30˚, 45˚ and 60˚. The proposed receiving antenna is facing the center location of the transmitting antenna at all angles. Since the transmitting antenna is symmetrical, the received power at other symmetrical angles, namely -15˚, -30˚, -45˚ and -60˚, is assumed to be the same. The measured results are shown in Fig. 6.21. The received power dropped from 6.2 μW to 1.3 μW due to the misalignment angle between the main beams of the antennas.

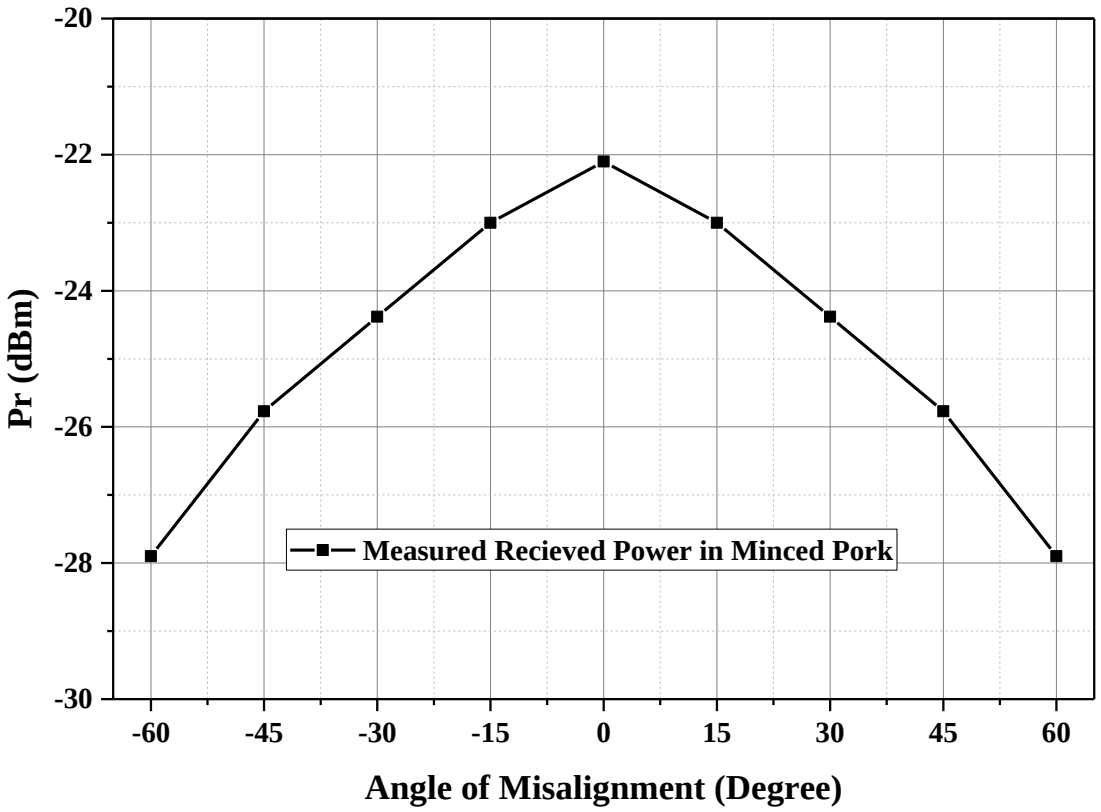

Fig. 6.21. The measured received power in minced pork with respect to rotation angle at a separation distance of 1 m between the transmitting and receiving antennas. The EIRP transmitted is 140 mW.

6.3.2 Experiment in a Rabbit

The proposed antenna was also implanted and tested in a rabbit. A 3 Kg male New Zealand type of rabbit was purchased from Envigo. The rabbit was maintained in a lab for 10 days and prepared following Schedule 1 for the experiment. The WPT experiment is carried out with the same setup as in the minced pork. The proposed antenna is implanted under the skin in the chest region of the rabbit. The antenna is connected using a micro coaxial cable to the power sensor to read the received power. In the experiment, the proposed antenna is tested in two orientations: horizontal for the scenario when a patient is sleeping and vertical for the scenario when a patient is standing. The measurement is done first to find out the received

power level at different separation distances from the transmitting antenna. The received power versus the separation range is depicted in Fig. 6.22.

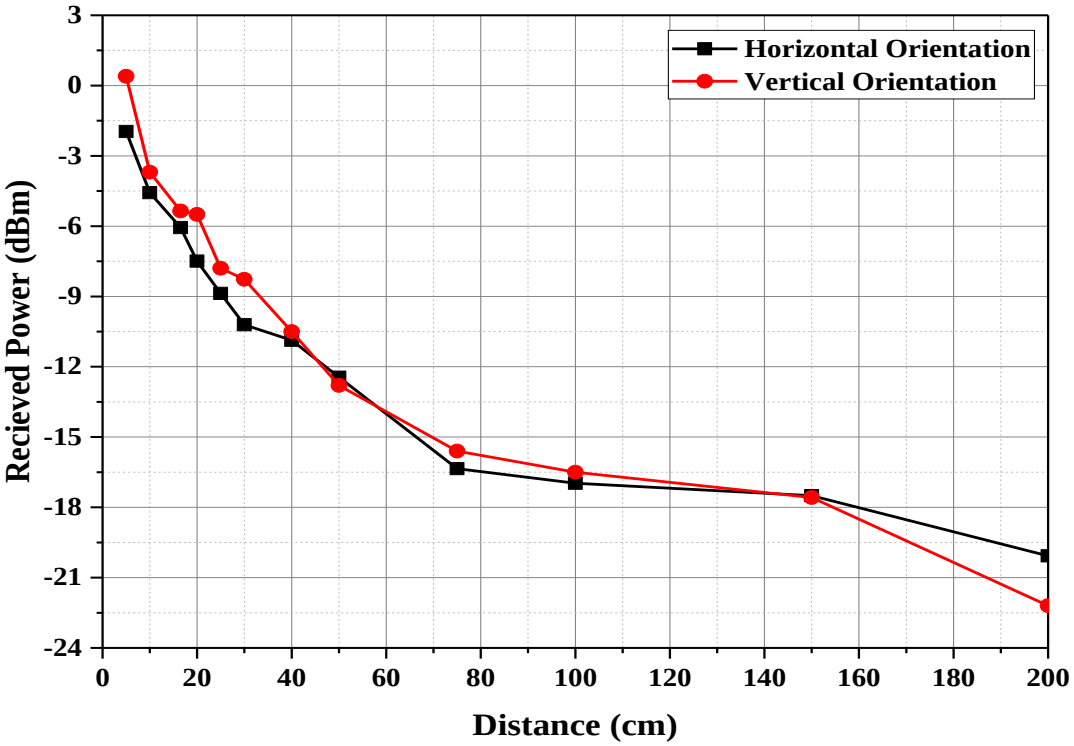

Fig. 6.22. The received power versus distance measured using the proposed antenna in a rabbit. The EIRP transmitted is 140 mW.

It can be seen from Fig. 6.22 that both orientations have similar receiving response with a slightly higher power in the vertical orientation. This advantage is counted to the proposed antenna where it can receive efficiently in two orientations. The power received at 1 m distance was 22.38 µW and 20.1 µW at the vertical and horizontal orientations, respectively. The transmit EIRP during the experiment was kept at 140 mW.

An experiment was then carried out to investigate the received power in different angles. Since the receiving antenna is embedded under the rabbit skin, it is kept in the same position and the angle of the transmitting antenna was rotated with respect to its azimuth from −60˚ to +60˚ with a rotation step of 15˚. The experiment is carried out for both horizontal and vertical orientations as shown in Fig. 6.23. The received power was not symmetrical because the radiation pattern of the receiving

antenna is not symmetrical in the vertical direction as shown in Fig. 6.14(a) and (b) and Fig. 6.15.

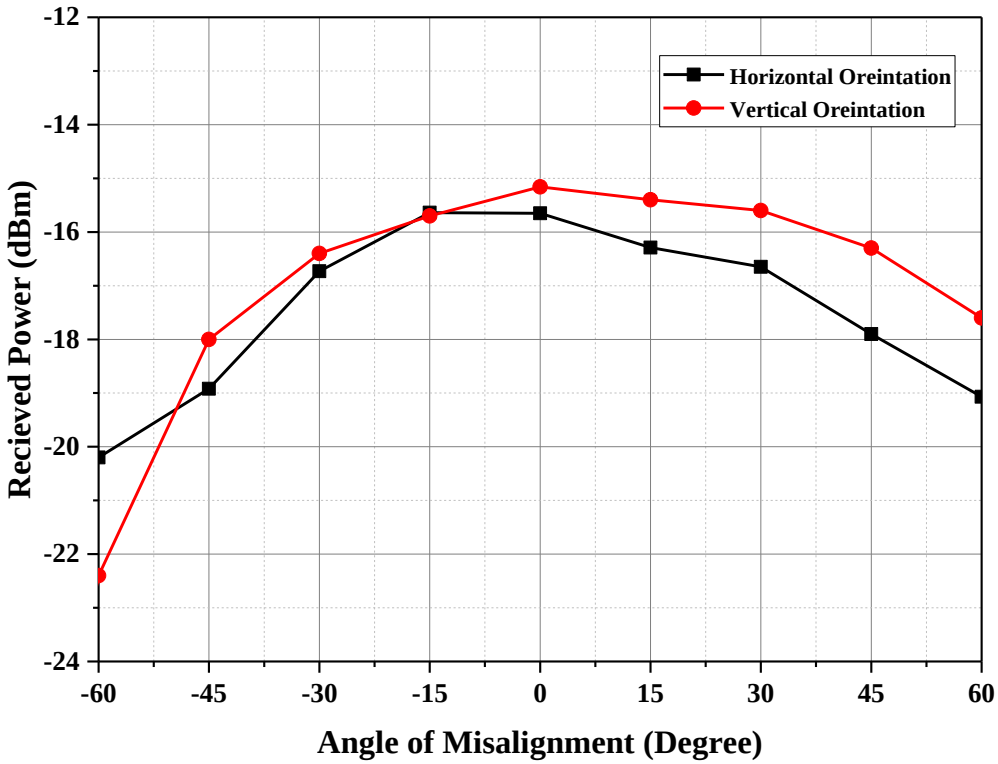

Fig. 6.23. The received power versus rotation angle measured in a rabbit with separation distance of 1 m between the transmitting and receiving antennas.

In general, the maximum transmit power by the transmitting antenna for far field WPT should be calculated according to the maximum exposure safety limits. According to IEEE standards for maximum exposure limits, the maximum power density at the body is 14.4 W/m² in a controlled environment and 2.165 W/m² in a public environment [28]. The gain of the transmitting antenna in the experiment was 2.3 dB. The maximum allowed EIRP at 1 m away from the transmitter in a public environment is 27 W. With this level of transmitted power, 4 mW can be received using the proposed antenna in the rabbit experiment and 1.2 mW in the minced pork experiment.

6.4 Communication Measurement

To demonstrate the ability of the proposed antenna for establishing a communication link, an experiment using a transceiver has been carried out. This transceiver is a part of a wireless temperature station. It has a temperature sensor and the transceiver works at 433.9 MHz. The proposed antenna covers both the MICS band of 402-405 MHz and the ISM band at 433 MHz. The proposed antenna was used in the experiment to work at 433.9 MHz.

The wireless weather Station has two parts: an indoor reader station that has a monopole receiving antenna with gain of 1.38 dB and an outdoor transmitting tag that contains a temperature sensor and an antenna with a gain of 1 dB, both at 433.9 MHz. The outdoor tag is modified so that the original antenna is replaced with the proposed one. The modified transceiver can be fitted inside the box as shown in Fig. 6.24. The transmit power of the tag transceiver is found out to be 25 μW. The modified communication system is demonstrated in vitro as follows:

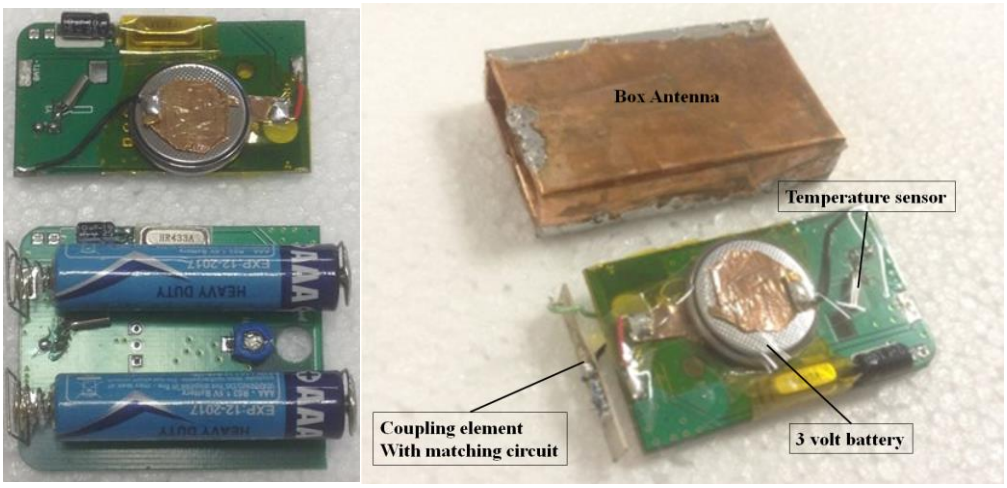

Fig. 6.24. The modified transceiver to be fit inside the proposed box antenna.

6.4.1 Experiment in Minced Pork and a Rabbit

The experiment setup including the proposed antenna with the modified transmitter was tested first in minced pork. A receiver station is used to read out the temperature. The experiment setup is shown in Fig. 6.25. It is worth mentioning that the antenna

was totally submerged in the minced pork during the experiment. The antenna can be seen in Fig. 6.25 just to show where the antenna was placed.

The temperature can be read within a range of 32 cm with the default transceiver transmit power of 25 µW. A longer range is expected if the transmit power is boosted to higher levels but within the safety limits. The receiving system can also be improved to increase the range. The result has verified that the proposed antenna can be used for effective communication.

The same experiment of communication is carried out in a rabbit as well. The housing antenna with the transceiver is implanted under the skin of the rabbit. A communication range of 1 m is achieved. The improved range is the consequence of the thin layer of the rabbit skin as compared with the 2 cm thick minced pork.

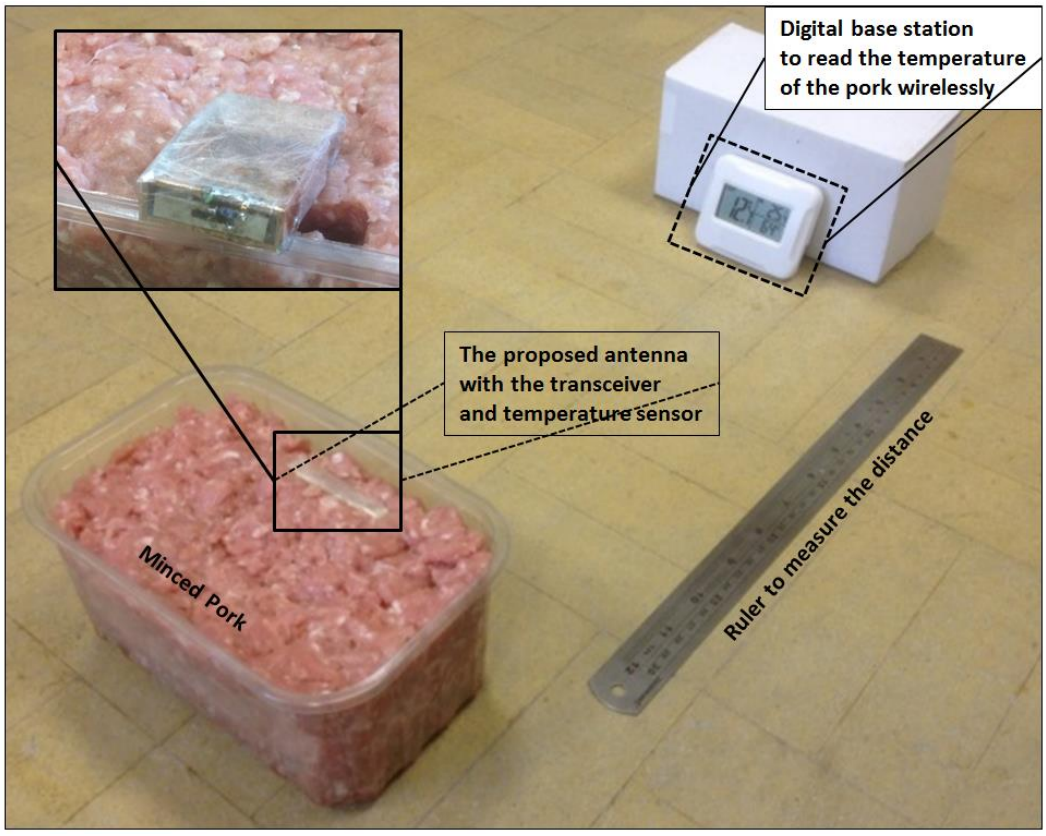

Fig. 6.25. The communication experiment of the proposed antenna to read the temperature in minced pork.

The proposed antenna to be used for communication should be verified for safety limits. The maximum transmit power from the proposed implanted antenna within the safety regulations can be computed according to the SAR. The FCC SAR regulation of 1.6 W/kg per 1-g averaging was considered to determine the usability of the proposed antenna. It is found by calculating the SAR using CST Microwave Studio that the proposed design can be used with a transmission power of up to 9 mW.

The experiment of communication is carried out with a transmit power of 25 µW which is fixed in the transmitter module. A communication range of 32 cm and 1 m is achieved inside minced pork and a rabbit respectively. A longer range is achievable with this antenna by increasing the transmit power up to 9 mW. By feeding the proposed antenna with this higher transmit power, it is estimated by calculation that a communication range of up to 19 m can be established.

6.5 Summary and Conclusions

This chapter has presented a novel antenna design using the housing case of a pacemaker. The proposed concept can be used for many other implantable devices with a conducting case. This housing antenna is optimized to work at the ISM band around 2.45 GHz in free space and then is optimized at the MICS band of 402 – 405 MHz and the ISM band around 433 MHz in body tissues. This design offers a radiation pattern with most power going out of the housing surface and off the body. It is suitable for implantable devices such as pacemakers due to the flexibility to choose the desired frequency band and a suitable radiation pattern.

The proposed antenna is tested for establishing communication links. This system established a communication link distance of 32 cm when the system was placed inside minced pork. The same experiment is carried out inside a rabbit and a communication range of 1 m has been achieved. This antenna can cover further range with a higher transmit power but within the safety limits.

A wireless power transfer experiment is also done to find out the capability of the proposed antenna for energy harvesting. The experiment shows promising results. A received power of 22.4 µW is demonstrated when an EIRP of 140 mW is transmitted from an antenna 1 m away. By boosting the transmitter with higher power but within

safety limits, a power of 4 mW can be received from the same distance. The received power can be potentially used to recharge a small battery.

If this design is implemented in a pacemaker, it can provide energy for communication and reserve the energy of the primary battery solely for the core function of the pacemaker. For long term of operation that is typically 5-7 years, this amount of reserved energy could be significant and help in extending the lifespan of the primary battery.

References

[1] NHS-Choices, "Pacemaker implantation," *http://www.nhs.uk/Conditions/PacemakerImplantation/Pages/Introduction.aspx,* 2015.

[2] "http://www.dailymail.co.uk/news/article-2958379/Heart-condition-woman-pleased-pacemaker-spent-3-500-matching-one-DOG.html."

[3] "http://myhealthblogs.com/heart-health/what-is-a-pacemaker.htmlhttp://myhealthblogs.com/heart-health/what-is-a-pacemaker.html."

[4] P. Arzuaga, "Cardiac Pacemakers: Past, Present and Future," *IEEE Instrumentation & Measurement Magazine,* vol. 17, pp. 21-27, Jun 2014.

[5] A. J. Shah, J. D. Brunett, J. P. Thaker, M. B. Patel, V. V. Liepa, K. Jongnarangsin, *et al.*, "Characteristics of telemetry interference with pacemakers caused by digital media players," *Pacing and Clinical Electrophysiology,* vol. 33, pp. 712-720, 2010.

[6] "http://www.medtees.com/ICDPhotos.html."

[7] "http://www.washingtonhra.com/pacemakers-icds/implantable-cardioverter-defibrillator-icd.php."

[8] H. D. Marlene, "FCC-03-32A1," *Federal Communications Commission Office of Engineering & Technology,* 2003.

[9] K. S. Nikita, *Handbook of biomedical telemetry*: John Wiley & Sons, 2014.

[10] H. S. Savci, A. Sula, Z. Wang, N. S. Dogan, and E. Arvas, "MICS transceivers: Regulatory standards and applications," *Proceedings of the*

IEEE SoutheastCon 2004, pp. 179-182, 2005.

[11] European Telecommunications Standards Institute, "Ultra Low Power Active Medical Implants (ULP-AMI) and Peripherals (ULP-AMI-P) operating in the frequency range 402 MHz to 405 MHz," 2009.

[12] F. C. W. Po, C. Delavaud, E. de Foucauld, J.-B. David, and P. Ciais, *An Efficient Adaptive Antenna-Impedance Tuning Unit Designed for Wireless Pacemaker Telemetry*: INTECH Open Access Publisher, 2011.

[13] W. Huang and A. A. Kishk, "Embedded Spiral Microstrip Implantable Antenna," *International Journal of Antennas and Propagation,* 2011.

[14] T. Houzen, M. Takahashi, and K. Ito, "Implanted antenna for an artificial cardiac pacemaker system," *Piers 2007 Prague: Progress in Electromagnetics Research Symposium, Proceedings,* pp. 51-54, 2007.

[15] S. Lee, W. Seo, K. Ito, and J. Choi, "Design of an implanted compact antenna for an artificial cardiac pacemaker system," *Ieice Electronics Express,* vol. 8, pp. 2112-2117, Dec 25 2011.

[16] P. Li, G. A. Mouchawar, J. Amely-Velez, and R. Imani, "Inverted E antenna with capacitance loading for use with an implantable medical device," US patent 2014/0002314 A1, Jan. 2, 2014.

[17] S. Vajha, K. R. Maile, D. E. Larson, D. A. Chizek, and J. M. Edgell, "Folded antennas for implantable medical devices," US patent 2012/0130451 A1, May 24, 2012.

[18] J. A. Von Arx, W. R. Mass, S. T. Mazar, and M. D. Amundson, "Antenna for an implantable medical device," US patent 7,483,752 B2, Jan. 27, 2009.

[19] M. D. Amundson, J. A. Von Arx, W. J. Linder, P. Rawat, and W. R. Mass, "Circumferential antenna for an implantable medical device," US patent 6,809,701 B2, Oct. 26, 2004.

[20] G. L. Dublin, W. D. Verhoef, and R. S. Wallace, "Optional telemetry antenna for implantable medical devices," U.S. patent 7,319,901 B2, Jan. 15, 2008.

[21] D. Aghassian, L. Freidin, and V. Dronov, "Implantable Medical Device Having A Slot Antenna In Its Case," U.S. patent 20100161002 A1, Dec. 22, 2008.

[22] R. Martens and D. Manteuffel, "Systematic design method of a mobile multiple antenna system using the theory of characteristic modes," *IET*

Microwaves, Antennas & Propagation, vol. 8, pp. 887-893, 2014.

[23] M. Cabedo-Fabres, E. Antonino-Daviu, A. Valero-Nogueira, and M. F. Bataller, "The Theory of Characteristic Modes Revisited: A Contribution to the Design of Antennas for Modern Applications," *IEEE Antennas and Propagation Magazine,* vol. 49, pp. 52-68, 2007.

[24] R. Valkonen, M. Kaltiokallio, and C. Icheln, "Capacitive Coupling Element Antennas for Multi-Standard Mobile Handsets," *IEEE Transactions on Antennas and Propagation,* vol. 61, pp. 2783-2791, May 2013.

[25] J. Villanen, J. Ollikainen, O. Kivekas, and P. Vainikainen, "Coupling element based mobile terminal antenna structures," *IEEE Transactions on Antennas and Propagation,* vol. 54, pp. 2142-2153, 2006.

[26] J. Holopainen, R. Valkonen, O. Kivekas, J. Ilvonen, and P. Vainikainen, "Broadband Equivalent Circuit Model for Capacitive Coupling Element-Based Mobile Terminal Antenna," *IEEE Antennas and Wireless Propagation Letters,* vol. 9, pp. 716-719, 2010.

[27] Z. Duan, Y. X. Guo, M. Y. Je, and D. L. Kwong, "Design and in Vitro Test of a Differentially Fed Dual-Band Implantable Antenna Operating at MICS and ISM Bands," *IEEE Transactions on Antennas and Propagation,* vol. 62, pp. 2430-2439, May 2014.

[28] IEEE Std C95.1™-2005, "IEEE Standard for Safety Levels with respect to Human exposure for RF electromagnetic fields 3 kHz to 300 GHz," *IEEE International Committee on Electromagnetic Safety (SCC39),* April 2006.

Chapter 7

Conclusions and Future Work

In this thesis, implantable and wearable antennas have been investigated in terms of communications and Wireless Power Transfer (WPT) with biomedical devices. Rectifier circuits have been designed to be integrated with these antennas to form a compact system. The conclusion of each Chapter is summarized:

In Chapter 1: Introduction and motivations of this thesis were given, with the following conclusions:

- Antennas are an essential part for RF telemetry system for medical devices. These antennas support the capability of remote home monitoring.
- Medical Implant Communication Service (MICS) band around 403 MHz is the main target for implantable antenna design since it is specified for medical communications only and limited with -16 dBm of transmitting power to reduce the interference effect from other applications.
- A compact antenna to handle both data communications and WPT is advantageous to reduce the implant size.
- The Industrial, Scientific and Medical (ISM) band around 433 MHz is the candidate for WPT. It is close to the MICS band so that it can be easily covered together with the MICS band using one antenna.
- Wearable antennas have several advantages to be adopted in data communication in terms of extending the communication range as a repeater. It has the advantage in WPT in terms of ability to utilize near field coupling and free mobility to the patient.

In Chapter 2: The safety standards have been discussed in terms of maximum exposure limits and SAR limits. The electromagnetic signal in terms of attenuation in

lossy media and reflection at boundary of tissue layers were presented. Types of implantable and wearable antennas were given. The WPT in terms of far field and near field were discussed further to the rectifier's designs. As a conclusion, this Chapter can be summarized in the following points:

- Low frequency bands that suitable for antenna designs are preferred for lower attenuation. MICS band and ISM band around 433 MHz are the target since they are relatively low frequency bands and suitable for implantable antenna design.
- High magnetic field antennas are preferred for higher level WPT in near field coupling.
- Flexible antennas are preferred for medical applications since it can be used in planar shape and conformal for implantable devices.
- A wearable antenna is a good choice to be adopted with implantable devices because of the close distance to the body. This has several advantages including: it can adopt inductive coupling for WPT; it can be used as a repeater to extend the communication range between the implantable antenna and an external reader.
- The power required for establishing a communication link between the implantable and wearable antenna is low so that the power consumption by the implants will be less and fall further below the SAR limit.
- Loop antenna is flexible and has large magnetic field in the near field region of the antenna. It can be used with planar and cylindrical implants as implantable antenna. It can be also used around all body parts as wearable antennas.
- Voltage doubler rectifier is good candidate since it only adopts two diodes in the circuit and has high RF to DC conversion efficiency.

In Chapter 3: Design of a voltage doubler rectifier circuit at 433 MHz band was investigated. Three rectifiers have been proposed for several purposes. The first rectifier was design on an FR4 substrate. This rectifier was used to charge a realistic

implantable battery. The second rectifier was designed on a Roger substrate. This rectifier was optimized on real available components; the overall components were optimized with the dimension of microstrip transmission lines to get smaller size. As a result this rectifier achieved around 50% reduction in size. This rectifier was integrated with a specific implantable antenna to be used for far field WPT experiment. The third rectifier was designed on a Roger substrate as well. This rectifier was miniaturized further than the second rectifier. The overall components have been tuned with reducing the size of the microstrip transmission lines. This process was repeated many times until getting the smallest size with high conversion efficiency. This rectifier was optimized for input impedance of 50 Ω to work with antennas as implantable rectennas. It is concluded that:

- A voltage doubler rectifier is useful to get high AC to DC conversion efficiency up to around 80%.
- Schottky diodes series HSMS-282x are used for input power levels greater than -20 dBm and frequency bands less than 4 GHz. This series is useful for WPT applications at 433 MHz.
- A rectifier circuit has been miniaturized to very small size by optimisation the overall components together including the transmission lines.

In Chapter 4: Wearable and implantable antenna designs have been introduced. The wearable antenna can be used on body for in body communications and for WPT. It can be used potentially as a repeater between the implantable antenna and a faraway external reader. In this Chapter, the conclusions are:

- Loop antennas can be used to cover several medical bands. This can be developed by adopting curve meandering technique so that several bands with wide bandwidths can be covered.
- Loop antennas with a wide bandwidth at 400 MHz can be used for communications at MICS band and for WPT at 433 MHz simultaneously.
- A strong magnetic field in the near field region of the antenna can be generated. This has been done by meandering the loop antenna in such way

the generated magnetic fields are combined constructively.

In Chapter 5: Experiments have been presented for both far field and near field WPT. In both types, our designs of wearable and implantable loop antennas and doubler rectifiers were used. Both techniques can provide sufficient power for direct powering of some implantable applications or recharging batteries that have small capacities around 10 mA•h. The results and key contributions with far field WPT can be summarized as:

- Antennas are demonstrated to be applicable for far field WPT at 433 MHz in experiments. It is potentially applicable for communications based on the far field antenna parameters.
- Sufficient values of power have been demonstrated within safety limits using the proposed designs. 4 mW can be received using far field WPT within 1 m away from the transmitting antenna. These values are applicable for directly powering some implantable applications or recharging small batteries.
- WPT experiment using liquid body model showed lower WPT efficiency than using pork. This is because that liquid absorbs more energy than the real tissues.
- Far field WPT has some drawback including the restricted movement for the patient and exposing all the body for radiation in order to power a specific spot.

In near field WPT, a system of the proposed wearable and implantable antennas with miniaturized doubler rectifier was used. It can be summarized as

- Orthogonal magnetic fields are an efficient approach to generate dense of magnetic field lines. As a result, a better coupling at several offsets between the wearable and implantable antennas was achieved. This was demonstrated using the proposed High Magnetic loop wearable and implantable antennas and compared with the performance of conventional square loop pair.

- The strong magnetic field that generated by constructive combination improves near field WPT. This was demonstrated using the proposed pair as compared with a pair of conventional square loop antennas.
- The proposed wearable and implantable antennas with miniaturized rectifier were able to deliver a DC power of more than 1 mW within safety limits. This amount of power is enough to directly power many common implantable medical devices including a pacemaker, a nerve stimulation device or a glucose measurement system.
- By adopting the near field WPT with wearable antenna, a free mobility for the patient is offered and the transmitting power is for the intended spot only.

In Chapter 6: A novel antenna design has been presented using the housing case of a pacemaker. The conclusion of this Chapter can be summarized as:

- Surface current modes on the housing case of pacemakers can be utilized for radiations at specific bands.
- The proposed concept can be used for many other implantable and wearable devices with a conducting case.
- Flexibility to choose the desired frequency band through applying the equivalent matching circuit to the excitation port.
- The proposed approach was demonstrated for communication and WPT at ISM band around 433 MHz with size comparable to a real pacemaker. This design can be generalized to similar devices such defibrillators, gastric stimulators and neuro stimulators.
- Sufficient power was received in *Vitro* measurement using the proposed design. This power can be used to directly power a specific application or recharge a battery with a relatively small capacity.

- If this design is implemented in a pacemaker, it can provide energy for communication and reserve the energy of the primary battery solely for the core function of the pacemaker. For long term of operation that is typically 5-

7 years, this amount of reserved energy could be significant and help in extending the lifespan of the primary battery.

There are also the following possible future works:

From Chapter 3, three rectifiers based on voltage doubler concept have been presented. Then DC combining based on parallel and series connections were discussed to get higher DC output power. However, cascading doubler rectifiers have not been discussed. Multistage doubler has the advantage of increasing the output voltage from the same input. However, it should be dealt with carefully since adding more stages means more dissipated power in diodes and lumped-element components. Furthermore, the rectifier size will be increased as well. A study for multistage voltage doubler for implantable applications is important so that the optimum number of stages with respect to the sweep of power input can be recommended. The extra size that associated with the multistage rectifier and how it fits to medical applications should be discussed as well.

From Chapter 4, wearable antennas have been designed to cover multiple wide bands and to improve the magnetic field in the near field region of the antenna. For the dual wideband butterfly antenna, the antenna size can be reduced further and it still covers the desired bands of MICS band and ISM around 433 MHz and 2.45 GHz. For the meandered wearable loop antennas that proposed for improving the magnetic field, a metamaterial layer can be added to the antenna to improve the magnetic field further. The induced surface current in the metamaterial lines can generate back magnetic fields. The generated magnetic field from the metamaterial can be combined with the generated one from the wearable antenna. The combined magnetic field would be stronger and it can improve WPT further. Furthermore, the metamaterial layer can act as insulator to the body from the electric field of the antenna. This can help to reduce the SAR effect of the antenna, and then higher power can be transmitted.

In chapter 5, the High Magnetic loop antenna design was presented for near field WPT. The design proposed a significant advantage of generating dense of orthogonal magnetic field lines by redirecting the surface current along two axes x and y, as a result a better receiving at different offsets is achieved as compared with

conventional loop antenna. This idea can be applied to coils. Several applications adopt coils for Near Field Coupling (NFC) such as mobile chargers and Radio Frequency Identification (RFID) equipped cards to manage building access. If this idea works with coils, then these applications can be improved significantly.

In Chapter 6, a housing case antenna was developed. This idea can be applied for devices that are contained in a conducting case such as Pacemakers, Defibrillators, Gastro stimulators, etc. the design approach was verified on a box shape antenna. Other shapes still not verified yet although the idea in principle can be applied. The antenna performance without insulation needs investigation. Furthermore, performance of the antenna with interference from external DC or other frequencies needs to be considered and investigated.